Breaking Symmetries: $\mathcal{N} = 2$ Spin Chains and Conformal Field Theory at Finite Temperature

Dissertation
zur Erlangung des Doktorgrades
an der Fakultät für Mathematik, Informatik und Naturwissenschaften
Fachbereich Physik
der Universität Hamburg

Vorgelegt von
Deniz Bozkurt

Hamburg
2026

Declaration on oath

I hereby declare and affirm that this doctoral dissertation is my own work and that I have not used any aids and sources other than those indicated.

If electronic resources based on generative artificial intelligence (gAI) were used in the course of writing this dissertation, I confirm that my own work was the main and value-adding contribution and that complete documentation of all resources used is available in accordance with good scientific practice. I am responsible for any erroneous or distorted content, incorrect references, violations of data protection and copyright law or plagiarism that may have been generated by the gAI.

25.03.2026

Date

Signature of doctoral candidate

Gutachter/innen der Dissertation:	Prof. Dr. Elli Pomoni Prof. Dr. Volker Schomerus
Zusammensetzung der Prüfungskommission:	Prof. Dr. Konstantinos Nikolopoulos Prof. Dr. Elli Pomoni Prof. Dr. Michael Potthoff Prof. Dr. Volker Schomerus Prof. Dr. Timo Weigand
Vorsitzende/r der Prüfungskommission:	Prof. Dr. Michael Potthoff
Datum der Disputation:	30.06.2026
Vorsitzender des Fach-Promotionsausschusses PHYSIK:	Prof. Dr. Johannes Haller
Leiter des Fachbereichs PHYSIK:	Prof. Dr. Markus Drescher
Dekan der Fakultät MIN:	Prof. Dr.-Ing. Norbert Ritter

Zusammenfassung

Konforme Feldtheorien (CFTs) und supersymmetrische Feldtheorien stellen spezielle Klassen von Quantenfeldtheorien dar, deren Anwendungen von kritischen Phänomenen und Confinement bis hin zur Quantengravitation im Rahmen der Holographie reichen. Ihre großen Symmetriegruppen machen sie zu idealen Testklassen für theoretische Entwicklungen und ermöglichen den Einsatz mächtiger und eleganter Methoden. Zu den erfolgreichsten Ansätzen zählen dabei der konforme Bootstrap und die Integrabilität.

In dieser Arbeit unternehmen wir Schritte, diese zwei Methoden über ihre herkömmlichen Anwendungsbereiche hinaus zu erweitern, indem wir die konforme Symmetrie durch endliche Temperatureffekte brechen und die Supersymmetrie durch Orbifold-Konstruktionen reduzieren. Für Spin-Ketten, die aus $\mathcal{N} = 2$-superkonformen Feldtheorien hervorgehen, welche durch Orbifold-Projektionen der $\mathcal{N} = 4$-Super-Yang–Mills-Theorie in vier Dimensionen gewonnen werden, verallgemeinern wir den Koordinaten-Bethe-Ansatz durch die Einbeziehung von Fernwechselwirkungs-Korrekturen.

Im Rahmen des konformen Bootstraps entwickeln wir nach dem Brechen der konformen Symmetrie durch die Formulierung der CFT auf einem d-dimensionalen Zylinder ein analytisches Framework auf Basis von Dispersionsrelationen. Wir wenden diese Methode auf verschiedene Theorien an, darunter große-N-CFTs in vier Dimensionen. Darüber hinaus kombinieren wir diesen analytischen Ansatz mit bestehenden numerischen Bootstrap-Methoden bei endlicher Temperatur, um neue thermische Korrelationsfunktionen in der dreidimensionalen Ising-CFT zu berechnen.

Abstract

Conformal field theories (CFTs) and supersymmetric field theories constitute special classes of quantum field theories with applications ranging from critical phenomena and confinement to quantum gravity via holography. Their large symmetry groups make them ideal testing grounds for theoretical developments, enabling the use of powerful and elegant methods. Among these, conformal bootstrap and integrability have proven particularly successful.

In this thesis, we take steps toward extending these methods beyond their conventional domains by breaking conformal symmetry through finite temperature effects and reducing supersymmetry via orbifolding. For spin chains arising from $\mathcal{N} = 2$ superconformal field theories obtained by orbifolding $\mathcal{N} = 4$ super Yang–Mills theory in four dimensions, we generalize the coordinate Bethe ansatz by incorporating long-range corrections.

On the conformal bootstrap side, after breaking conformality by placing the CFT on a d-dimensional cylinder, we develop an analytic framework based on dispersion relations. We apply this method to several theories, including large-N CFTs in four dimensions. Furthermore, we combine this analytic approach with existing numerical bootstrap techniques at finite temperature to compute new thermal correlation functions in the three-dimensional Ising CFT.

Acknowledgments

I would first like to express my deepest gratitude to my supervisor, Elli Pomoni, for her invaluable guidance, constant support, and the many stimulating discussions that have shaped my Ph.D. journey. I am especially grateful for her openness, her encouragement to push beyond my limits, and her trust in allowing me the space to grow into an independent researcher. Beyond physics, I have also learned from her in ways that extend far into life.

I would also like to sincerely thank Timo Weigand for his continuous support and understanding throughout both my master's and doctoral studies. His encouragement and belief in me have made a lasting difference. I am further grateful to Volker Schomerus and Gleb Arutyunov for their support and for the insightful advice they have generously shared.

I am also deeply grateful to my bachelor's advisor, Ilmar Gahramanov, for preparing me for the path toward my Ph.D. and for his constant support over the years. Even from Istanbul, he has remained a steady source of encouragement and guidance and has maintained a research group that continues to feel like an academic home to me.

During my Ph.D., I greatly benefited from the wonderful environment in Hamburg, and at DESY in particular. I thank the entire group for their support and the many valuable discussions. I am especially thankful to those who made DESY more than a workplace and supported me through difficult times: Alessio, Alain, Craig, Davide (Lai), Enrico, Julien, Lorenzo, Margaritha, and Sara. I also thank all those who made DESY a warm and joyful place: Ana, Carlos, Davide (Bonomi), Davide (Polvara), Fabio, Federico, Francesco, Gabrielle, Giovanni, Guido, Mateo, Nika, Paul, Peter, Rigers, Sebastian, Tabea, Torben, and Waltraut. Among them, I owe special thanks to my collaborators Alessio, Enrico, and Julien for the many hours spent working together with Mathematica, for the countless discussions, and for their constant support. I also acknowledge my collaborators Juan Miguel and Ziwen for sharing the challenges of a particularly demanding project with me.

My deepest gratitude goes to my friends, who turned Hamburg into a true home for me. They listened to every story, endured my grumpiest moments, and found countless reasons to celebrate life together. Through their music, food, and our many shared adventures, they filled my life with joy and meaning: Andres, Cosima, Daniel, David, Enrico, Felipe, Felix, Isabela, Julia, Leo, Mateo, Paul, Paula, Rafael, and Tobias.

To my love, Alejandro, thank you for filling my life with joy, laughter, and unwavering support at every step of this journey. Having you by my side has been one of my greatest fortunes.

Finally, to my parents, Nilgün and Durali, to my closest friends, Berivan, Dicle, and Tuna, and to all my friends back in Turkey: I owe you more than words can express. You are my foundation and my roots. It is because of you that I find the strength to move forward, and because of you that I always know who I am and where I belong.

Author's contributions

This thesis is based on the following works by the author:

- Long-range to the rescue of Yang-Baxter I [1],
- Long-range to the rescue of Yang-Baxter II [2],
- The analytic bootstrap at finite temperature [3],
- Analytic thermal bootstrap meets holography [4].

Contents

Chapter 1

Introduction

From a bird's-eye view, fundamental theoretical physics seeks to understand the basic forces of nature and the interactions they govern. In the modern picture, four fundamental interactions are known: electromagnetism, the weak interaction, the strong interaction, and gravity. Ever since Maxwell unified electricity and magnetism within a single theory of electromagnetism [5], physicists have been led by the conviction that a deeper understanding of the laws of nature may be achieved by revealing how these apparently distinct interactions arise from a more unified framework. The pursuit of such unification has therefore become one of the central themes of modern physics.

However, this picture is only a simplified one. The development of modern physics has been shaped by a sequence of profound unifications, each of which transformed our understanding of nature. Among the most striking achievements of the twentieth century were the development of quantum mechanics and relativity [6–8]. One of the key insights that contributed to the emergence of quantum mechanics was the unification of wave and particle concepts [9, 10]. This new framework radically changed the classical view of nature as fundamentally deterministic and opened the way to a deeper understanding of the microscopic world [11, 12]. Relativity, on the other hand, revolutionized our conception of space and time by showing that they are not independent entities but rather aspects of a single underlying structure: spacetime.

Immediately after these two great discoveries, Dirac succeeded in combining the principles of special relativity with those of quantum mechanics [13]. The result of this synthesis is quantum field theory (QFT), one of the most precise and comprehensive frameworks currently available for describing physical phenomena. The second half of the twentieth century was marked by the explorations that became possible within the framework of QFT. Remarkably, QFT provides a common language for a vast range of subjects, from condensed matter and statistical physics to high-energy physics. Moreover, if gravity is set aside, the remaining three interactions, namely electromagnetism, the weak interaction, and the strong interaction, are all successfully described within the framework of QFT. More specifically, they are understood as gauge theories, and their unification into the Standard Model stands as one of the great achievements of modern physics, providing an extraordinarily successful description of the subatomic world [14–16].

Yet, despite the extraordinary success of QFT and the Standard Model, one fundamental problem remains open: the construction of a consistent quantum theory of gravity, indicating that an even deeper conceptual framework is required. Among the proposed approaches, string theory stands out as one of the most elegant and potentially far-reaching. In this framework, gravity emerges naturally within a quantum-consistent setting, offering a compelling route toward unification. For this reason, it has long been regarded as one of the leading candidates for a unified description of all fundamental interactions [17–19]. However, it remains an open question whether string theory provides the correct description of quantum gravity for our nature.

A key insight underlying these developments is that physical theories are most naturally understood in terms of the symmetries that govern them. This perspective, first made precise in the seminal work of Emmy Noether [20], establishes a deep connection between continuous symmetries and conservation laws. In modern physics, symmetry principles play a central role in organizing our understanding of quantum field theories and in enabling powerful computational techniques.

Despite the significant progress in our understanding of fundamental interactions, quantum field theories remain notoriously difficult to analyze in general. In practice, exact or controlled results can typically be obtained only in the presence of a large amount of symmetry. Among the various possibilities, two types of symmetries play a particularly important role in simplifying the study of quantum field theories: supersymmetry and conformal symmetry.

Conformal field theories (CFTs) play a central role in contemporary theoretical physics, with applications ranging from critical phenomena to string theory, and, via the holographic correspondence, to quantum gravity. One of the main reasons for their importance is the combination of this broad range of applications with a rich set of powerful methods that exploit conformal symmetry [21–24]. The large symmetry group underlying CFTs allows for the use of a wide variety of techniques, including renormalization group (RG) methods, integrability, conformal bootstrap, Monte Carlo simulations, and tensor network approaches. In two dimensions, the infinite-dimensional Virasoro symmetry further enhances this structure, enabling the exact computation of a large class of physical observables.

Supersymmetric quantum field theories play an equally central role in modern theoretical physics, providing a powerful framework in which non-perturbative aspects of QFT can be studied with remarkable precision. In particular, theories with extended supersymmetry, such as $\mathcal{N} = 4$ supersymmetric Yang–Mills (SYM) theory, have become paradigmatic examples due to their exceptional degree of symmetry and mathematical structure. A key reason for their importance lies in the wide array of exact techniques that supersymmetry makes available [25, 26]. These include supersymmetric localization [27], which enables the exact computation of certain observables; integrability [28], which allows for the determination of spectra and correlation functions; electromagnetic duality [29], which relates strongly and weakly coupled regimes; and various 4d/2d correspondences [30], which connect four-dimensional gauge theories to two-dimensional conformal field theories. Together, these methods provide deep insights into the non-perturbative dynamics of quantum field theories and continue to play a central role in the study of strongly coupled systems.

High-energy theoretical physics has benefited greatly over the last fifty years from the presence of these two symmetries. A paradigmatic example in which the superconformal symmetry group plays a crucial role is the AdS/CFT correspondence [31, 32]. The AdS/CFT correspondence provides a powerful framework for studying strongly coupled gauge theories through their dual weakly coupled gravitational descriptions, while simultaneously offering deep insights into the nature of quantum gravity. As a concrete realization of gauge/gravity duality, it relates maximally supersymmetric Yang–Mills theory in four dimensions to Type IIB superstring theory in ten-dimensional spacetime. Over the past three decades, the rich structure of superconformal symmetry, together with a variety of powerful theoretical techniques, has enabled detailed investigations of this correspondence, leading to numerous non-trivial checks and a deeper understanding of its underlying principles.

At the same time, this reliance on symmetry presents a fundamental limitation. Although superconformal field theories (SCFTs) provide a remarkable testing ground for many of our modern theoretical ideas, they are not, in their most symmetric form, directly realized in nature. In particular, when compared with experimental observations, such highly symmetric models are often too idealized to capture the full complexity of physical systems. To make closer contact with reality, it is therefore necessary to consider theories in which these symmetries are partially or completely broken.

At the same time, the powerful techniques developed for studying highly symmetric theories remain extremely valuable. A central challenge is therefore to understand how these methods can be extended beyond the superconformal setting. In practice, this involves systematically breaking supersymmetry and conformal symmetry and carefully tracking how physical observables and theoretical structures are modified under such deformations. In this way, one aims to retain as much analytical control as possible while moving toward more realistic models of fundamental interactions [33–35].

There are many established techniques to break these symmetry groups. Among them, the most studied approaches include adding operators to the Lagrangian to deform the theory, keeping a symmetric Lagrangian but choosing a non-symmetric vacuum (spontaneous breaking) [35, 36], or considering cases where quantum effects (anomalies) break these symmetries. In this thesis, we use orbifolding to break supersymmetry, which involves projecting the R-symmetry group to a smaller group using a discrete group, and we place the CFT on a d-dimensional manifold that is not conformally equivalent to flat space in order to introduce a scale.

Both of these deformations are well motivated and give rise to long-term research programs. For the breaking of supersymmetry, orbifolding provides access to a large portion of the theory space of $\mathcal{N}=2$ SCFTs. In this case, we focus on the diagonalization of the Hamiltonian, which corresponds to computing the anomalous dimensions of all single-trace operators at one loop. This problem, in the context of $\mathcal{N}=4$ SYM, was solved using the coordinate Bethe ansatz (CBA) technique [37], and we extend this method so that it applies to marginally deformed orbifold theories. We expect that it can be applied to other $\mathcal{N}=2$ orbifold cases and further extended to incorporate $\mathcal{N}=1$ orbifolds.

For the breaking of conformality, placing the theory on a d-dimensional manifold provides the simplest setup in which we can develop finite-temperature bootstrap techniques [38] and compute additional one-point functions. By developing these techniques, we move closer to addressing more complicated and physically relevant cases, such as $S^1 \times S^{d-1}$, for which we also have some preliminary results. We hope that these explorations will guide us toward formulating CFTs in a way that is less dependent on the special features of flat space and will allow us to probe phenomena such as phase transitions and hydrodynamics.

To provide a detailed account of how we implement these ideas, namely the breaking of these symmetries and the development of techniques to address the resulting novel features, we summarize the structure of the thesis as follows.

1.1 Summary of Thesis

In this thesis, we begin by reviewing the background material necessary to present our contributions to the literature. We then turn to the two main chapters, which consider the breaking of supersymmetry and conformal symmetry, respectively.

Background. Chapter 2 is divided into three sections, covering the three main topics of this thesis: supersymmetry, conformal symmetry and thermodynamics. The discussion of these topics is self-contained but not exhaustive.

In Section 2.1, we review the background material necessary to study supersymmetric quantum field theories and briefly introduce $\mathcal{N} = 4$ SYM. Since we focus on integrability as the primary example of a technique that depends on the presence of supersymmetry, we briefly present spin chains arising from $\mathcal{N} = 4$ SYM. We then review the orbifolding procedure to break supersymmetry and arrive at the theories that are the focus of this thesis.

In Section 2.2, we cover the basics of conformal symmetry and describe the main techniques essential for this work. The discussion of CFT includes the main tools such as the operator product expansion, radial quantization, and aspects of the analytic conformal bootstrap.

Lastly, in Section 2.3, we cover the basics of thermodynamics, in particular the Matsubara formalism. This provides the necessary framework for breaking conformality by introducing temperature, and for discussing the fundamental aspects of the dynamics that play an essential role.

Spin Chains Arising from $\mathcal{N} = 2$ SCFTs Chapter 3 considers an $\mathcal{N} = 2$ SCFT obtained by systematically breaking the supersymmetry of $\mathcal{N} = 4$ SYM, and develops a long-range generalization of the CBA for this setup.

In Section 3.1, we introduce the novel properties of the marginally deformed $\mathbb{Z}_2$ orbifold of $\mathcal{N} = 4$ SYM.

In Section 3.2, we focus on a subsector of the spin-chain model arising from this SCFT and present the limitations of the CBA in this context.

In Section 3.3, we introduce the long-range Bethe ansatz and solve the three-magnon problem. We demonstrate that, by imposing additional permutation symmetry constraints, we are able to find a family of solutions with manifest permutation symmetry.

In Section 3.4, we introduce the long-range ansatz for the four-magnon problem and generalize the solution to this sector.

In Section 3.5, since the symmetry constraints used for the three-magnon solution turn out to be insufficient to fully constrain the four-magnon solution, we explore the connection between solutions with different numbers of magnons and derive a physical limiting procedure to further constrain the solution.

In Section 3.6, we apply the conditions derived from the limiting procedure to the special solution of the four-magnon problem and obtain a particular family of solutions.

In Section 3.7, we apply the Yang operator formalism to the special solutions of the three- and four-magnon problems and demonstrate the manifest permutation symmetry in detail.

In Section 3.8, we impose periodic boundary conditions on the two- and four-magnon solutions and show that the long-range solution developed in this thesis is compatible with these boundary conditions.

Conformal Field Theory at Finite Temperature In Chapter 4, we change gears and consider the breaking of conformal symmetry by placing it on a d-dimensional cylinder.

In Section 4.1, we introduce the finite-temperature setup and consider the most fundamental aspects of CFTs on d-dimensional cylinders.

In Section 4.2, we present the analytic structure of the correlators at finite temperature and construct a dispersion relation with it. After obtaining the main analytic bootstrap results, we apply them to various examples like GFF models and the $O(N)$ model.

In Section 4.3, we apply the dispersion relation technique developed in the previous section to holographic setups. In this case, the holographic setup brings new challenges like OPE coefficients with poles and we overcome these challenges in the framework we developed previously.

In Section 4.4, we combine the results of the analytic bootstrap with the sum rules derived from the KMS condition. In this way, we are able to compute thermal correlation functions for the $3d$ Ising model.

Chapter 2

Background

QFTs are a central part of our current understanding of physics. Although there are several ways to formulate a QFT, these theories remain notoriously difficult to study. Their symmetries provide one of the most powerful tools for organizing their structure. In special cases where the symmetry algebra is especially large, one can derive strong constraints and obtain detailed information about the properties of the theory.

In this thesis, we focus on two important examples of such extended symmetry algebras: supersymmetry and conformal symmetry. Both profoundly reshape our perspective on QFTs and enable the development of powerful and far-reaching methods for their analysis. Therefore, in this chapter, we review the basic features that characterize these two special classes of QFTs and briefly discuss some of the powerful tools that emerge in the presence of these symmetries. This review is not intended to be exhaustive and is largely guided by the existing literature; further details can be found in [39–43].

First, we consider the supersymmetry algebra and its representations. We then focus on maximally supersymmetric Yang–Mills theory in four dimensions to demonstrate how integrable spin chains arise in this context. Before turning to conformal symmetry, we review the orbifolding procedure, which partially breaks supersymmetry and yields theories with reduced supersymmetry. Next, we review the conformal symmetry algebra and its representations. We focus on the radial quantization picture, which makes many features of conformal symmetry, such as the state-operator correspondence manifest. We conclude this part by discussing aspects of the conformal bootstrap, both from numerical and analytical perspectives, to set the stage for the breaking of conformality by temperature. Finally, we review various aspects of interacting QFTs at finite temperature.

2.1 Supersymmetric Field Theory

Even though supersymmetry has not yet been observed experimentally, it remains a powerful framework for the rigorous study of non-perturbative phenomena in quantum field theory. Remarkably, supersymmetry constrains the dynamics of a quantum field theory so strongly that certain strongly coupled regimes become exactly computable. This does not imply, however, that supersymmetric quantum field theories are devoid of interesting phenomena. On the contrary, they provide an important class of toy models that allow us to explore regimes of quantum field theory where analytic control would otherwise be very limited.

A particularly celebrated example is the study of confinement. Although a first-principles understanding of confinement in QCD remains out of reach, there exist supersymmetric gauge theories closely related to QCD in which confinement can be demonstrated analytically. A prominent example is the celebrated Seiberg-Witten solution of $\mathcal{N} = 2$ supersymmetric gauge theories [44, 45].

Another remarkable achievement of supersymmetry is the deep and unexpected connections it has revealed between quantum field theory and various areas of mathematics. Unlike many other areas of physics, supersymmetric quantum field theories can often be studied with a high degree of mathematical rigor, which has led to several striking contributions to mathematics. Among the most celebrated examples is the development of new perspectives on Morse theory and index theorems following the seminal work of Witten [46]. In this work, rather than merely uncovering an interesting relationship between physics and mathematics, Witten introduced a new analytic method for proving and understanding Morse theory, now known as the Witten deformation of the de Rham complex. Conversely, ideas from index theory have also led to important physical insights; for instance, they play a central role in the understanding of quantum anomalies [47].

In this section, we briefly review the supersymmetry algebra and some of its basic consequences. We then focus on maximally supersymmetric Yang–Mills theory in four dimensions to illustrate one of the powerful tools made possible by supersymmetry in this context. Later in this thesis, we reduce the amount of supersymmetry and adapt this tool to study theories with less supersymmetry.

2.1.1 Supersymmetry Group

To define the supersymmetry group (more precisely, the super-Poincaré algebra) in a simple manner, we consider the Lorentzian analogue of the rotation group, given by $SO(1, d-1)$.[1] Combining this group with the translations (2.2.9) yields the Poincaré group, which serves as the symmetry group of a relativistic quantum field theory.

To study spinor representations in this setting, we must consider the double cover of the Lorentz group. In four dimensions, for example, we have

$$SO(1,3) \cong \mathrm{Spin}(1,3)/\mathbb{Z}_2\,. \tag{2.1.1}$$

At the level of Lie algebras, this can be expressed as

$$\mathfrak{so}(1,3) \cong \mathfrak{su}(2) \oplus \mathfrak{su}(2)\,, \tag{2.1.2}$$

such that the spinor generators decompose into left-handed and right-handed components, corresponding to the two $\mathfrak{su}(2)$ factors.[2]

The Lorentzian signature slightly modifies the commutation relations between the symmetry generators.[3] In particular, the Lorentzian version uses the Minkowski metric

$$\eta_{\mu\nu} = \mathrm{diag}(+1, -1, \cdots, -1)\,. \tag{2.1.3}$$

In this case, the Poincaré algebra is defined in terms of the commutation relations,

$$[M_{\mu\nu}, P_\rho] = i\left(\eta_{\nu\rho}P_\mu - \eta_{\mu\rho}P_\nu\right)\;, \tag{2.1.4}$$

$$[M_{\mu\nu}, M_{\rho\sigma}] = i\left(\eta_{\nu\rho}M_{\mu\sigma} - \eta_{\mu\rho}M_{\nu\sigma} + \eta_{\mu\sigma}M_{\nu\rho} - \eta_{\nu\sigma}M_{\mu\rho}\right)\;. \tag{2.1.5}$$

A natural question to ask is whether we can extend this symmetry algebra by generators that have non-trivial commutation relations with the generators of the Poincaré algebra. It was proven in [48] that under certain physical assumptions such as non-trivial scattering and a finite number of particle types below any fixed energy, the symmetry algebra of an interacting relativistic quantum field theory in spacetime dimension greater than two factorizes into a direct product of the Poincaré algebra and an internal symmetry algebra (Poincaré $\times$ Internal). Crucially, the Coleman-Mandula

[1] The Euclidean rotation group will be discussed in Section 2.2.

[2] Here we refer to the chirality of the spinor generators. Below, when discussing massless representations of the Lorentz group, we will treat chirality and helicity as equivalent. This equivalence does not hold for massive representations.

[3] Recall that the Euclidean version of these generators appeared in (2.2.16).

theorem concerns a QFT with a mass gap.[4] Indeed, when there is no mass gap in the IR, the Poincaré symmetry can be extended, and this is the focus of Section 2.2. Another important loophole of the Coleman-Mandula theorem is that it assumes the symmetry generators form a Lie algebra. Supersymmetry is possible because of this loophole, since it is characterized by a $\mathbb{Z}_2$-graded Lie algebra.

This structure is achieved by adding a left-handed Weyl spinor Q_α and its right-handed counterpart, where $\alpha = 1, 2$ in four dimensions, exactly because of the relation given in (2.1.2). These generators are called *supercharges*. In this case, the generators satisfy the anti-commutation relation,[5]

$$\{Q_\alpha, \bar{Q}_{\dot{\alpha}}\} = 2\sigma^\mu_{\alpha\dot{\alpha}} P_\mu \ , \tag{2.1.6}$$

where $\sigma^\mu_{\alpha\dot{\alpha}}$ is a component of the gamma matrices that generate the Clifford algebra. Combined with the commutation relations given in (2.1.4) and (2.1.5), the supersymmetry algebra consists of

$$[M^{\mu\nu}, Q_\alpha] = (\sigma^{\mu\nu})_\alpha^{\ \beta} Q_\beta \qquad [Q_\alpha, P_\mu] = \{Q_\alpha, Q_\beta\} = 0 \ , \tag{2.1.7}$$

together with the right-handed version of these commutation and anti-commutation relations. Like the Poincaré algebra, all internal symmetries must also commute with the supercharges, with one exception. The *R-symmetry* generators commute with the Poincaré algebra generators, but they do not commute with the supercharges[6],

$$[R, Q_\alpha] = -Q_\alpha \ , \qquad [R, \bar{Q}_{\dot{\alpha}}] = \bar{Q}_{\dot{\alpha}} \ . \tag{2.1.8}$$

This completes the review of the supersymmetry algebra. By taking the supercharges into account, we obtain a QFT that remains invariant under the exchange of bosons and fermions. Schematically, we can summarize this as

$$Q\,|\text{fermion}\rangle = |\text{boson}\rangle \ , \qquad Q\,|\text{boson}\rangle = |\text{fermion}\rangle \ . \tag{2.1.9}$$

We now turn to the classification of the states of a supersymmetric field theory. Since our interest lies in superconformal field theories, we restrict our attention to *massless*

[4]More precisely, the Coleman–Mandula theorem relies on a collection of assumptions about the existence of a non-trivial relativistic S-matrix, the analyticity and non-degeneracy of scattering amplitudes, and the structure of the particle spectrum, in particular that there are only finitely many particle species below any fixed mass.

[5]This anti-commutation relation is very powerful. Already at this level it implies that the energy of any state in a supersymmetric theory is necessarily positive, $\langle\phi|P_0|\phi\rangle \geq 0$.

[6]Note that these are the commutation relations for $U(1)$ R-symmetry. For extended supersymmetry, the R-symmetry group must also be extended and the commutation relations adjusted accordingly.

representations. Because the symmetry algebra under consideration is non-compact, it does not admit finite-dimensional unitary representations. Consequently, the analysis of particle states is performed by first working in a convenient reference frame and subsequently generating the full set of states by applying Lorentz transformations.

To determine the massless representations of the supersymmetry algebra, we choose the momentum of the state to be

$$p^{\mu} = (E, 0, 0, E). \tag{2.1.10}$$

We fix a reference frame for arbitrary $E \in \mathbb{R}$. This corresponds to a null momentum vector and therefore describes a massless particle. This is simply a convenient choice of frame, since any null momentum can be brought to this form by an appropriate Lorentz transformation. The subgroup of the Lorentz group that leaves this momentum invariant is the *little group*, which in this case reduces to $SO(2)$, generated by M_{12}.

With this choice of momentum, the essential supersymmetry algebra anti-commutation relation given in (2.1.6) simplifies to

$$\{Q_{\alpha}, \bar{Q}_{\dot{\alpha}}\} = 4E \begin{pmatrix} 1 & 0 \\ 0 & 0 \end{pmatrix}_{\alpha\dot{\alpha}} . \tag{2.1.11}$$

This suggests that we can interpret the operators Q_1 and $\bar{Q}_{\dot{1}}$ as fermionic annihilation and creation operators and use them to build the states of the theory. Depending on the number of supercharges $a = 1, \cdots, \mathcal{N}$, we can start with a Clifford vacuum,

$$|\lambda\rangle \xrightarrow{\bar{Q}^1_{\dot{1}}} |\lambda + \frac{1}{2}\rangle \xrightarrow{\bar{Q}^2_{\dot{1}}} \cdots \xrightarrow{\bar{Q}^{\mathcal{N}}_{\dot{1}}} |\lambda + \frac{\mathcal{N}}{2}\rangle \ , \tag{2.1.12}$$

where the increase by $\frac{1}{2}$ refers to the helicity charge arising from the commutation relation between M_{12} and the supercharges given in (2.1.7). Since helicity is flipped by CPT, we must always include both $|\lambda\rangle$ and $|-\lambda\rangle$ states in order to construct a physical theory. Therefore, when we count the number of states, we add the CPT conjugates when necessary and obtain

$$n = 2^{\mathcal{N}} \times \begin{cases} 1 & \text{if the multiplet is CPT complete} \\ 2 & \text{if the CPT conjugate has to be added} \end{cases} . \tag{2.1.13}$$

All states with a given helicity in (2.1.12) that are related to each other constitute a *supersymmetric multiplet*. In four dimensions, allowing for all possible helicities, the different multiplets are summarized in Table 2.1.[7]

[7] We restrict to helicity ≤ 1 because we are interested in renormalizable interacting quantum field theories in four dimensions. Such theories cannot consistently contain massless particles with spin greater than one. More generally, interacting massless particles with spin $s > 1$ cannot exist in a local QFT unless the theory includes gravity [49].

$\lambda \leq 1$	$\mathcal{N}=1$ vector	$\mathcal{N}=1$ chiral	$\mathcal{N}=2$ vector	$\mathcal{N}=2$ hyper	$\mathcal{N}=3$ vector	$\mathcal{N}=4$ vector
1	1	0	1	0	1	1
1/2	1	1	2	1+1	3+1	4
0	0	1+1	1+1	2+2	3+3	6
−1/2	1	1	2	1+1	1+3	4
−1	1	0	1	0	1	1
Total #	2×2	2×2	2×4	2×4	2×8	16

Table 2.1: *All possible massless supersymmetry multiplets in four dimensions with numbers of massless states as a function of $\mathcal{N}$ and helicity $\lambda \leq 1$.*

A very convenient way of organizing supersymmetric multiplets is through the $\mathcal{N}=1$ *superspace formalism.* In four spacetime dimensions, the superspace coordinates are obtained by extending the ordinary spacetime coordinates as

$$x^\mu \to (x^\mu, \theta_\alpha, \bar{\theta}_{\dot{\alpha}}), \qquad \alpha, \dot{\alpha} = 1, 2. \tag{2.1.14}$$

Here θ_α and $\bar{\theta}_{\dot{\alpha}}$ are Grassmann coordinates. They commute with the Minkowski coordinates x^μ but anticommute among themselves,

$$\theta_\alpha \theta_\beta = -\theta_\beta \theta_\alpha, \qquad \theta_\alpha \bar{\theta}_{\dot{\beta}} = -\bar{\theta}_{\dot{\beta}} \theta_\alpha. \tag{2.1.15}$$

In superspace the supercharges appearing in (2.1.6) can be represented as differential operators acting on both the spacetime and Grassmann coordinates. Using these coordinates, the component fields of a supersymmetric multiplet can be combined into a single object called a *superfield.*

The most general superfield in $\mathcal{N}=1$ superspace has the expansion

$$\begin{aligned} \Phi(x, \theta, \bar{\theta}) = \phi(x) + \theta\psi(x) + \bar{\theta}\bar{\chi}(x) + \theta^2 F(x) + \bar{\theta}^2 G(x) \\ + \theta\sigma^\mu\bar{\theta}\, A_\mu(x) + \theta^2\bar{\theta}\,\bar{\lambda}(x) + \bar{\theta}^2\theta\,\rho(x) + \theta^2\bar{\theta}^2 D(x). \end{aligned} \tag{2.1.16}$$

The component fields appearing with an even number of Grassmann coordinates, such as ϕ, A_μ, and D, are bosonic fields transforming in various representations of the Poincaré group. The remaining components are fermionic fields transforming in spinor representations of the Poincaré group. By imposing additional constraints on a superfield, one can obtain superfields with fewer component fields, and therefore shorter supersymmetric multiplets.

Before concluding the discussion of the superspace formalism, we note that supersymmetric Lagrangians can be constructed by integrating over the Grassmann coordinates of superspace,

$$\int d^2\theta, d^2\bar{\theta}\, \mathcal{K}(\Phi^i, \bar{\Phi}^{\bar{i}}), \qquad \int d^2\theta\, \mathcal{W}(\Phi^i). \tag{2.1.17}$$

The first expression corresponds to an integral over the entire Grassmann superspace. It generates the kinetic terms of the theory and may also produce non-renormalizable interaction terms containing derivatives. The function $\mathcal{K}(\Phi^i, \bar{\Phi}^{\bar{i}})$ is known as the *Kähler potential.*

Renormalizable, non-derivative interaction terms arise instead from integrating over half of the Grassmann coordinates, as in the second expression. This produces holomorphic terms determined by the function $\mathcal{W}(\Phi^i)$, which is called the *superpotential.* The superpotential plays a central role in characterizing the interactions of a supersymmetric theory.

Superconformal symmetry. Supersymmetry can be consistently combined with conformal symmetry, leading to an enlarged symmetry algebra known as the superconformal algebra.[8] In addition to the generators of the conformal algebra, it contains the supersymmetry generators Q together with the conformal supercharges S, resulting in twice as many fermionic generators. Operators in a superconformal field theory organize into representations of this algebra, known as superconformal multiplets.

These multiplets are built from a superconformal primary operator, defined as an operator annihilated by the special conformal generators K_μ and the conformal supercharges S. The remaining operators in the multiplet are obtained by acting with the supersymmetry generators Q and the translation generators P_μ. From the point of view of the conformal algebra, a superconformal multiplet decomposes into several conformal multiplets that are related to each other through the action of the supersymmetry generators [43, 50, 51].[9]

Once the possible multiplets for different supersymmetry groups, listed in Table 2.1, and their superfield representations are established, one can construct Lagrangians from the restricted set of terms allowed by supersymmetry, namely the Kähler potential and the superpotential. From this analysis one finds that the Lagrangian $\mathcal{N} = 4$ theory

[8] This point will become clear after Section 2.2.

[9] Depending on the representation, additional shortening conditions may arise, leading to shorter or protected multiplets.

is unique up to the choice of gauge group. It is widely believed that there are no other interacting four-dimensional quantum field theories with $\mathcal{N} = 4$ supersymmetry besides $\mathcal{N} = 4$ SYM. Moreover, $\mathcal{N} = 4$ SYM is conformally invariant since its beta function vanishes, a property ensured by the large amount of supersymmetry present in the theory.

The situation is considerably more complicated for $\mathcal{N} = 2$ theories, as the landscape of possible theories becomes very vast. In [52], the building blocks of Lagrangian SCFTs in four dimensions were classified. According to this classification, each Lagrangian SCFT can be represented by a quiver diagram consisting of nodes, boxes, and lines connecting them. These elements correspond to gauge groups, flavor groups, and hypermultiplets transforming in representations of these groups, respectively.

In addition, these SCFTs can be deformed by terms of the form $mQ\tilde{Q}$[10], which break conformal symmetry while preserving $\mathcal{N} = 2$ supersymmetry; such deformations are referred to as *mass deformations*. The only marginal deformations they admit arise from the conformal multiplet containing the operator $\mathrm{tr}(\phi^2)$.

According to this classification, orbifold theories span a large portion of the landscape of Lagrangian $\mathcal{N} = 2$ SCFTs. They are also connected to many other theories in the $\mathcal{N} = 2$ landscape through various deformations, of which we have only mentioned a small subset, namely mass deformations and marginal deformations. For this reason, after demonstrating the powerful techniques of integrability applied to $\mathcal{N} = 4$ SYM in the next section, we will turn our attention to orbifold theories. We will then explore the fate of these integrability techniques as supersymmetry is reduced from $\mathcal{N} = 4$ to $\mathcal{N} = 2$ via orbifolding and as we move along the conformal manifold (a subsector of the landscape) through marginal deformations.

2.1.2 $\mathcal{N} = 4$ Super Yang–Mills

One of the most symmetric quantum field theories in four dimensions is maximally supersymmetric Yang–Mills theory, which possesses four independent sets of supercharges.[11] The field content of $\mathcal{N} = 4$ SYM consists of a gauge field A_μ, six real scalar fields ϕ_i, and four Majorana fermions ψ, all transforming in the adjoint representation of the gauge group. The action is

[10] Here, Q and $\tilde{Q}$ refer to distinct hypermultiplets in conjugate representations of the gauge group.

[11] In four dimensions, $\mathcal{N} = 4$ supersymmetry corresponds to 16 real Poincaré supercharges. Since the theory is also superconformal, it contains an additional set of 16 conformal supercharges, yielding a total of 32 fermionic generators that form the superconformal algebra.

$$S_{\mathcal{N}=4} = \frac{1}{g_{YM}^2} \int d^4x \ \mathrm{tr}\Big[-\frac{1}{2} F_{\mu\nu}F^{\mu\nu} - D_\mu\phi_i D^\mu\phi_i \\ + i\psi\Gamma^\mu D_\mu\psi + \psi\Gamma^i[\phi_i, \psi] + \frac{1}{2}[\phi_i, \phi_j][\phi_i, \phi_j]\Big] \quad (2.1.18)$$

where the field strength $F_{\mu\nu}$ and the covariant derivatives D_μ are defined in the usual way:

$$\begin{aligned} F_{\mu\nu} &= \partial_\mu A_\nu - \partial_\nu A_\mu - i[A_\mu, A_\nu]\,, \\ D_\mu\phi_i &= \partial_\mu\phi_i - i[A_\mu, \phi_i]\,, \qquad D_\mu\psi = \partial_\mu\psi - i[A_\mu, \psi]\,. \end{aligned} \quad (2.1.19)$$

This theory is also manifestly conformally invariant. The theory also enjoys an $\mathfrak{su}(4)_R \simeq \mathfrak{so}(6)$ R-symmetry under which the six scalars transform in the vector representation. As shown in Table 2.1, the $\mathcal{N}=4$ supersymmetry algebra admits a single short massless representation, namely the vector multiplet. No other multiplets are allowed, implying that the theory is uniquely determined up to the choice of gauge group G. All fields transform in the adjoint representation of G, and gauge-invariant local composite operators can be constructed by taking traces of products of fields that transform covariantly under the gauge group, *e.g.* $\mathcal{O} = \mathrm{tr}(\phi_1\phi_2 F^2 \ldots)$. In addition to such single-trace operators, one can also form multi-trace operators by taking products of traces, for example $\mathrm{tr}(\phi_1\phi_2)\,\mathrm{tr}(\phi_3\phi_4)$.

In the superspace formalism, the superpotential of this theory can be written as

$$\mathcal{W} = \frac{i\,g}{3!}\epsilon_{ijk}\,\mathrm{Tr}\left(\Phi^i\Phi^j\Phi^k\right)\,. \quad (2.1.20)$$

Here Φ^i denote the $\mathcal{N}=1$ chiral multiplets obtained by expressing the $\mathcal{N}=4$ vector multiplet in $\mathcal{N}=1$ superspace. These chiral multiplets contain the complex scalar fields

$$\begin{aligned} X \equiv \Phi^1(x, \theta=0) = \phi_1 + i\phi_2\,, \qquad Y \equiv \Phi^2(x, \theta=0) = \phi_3 + i\phi_4 \\ Z \equiv \Phi^3(x, \theta=0) = \phi_5 + i\phi_6\,. \end{aligned} \quad (2.1.21)$$

The six real scalar fields ϕ_i can be interpreted as parametrizing the transverse directions of type IIB string theory, in which $\mathcal{N}=4$ SYM arises as the low-energy effective theory on a stack of N coincident $D3$-branes. Here, N denotes the rank of the gauge group G. From this perspective, the action (2.1.18) can be obtained via dimensional reduction of ten-dimensional $\mathcal{N}=1$ SYM to four dimensions.

An alternative realization of $\mathcal{N}=4$ SYM arises from considering type IIB string theory on $AdS_5 \times S^5$. In this setup, the gauge theory is defined on the conformal boundary of

AdS_5, leading to the celebrated *AdS/CFT correspondence* [31]. This perspective will play a central role in this thesis, and a more detailed discussion will be presented in Section 4.3.1.

$\mathcal{N} = 4$ SYM with 't Hooft coupling $\lambda = g_{YM}^2 N$ is weakly coupled when $\lambda \ll 1$. The limit $N \to \infty$ is known as the *'t Hooft (or planar) limit*, in which $g_{YM} \to 0$ and $N \to \infty$ while the 't Hooft coupling λ is kept fixed [53]. In this limit only planar Feynman diagrams contribute to correlation functions. As a consequence, interactions that lead to the splitting and joining of traces are suppressed. It is therefore sufficient to consider operators with a fixed number of traces, such as single-trace operators.

Taking the planar limit significantly reduces the combinatorial complexity of Feynman diagrams, changing their growth from factorial to exponential. As a result, the radius of convergence of the perturbative series becomes finite. This regime will be the main focus of Section 3.[12]

Spectral problem. As discussed above, we work in the limit $g_{YM} \to 0$ and $N \to \infty$. In this regime the spectral problem consists of determining the spectrum of conformal dimensions Δ of local operators. The difference $\Delta - \Delta^{(0)}$ between the full conformal dimension and the classical one is referred to as the anomalous dimension.

For concreteness, let us consider single-trace operators in the SU(2) sector with classical conformal dimension $\Delta^{(0)} = L$. These operators span a vector space generated by operators of the form

$$\mathcal{O} = \Psi^S \; \mathrm{tr}[\phi_{s_1} \dots \phi_{s_L}] \,, \tag{2.1.22}$$

where $s_i = \uparrow, \downarrow$, $S = s_1, \cdots, s_L$ and we identify $\phi_\uparrow = X$ and $\phi_\downarrow = Y$. Because of the cyclicity of the trace, the coefficient Ψ^S must be invariant under cyclic permutations,

$$\Psi^{\{s_1, s_2, \dots, s_L\}} = \Psi^{\{s_L, s_1, s_2, \dots, s_{L-1}\}}. \tag{2.1.23}$$

It is therefore natural to view Ψ as a vector in the tensor product space $\bigotimes_L \mathbb{C}^2 = \mathbb{C}^{2^L}$, since each index s_i can take two possible values.

[12]On the other hand, the limit $\lambda \to \infty$ corresponds to the strongly coupled regime of $\mathcal{N} = 4$ SYM, which is dual to a classical string theory on $AdS_5 \times S^5$. In this picture the string worldsheet theory is weakly coupled. Corrections in $\frac{1}{\lambda}$ correspond to α' corrections on the string side, while corrections in $\frac{1}{N}$ correspond to string loop effects. Various integrability techniques can be applied in these regimes; for a review see [54]. Additionally, unlike QCD, $\mathcal{N} = 4$ SYM is not a confining theory. However, in the planar limit and when placed on a finite volume it exhibits confinement-like behavior [55, 56].

One can then compute the two-point function of two such operators to one-loop order using dimensional regularization. The result takes the form [57, 58]

$$\langle \mathcal{O}_1(x)\bar{\mathcal{O}}_2(y)\rangle_\epsilon = L\, 4^L g^{2L}\left[\frac{\pi^\epsilon \mu^{2\epsilon}\Gamma(1-\epsilon)}{[(x-y)^2]^{1-\epsilon}}\right]^L \times \langle \Psi_2|1 - g^2\left(\frac{1}{\epsilon}+1+\gamma_E+\log(\pi|x-y|^2)\right)\mathcal{H}|\Psi_1\rangle + g^2 O(\epsilon) + O(g^4)\,. \quad (2.1.24)$$

Here the inner product $\langle\Psi_2|\Psi_1\rangle = (\Psi_2^S)^\dagger \Psi_1^S$ is the standard inner product on $\mathbb{C}^{2^L}$, and we have introduced the coupling constant $g^2 = \lambda/16\pi^2$. The operator $\mathcal{H}$ appearing in (2.1.24) is given by

$$\mathcal{H} = 2\sum_{i=1}^{L}(1-\mathbb{P}_{i,i+1})\,, \quad (2.1.25)$$

where $\mathbb{P}_{i,i+1}$ denotes the operator that permutes two neighboring spins,

$$(\mathbb{P}_{i,i+1}\Psi)^{\{s_1,\dots,s_L\}} = \Psi^{\{s_1,\dots,s_{i-1},s_{i+1},s_i,s_{i+2},\dots,s_L\}}\,. \quad (2.1.26)$$

The Hamiltonian $\mathcal{H}$ is therefore identified with that of the celebrated Heisenberg XXX spin chain [59].

Heisenberg spin chain. This is a one-dimensional lattice model used to describe magnetization in one-dimensional metals. Unlike the Ising lattice model (2.2.3), which we study in this thesis, the Heisenberg chain is a quantum mechanical model. The Hamiltonian given in (2.1.25) possesses $SU(2)$ symmetry, and its spectral problem can be elegantly solved using various techniques. One technique that is central to understanding the integrability of the model is the *coordinate Bethe ansatz*. This will also be the main technique that we generalize in Section 3. To demonstrate how the spectral problem of the XXX model can be solved using the CBA, we begin with an ansatz. We define

$$|\Psi(p_1,\cdots,p_M)\rangle = \sum_{x_1<\cdots<x_M}\sum_{\sigma\in\mathcal{S}_M} A_\sigma\, e^{i\sum_i p_i x_i}\,|x_1,\cdots,x_M\rangle\,, \quad (2.1.27)$$

where, analogously to $\Psi^{s_1\cdots s_L}$, the state $|x_1,\cdots,x_M\rangle$ denotes the positions of the $\uparrow$ spins in a sea of $\downarrow$ spins,

$$|x_1,\cdots,x_M\rangle \in \otimes_L \mathbb{C}^2\,. \quad (2.1.28)$$

Since the spin chain is $SU(2)$ symmetric, there is no distinction between choosing $\uparrow$ or $\downarrow$ as the excited state. Additionally, in (2.1.27), the coefficients A_σ are functions of the momentum variables called *scattering coefficients*, and $\mathcal{S}_M$ is the symmetric group on M elements, where M counts the number of *magnons*.

For a single excitation, $\mathcal{S}_1$ consists only of the identity element, and $A_{\mathbf{1}}$ becomes an overall coefficient for the state $|\Psi(p)\rangle$. Therefore, solving the eigenvalue equation

$$\mathcal{H}\,|\Psi(p)\rangle = E(p)\,|\Psi(p)\rangle \ , \tag{2.1.29}$$

yields the dispersion relation of the model,

$$E(p) = 4\sin^2\left(\frac{p}{2}\right) \ . \tag{2.1.30}$$

Moreover, due to the additive structure of the energy spectrum—manifest from the nearest-neighbour form of the Hamiltonian—we find that

$$\mathcal{H}\,|\Psi(p_1,\cdots,p_M)\rangle = \left(\sum_{i=1}^{M} E(p_i)\right)|\Psi(p_1,\cdots,p_M)\rangle \ , \tag{2.1.31}$$

which reflects the factorization of scattering. The corresponding Bethe wavefunction is given in (2.1.27), where the amplitudes factorize into two-body scattering matrices,

$$A(\sigma) = \prod_{i<j} S_{\sigma(i)\sigma(j)} \ , \tag{2.1.32}$$

with

$$S_{ij} = -\frac{1+e^{i(p_i+p_j)}-2e^{ip_j}}{1+e^{i(p_i+p_j)}-2e^{ip_i}} \ . \tag{2.1.33}$$

In expressing the permutation $\sigma \in \mathcal{S}_M$ in terms of elementary transpositions, it is useful to keep in mind its decomposition into a product of two-cycles,

$$\sigma = (ijk\cdots) = \prod_{i<j}(ij) \ . \tag{2.1.34}$$

Here, the decomposition of a permutation (i.e. an element of the symmetric group) into transpositions is not unique. Nevertheless, for any such decomposition, the corresponding composition of two-body scattering factors S_{ij} yields the same result. This property follows from the associativity of successive permutations of adjacent momentum states and is encoded in the *Yang–Baxter equation* (YBE),

$$(23)(13)(12) = (12)(13)(23)\,, \tag{2.1.35}$$

which can be interpreted as the equivalence of different sequences of pairwise scattering processes. This equivalence can be represented diagrammatically, where different orderings of pairwise scattering processes lead to the same final configuration,

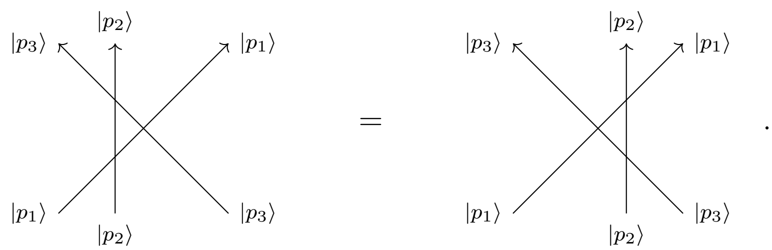

. (2.1.36)

Finally, after obtaining the solution for the open, infinite chain as described above, one can additionally impose boundary conditions and solve them in order to determine the allowed momenta (or spectrum) of the spin chain. The simplest and most common boundary conditions are the periodic ones, which are also the natural boundary conditions for the single-trace operators of $\mathcal{N} = 4$ SYM, as demonstrated in (2.1.23). The periodic boundary conditions lead to the Bethe equations for a fixed spin-chain length L,

$$e^{ip_i L} = \prod_{j \neq i} S_{ij} \ , \qquad \forall i \in \{1, \cdots, M\} \ . \tag{2.1.37}$$

Solving these highly nonlinear equations then determines the allowed states of the Hilbert space for the specified boundary conditions. Therefore, by knowing the two-body scattering matrix (2.1.33) and the dispersion relation of the model (2.1.30), we obtain a complete diagonalization of the model.[13] Additionally, thanks to the connection between integrable spin chains and $\mathcal{N} = 4$ SYM, this result determines the one-loop anomalous dimensions of the single-trace operators belonging to the $SU(2)$ sector (2.1.22).

A complementary and more algebraic approach to the coordinate Bethe ansatz (CBA) is the *algebraic Bethe ansatz* (ABA), which is based on encoding the scattering data of the model into an R-matrix that acts on two adjacent spin states. This perspective arises from interpreting the one-dimensional spin chain and its time evolution (i.e. a $(1+1)$-dimensional system) as a two-dimensional classical statistical model, in which Boltzmann weights are assigned to vertices or faces of a lattice. In this framework, the

[13] At this stage it is far from obvious that the resulting solution provides a complete set of states. To verify this, one must ensure that the solutions of (2.1.37) generate all highest-weight states of $\otimes_L \mathbb{C}^2$ viewed as a representation of $SU(2)$. The $SU(2)$ raising and lowering operators then generate the remaining states in each multiplet. This is indeed the case for the solutions of the Bethe equations, and a proof is given in [60].

associativity condition depicted in (2.1.36) is expressed in terms of these R-matrices and corresponds to the Yang–Baxter equation. By imposing appropriate boundary conditions, the spin chain can be realized as a representation of a quantum group [61].

2.1.3 Orbifolding

In this section, we will break the supersymmetry group of $\mathcal{N} = 4$ down to $\mathcal{N} = 2$ by orbifolding. This procedure retains a large part of the properties of $\mathcal{N} = 4$ SYM and allows us to test AdS/CFT or integrability in a much more involved setting. Here, we consider the simplest form of orbifolding which is to quotient the symmetry groups of the SCFT with a $\mathbb{Z}_L$ discrete group. A full treatment for all possible discrete groups is given in [62–67].

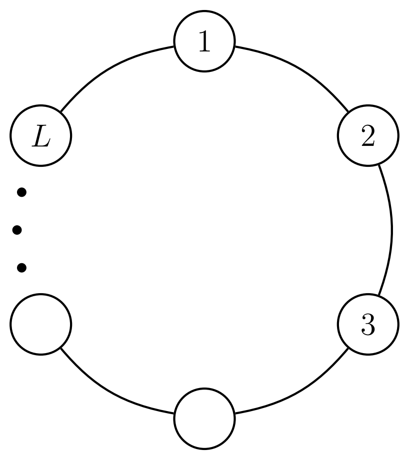

Figure 2.1: *The quiver diagram of a circular quiver theory obtained by orbifolding $\mathcal{N} = 4$ SYM by the group $\mathbb{Z}_L$. Each node corresponds to an $\mathcal{N} = 2$ vector multiplet transforming in the adjoint representation of* $\mathrm{SU}(N)$*, a subgroup of the gauge group. The links between neighboring nodes represent $\mathcal{N} = 2$ hypermultiplets transforming in the bifundamental representation of* $\mathrm{SU}(N_i) \times \mathrm{SU}(N_{i+1})$ *which is also a subgroup of the gauge group. For the special case $L = 2$, an additional* $\mathrm{SU}(2)$ *symmetry appears, acting on the pair of hypermultiplets connecting the two gauge nodes.*

On the field theory side, the $\mathbb{Z}_L$ orbifold projection can be implemented on four-dimensional $\mathcal{N} = 4$ SYM with gauge group $\mathrm{SU}(LN)$. This procedure produces an $\mathcal{N} = 2$ superconformal gauge theory with gauge group $\mathrm{SU}(N)^L$. The matter content of the resulting theory is naturally encoded in the quiver diagram shown in Figure 2.1. The gauge couplings associated with the different nodes are taken to be identical, $g_{\mathrm{YM},i} = g_{\mathrm{YM}}$.

From the string theory perspective, the dual background is obtained by performing an orbifold identification on the S^5 factor. Concretely, the $\mathbb{Z}_L$ action acts on the complex embedding coordinates of the flat space $\mathbb{C}^3 \supset S^5$ according to

$$\Gamma_L : (X, Y, Z) \mapsto \left(e^{\frac{2\pi i}{L}} X,\ e^{-\frac{2\pi i}{L}} Y,\ Z \right) , \tag{2.1.38}$$

where these transverse coordinates correspond to the complex scalar fields defined in (2.1.21). The fixed-point set of this $\mathbb{Z}_L$ action forms a six-dimensional submanifold given by $\mathrm{AdS}_5 \times S^1$. In the neighbourhood of this locus, the geometry locally takes the form $\mathrm{AdS}_5 \times S^1 \times \mathbb{C}^2/\mathbb{Z}_L$. Consequently, the full orbifold space $\mathrm{AdS}_5 \times S^5/\mathbb{Z}_L$ can be interpreted as the near-horizon limit of a stack of D3-branes placed at the singular point of the locally flat orbifold geometry $\mathbb{R}^{1,5} \times \mathbb{C}^2/\mathbb{Z}_L$.[14]

In addition to the breaking of the R-symmetry group described in the string theory language, from the perspective of the flat orbifold geometry, the breaking of the gauge group is implemented through the $LN \times LN$ projection matrix

$$\gamma = \begin{pmatrix} \mathbf{1} & 0 & 0 & \cdots \\ 0 & e^{\frac{2\pi i}{L}} \mathbf{1} & 0 & \cdots \\ 0 & 0 & e^{2\frac{2\pi i}{L}} \mathbf{1} & \cdots \\ \vdots & \vdots & \vdots & \ddots \end{pmatrix} , \tag{2.1.39}$$

together with the identification of each field with its orbifold image:

$$Z \sim \gamma Z \gamma^{-1} , \qquad X \sim -\gamma X \gamma^{-1} , \qquad Y \sim -\gamma Y \gamma^{-1} . \tag{2.1.40}$$

After performing these projections for the R-symmetry group and the gauge group, we obtain an $\mathcal{N} = 2$ elliptic quiver gauge theory with gauge group $SU(N)^L$, whose superpotential is given by

$$\mathcal{W}_{\mathcal{N}=2\,\text{orb.}} = i\, g \sum_{n=1}^{L} \left(\tilde{Q}_{(n)} \Phi_{(n)} Q_{(n)} - Q_{(n)} \Phi_{(n+1)} \tilde{Q}_{(n)} \right) , \tag{2.1.41}$$

where $\tilde{Q}_{(n)}$ and $Q_{(n)}$ are hypermultiplets, while the $\Phi_{(n)}$ are $\mathcal{N} = 2$ chiral multiplets. As shown in [62], the orbifolding procedure produces theories in which all gauge couplings are equal and coincide with the Yang–Mills coupling constant of the parent $\mathcal{N} = 4$ SYM theory. This point in parameter space is known as the *orbifold point*.

These orbifold theories are known to be integrable in the planar limit [71, 72]. As in the case of $\mathcal{N} = 4$ SYM, the coordinate Bethe ansatz is sufficient to diagonalize the

[14] A detailed discussion of the twisted and untwisted sectors of these orbifold theories, as well as recent developments, can be found in [68–70].

Hamiltonian of the spin chains arising from the one-loop mixing matrix. Although the Hilbert space of the spin chain consists of two copies of that of $\mathcal{N} = 4$ SYM and loses its simple tensor-product structure due to the orbifold projection, the dispersion relation (2.1.30) and the scattering coefficients (2.1.33) remain unchanged. The corresponding Bethe equations were studied in [71, 73–75], the associated Y-system in [76], and the thermodynamic Bethe ansatz in [77, 78]. More recently, the hexagon formalism has been generalized to these theories [69, 79].

A natural next step in exploring the landscape of $\mathcal{N} = 2$ theories is to consider their marginal deformations and investigate the SCFTs that arise in the vicinity of these orbifold points. Such marginal deformations preserve the structural form of the superpotential (2.1.41), while allowing the coupling constants to become independent. The resulting superpotential takes the form

$$\mathcal{W}_{\mathcal{N}=2\,\mathrm{m.orb.}} = i \sum_{n=1}^{L} \left(g_n \, \tilde{Q}_{(n)} \Phi_{(n)} Q_{(n)} - g_{n+1} \, Q_{(n)} \Phi_{(n+1)} \tilde{Q}_{(n)} \right) . \tag{2.1.42}$$

These models, together with their highly non-trivial AdS duals, provide a valuable framework for extending the AdS/CFT correspondence beyond the realm of maximally supersymmetric theories. In particular, they offer a setting in which to study theories with reduced supersymmetry that are not directly connected to $\mathcal{N} = 4$ SYM. The investigation of such models from this perspective was initiated in [80, 81].

A central question in this program concerns the fate of integrability in this more general setting. While the rational integrable structures present in $\mathcal{N} = 4$ SYM and at the orbifold point are known to break down under these deformations, it has been conjectured that a form of elliptic integrability may emerge instead. This perspective was put forward in [82], and our contribution to this line of research is presented in Section 3.

2.2 Conformal Field Theory

A useful way to think about a UV-complete QFT is in terms of the RG flow between the ultraviolet (UV) and infrared (IR) regimes. More precisely, one may regard a QFT as an RG flow connecting two CFTs: one describing the UV fixed point and the other the IR fixed point,

$$\mathrm{CFT}_{\mathrm{UV}} \xrightarrow{\mathrm{QFT}} \mathrm{CFT}_{\mathrm{IR}} \,. \tag{2.2.1}$$

A simple and particularly instructive example of an RG flow is provided by the three-dimensional ϕ^4 theory, defined by the Euclidean action

$$S = \int d^3x \, \left(\frac{1}{2} \left(\partial\phi\right)^2 + \frac{1}{2} m^2 \phi^2 + \frac{1}{4!} g \phi^4 \right) \,. \tag{2.2.2}$$

At very high energies, this theory reduces to the free scalar theory. In the IR, for a special value of the ratio $\frac{g^2}{m^2}$,[15] the theory flows to an interacting CFT.

Another route to the same interacting IR CFT is provided by the three-dimensional Ising lattice model in the UV. This is a classical lattice model with partition function

$$Z_{\mathrm{Ising}} = \sum_{\{s_i\}} \exp \left(-J \sum_{\langle i,j \rangle} s_i s_j \right) , \tag{2.2.3}$$

where i, j label lattice sites and the notation $\langle i, j \rangle$ indicates that the sum runs only over nearest-neighbour pairs. The variables s_i take the values ± 1 on each lattice site. At the critical coupling, this model flows in the IR to the same interacting CFT that arises from the ϕ^4 theory. We will refer to this interacting CFT as the *Ising CFT*. This means that the two theories defined in (2.2.2) and (2.2.3) belong to the same *universality class.*

More generally, theories with very different UV behaviour can flow to the same IR fixed point and therefore belong to the same universality class. Studying such IR CFTs allows us to uncover features that are common to physical systems arising in very different settings and across a wide range of energy scales. To study these CFTs in greater detail, we begin by taking a closer look at the symmetries that characterize them.

[15] This value lies between two other IR regimes. If m^2 is large and positive, the IR theory is massive and preserves the $\mathbb{Z}_2$ symmetry. If m^2 is negative, the IR theory is again massive, but the $\mathbb{Z}_2$ symmetry is spontaneously broken.

2.2.1 Conformal Symmetry Group

Every local QFT possesses a stress-energy tensor satisfying the *conservation equation*

$$\partial_\mu T^{\mu\nu} = 0 \; , \tag{2.2.4}$$

at the operator level. In the presence of additional operator insertions, this conservation equation implies Ward identities for the correlation functions of the theory,

$$\partial_\mu \langle T^{\mu\nu}(x)\mathcal{O}_1(x_1)\cdots\mathcal{O}_n(x_n)\rangle = -\sum_i \delta(x-x_i)\partial_i^\nu \langle\mathcal{O}_1(x_1)\cdots\mathcal{O}_n(x_n)\rangle \; . \tag{2.2.5}$$

In addition to the conservation law (2.2.4), one may consider local diffeomorphisms generated by vector fields $\epsilon = \epsilon^\mu(x)\partial_\mu$. These give rise to currents of the form

$$\epsilon_\nu T^{\mu\nu} \; , \tag{2.2.6}$$

whose conservation requires

$$\partial_\mu \left(\epsilon_\nu T^{\mu\nu}\right) = 0 \; . \tag{2.2.7}$$

This implies the condition

$$\left(\partial_\mu \epsilon_\nu + \partial_\nu \epsilon_\mu\right) T^{\mu\nu} = 0 \; , \tag{2.2.8}$$

which is satisfied by the vector fields

$$p_\mu = \partial_\mu \tag{2.2.9}$$

$$m_{\mu\nu} = x_\nu \partial_\mu - x_\mu \partial_\nu \; , \tag{2.2.10}$$

corresponding to translations and rotations, respectively.

Furthermore, if the action of the QFT is invariant under infinitesimal local rescalings of the metric, known as *Weyl transformations*, $g \to e^{2\delta\omega(x)} g$, then the stress-energy tensor additionally satisfies the tracelessness condition

$$T^\mu_{\ \mu} = 0 \; . \tag{2.2.11}$$

This allows the Killing equation to be relaxed to

$$\partial_\mu \epsilon_\nu + \partial_\nu \epsilon_\mu = f(x)\delta_{\mu\nu} \; , \tag{2.2.12}$$

where $f(x)$ is a scalar function. In this case, in addition to translations and rotations, the action is also invariant under scalings[16] and special conformal transformations,

$$d = x^\mu \partial_\mu \ , \tag{2.2.13}$$

$$k_\mu = 2x_\mu (x^\rho \partial_\rho) - x^2 \partial_\mu \ . \tag{2.2.14}$$

Taken together, these local diffeomorphism invariances can be promoted to spacetime symmetry generators by defining the corresponding charges P_μ, $M_{\mu\nu}$, D, and K_μ,

$$Q(\Sigma) = -\int_\Sigma \epsilon_\nu(x) T^{\mu\nu}(x) \ . \tag{2.2.15}$$

Conformal symmetry algebra. These generators form the conformal symmetry algebra, characterized by the commutation relations

$$\begin{gathered} [M_{\mu\nu}, P_\rho] = \delta_{\nu\rho} P_\mu - \delta_{\mu\rho} P_\nu \ , \qquad [M_{\mu\nu}, K_\rho] = \delta_{\nu\rho} K_\mu - \delta_{\mu\rho} K_\nu \ , \\ [M_{\mu\nu}, M_{\rho\sigma}] = \delta_{\nu\rho} M_{\mu\sigma} - \delta_{\mu\rho} M_{\nu\sigma} + \delta_{\mu\sigma} M_{\nu\rho} - \delta_{\nu\sigma} M_{\mu\rho} \ , \\ [D, P_\mu] = P_\mu \ , \qquad [D, K_\mu] = -K_\mu \ , \qquad [K_\mu, P_\nu] = 2\delta_{\mu\nu} D - 2M_{\mu\nu} \ . \end{gathered} \tag{2.2.16}$$

From these commutation relations, we see that the generators $M_{\mu\nu}$ span the rotation algebra $\mathfrak{so}(d)$,[17] while the translation and special conformal generators transform as vectors under its action. Taken together, all generators furnish the algebra $\mathfrak{so}(d+1,1)$.

Using the algebra in (2.2.16), we classify CFT operators according to representations of the conformal group. Representations of the rotation subgroup are labeled by the spin quantum numbers of the operators, which determine how they transform under rotations. In the presence of dilatation invariance generated by (2.2.13), one must also specify the scaling dimension of each operator. We therefore diagonalize the action of the dilatation generator on operators inserted at the origin,

$$[D, \mathcal{O}(0)] = \Delta \mathcal{O}(0) \ . \tag{2.2.17}$$

In this framework, the translation generators act as raising operators, while the special conformal generators act as lowering operators. Primary operators are defined as those

[16] A natural question at this stage is whether scale invariance implies conformal invariance. This question is still the subject of active research. In two and four dimensions, it has been shown that Lorentz invariance and unitarity are sufficient to imply that scale invariance enhances to conformal invariance [83–85]. Later on, it was also shown that unitarity is indeed a necessary condition [86]. However, in other dimensions, the necessary and sufficient conditions remain unknown.

[17] In the previous section we considered the Lorentzian version of this algebra given in (2.1.4) and (2.1.5).

annihilated by all special conformal generators, corresponding to highest weight states with respect to the dilatation operator,

$$[K_\mu, \mathcal{O}(0)] = 0 \ . \tag{2.2.18}$$

The action of translations then generates the *descendant operators*, which are obtained from the primary operators as

$$[D, P_{\mu_1} \cdots P_{\mu_n} \mathcal{O}(0)] = (\Delta + n)\, P_{\mu_1} \cdots P_{\mu_n} \mathcal{O}(0) \ . \tag{2.2.19}$$

Having established the symmetry algebra of the CFT and the structure of its representations, we now examine how this symmetry algebra constrains the operators and states of the theory.

2.2.2 Radial Quantization

A particularly direct way to characterize a QFT is through the path integral formulation. However, a path integral can be interpreted in terms of different notions of time evolution and, correspondingly, different Hilbert spaces. We refer to each such interpretation of the path integral as a distinct *quantization* of the same theory. Concretely, one chooses a time direction and defines states on hypersurfaces orthogonal to the corresponding time evolution. In a rotationally invariant Euclidean theory on $\mathbb{R}^d$, for example, any direction may be chosen as time, and the resulting quantizations are equivalent.

Although different quantizations of a given theory correspond to different Hilbert spaces and different sets of operators, the action of the symmetry generators on the Hilbert space and on the operators of the theory remains the same.[18] This is why symmetries provide one of the most powerful organizational principles in QFT.

For scale-invariant theories, a natural way to foliate flat d-dimensional spacetime is by spheres centered at the origin, with the evolution of states from smaller spheres to larger spheres generated by the dilatation operator. This construction is known as *radial quantization*,

$$ds^2_{\mathbb{R}^d} = e^{2\tau} ds^2_{\mathbb{R}\times S^{d-1}} \ , \tag{2.2.20}$$

[18] In general, the way local operators transform under symmetries is insensitive to IR effects such as spontaneous symmetry breaking or finite temperature. This observation will form the basis of our study of CFTs at finite temperature.

where, for $\vec{x} \in \mathbb{R}^d$, the radial coordinate is defined by $|\vec{x}| = e^\tau$. This implies that time evolution on the cylinder $\mathbb{R} \times S^{d-1}$ is generated by the dilatation operator,

$$H_{\text{rad}} = \frac{D}{R}\,, \tag{2.2.21}$$

where H_{rad} is the Hamiltonian and R is the radius of the $(d-1)$-dimensional sphere.

To define the *vacuum state* in radial quantization, we consider the path integral over the interior of a sphere B with no operator insertions. The state $|0\rangle$ is then defined on the boundary ∂B of this sphere. Similarly, by inserting operators inside B, we can prepare states of the form $\mathcal{O}\,|0\rangle$.

Conversely, eigenstates of the dilatation operator can be interpreted through a cutting-and-gluing procedure along spheres, which allows one to construct local operators from the corresponding states. Combining these two viewpoints, we associate local operators with eigenstates of the dilatation operator D in radial quantization. This relation is known as the *state–operator correspondence* in a CFT.[19]

In choosing a quantization and defining the states and operators of the system, we require a positive-definite inner product. In Lorentzian signature, the existence of such an inner product is closely tied to unitarity, which requires conserved charges, such as the Hamiltonian in (2.2.21), to be represented by Hermitian operators. Since Hermitian operators generate unitary transformations, both time evolution and symmetry transformations preserve probabilities. Upon analytic continuation to Euclidean signature, this requirement of unitarity is replaced by the condition known as *reflection positivity.*

Multiplets of conformal symmetry. Using the state–operator correspondence together with the appropriate notion of a positive-definite inner product in Euclidean CFT, one can show that the spectrum of states consists entirely of primary and descendant states/operators.[20] We may therefore describe a generic conformal multiplet in terms of its conformal primary, defined in (2.2.18), with the remaining operators in the multiplet generated by the descendants defined in (2.2.19):

$$\mathcal{A}^{\Delta}_{j,\bar{j}} = \operatorname{span}\left(\{P_{\mu_1}\cdots P_{\mu_n}\mathcal{O}\}\right)\,. \tag{2.2.22}$$

Operator-product expansion. Finally, combining the state–operator correspondence with the description of operators in terms of primaries and descendants, we

[19]In Section 4.1.1, we will consider different quantizations of the d-dimensional cylinder and use them to illuminate various aspects of thermal CFTs.

[20]This is also related to the requirement that the partition function on $S^1 \times S^{d-1}$ be finite, a statement sometimes referred to as the spectral theorem [39].

arrive at the *operator-product expansion* (OPE) for two scalar operators $\mathcal{O}_1$ and $\mathcal{O}_2$,[21]

$$\mathcal{O}_1(\vec{x}) \times \mathcal{O}_2(0) = \sum_{\mathcal{O}_3 \in \mathcal{O}_1 \times \mathcal{O}_2} \frac{f_{\mathcal{O}_1\mathcal{O}_2\mathcal{O}_3}}{c_{\mathcal{O}_3}} |\vec{x}|^{\Delta_{\mathcal{O}_3} - \Delta_{\mathcal{O}_2} - \Delta_{\mathcal{O}_1} - J} x_{\mu_1} \cdots x_{\mu_J} \mathcal{O}_3^{\mu_1 \cdots \mu_J} \,. \tag{2.2.23}$$

Here, $f_{\mathcal{O}_1\mathcal{O}_2\mathcal{O}_3}$ denotes the coefficient appearing in the three-point function, while $c_{\mathcal{O}}$ denotes the coefficient of the two-point function. These coefficients will be defined more precisely in the following section.

2.2.3 Towards a Non-Perturbative Formulation of CFT

A striking consequence of conformal symmetry is that the form of all two- and three-point functions in a CFT is completely fixed,

$$\langle \mathcal{O}_1(x)\mathcal{O}_2(0)\rangle = \frac{c_{12}}{|x|^{\Delta_1+\Delta_2}} \,, \tag{2.2.24}$$

$$\langle \mathcal{O}_1(x)\mathcal{O}_2(y)\mathcal{O}_3(0)\rangle = \frac{f_{\mathcal{O}_1\mathcal{O}_2\mathcal{O}_3}}{|x-y|^{\Delta_1+\Delta_2-\Delta_3}|x|^{\Delta_1+\Delta_3-\Delta_2}|y|^{\Delta_2+\Delta_3-\Delta_1}} \,. \tag{2.2.25}$$

Furthermore, higher-point functions can be decomposed into two- and three-point functions by means of the OPE (2.2.23). This observation leads to the important idea that a CFT can be specified by a reduced set of data, known as the *CFT data*,

$$\langle \mathcal{O}_1(x_1)\cdots\mathcal{O}_n(x_n)\rangle, \;\; \forall n \quad \leftrightarrows \quad \{\Delta_{\mathcal{O}}, f_{\mathcal{O}_1\mathcal{O}_2\mathcal{O}_3}\} \,. \tag{2.2.26}$$

This viewpoint suggests that a CFT may, in principle, be defined non-perturbatively entirely in terms of this data without needing a Lagrangian description. This idea was first explored in [93–95] and is called *conformal bootstrap*. However, several conceptual questions remain open. For instance, it is not yet fully understood under what conditions a consistent set of CFT data uniquely determines a CFT. Moreover, additional information associated with extended operators, such as line or surface operators, may also play an essential role in characterizing the full theory. Finally, placing a CFT on geometries other than flat space imposes further constraints on correlation functions, potentially yielding new insights into the structure of the theory. This last point will be one of the main themes explored in Section 4.

To illustrate how conformal data characterizes a CFT, we consider the four-point function of four identical scalar operators,

$$\langle \phi(x_1)\phi(x_2)\phi(x_3)\phi(x_4)\rangle \,. \tag{2.2.27}$$

[21] If these operators carry spin the OPE can still be derived, however it would have a much more complicated tensor structure [87–92].

Using the OPE in (2.2.23), we can decompose this correlation function by choosing a particular OPE channel,

$$\langle \overbrace{\phi(x_1)\phi(x_2)} \quad \overbrace{\phi(x_3)\phi(x_4)} \rangle = \frac{1}{|x_1-x_2|^{2\Delta_\phi}|x_3-x_4|^{2\Delta_\phi}} \sum_{\mathcal{O}} f^2_{\phi\phi\mathcal{O}}\, g_{\Delta_{\mathcal{O}},J_{\mathcal{O}}}(u,v)\ , \quad (2.2.28)$$

where the sum runs over all primary operators $\mathcal{O}$ of the theory, $x_{ij}^2 \equiv |x_i - x_j|^2$ and *conformal blocks* $g_{\Delta_{\mathcal{O}},J_{\mathcal{O}}}$ are defined in terms of two cross-ratios,

$$u = \frac{x_{12}^2 x_{34}^2}{x_{13}^2 x_{24}^2}\ , \quad v = \frac{x_{14}^2 x_{23}^2}{x_{13}^2 x_{24}^2}\ . \quad (2.2.29)$$

Here, we assume the canonical normalization of two-point functions,

$$\langle \mathcal{O}_a(x)\mathcal{O}_b(0)\rangle = \frac{\delta_{ab}}{|x|^{2\Delta_{\mathcal{O}_a}}}\ . \quad (2.2.30)$$

The conformal blocks encode the contributions of a primary operator $\mathcal{O}$ and all of its descendants. They depend on particular combinations of the relative distances between the operator insertions, such as x_{12}, x_{23}, and so on, determined by the chosen OPE channel, and they incorporate the contraction of all spacetime indices appearing in the OPE (2.2.23).

Conformal blocks. Conformal blocks can be computed elegantly using the Casimir operators of the conformal group [96]. For example, in four dimensions they take the form

$$g^{(4d)}_{\Delta,\ell}(u,v) = \frac{z\bar{z}}{z-\bar{z}}\left(k_{\Delta+\ell}(z)k_{\Delta-\ell-2}(\bar{z}) - k_{\Delta-\ell-2}(z)k_{\Delta+\ell}(\bar{z})\right), \quad (2.2.31)$$

$$k_\beta(x) \equiv x^{\beta/2}\,{}_2F_1\left(\frac{\beta}{2},\frac{\beta}{2},\beta,x\right). \quad (2.2.32)$$

In any spacetime dimension, conformal blocks depend on two independent conformal cross-ratios,[22] which may be denoted by u, v as given in (2.2.29) or, equivalently, by $z, \bar{z}$.[23]

$$u = z\bar{z}\ , \quad v = (1-z)(1-\bar{z})\ . \quad (2.2.33)$$

[22]The four insertion points of the operators give rise to four independent coordinates, but conformal symmetry reduces the dependence to two independent variables. One way to see this is to use conformal transformations to place one operator at the origin, $x_1^\mu = (0,\cdots,0)$, and another at infinity.

[23]In Euclidean signature, z and $\bar{z}$ are complex conjugates of one another, whereas after suitable analytic continuations to Lorentzian signature they become independent complex variables.

The different ways of applying the OPE to the four-point function (2.2.27) give rise to different OPEs. The key idea is that the same correlation function can be decomposed by first fusing different pairs of operators. For example, one may first apply the OPE to the operators at x_1 and x_2, and independently to those at x_3 and x_4. This yields an expansion in terms of intermediate operators $\mathcal{O}_i$ that propagate between the two pairs. Alternatively, one may first fuse the operators at x_1 and x_4, and those at x_2 and x_3, leading to a different decomposition of the same four-point function.

Although these decompositions correspond to different choices of *OPE channels*, they must describe the same physical correlation function. Therefore, the sums over intermediate operators appearing in the two expansions must agree. This consistency condition is known as *crossing symmetry*. Diagrammatically, it corresponds to exchanging the order in which the operators are fused, or equivalently exchanging the operators inserted at different spacetime points. The resulting equality between different OPE decompositions can be represented schematically as

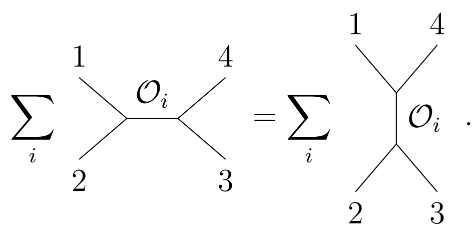

(2.2.34)

Crossing symmetry therefore imposes highly non-trivial constraints on the spectrum of operators and on their OPE coefficients through the associativity of the OPE,[24]

$$\overbrace{\overbrace{\mathcal{O}_1\mathcal{O}_2}\,\mathcal{O}_3} = \overbrace{\mathcal{O}_1\,\overbrace{\mathcal{O}_2\mathcal{O}_3}}\ . \tag{2.2.35}$$

In practice, the equality between different OPE channels translates into a set of functional equations for the conformal blocks appearing in the decomposition of the four-point function. The systematic study of these constraints, without relying on a Lagrangian description of the theory, forms the basis of the modern *conformal bootstrap program*, which was revitalized by the numerical approach to bounding operator dimensions and OPE coefficients [97].

To illustrate the core idea of the numerical conformal bootstrap, we use unitarity and reflection positivity. These imply that the three-point function coefficients $f_{\phi\phi\mathcal{O}}$ are real, and therefore that the coefficients $f^2_{\phi\phi\mathcal{O}}$ appearing in the OPE decomposition (2.2.28) are positive. The basic strategy of the numerical conformal bootstrap is to combine

[24]This is in spirit very similar to the associativity condition formulated in (2.1.36).

the positivity property with crossing symmetry in order to derive rigorous constraints on the CFT data. Writing the crossing equation in the form

$$\sum_{\mathcal{O}} f_{\phi\phi\mathcal{O}}^2\, F_{\Delta,\ell}(u,v) = 0\ , \tag{2.2.36}$$

with

$$F_{\Delta,\ell}(u,v) \equiv v^{\Delta_\phi} g_{\Delta,\ell}(u,v) - u^{\Delta_\phi} g_{\Delta,\ell}(v,u)\ , \tag{2.2.37}$$

one sees that crossing symmetry imposes a non-trivial linear relation among the conformal blocks appearing in the $\phi \times \phi$ OPE. Because unitarity implies $f_{\phi\phi\mathcal{O}}^2 \geq 0$, the crossing equation becomes a positivity constraint on the allowed spectrum of operator dimensions and OPE coefficients. Then we can apply linear functionals to (2.2.36). If one can construct a functional that acts positively on all contributions compatible with a hypothetical spectrum, while yielding a negative value on the identity contribution, one arrives at a contradiction and thereby rules out the assumed spectrum. In this way, crossing symmetry and unitarity are translated into rigorous constraints on the admissible CFT data, providing a powerful non-perturbative framework for conformal field theory. These bounds can be pushed to remarkably high precision, effectively amounting to a direct numerical determination of the CFT data. Indeed, following its modern revival, the numerical conformal bootstrap developed rapidly, incorporating spinning correlators and leading to striking results, beginning with the discovery of the three-dimensional Ising island [98–101]. Moreover, this program continues to be systematically refined and extended [102, 103].

An additional important structural consequence of crossing symmetry emerges from studying the limit $z \to 0$ of the four-point crossing equation. In this limit, the conformal blocks behave as $g_{\Delta,\ell}(u,v) \sim (z\bar{z})^{\Delta/2}$,[25] so the direct-channel expansion is dominated by the operator of smallest dimension appearing in the OPE, namely the identity. However, after crossing, $(z,\bar{z}) \to (1-z, 1-\bar{z})$, each conformal block behaves as $z^{2\Delta_\phi} \log z$, and any finite sum of such terms vanishes as $z \to 0$. Therefore, the crossing equation cannot be satisfied by a finite number of primary operators, implying that the $\phi \times \phi$ OPE must contain an infinite tower of primaries. More precisely, the crossed-channel sum reproduces the identity contribution through the collective effect of operators with increasingly large scaling dimensions, and one can show that the dominant contributions come from operators with $\Delta \sim 1/\sqrt{z}$ as $z \to 0$ [104]. This phenomenon, sometimes referred to as large-Δ dominance, highlights the fact that crossing symmetry relates

[25] This behaviour is manifest in the four-dimensional conformal blocks given in (2.2.32), but it also holds in any spacetime dimension.

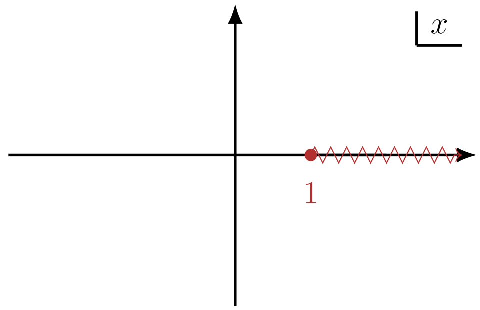

Figure 2.2: *The analytic structure of the function $f(x)$ given in* (2.2.39)*.*

low-dimension operators in one channel to the asymptotic large-dimension spectrum in the crossed channel. It also plays a crucial role in the finite-temperature bootstrap explored in Section 4.

2.2.4 Dispersion Relations in Analytic Bootstrap

Since one of the main topics of this thesis is the extension of analytic bootstrap methods based on dispersion relations to the thermal setting, we now take a closer look at the role these relations play in the conformal bootstrap. Dispersion relations are non-perturbative formulas that relate the ultraviolet and infrared behaviour of an observable, and they have wide-ranging applications in linear response theory, QFT scattering amplitudes, and conformal correlators. The term derives from the seminal work of Froissart and Gribov [105, 106].

In the context of CFTs, dispersion relations appear in two main ways: in the inversion formula [107], and in the Polyakov bootstrap in Mellin space [108–110]. In both scenarios, they establish a direct connection between the known analytic structure of the correlator under consideration and the associated CFT data.[26]

Inversion formula. When we consider the OPE decomposition of a four-point function, as in (2.2.28), we find that it takes the general form

$$G(z,\bar{z}) = \sum_{\Delta,J} a_{\Delta,J} G_{\Delta,J}(z,\bar{z}) \,, \tag{2.2.38}$$

where $G_{\Delta,J}(z,\bar{z}) = (z\bar{z})^{\frac{\Delta-J}{2}} g_{\Delta,J}(z,\bar{z})$, and $g_{\Delta,J}(z,\bar{z})$ denotes the conformal block introduced in (2.2.28). Each contribution $a_{\Delta,J}G_{\Delta,J}(z,\bar{z})$ corresponds to the exchange of a primary operator with quantum numbers Δ, J and its descendants between the

[26]For a comprehensive review see [111].

four external operators. The central insight of the inversion formula is that the OPE coefficients $a_{\Delta,J}$ are not arbitrary. Rather, they depend on the spin J and the scaling dimension Δ in such a way as to reproduce the analytic structure of the correlator.

Following [107], one can illustrate the basic idea of the inversion formula in a simple setting. Consider a function expanded as a power series,

$$f(x) = \sum_{j=1}^{\infty} f_j x^j \,. \tag{2.2.39}$$

Assume that it is analytic in the complex plane except for a branch cut along the real axis for $x > 1$, and that it satisfies $f(x)/x \to 0$ as $x \to \infty$. By Cauchy's theorem, the coefficients f_j can be written as

$$f_j = \frac{1}{2\pi i} \oint \frac{dx}{x}\, x^{-j} f(x) \,. \tag{2.2.40}$$

By deforming the contour so that it wraps around the branch cut, and using the asymptotic condition at infinity, this becomes

$$f_j = \frac{1}{2\pi} \int_1^{\infty} \frac{dx}{x}\, x^{-j}\, \mathrm{Disc}\, f(x) \,. \tag{2.2.41}$$

Here,

$$\mathrm{Disc}\, f(x) = -i\Big(f(x+i0) - f(x-i0)\Big) \,. \tag{2.2.42}$$

This shows that the coefficients are determined entirely by the discontinuity of the function, and that they are analytic in j for $\mathrm{Re}(j) \geq 1$.

An analogous structure appears in conformal field theory when one considers the decomposition in (2.2.38), or more generally the decomposition into conformal partial waves [112],

$$G(z,\bar{z}) = \delta_{12}\delta_{34} + \sum_{J=0}^{\infty} \int \frac{d\Delta}{2\pi i}\, c(J,\Delta)\, F_{J,\Delta}(z,\bar{z}) \,. \tag{2.2.43}$$

Here $c(J,\Delta)$ is a spectral function encoding the OPE data. Using the orthogonality of the functions $F_{J,\Delta}$, one can invert this decomposition and obtain

$$c(J,\Delta) = \mathcal{N}(J,\Delta) \int d^2z\, \mu(z,\bar{z})\, F_{J,\Delta}(z,\bar{z})\, G(z,\bar{z}) \,. \tag{2.2.44}$$

This expresses the OPE data directly in terms of the analytic structure of the correlator. So far, all of this has been formulated in Euclidean signature. To pass to Lorentzian signature, one must change the parametrization [113] and replace the discontinuity by the double-discontinuity,

$$\mathrm{dDisc}\,[G(z,\bar{z})] = G_{\mathrm{Eucl}}(z,\bar{z}) - \frac{1}{2}\,G_{\circlearrowleft}(z,\bar{z}) - \frac{1}{2}\,G_{\circlearrowright}(z,\bar{z})\ . \tag{2.2.45}$$

Here $G_{\mathrm{Eucl}}(z,\bar{z})$ is the Euclidean correlator, while the other terms correspond to the two possible analytic continuations around the branch point $\bar{z}=1$. With these two modifications, one arrives at the Lorentzian inversion formula [107].

Polyakov bootstrap. In the modern formulation of the Polyakov bootstrap, one considers Mellin amplitudes in order to express the four-point function in terms of Witten diagrams [108–110, 114]. This makes it possible to expand the correlator in crossing-symmetric building blocks, and the bootstrap conditions can then be systematically recast in terms of this expansion.

To illustrate the central idea, we begin by performing the Mellin transform of the four-point function (2.2.27),

$$G(u,v) = \int_{-i\infty}^{i\infty} \frac{ds\,dt}{(4\pi i)^2}\, u^{\frac{s}{2}} v^{\frac{t}{2}-\Delta_\phi} M(s,t)\mu(s,t)\ , \tag{2.2.46}$$

where the parameters u, v are defined in (2.2.33), and the measure factor μ is given by

$$\mu(s,t) = \Gamma^2\Big(\Delta_\phi - \frac{s}{2}\Big)\,\Gamma^2\bigg(\Delta_\phi - \frac{t}{2}\bigg)\,\Gamma^2\Big(\Delta_\phi - \frac{u}{2}\Big)\ , \tag{2.2.47}$$

with

$$s + t + u = 4\Delta_\phi\ . \tag{2.2.48}$$

Here, $M(s,t)$ is called the *Mellin amplitude*. The double poles in the measure factor correspond to the contributions of double-twist operators with dimensions $\Delta = 2\Delta_\phi + 2n + J$. In a generic interacting CFT without supersymmetry, however, the spectrum is not expected to consist of exact towers of double-twist operators with integer spacing. Instead, these poles must combine with the Mellin amplitude in such a way that the naive double-twist contributions are cancelled and replaced by the physical spectrum. These cancellation conditions lie at the heart of the Polyakov bootstrap.

In order to make this structure manifest, and to clarify the role played by the dispersion relation, it is convenient to replace the Mandelstam variables in (2.2.48) by a new set of parameters,

$$s = 2s_1 + \frac{4\Delta_\phi}{3}\ , \quad t = 2s_2 + \frac{4\Delta_\phi}{3}\ , \quad u = 2s_3 + \frac{4\Delta_\phi}{3}\ , \tag{2.2.49}$$

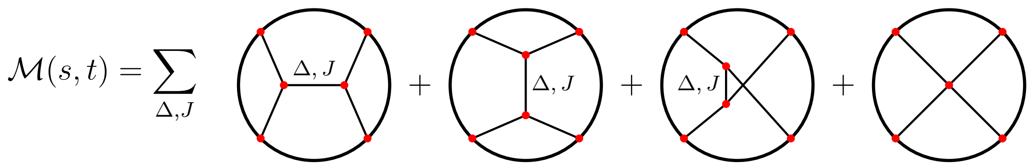

Figure 2.3: *We can expand the Mellin amplitude in a basis of crossing symmetric AdS exchange Witten diagrams which include the contact diagrams. Each of these diagrams is crossing symmetric on their own.*

so that $s_1+s_2+s_3=0$. In this parametrization, crossing symmetry becomes invariance under permutations of the s_i. The Mellin amplitude can then be written in the form of a dispersion relation,

$$M(s_1,s_2) = M(0,0) + \frac{1}{\pi}\int_\sigma^\infty \frac{ds_1'}{s_1'}\,\mathcal{A}(s_1';s_2^+(s_1',a))\,H_2(s_1';s_1,s_2,s_3)\;, \tag{2.2.50}$$

where

$$H_2(s;s_1,s_2,s_3) = \left(\frac{s_1}{s-s_1}+\frac{s_2}{s-s_2}+\frac{s_3}{s-s_3}\right)\;, \tag{2.2.51}$$

is a manifestly crossing-symmetric kernel. The lower limit σ marks the point at which the sequence of poles in the Mellin variable s_1 begins. The quantity $\mathcal{A}(s_1;s_2)$ denotes the s-channel discontinuity of the Mellin amplitude. In this language, the cancellation of the tower of double-twist operators is encoded in the *Polyakov conditions*,

$$M\left(s_1 = \frac{\Delta_\phi}{3}+p, s_2\right) = 0\;, \tag{2.2.52}$$

$$\partial_{s_1} M\left(s_1 = \frac{\Delta_\phi}{3}+p, s_2\right) = 0\;, \tag{2.2.53}$$

for all positive integers p. The validity of these conditions in this context was established in [115].

Moreover, imposing the Polyakov conditions (2.2.52) and (2.2.53) leads to an expansion of the Mellin amplitude in a basis of crossing-symmetric AdS exchange Witten diagrams, illustrated in Figure 2.3, together with contact diagrams. The crossing-symmetric dispersion relation in (2.2.50) fixes this basis.

As these two examples of analytic bootstrap illustrate, dispersion relations are crucial for systematically understanding the structure of four-point functions and have led to many illuminating connections, such as that between Mellin amplitudes and contact Witten diagrams. These techniques have been used to bootstrap various theories in the

ϵ-expansion [108–110, 114], leading to a deeper understanding of distinct theories as well as of their large-Δ behaviour. In Section 4, we will develop analogous techniques for CFTs at finite temperature and demonstrate that, although conformal symmetry is broken, similarly powerful methods can still be applied.

2.3 Thermodynamics

In this section, we adopt a statistical–mechanical perspective on quantum field theories and focus on macroscopic thermodynamic quantities such as temperature, energy density, and entropy. Depending on the thermal regime under consideration, the appropriate field-theoretic tools may vary significantly. Before turning to these methods in detail, we first review the basic concepts and quantities of thermodynamics that will be used throughout this discussion.

In equilibrium statistical mechanics, the *microcanonical ensemble* provides the appropriate description of an isolated system with fixed energy, particle number, and volume. These are the natural thermodynamic variables of the microcanonical ensemble, while quantities such as temperature are derived from them.

The *canonical ensemble* describes a system in thermal contact with a heat reservoir, so that the temperature, particle number, and volume are fixed, while energy may be exchanged with the reservoir.

Finally, the *grand canonical ensemble* corresponds to the situation in which both energy and particles can be exchanged with the environment, while the temperature and volume remain fixed.[27]

Using the time-evolution operator introduced in Section 2.2.2, together with the total particle number operator N, one can define the density operator as

$$\rho = \exp\left(-\beta\left(H - \mu N + \cdots\right)\right) \ , \tag{2.3.1}$$

where $\beta = \frac{1}{T}$ acts as a Lagrange multiplier enforcing the average-energy constraint, and μ denotes the chemical potential. From this density operator, we define the *grand canonical partition function* by

$$Z = \mathrm{Tr}(\rho) \ . \tag{2.3.2}$$

The partition function provides a unified framework from which thermodynamic quantities can be derived. In particular,

$$P = \frac{\partial(T \ln Z)}{\partial V} \ , \quad N = \frac{\partial(T \ln Z)}{\partial \mu} \ , \quad S = \frac{\partial(T \ln Z)}{\partial T} \ , \tag{2.3.3}$$

[27] In relativistic quantum systems, where particle creation and annihilation occur naturally, the grand canonical ensemble provides the most natural description.

yield the pressure, particle number, and entropy, respectively. Combining these relations, the internal energy may be written as

$$E = -PV + TS + \mu N \ . \tag{2.3.4}$$

A detailed discussion of the thermodynamic quantities introduced above, and of their treatment within quantum field theory, can be found in [33, 116, 117]. Several complementary frameworks have been developed for studying quantum field theories at finite temperature, each suited to different physical questions. Prominent examples include the *thermofield double formalism*, the *Matsubara (imaginary-time) formalism*, and the *Schwinger–Keldysh formalism*. In this work, we will primarily employ the Matsubara formalism, which provides a particularly convenient framework for computing equilibrium thermodynamic quantities.

2.3.1 Matsubara Formalism

We consider the imaginary-time formalism, as originally introduced in [38], with $\tau = it$,

$$\mathcal{O}(\tau, x) = e^{\tau H}\mathcal{O}(x)e^{-\tau H} \ , \tag{2.3.5}$$

where H is the appropriate time-evolution operator. The spectral decomposition of a thermal correlator in the canonical ensemble is given by

$$\langle \mathcal{O}_1(\tau_1, x_1)\cdots\mathcal{O}_n(\tau_n, x_n)\rangle_\beta = \frac{\mathrm{Tr}\Big[\rho\mathcal{O}_1(\tau_1, x_1)\cdots\mathcal{O}_n(\tau_n, x_n)\Big]}{\mathrm{Tr}[\rho]} \tag{2.3.6}$$

$$= \frac{\sum_\alpha \langle\varepsilon_\alpha|e^{-\beta\varepsilon_\alpha}\mathcal{O}_1(x_1)\cdots\mathcal{O}_n(x_n)|\varepsilon_\alpha\rangle}{\sum_\alpha \langle\varepsilon_\alpha|e^{-\beta\varepsilon_\alpha}|\varepsilon_\alpha\rangle} \ . \tag{2.3.7}$$

Combining the imaginary-time formalism with the density operator $\rho = e^{-\beta H}$, we obtain

$$\langle \mathcal{O}_1(\tau_1, x_1)\cdots\mathcal{O}_n(\tau_n, x_n)\rangle_\beta = \frac{\mathrm{Tr}\Big[e^{-\beta H+\tau_1 H}\mathcal{O}_1(x_1)e^{-H(\tau_1-\tau_2)}\cdots\mathcal{O}_n(x_n)e^{-\tau_n H}\Big]}{\mathrm{Tr}[\rho]} \ . \tag{2.3.8}$$

Cyclicity of the trace implies that the correlation functions must satisfy a periodicity relation. In the case of two-point functions, which will be the focus of Section 4, this periodicity relation is known as the *Kubo–Martin–Schwinger (KMS) condition* [118],

$$\langle \mathcal{O}_1(\tau, x)\mathcal{O}_2(0,0)\rangle_\beta = \langle \mathcal{O}_1(\tau+\beta, x)\mathcal{O}_2(0,0)\rangle_\beta \ . \tag{2.3.9}$$

Therefore, the UV divergence arising from coincident operators, $\langle \mathcal{O}_1(0,0)\mathcal{O}_2(0,0)\rangle_\beta$, is repeated at each $\tau = n\beta$ for all $n \in \mathbb{Z}$. Importantly, when one considers the momentum-space correlation function, one finds that it also has poles at discrete purely imaginary frequencies separated by integer multiples of $2\pi T$, known as *Matsubara poles*. These two closely related observations provide the heuristic justification for interpreting the temperature entering the correlation functions through the density matrix ρ geometrically, namely as arising from an S^1 factor in spacetime.

2.3.2 Interacting QFTs at Finite Temperature

Using the imaginary-time formalism, we consider a generic interacting QFT. As discussed at the beginning of this section, the partition function is given by

$$Z_\beta = \int [\phi] e^{S_0 + S_I} \ , \tag{2.3.10}$$

where S_0 denotes the free part of the action, containing at most quadratic terms and corresponding to the ideal-gas contribution. On the other hand, S_I denotes the interacting part of the action. Expanding the partition function in powers of the interaction term allows us to separate the ideal-gas contribution from the interacting corrections,

$$\ln Z = \ln\left(\int [\phi] e^{S_0}\right) + \ln\left(1 + \frac{1}{\int [\phi] e^{S_0}} \sum_{i=1}^{\infty} \frac{1}{i!} \int [\phi] e^{S_0} S_I^i\right) \ . \tag{2.3.11}$$

This separation is particularly useful for weakly interacting theories. In that case, one can further expand both contributions in terms of bubble diagrams and compute the partition function order by order [33]. Similarly, the same techniques can be used to compute thermal correlation functions. When we consider vector models with interaction $g(\phi_i\phi_i)^2$ (given in (2.2.2) for $N = 1$) in $4-\epsilon$ dimensions, the theory becomes weakly coupled. Therefore, the thermal correlation functions can be computed perturbatively for small g.

The Feynman rules. We first present the Feynman rules for the theory at the Wilson–Fisher fixed point

$$\frac{g_\star}{(4\pi)^2} = \frac{3\varepsilon}{N+8} + O(\varepsilon^2) \ . \tag{2.3.12}$$

Using the geometric interpretation of temperature and viewing the time direction as compactified, as explained in Section 2.3.1, the scalar propagator takes the form[28]

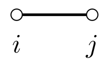

$$= \delta^{ij} \frac{\Gamma(d/2-1)}{4\pi^{d/2}} \sum_{m=-\infty}^{\infty} \frac{1}{((\tau-m)^2+x^2)^{d/2-1}} \ , \tag{2.3.13}$$

while the insertion of a vertex gives rise to the following integral and index contractions:

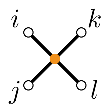

$$= -\frac{\lambda_\star}{4!} \left(\delta^{ij}\delta^{kl} + \delta^{ik}\delta^{jl} + \delta^{il}\delta^{jk}\right) \int \mathrm{d}^{d-1}x \int_0^1 \mathrm{d}\tau \ . \tag{2.3.14}$$

The correlator. We now compute the thermal correlator $\langle\, \phi(0)\phi(\tau,x)\,\rangle_\beta$. The operator is normalized so that the zero-temperature correlator takes the form,

$$\langle\, \phi(0)\phi(\tau)\,\rangle = \frac{1}{\tau^{2\Delta_\phi}} \ . \tag{2.3.15}$$

We therefore write the interacting part of the correlator as

$$g(\tau,x) - g_{\text{free}}(\tau,x) = \frac{1}{n_\phi} Z_\phi^{-2} \Bigg(\quad + O(\lambda^2) \Bigg) \ , \tag{2.3.16}$$

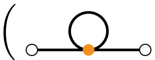

where n_ϕ is the normalization constant ensuring (2.3.15), while the diagram is built from unnormalized fields. The factor Z_ϕ is the usual wave-function renormalization constant; however, at this order in λ, the operator does not renormalize:

$$Z_\phi^{-2} = 1 + O(\lambda^2) \ . \tag{2.3.17}$$

For our calculation, we only need the leading term in the normalization constant, which is simply

$$\frac{1}{n_\phi} = 4\pi^2 + O(\varepsilon) \ . \tag{2.3.18}$$

After manipulating the integrals, we obtain,

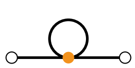

$$= \frac{\lambda_\star(N+2)}{576\pi^2} \sum_{n=-\infty}^{\infty} \left[\frac{1}{\varepsilon} + 12\log A - \log 2 + \frac{1}{2}\log[(n+z)(n+\bar{z})] + O(\varepsilon) \right] \ , \tag{2.3.19}$$

where $A = 1.282427\ldots$ is the Glaisher–Kinkelin constant, and we have introduced the coordinates $z = \tau + ix$ for simplicity. It is worth noting that the correlator contains

[28] A very straightforward way to see this is to take the propagator in momentum-space then transform to position-space as it is $\mathbb{R}^d$ and apply Poisson resummation [3].

only transcendental terms of homogeneous weight 1. To conclude, note that the contributions computed explicitly here do not exhaust the full $O(\varepsilon)$ correction. Since the theory lives in $d = 4 - \varepsilon$, there is an additional contribution at order ε coming from the free propagator. This results in the following OPE coefficients,

$$a_{[\phi\phi]_{0,J>0}} = 2\zeta(2+J) - 2\varepsilon\zeta'(2+J) + O(\varepsilon^2)\ . \tag{2.3.20}$$

The details of this computation can be found in [3]. This example illustrates the basic properties of thermal correlators discussed in this section. Later, we will reproduce this result using the analytic bootstrap method developed in this thesis.

One of the main motivations for computing a correlator in a weakly coupled theory is to show that finite-temperature calculations do not introduce any additional ultraviolet divergences associated with high momenta or very short distances. Any such divergences are the same as those already present at zero temperature, so the regularization and renormalization required at $T = 0$ remain sufficient for $T > 0$, up to the additional zeta-function regularization needed to implement the method of images. There are three ways to see this [33]. First, if one could explicitly construct the full set of Hamiltonian eigenstates with energies E_S, then the partition function would simply be

$$Z = \sum_S e^{-\beta E_S}, \tag{2.3.21}$$

and there would be no source of new thermal divergences. Second, one can start from the real-time transition amplitude and obtain the thermodynamic partition function by analytic continuation to imaginary time, which does not generate new ultraviolet problems. Third, in perturbation theory, each loop contains a frequency sum that can be separated into a zero-temperature contour integral and a finite-temperature contribution. The zero-temperature part is the one that can generate the usual quadratic or logarithmic ultraviolet divergences, whereas the thermal part is exponentially suppressed at large frequencies. In other words, finite temperature does not modify the very short-distance behaviour of the theory.

This concludes our review of supersymmetry, conformal field theory, and thermal quantum field theory. In the next two chapters, we turn to the main theme of this thesis: the controlled breaking of these symmetries and the extent to which the powerful methods these symmetries underpin can be generalized to less symmetric settings.

Chapter 3

Spin Chains Arising From $\mathcal{N} = 2$ SCFTs

The connection between one-dimensional spin-chain models and supersymmetric gauge theories was first established in the seminal work [37] for maximally supersymmetric $SU(N)$ gauge theory in four dimensions. This observation led to the realisation that $\mathcal{N} = 4$ SYM is very likely an integrable quantum field theory, and placing this statement on a firm mathematical footing remains an important and active direction of research. Over the past two decades, integrability has proved to be an extremely powerful tool, enabling the computation of a wide range of physical quantities, including anomalous dimensions and Wilson line expectation values. These developments were reviewed in Section 2.1.2.

In the case of $\mathcal{N} = 4$ SYM, translating the physical observables of interest into the language of spin chains leads to a drastic simplification of the problem, since the resulting models are well-known rational integrable spin chains that admit exact solutions via the Bethe ansatz. As the amount of supersymmetry is reduced, however, establishing and exploring this correspondence becomes less straightforward and increasingly computationally challenging [119, 120]. Nevertheless, the connection remains fruitful even in the absence of integrability, both for the underlying quantum field theories and for the associated spin-chain models.

The next natural step beyond $\mathcal{N} = 4$ SYM involves its orbifolds, which, at the orbifold point of the conformal manifold, lead to integrable superconformal field theories (SCFTs) [71]. Further marginal deformations away from this point give rise to quiver SCFTs, which span a significant portion of the landscape of Lagrangian SCFTs with known gravity duals [63, 64]. In this work, we focus on the simplest such $\mathcal{N} = 2$

SCFT: the marginally deformed $\mathbb{Z}_2$ orbifold of $\mathcal{N}=4$ SYM, which has been the subject of extensive study [42, 80–82, 121–134]. This theory interpolates between the $\mathbb{Z}_2$ orbifold of $\mathcal{N}=4$ SYM—an integrable theory with a well-understood AdS dual—and $\mathcal{N}=2$ superconformal QCD (SCQCD), conjectured to be dual to a non-critical string theory [80] (see also [135]).

As will become clear from the example we consider, spin-chain models associated with SCFTs possessing less than maximal supersymmetry begin to exhibit a variety of novel features that have not been systematically studied in the existing literature. Consequently, a careful analysis of these models and a thorough understanding of their fundamental properties are necessary before addressing the question of whether they are integrable, and in what precise sense such integrability may hold. Also, recent developments have uncovered hidden structures [82, 136] indicating that it may belong to a novel class of integrable systems governed by a *dynamical* Yang–Baxter equation (DYBE) [137, 138], specifically of the type studied in [139–141].

In this thesis, we study the fundamental properties of a simple example that captures the essential intricacies of $\mathcal{N}=2$ SCFTs. As explained in Section 2.1, the landscape of $\mathcal{N}=2$ theories was elegantly classified in [52]. Within this classification, orbifolds of $\mathcal{N}=4$ SYM, together with their marginal deformations, occupy a large region of the landscape. Moreover, it was shown that such orbifolds preserve integrability essentially in the same sense as the parent $\mathcal{N}=4$ SYM theory [71].

Orbifold theories therefore provide a particularly suitable testing ground. Since the orbifold point is integrable, one can begin with a Bethe ansatz solution and then, by marginally deforming the theory away from this point, track how the Bethe ansatz, and more generally the integrable structure deforms. To implement this strategy, we consider the simplest possible orbifold construction, namely the $\mathbb{Z}_2$ orbifold of $\mathcal{N}=4$ SYM. This chapter is primarily based on the work [1, 2].

3.1 Introduction to $\mathbb{Z}_2$ Orbifold of $\mathcal{N}=4$ SYM

In this section, we introduce the details of the $\mathcal{N}=2$ SCFT under study and the corresponding spin-chain models. We review the relevant literature and set up the spectral problem.

3.1.1 The Gauge Theory

Building on the discussion of orbifolding given in Section 2.1.3, the $\mathbb{Z}_2$ orbifold of $\mathcal{N} = 4$ SYM has $SU(N)_1 \times SU(N)_2$ gauge group and $SU(2)_R \times U(1)_r$ R-symmetry. The field content is captured by the quiver diagram depicted in Figure 3.1 and includes two bifundamental hypermultiplets as well as two adjoint $\mathcal{N} = 2$ vector multiplets. Following the notation of [1, 82], these fields descend from the three complex scalars of $\mathcal{N} = 4$ in the following manner (2.1.40),

$$X \to \begin{pmatrix} & Q_{12} \\ Q_{21} & \end{pmatrix} , \qquad Y \to \begin{pmatrix} & \tilde{Q}_{12} \\ \tilde{Q}_{21} & \end{pmatrix} , \qquad Z \to \begin{pmatrix} \phi_1 & \\ & \phi_2 \end{pmatrix} . \tag{3.1.1}$$

The scalars ϕ_1 and ϕ_2 transform in the adjoint representation of one of the $SU(N)_{i=1,2}$ gauge groups, respectively. The two hypermultiplets include the bifundamental scalars $Q_{12}, \tilde{\bar{Q}}_{12}$ and $Q_{21}, \tilde{\bar{Q}}_{21}$, where the first index refers to the gauge node for which the field is in the fundamental representation, and the second index refers to the gauge node for which the scalar field is in the anti-fundamental representation. Marginally deforming away from the orbifold point with the parameter $\kappa = g_2/g_1$ gives a theory with two distinct coupling constants as given in (2.1.41),

$$\mathcal{W}_{\mathbb{Z}_2} = ig_1 \mathrm{tr}_2 \left(\tilde{Q}_{21}\phi_1 Q_{12} - Q_{21}\phi_1 \tilde{Q}_{12} \right) - ig_2 \mathrm{tr}_1 \left(Q_{12}\phi_2 \tilde{Q}_{21} - \tilde{Q}_{12}\phi_2 Q_{21} \right) , \tag{3.1.2}$$

with the parameter $\kappa \in [0, 1]$. In addition to the $SU(2)_R \times U(1)_r$ R-symmetry, this theory has an extra $SU(2)_L$ global symmetry such that the adjoint scalars ϕ_i are singlets under the $SU(2)_L$ symmetry, while Q_{ij} and $\tilde{Q}_{ij}$ are bifundamentals forming two $SU(2)_L$ doublets [81],

$$Q_{\hat{I}} = \begin{pmatrix} Q_{12} \\ \tilde{Q}_{12} \end{pmatrix} , \qquad \tilde{Q}_{\hat{I}} = \begin{pmatrix} \tilde{Q}_{21} \\ Q_{21} \ . \end{pmatrix} \tag{3.1.3}$$

This is a special feature of the $\mathbb{Z}_2$ orbifold theory and this global symmetry is no longer present when we consider $\mathbb{Z}_k$ orbifolds with $k > 2$. The $\mathbb{Z}_2$ orbifold point theory (at $\kappa = 1$) has a well understood $AdS_5 \times S^5/\mathbb{Z}_2$ gravity dual [63, 64, 80]. Because this is a $\mathbb{Z}_2$ orbifold, there is only one marginal deformation which allows us to explore the real two-dimensional conformal manifold of the $g_1 \neq g_2$ exactly marginal YM couplings which are given inside the superpotential (3.1.2).

Also, the theory interpolates between the orbifold point theory for $\kappa = 1$ and the $\mathcal{N} = 2$ superconformal QCD (SCQCD) with the $U(N_f) = U(2N)$ flavor symmetry for $\kappa = 0$ [80]. The study of this theory after marginal deformation was initiated in [80, 81] where a complete one-loop hamiltonian for the scalar operators of the theory was computed.

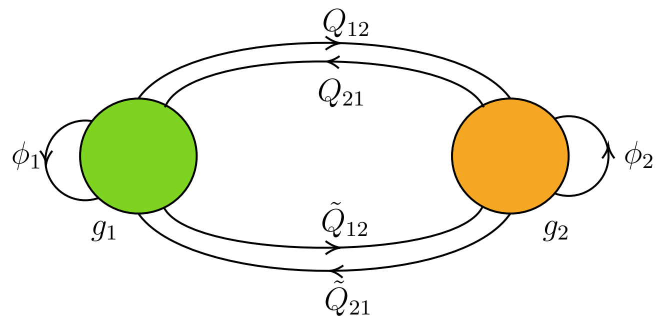

Figure 3.1: *The $\mathbb{Z}_2$ orbifold theory with $SU(N)_1 \times SU(N)_2$.*

In the interpolating $\mathcal{N} = 2$ theory, the breaking of the mother $SU(4)_R$ is such that there are three distinct $SU(2)$ subsectors which we can read off from the one-loop Hamiltonian. These subsectors are named with respect to their $\mathcal{N} = 4$ origins as given in (3.1.1), namely the XY-subsector, the XZ-subsector and the YZ-subsector. In the XY-subsector the $SU(2)$ symmetry is unbroken and it coincides with the $SU(2)_R$ symmetry. On the other hand, the XZ- and YZ- sectors are described by the same spin chain and for them the $SU(2)$ is broken and it coincides with the $SU(2)_R$ symmetry that is broken through the orbifolding process. Here, we will present these different subsectors in the following section after passing to the spin chain picture and then focus on the subsector that exhibits the breaking of the R-symmetry most severely.

3.1.2 The Spin Chain

A number of the novel features of $\mathcal{N} = 2$ SCFT spin chains that we aim to highlight in this thesis are already captured by the $\mathbb{Z}_2$ orbifold of $\mathcal{N} = 4$ SYM. To construct the Hilbert space of the spin chain for this theory, we consider single-trace operators built from two of the three complex scalar fields introduced in (3.1.1).

The fact that these fields are in different representations of the gauge group restricts the allowed single-trace operators in the planar limit and gives rise to a dynamical spin chain model [82]. More explicitly the color contraction rules for the bifundamental Q_{ij} for $ij \in \{12, 21\}$, which are in the $\square_i \times \bar{\square}_j$ representation of the $SU(N)_1 \times SU(N)_2$ gauge group, strictly prohibit having the following configurations inside the single trace operators:

$$\begin{gathered}\operatorname{tr}(\cdots \cancel{Q_{12}Q_{12}} \cdots)\ ,\ \operatorname{tr}(\cdots \cancel{Q_{21}Q_{21}} \cdots)\ ,\ \operatorname{tr}(\cdots \cancel{Q_{12}\phi_1} \cdots)\ ,\ \operatorname{tr}(\cdots \cancel{\phi_1 Q_{21}} \cdots)\ ,\\ \operatorname{tr}(\cdots \cancel{\phi_2 Q_{12}} \cdots)\ ,\ \operatorname{tr}(\cdots \cancel{Q_{21}\phi_2} \cdots)\ ,\ \operatorname{tr}(\cdots \cancel{\phi_2\phi_1} \cdots)\ ,\ \operatorname{tr}(\cdots \cancel{\phi_1\phi_2} \cdots)\ . \end{gathered} \tag{3.1.4}$$

Moreover, because of the color contraction rules, single-trace operators can only include an even number of bifundamental fields and the bifundamental fields, Q_{12}, Q_{21}, $\tilde{Q}_{12}$, and $\tilde{Q}_{21}$ should always appear in an alternating fashion with or without ϕ's in between. Examples of the possible configurations include,

$$\mathrm{tr}_1\left(\phi_1^L\right)\ , \quad \mathrm{tr}\left(\phi_1^{L-A}Q_{12}\phi_2^A Q_{21}\right)\ , \quad \mathrm{tr}\left(\phi_1^{L-A-B-C}Q_{12}\phi_2^A Q_{21}\phi_1^B Q_{12}\phi_2^C Q_{21}\right)\ , \tag{3.1.5}$$

additionally, we could have

$$\mathrm{tr}_1\left(Q_{12}Q_{21}Q_{12}\cdots Q_{12}\right)\ , \qquad \mathrm{tr}_1\left(Q_{12}\tilde{Q}_{21}\tilde{Q}_{12}\cdots Q_{12}\right)\ . \tag{3.1.6}$$

In terms of the spin chain picture this spoils the tensor product structure of the Hilbert space. And implicitly adds non-local effects into the model. Before going into the details of the specific spin chain models, we introduce the distinct $SU(2)$-like subsectors of this theory by looking at the scalar one-loop Hamiltonian [81].

The XY-sector. This is the sector which includes all the (holomorphic) bifundamental fields. To derive the Hamiltonian, let us start by considering the ϕ_i F-terms:

$$F_{\phi_1} = g_1(Q_{12}\tilde{Q}_{21} - \tilde{Q}_{12}Q_{21})\ , \quad F_{\phi_2} = g_2(Q_{21}\tilde{Q}_{12} - \tilde{Q}_{21}Q_{12}) \tag{3.1.7}$$

After taking out an overall factor of g_1g_2 and defining $\kappa = g_2/g_1$, we find the Hamiltonian:

$$\mathcal{H}_{\ell,\ell+1} = \begin{array}{c} \\ \scriptstyle Q_{12}Q_{21} \\ \scriptstyle Q_{12}\tilde{Q}_{21} \\ \scriptstyle \tilde{Q}_{12}Q_{21} \\ \scriptstyle \tilde{Q}_{12}\tilde{Q}_{21} \\ \scriptstyle Q_{21}Q_{12} \\ \scriptstyle Q_{21}\tilde{Q}_{12} \\ \scriptstyle \tilde{Q}_{21}Q_{12} \\ \scriptstyle \tilde{Q}_{21}\tilde{Q}_{12} \end{array} \begin{array}{c} \begin{array}{cccccccc} \scriptstyle Q_{12}Q_{21} & \scriptstyle Q_{12}\tilde{Q}_{21} & \scriptstyle \tilde{Q}_{12}Q_{21} & \scriptstyle \tilde{Q}_{12}\tilde{Q}_{21} & \scriptstyle Q_{21}Q_{12} & \scriptstyle Q_{21}\tilde{Q}_{12} & \scriptstyle \tilde{Q}_{21}Q_{12} & \scriptstyle \tilde{Q}_{21}\tilde{Q}_{12} \end{array} \\ \left(\begin{array}{cccc|cccc} 0 & 0 & 0 & 0 & 0 & 0 & 0 & 0 \\ 0 & 1/\kappa & -1/\kappa & 0 & 0 & 0 & 0 & 0 \\ 0 & -1/\kappa & 1/\kappa & 0 & 0 & 0 & 0 & 0 \\ 0 & 0 & 0 & 0 & 0 & 0 & 0 & 0 \\ \hline 0 & 0 & 0 & 0 & 0 & 0 & 0 & 0 \\ 0 & 0 & 0 & 0 & 0 & \kappa & -\kappa & 0 \\ 0 & 0 & 0 & 0 & 0 & -\kappa & \kappa & 0 \\ 0 & 0 & 0 & 0 & 0 & 0 & 0 & 0 \end{array}\right) \end{array} . \tag{3.1.8}$$

Here, the indices ℓ and $\ell+1$ label nearest-neighbour sites along the spin chain. Despite the presence of four elementary fields, the resulting Hilbert space is only eight-dimensional rather than sixteen-dimensional, as one might naively expect. This reduction arises from the constraints imposed by color contraction rules. A systematic way to account for this restricted structure—initiated in [82] and further developed in [136]—is to exploit the $\mathcal{N}=4$ origin of the theory and encode the $\mathcal{N}=2$ color structure into a single overall index taking values in $\{1,2\}$.

Concretely, a state such as $|XYXYYX\cdots\rangle$ in the $\mathcal{N}=4$ description decomposes into two distinct states in the $\mathcal{N}=2$ picture, namely

$$|Q_{12}\tilde{Q}_{21}Q_{12}\tilde{Q}_{21}\tilde{Q}_{12}Q_{21}\cdots\rangle \quad \text{and} \quad |Q_{21}\tilde{Q}_{12}Q_{21}\tilde{Q}_{12}\tilde{Q}_{21}Q_{12}\cdots\rangle\,. \tag{3.1.9}$$

These two states are related by exchanging the gauge groups. In the XY formulation, the specific chain under consideration is uniquely fixed by specifying the gauge group to the left of a given site, that is, by the first index of the bifundamental field at that site. Without loss of generality, we choose this reference to be the first site of the chain.

Similarly, the action of the Hamiltonian decomposes into the action of *two* distinct Hamiltonians when expressed in the XY basis. Which of the two blocks is realised depends, once again, on the choice of gauge group to the left of the first site on which the Hamiltonian acts. We denote these two Hamiltonians by $\mathcal{H}_1$ and $\mathcal{H}_2$, with

$$\mathcal{H}_1 = \begin{pmatrix} 0 & 0 & 0 & 0 \\ 0 & \kappa^{-1} & -\kappa^{-1} & 0 \\ 0 & -\kappa^{-1} & \kappa^{-1} & 0 \\ 0 & 0 & 0 & 0 \end{pmatrix} \quad \text{and} \quad \mathcal{H}_2 = \begin{pmatrix} 0 & 0 & 0 & 0 \\ 0 & \kappa & -\kappa & 0 \\ 0 & -\kappa & \kappa & 0 \\ 0 & 0 & 0 & 0 \end{pmatrix}\,, \quad \text{in the basis} \begin{pmatrix} XX \\ XY \\ YX \\ YY \end{pmatrix}_{i=1,2} \tag{3.1.10}$$

where the notation is that $\mathcal{H}_1$ acts on the basis labelled by $i=1$ in the representation $\square_1 \times \overline{\square}_1$ of the color group, while $\mathcal{H}_2$ acts on the basis with $i=2$ in the representation $\square_2 \times \overline{\square}_2$. Given that the XY-sector consists solely of bifundamental fields, the gauge group necessarily alternates at consecutive sites along the chain, independently of whether the field at a given site is an X or a Y. As a consequence, the Hamiltonian in this sector alternates between $\mathcal{H}_1$ and $\mathcal{H}_2$. For example, if we fix the gauge group to the left of the first site to be the first one, then $\mathcal{H}_1$ acts on odd–even sites, while $\mathcal{H}_2$ acts on even–odd sites.

It is also possible to describe the XY-sector of the interpolating theory as an alternating XXX-model Hamiltonian. This model was studied in detail in [82] and the one- and two-magnon problems were solved by using contact terms in center-of-mass limit. Furthermore, the idea of the dynamical basis which we demonstrated above is further developed in [136], both for the Hilbert space of operators and the symmetry generators that act on them, using the algebroid/groupoid structures.

With these in mind, we turn our attention to the other distinct $SU(2)$-like spin chain arising from the scalar sector of the $\mathbb{Z}_2$ orbifold of $\mathcal{N}=4$ SYM. This model will be the main focus of this chapter.

XZ-sector. In this sector we will consider operators composed of the bifundamental field X and the adjoint field Z. To find the Hamiltonian we will need the $\tilde{Q}_{ij}$ F-terms:

$$F_{\tilde{Q}_{12}} = i(g_2\phi_2 Q_{21} - g_1 Q_{21}\phi_1) \ , \quad F_{\tilde{Q}_{21}} = i(g_1\phi_1 Q_{12} - g_2 Q_{12}\phi_2) \tag{3.1.11}$$

As in the previous case, the basis the Hamiltonian acts upon is not the sixteen-dimensional two-site tensor product space of a four-dimensional vector space with the basis vectors $\{|\phi_1\rangle, |\phi_2\rangle, |Q_{12}\rangle, |Q_{21}\rangle\}$. But it has to be projected to an eight-dimensional one according to the color contraction rules. The projection is required for any spin chain length and cannot be avoided. As discussed in [136], these four-dimensional basis vectors can be organized into two doublet representations,

$$\begin{pmatrix} |\phi_1\rangle \\ |Q_{12}\rangle \end{pmatrix} \quad \overset{\mathbb{Z}_2}{\longleftrightarrow} \quad \begin{pmatrix} |\phi_2\rangle \\ |Q_{21}\rangle \end{pmatrix} \ , \tag{3.1.12}$$

which are related to each other by the $\mathbb{Z}_2$ transformation of the quiver under the exchange of color indices $1 \leftrightarrow 2$. We can construct the spin chain states for any length by starting with one of these doublets and substituting the other whenever a $|Q_{ij}\rangle$ state is used. For example, spin chain states with length two can be written in the basis,

$$\begin{pmatrix} |\phi_1\phi_1\rangle \\ |\phi_1 Q_{12}\rangle \\ |Q_{12}\phi_2\rangle \\ |Q_{12}Q_{21}\rangle \end{pmatrix} \quad \overset{\mathbb{Z}_2}{\longleftrightarrow} \quad \begin{pmatrix} |\phi_2\phi_2\rangle \\ |\phi_2 Q_{21}\rangle \\ |Q_{21}\phi_1\rangle \\ |Q_{21}Q_{12}\rangle \end{pmatrix} \ . \tag{3.1.13}$$

As usual, to study the spectral problem of this spin chain we first consider infinitely long open spin chains. The two (degenerate) vacua constructed by the adjoint scalars of the theory are[1]

$$|\text{vac}\rangle_i = |\cdots\phi_i\phi_i\phi_i\cdots\rangle \ , \qquad \text{for} \quad i = 1, 2 \ . \tag{3.1.14}$$

On these vacua, we have two types of magnon excitations, given by Q_{12} and Q_{21}. Although spin chain states with any number of magnons are allowed, only the ones with a even number of magnons admit periodic boundary conditions. For example,

$$|{\phi_1}^{a_1}_{a_2}{\phi_1}^{a_2}_{a_3}\cdots{\phi_1}^{a_{L-1}}_{a_1}\rangle \longleftrightarrow \text{tr}\left({\phi_1}^L\right) \ , \tag{3.1.15}$$

[1] $\mathcal{N} = 2$ SCFTs have two types of BPS operators which could be used as vacua around which we study the n-magnon problem. These are operators either with $\Delta = \pm r$ with r being the $U(1)_r$ symmetry charge or $\Delta = 2R$ with R being the $SU(2)_R$ symmetry Cartan eigenvalue. In this work, we consider the vacua with $\Delta = \pm r$ which we also refer to as ϕ-vacua. In [82] the study of the Q-vacuum was pursued.

$$|\phi_1{}^{a_1}_{a_2} Q_{12}{}^{a_2}_{\bar a_1} \phi_2{}^{\bar a_1}_{\bar a_2} \cdots \phi_2{}^{\bar a_{L-1}}_{\bar a_L}\rangle \longleftrightarrow \text{(cannot be closed)} \,, \tag{3.1.16}$$

$$|\phi_1{}^{a_1}_{a_2} Q_{12}{}^{a_2}_{\bar a_1} \phi_2{}^{\bar a_1}_{\bar a_2} \cdots Q_{21}{}^{\bar a_{L-1}}_{a_1}\rangle \longleftrightarrow \mathrm{tr}\left(\phi_1 Q_{12} \phi_2^{L-4} Q_{21}\right) \,. \tag{3.1.17}$$

The Hamiltonian of the "broken $SU(2)$ sector" is of nearest-neighbor[2] type and can be taken from [81],

$$\mathcal{H} = \sum_l \mathcal{H}_{l,l+1} \,, \tag{3.1.18}$$

where

$$\mathcal{H}_{\ell,\ell+1} = \begin{array}{c} \\ \phi_1\phi_1 \\ \phi_1 Q_{12} \\ Q_{12}\phi_2 \\ Q_{12}Q_{21} \\ \phi_2\phi_2 \\ \phi_2 Q_{21} \\ Q_{21}\phi_1 \\ Q_{21}Q_{12} \end{array} \begin{array}{c} \begin{array}{cccccccc} \phi_1\phi_1 & \phi_1 Q_{12} & Q_{12}\phi_2 & Q_{12}Q_{21} & \phi_2\phi_2 & \phi_2 Q_{21} & Q_{21}\phi_1 & Q_{21}Q_{12} \end{array} \\ \left(\begin{array}{cccc|cccc} 0 & 0 & 0 & 0 & 0 & 0 & 0 & 0 \\ 0 & 1/\kappa & -1 & 0 & 0 & 0 & 0 & 0 \\ 0 & -1 & \kappa & 0 & 0 & 0 & 0 & 0 \\ 0 & 0 & 0 & 0 & 0 & 0 & 0 & 0 \\ \hline 0 & 0 & 0 & 0 & 0 & 0 & 0 & 0 \\ 0 & 0 & 0 & 0 & 0 & \kappa & -1 & 0 \\ 0 & 0 & 0 & 0 & 0 & -1 & 1/\kappa & 0 \\ 0 & 0 & 0 & 0 & 0 & 0 & 0 & 0 \end{array}\right) \end{array} \,. \tag{3.1.19}$$

By organizing the two-site basis vectors into two subsets that are related to each other under the exchange of color indices i, j of the fundamental fields, ϕ_i and Q_{ij}, we bring the Hamiltonian to a block diagonal form. Under the exchange of color indices, together with inverting κ to $1/\kappa$, we can map these two blocks of the Hamiltonian to each other. This $\mathbb{Z}_2$ symmetry of the Hamiltonian corresponds to the $\mathbb{Z}_2$ symmetry of the quiver diagram in Figure 3.1. More explicitly, the transformation,

$$\mathbb{Z}_2 : \begin{pmatrix} \phi_1 \\ Q_{12} \end{pmatrix} \leftrightarrow \begin{pmatrix} \phi_2 \\ Q_{21} \end{pmatrix} \quad \text{together with} \quad \kappa \leftrightarrow 1/\kappa \,, \tag{3.1.20}$$

leaves the Hamiltonian invariant,

$$[\mathbb{Z}_2, \mathcal{H}] = 0 \,. \tag{3.1.21}$$

This will play a crucial role when we start constructing eigenvectors. Additionally, we can also express this Hamiltonian in the form given in (3.1.10).

[2] Although the form of the Hamiltonian as a sum over two-site Hamiltonian densities suggests nearest neighbor interactions, the restricted form of the Hilbert space brings highly non-local effects which we explore by using a long-range ansatz in the following section.

Each one of the blocks we see inside the Hamiltonian resembles a Temperley-Lieb Hamiltonian with quantum parameter κ or $\frac{1}{\kappa}$. However, since the basis of the Hilbert space is highly non-trivial, this model is not equivalent to two copies of the Temperley-Lieb model. The constraints coming from the color contraction rules, together with the $\mathbb{Z}_2$ symmetry, make this model a dynamical spin chain model [82]. Nevertheless, taking $\kappa \to 1$ reduces the Hamiltonian given in (3.1.19) to two copies of the Heisenberg XXX model,[3] which is integrable as discovered by [71]. This limit corresponds to the orbifold point limit from the gauge theory side. Our solution must recover the eigenvalues and eigenvectors of these two XXX models as we take the $\kappa \to 1$ limit. We will show that this is indeed the case.

In addition to the $\mathbb{Z}_2$ symmetry, the fact that the Hamiltonian (3.1.18) is the sum of infinite local Hamiltonian densities implies that the overall Hamiltonian commutes with the operator that shifts all positions by one site

$$[e^{iP}, \mathcal{H}] = 0 \,, \tag{3.1.22}$$

Note that the permutation operators that we need to define the shift operator,

$$e^{iP} = \cdots P_{N,N-1} P_{N-1,N-2} \cdots P_{21} P_{1,0} P_{0,-1} \cdots P_{-N,-N-1} \cdots \tag{3.1.23}$$

are also defined in the dynamical basis,

$$P^1_{ij} = \begin{array}{c} \\ \phi_1\phi_1 \\ \phi_1 Q_{12} \\ Q_{12}\phi_2 \\ Q_{12}Q_{21} \end{array} \begin{array}{c} \begin{array}{cccc} \phi_1\phi_1 & \phi_1 Q_{12} & Q_{12}\phi_2 & Q_{12}Q_{21} \end{array} \\ \begin{pmatrix} 1 & 0 & 0 & 0 \\ 0 & 0 & 1 & 0 \\ 0 & 1 & 0 & 0 \\ 0 & 0 & 0 & 1 \end{pmatrix} \end{array} , \quad P^2_{ij} = \begin{array}{c} \\ \phi_2\phi_2 \\ \phi_2 Q_{21} \\ Q_{21}\phi_1 \\ Q_{21}Q_{12} \end{array} \begin{array}{c} \begin{array}{cccc} \phi_2\phi_2 & \phi_2 Q_{21} & Q_{21}\phi_1 & Q_{21}Q_{12} \end{array} \\ \begin{pmatrix} 1 & 0 & 0 & 0 \\ 0 & 0 & 1 & 0 \\ 0 & 1 & 0 & 0 \\ 0 & 0 & 0 & 1 \end{pmatrix} \end{array} \tag{3.1.24}$$

Another important symmetry of the XXX spin chain is parity. In this context, parity is defined according to keeping the color indices of the adjoint scalars ϕ_i and reflecting the position coordinates. However, we observe that this operator only commutes with the action of the Hamiltonian for states which have an even number of Q's, therefore we conclude that the parity is broken,

$$[\mathcal{H}, \mathcal{P}] \neq 0 \,. \tag{3.1.25}$$

Later on we will show that we can recover the action of parity by combining it with $\mathbb{Z}_2$ operator,

$$[(\mathbb{Z}_2)^M \mathcal{P}, \mathcal{H}] = 0 \,, \tag{3.1.26}$$

[3] We can also obtain the Heisenberg XXX model for open infinite spin chains by taking the quantum parameter of a Temperley-Lieb model to 1.

where M is the total number of magnons. In the following section, we present the CBA method and various ways to generalize the CBA in the cases that it fails to capture the dynamical nature of the spin chains. We also analyze the implications of these symmetries in more detail for different numbers of magnons.

In developing a method to solve the spectral problem for the XZ-sector, we focus on open infinite spin chains. Incorporating boundary conditions into such systems within the CBA framework is a challenging task, and it lies outside our scope; our present aim is to connect to gauge theory for an odd number of excitations. Notably, closed spin chain states with periodic or twisted boundary conditions correspond to single-trace operators of scalar fields. In this model, spin chain states can only be closed for an even number of excitations. As a result, the discussion of closed boundary conditions and the associated Bethe equations is done in [2] and it is the subject of Section 3.8, where we will apply the methods described in this thesis to states with four magnons and solve periodicity relations for long-range Bethe ansatz solution. Furthermore, open boundary conditions also correspond to operators on the gauge theory side, but addressing this requires the inclusion of flavor branes in the theory [142, 143], a topic that will not be explored here.

3.2 Coordinate Bethe Ansatz

We begin by considering the spectral problem and solving it for a fixed number of excitations using the CBA. We show that starting from the three-magnon problem, this approach is no longer sufficient to solve the system.

One-magnon problem. We consider one excited state in a sea of ϕ's. Depending on the color indices we start with, we have two distinct one-magnon states. The CBA for one-magnon is given by the state,

$$|\Psi(p)\rangle_{12} = \sum_{l=-\infty}^{\infty} e^{ipl} \, |\ldots \phi_1\phi_1 Q_{12}(l)\phi_2\phi_2 \ldots\rangle \ , \tag{3.2.1}$$

$$|\Psi(p)\rangle_{21} = \sum_{l=-\infty}^{\infty} e^{ipl} \, |\ldots \phi_2\phi_2 Q_{21}(l)\phi_1\phi_1 \ldots\rangle \ , \tag{3.2.2}$$

where the fields Q_{12} and Q_{21} sit in position l. We represent the position vector using the coordinate of the magnon. Each position state is dressed with a plane wave factor, and we sum over all possible positions that the excited state can occupy to construct the

CBA for the one-magnon state. To differentiate between the two types of momentum states, we assign two color indices to the momentum space states: the first index corresponds to the color of the ϕ states at the far left of the spin chain, while the second index corresponds to the color of the ϕ states at the far right of the position states of the spin chain.

We derive the dispersion relation of the model by solving the eigenvalue equation,

$$\mathcal{H}\left|\Psi(p)\right\rangle_{ij} = E(p)\left|\Psi(p)\right\rangle_{ij} \ , \quad \text{for} \quad ij \in \{12, 21\} \ . \tag{3.2.3}$$

The dispersion relation is identical for both states,

$$E_1(p) = \left(\sqrt{\kappa} - \frac{1}{\sqrt{\kappa}}\right)^2 + 4\sin^2\left(\frac{p}{2}\right) \ . \tag{3.2.4}$$

The agreement between the dispersion relations of two states is a consequence of a $\mathbb{Z}_2$ symmetry of the Hamiltonian (3.1.20). This operator maps distinct one-magnon states to each other,

$$\mathbb{Z}_2\left|\Psi(p)\right\rangle_{ij} = \left|\Psi(p)\right\rangle_{ji} \ , \qquad \text{for} \qquad ij \in \{12, 21\} \ . \tag{3.2.5}$$

It is also worth mentioning that the dispersion relation (3.2.4) coincides with the dispersion relation of a Heisenberg XXZ spin chain with the anisotropy parameter, $\Delta = (\kappa + 1/\kappa)/2$. Indeed, when we take $\kappa \to 1$, the mass gap closes and we obtain the dispersion relation for the Heisenberg XXX model. At the orbifold point, we obtain two copies of the Heisenberg XXX model, which is integrable for infinite open spin chains.

Another important transformation in the context of spin chains is parity, $\mathcal{P}$, which reverses the ordering of the states of our chain (supplemented in our case with the transformation $Q_{12} \leftrightarrow Q_{21}$ for consistency in the color indices)

$$\begin{aligned}
\mathcal{P}\left|\Psi(p)\right\rangle_{12} &= \sum_{l=-\infty}^{\infty} e^{ipl}\mathcal{P}\left|\cdots\phi_1 Q_{12}(l)\phi_2\cdots\right\rangle \\
&= \sum_{l=-\infty}^{\infty} e^{ipl}\left|\cdots\phi_2 Q_{21}(-l)\phi_1\cdots\right\rangle \\
&= \left|\Psi(-p)\right\rangle_{21} \ .
\end{aligned} \tag{3.2.6}$$

At first glance, the parity of the model seems broken due to the distinction between the magnons, Q_{12} and Q_{21}.[4] However, by employing the $\mathbb{Z}_2$ symmetry of the Hamiltonian,

[4]Here the breaking of the parity can be seen in the fact that parity maps the distinct one-magnon states to each other instead of just reversing the sign of the momentum parameter.

we observe that the operator given in (3.1.26) takes the role of parity operator,

$$\mathbb{Z}_2\mathcal{P}\,|\Psi(p)\rangle_{ij} = |\Psi(-p)\rangle_{ij} \ . \tag{3.2.7}$$

This is a property of our spin chains which we will use to characterize the three-magnon solution better. We first consider the two-magnon eigenvalue problem.

Two-magnon problem. We proceed by solving the eigenvalue problem for two-magnon spin chain states,

$$\mathcal{H}\,|\Psi(p_1,p_2)\rangle = E_2(p_1,p_2)\,|\Psi(p_1,p_2)\rangle \ . \tag{3.2.8}$$

The eigenvalue of the two-magnon states is given by summing over the one-magnon energy eigenvalue,[5] (3.2.4) for the independent momentum variables,

$$E_2(p_1,p_2) = E_1(p_1) + E_1(p_2) \ . \tag{3.2.9}$$

The CBA for two magnons is given by summing over all possible configurations of the magnons with a fixed ordering. Depending on the order of the magnons on the spin chain we can have two distinct eigenvectors,

$$\cdots\phi_1 Q_{12}\phi_2\cdots\phi_2 Q_{21}\phi_1\cdots \ , \qquad\qquad \cdots\phi_2 Q_{21}\phi_1\cdots\phi_1 Q_{12}\phi_2\cdots \ .$$

As with the one-magnon eigenvectors, these two configurations are labeled by the color indices of ϕ states at the far left and far right of the spin chain. According to those color indices, two magnons, Q_{ij}, always appear with opposite color indices. We introduce a wave function for each state in position space, incorporating the two possible ways the magnons can carry the momentum, p_1 and p_2. Initially, the CBA for two excited states takes the form

$$|\Psi(p_1,p_2)\rangle_{ii} = \sum_{l_1<l_2}\psi_{ii}(p_1,p_2;l_1,l_2)\,|Q_{ij}(l_1),Q_{ji}(l_2)\rangle \ , \tag{3.2.10}$$

such that the wave function under a particular choice of normalization is expressed as

$$\psi_{ii}(p_1,p_2;l_1,l_2) = (e^{il_1p_1+il_2p_2} + S_{ii}(p_1,p_2)e^{il_1p_2+il_2p_1}) \ , \tag{3.2.11}$$

for $i\in\{1,2\}$. The first coefficient of the weighted sum of plane waves is set to one for simplicity, while the second one is the *scattering coefficient*. This coefficient is fixed by

[5]The additive energy is a consequence of having a nearest-neighbor Hamiltonian and the requirement that asymptotically two magnon states are given by two one-magnon states. It is equivalent to $\langle l_1,l_2|\mathcal{H}-E_2|\Psi(p_1,p_2)\rangle_{ii}=0$ for $l_1<l_2$.

demanding that the wave function be a solution of the eigenvalue problem (3.2.8) when the two excitations are adjacent,

$$\langle l_1, l_1+1|\mathcal{H} - E_2|\Psi(p_1,p_2)\rangle_{ii} = 0 \ , \tag{3.2.12}$$

for $i \in \{1,2\}$ separately. Remaining equations that capture the eigenvalue problem for the non-interacting configurations, $\langle l_1, l_2|\mathcal{H} - E_2|\Psi(p_1,p_2)\rangle_{ii}$ vanish, for all $l_1 < l_2 - 1$ because of additive energy (3.2.9). Furthermore, the eigenvalue problem projected onto the interacting magnons state, (3.2.12) is given by

$$S_\kappa(p_1,p_2) = -\frac{1+e^{ip_1+ip_2} - 2\kappa e^{ip_2}}{1+e^{ip_1+ip_2} - 2\kappa e^{ip_1}} \ , \tag{3.2.13}$$

such that the scattering coefficients of the two eigenvectors are related to each other by $\kappa \to 1/\kappa$ transformation,

$$S_{11} = S_\kappa(p_1,p_2) \ , \tag{3.2.14}$$

whereas

$$S_{22} = S_{1/\kappa}(p_1,p_2) \ . \tag{3.2.15}$$

This is a consequence of the $\mathbb{Z}_2$ symmetry (3.1.20). Notably, the distinction between the eigenstates of this model and those of two copies of the Heisenberg XXZ spin chain becomes evident only at the two-magnon level. For an XXZ spin chain with anisotropy parameter $\Delta = \frac{1}{2}\left(\kappa + \frac{1}{\kappa}\right)$, the two-magnon scattering coefficients take the form $S_{\frac{1}{2}\left(\kappa+\frac{1}{\kappa}\right)}(p_1,p_2)$ in terms of (3.2.13). Here, we observe that the parameter $(\kappa + 1/\kappa)/2$, extracted from the dispersion relation (3.2.4), splits into two components, each of which parametrizes the scattering coefficients. This splitting highlights the unique features of the model and underscores the role of $\mathbb{Z}_2$ symmetry in differentiating it from the Heisenberg XXZ spin chain. Additionally, taking the orbifold limit would make the distinct scattering coefficients (3.2.14) and (3.2.15) coincide and we would obtain the result for two copies of the Heisenberg XXX chain as anticipated. Other than $\kappa = \pm 1$ and $\kappa = 0$, the scattering coefficients also coincide under the kinematic limit, $p_1 + p_2 = \pi$,

$$S_\kappa(p_1, \pi - p_1) = S_{1/\kappa}(p_1, \pi - p_1) \ , \tag{3.2.16}$$

for arbitrary p_1 and κ. This turns out to be crucial for the three-magnon CBA with contact terms, which is presented in Appendix A in [1].

Furthermore, the parity operator acts by reversing the sign of the momentum variables and does not need to be combined with the $\mathbb{Z}_2$ operator. This phenomenon is deeply connected with the fact that two magnon states, as well as all other states with an even number of excitations, admit periodic boundary conditions. Since the states at the far left and far right of the spin chain agree, we observe,

$$\mathcal{P}\,|\Psi(p_1,p_2)\rangle_{ii} = S_{ii}(p_1,p_2)\,|\Psi(-p_1,-p_2)\rangle_{ii} \ . \tag{3.2.17}$$

The periodic boundary conditions imply the following Bethe equations, which were analyzed in [81],

$$e^{ip_a L} = S_{ii}(p_a,p_b) \qquad \text{for} \qquad a,b,i=1,2 \ \text{ and } \ a\neq b \ , \tag{3.2.18}$$

we will discuss them in detail in Section 3.8. Here, as a preparation for the next section, we take a detour to consider deforming the two-body CBA. We insert *contact terms* to the wave function which only play a role when the magnons are interacting, [82, 144],

$$\begin{aligned}|\Phi(p_1,p_2)\rangle_{11} = \sum_{l_1<l_2} \Big(&(A_{12} + D_{12}\,\delta(l_2,l_1+1))\, e^{ip_1 l_1 + ip_2 l_2} \\ &+ (A_{21} + D_{21}\,\delta(l_2,l_1+1))\, e^{ip_2 l_1 + ip_1 l_2}\Big)\, |l_1,l_2\rangle_{11} \ .\end{aligned} \tag{3.2.19}$$

As scattering coefficients, contact terms are functions of momentum variables. The eigenvalue problem imposes the following relations among scattering coefficients and contact terms,

$$\frac{A_{21}}{A_{12}} = S_\kappa(p_1,p_2) \ , \qquad\qquad D_{21} = -e^{ip_2 - ip_1} D_{12} \ . \tag{3.2.20}$$

Since the contact terms only become non-trivial for $l_2 = l_1 + 1$, we observe that the relation given above implies that the contribution from the contact terms vanishes. Although we can generalize the idea of the contact terms by replacing $D_{ij}\delta(l_2, l_1 + 1)$ with an infinite sum $\sum_n D^n_{ij}\delta(l_2, l_1 + n)$, the solution of the eigenvalue problem would still wash out the contact term contributions. Therefore, we state that the two-magnon eigenvector cannot be generalized by the contribution of the contact terms. This point was considered in depth in Appendix A of [1].

How CBA fails for the three-magnon problem. The eigenvalue problem for three magnons is a natural extension of the two-magnon case. We consider the eigenvalue problem,

$$\mathcal{H}\,|\Psi(p_1,p_2,p_3)\rangle = E_3(p_1,p_2,p_3)\,|\Psi(p_1,p_2,p_3)\rangle \ , \tag{3.2.21}$$

such that the eigenvalue of the three-magnon state is the sum of the energy eigenvalues for each momentum variable,

$$E_3(p_1, p_2, p_3) = E_1(p_1) + E_1(p_2) + E_1(p_3) \ . \tag{3.2.22}$$

The natural extension of the CBA to states with three excitations should naively have the following form,

$$|\varphi(p_1, p_2, p_3)\rangle_{12} = \sum_{l_1<l_2<l_3} \varphi_{12}(p_1, p_2, p_3; l_1, l_2, l_3)\, |l_1, l_2, l_3\rangle_{12} \ , \tag{3.2.23}$$

$$\varphi_{12}(p_1, p_2, p_3; l_1, l_2, l_3) = \left(\sum_{\sigma\in\mathcal{S}_3} A_\sigma \ e^{ip_{\sigma(1)}l_1 + ip_{\sigma(2)}l_2 + ip_{\sigma(3)}l_3} \right) \ . \tag{3.2.24}$$

Here, the wave function includes a sum over all elements of the symmetric group, $\mathcal{S}_3$.[6] The group elements can be represented as the possible permutations of the three momentum parameters. As in the case of one and two magnons, the momentum space vector is labeled by the indices of the ϕ states at the leftmost end of the spin chain, while the second index corresponds to the color of the ϕ states at the rightmost end of the spin chain. This is enough to fully characterize the color structure of the magnons, as the Q_{12} and Q_{21} states are arranged in alternating order. Additionally, there exists another state, $|\varphi(p_1, p_2, p_3)\rangle_{21}$, corresponding to the image of the state given in (3.2.23) under the action of $\mathbb{Z}_2$.

By using the CBA given in (3.2.23) we attempt to solve the three-magnon eigenvalue problem. We observe that the eigenvalue problem is immediately satisfied for well-separated magnons,

$$\langle l_1, l_2, l_3|\mathcal{H} - E_3|\varphi(p_1, p_2, p_3)\rangle = 0 \ , \quad \text{for all} \quad l_2 - l_1 > 1, \ l_3 - l_2 > 1 \ . \tag{3.2.25}$$

When two or more magnons are next to each other, we obtain a finite set of linear equations for the scattering coefficients A_σ. Here we consider the configurations that have only two interacting magnons and the third one is far away. For this ansatz (3.2.23), the equations associated with the configurations with three interacting magnons are a linear combination of the former. This is a feature of the CBA with factorized scattering coefficients. The two-magnon interacting equations fully fix the three-magnon scattering coefficients as products of two-magnon scattering coefficients. As a consequence, the three-magnon interacting equation does not add any new piece of information.

[6] In this article we denote the permutation $\sigma \in \mathcal{S}_3$ that maps $\sigma(1) = i$, $\sigma(2) = j$ and $\sigma(3) = k$ as the string (ijk). This notation differs from the cyclic notation, so it is important to avoid any confusion between the two. Composition of permutations is defined by the rule $(\tau\sigma)(i) = \tau(\sigma(i))$.

Depending on whether the pair of interacting magnons is located at the left or right of the third one,

$$\cdots \phi_1 Q_{12} Q_{21} \phi_1 \cdots \phi_1 Q_{12} \phi_2 \cdots \ , \qquad\qquad \cdots \phi_1 Q_{12} \phi_2 \cdots \phi_2 Q_{21} Q_{12} \phi_2 \cdots \ ,$$

the equations we obtain are different,

$$\begin{aligned} &\langle l_1, l_1+1, l_3 | \mathcal{H} - E_3 | \varphi(p_1,p_2,p_3) \rangle_{12} = e^{il_1(p_1+p_2+p_3)} \\ &\qquad \times \sum_{ij\in\{12,13,23\}} \left(A_{jik} a(p_i,p_j,\kappa) + A_{ijk} a(p_j,p_i,\kappa)\right) e^{i(l_3-l_1)p_k} \ , \end{aligned} \tag{3.2.26}$$

$$\begin{aligned} &\langle l_1, l_3-1, l_3 | \mathcal{H} - E_3 | \varphi(p_1,p_2,p_3) \rangle_{12} = e^{il_3(p_1+p_2+p_3)} \\ &\qquad \times \sum_{ij\in\{12,13,23\}} \left(A_{kji} a(p_i,p_j,\kappa^{-1}) + A_{kij} a(p_j,p_i,\kappa^{-1})\right) e^{i(l_1-l_3)(p_i+p_j)} \ , \end{aligned} \tag{3.2.27}$$

The function

$$a(p_1,p_2,\kappa) = 1 + e^{ip_1+ip_2} - 2\kappa e^{ip_1} \ , \tag{3.2.28}$$

is the denominator of the scattering coefficient given in (3.2.13). We assume that the scattering coefficients are independent of the coordinates of the magnons, meaning that each of the three terms of the sums in the previous equations has to separately vanish. We write these six equations in the matrix form,

$$\begin{pmatrix} a(p_3,p_2;1/\kappa) & a(p_2,p_3;1/\kappa) & 0 & 0 & 0 & 0 \\ a(p_2,p_1;\kappa) & 0 & a(p_1,p_2;\kappa) & 0 & 0 & 0 \\ 0 & a(p_3,p_1;\kappa) & 0 & 0 & a(p_1,p_3;\kappa) & 0 \\ 0 & 0 & a(p_3,p_1;1/\kappa) & a(p_1,p_3;\kappa) & 0 & 0 \\ 0 & 0 & 0 & a(p_3,p_2;\kappa) & 0 & a(p_2,p_3;\kappa) \\ 0 & 0 & 0 & 0 & a(p_2,p_1;1/\kappa) & a(p_1,p_2;1/\kappa) \end{pmatrix} \begin{pmatrix} A_{123} \\ A_{132} \\ A_{213} \\ A_{231} \\ A_{312} \\ A_{321} \end{pmatrix} = 0 \ . \tag{3.2.29}$$

We can check that the determinant of the matrix of coefficients does not vanish, implying that only the trivial solution exists. Therefore, the CBA given in (3.2.23) fails to provide a solution for the eigenvectors of the three-body eigenvalue problem, (3.2.21), (3.2.22) and (3.2.23).

We can understand the failure of the CBA from a different perspective. On one hand, solving the equations (3.2.26) implies that the scattering coefficients have to fulfill the relations

$$\frac{A_{213}}{A_{123}} = S_\kappa(p_1,p_2) \ , \qquad \frac{A_{312}}{A_{132}} = S_\kappa(p_1,p_3) \ , \qquad \frac{A_{321}}{A_{231}} = S_\kappa(p_2,p_3) \ . \tag{3.2.30}$$

On the other hand, we obtain the following relations between the scattering coefficients when we only solve (3.2.27),

$$\frac{A_{321}}{A_{312}} = S_{1/\kappa}(p_1, p_2) \ , \qquad \frac{A_{231}}{A_{213}} = S_{1/\kappa}(p_1, p_3) \ , \qquad \frac{A_{132}}{A_{123}} = S_{1/\kappa}(p_2, p_3) \ . \tag{3.2.31}$$

When we combine these results, the failure of the CBA can be mapped to the fact that the scattering coefficients of the CBA do not fulfill the YBE

$$S_\kappa(p_2, p_3)S_{1/\kappa}(p_1, p_3)S_\kappa(p_1, p_2) \neq S_{1/\kappa}(p_1, p_2)S_\kappa(p_1, p_3)S_{1/\kappa}(p_2, p_3) \ . \tag{3.2.32}$$

This observation was initially made in [81]. It becomes evident that this issue recurs for all higher numbers of magnons due to the permutation symmetric, factorizable nature of the CBA. It is clear that as long as we use a permutationally symmetric form for the eigenvector ansatz, the YBE will arise. The goal of this thesis is to present a systematic way to upgrade the factorization of the scattering coefficients which do not satisfy YBE so that they satisfy a form of YBE which resembles dynamical Yang–Baxter equation (DYBE) [137]. We will clarify this point of view further when we look for the special solution of the three-magnon problem and impose additional conditions to make the connection more precise in Section 3.3.2. Additionally, as detailly discussed in [1] adding finitely many contact terms does not resolve this problem.

To address this, in the next section, we introduce position-dependent corrections for every configuration in position space. Starting with the most general ansatz that preserves shift symmetry, we construct eigenvectors for the spectral problem with arbitrary momenta and $\kappa \in [0, 1]$. Furthermore, leveraging the symmetries of the model allows us to constrain the general form of the solution and investigate the spectrum of the spin chain model.

3.3 Three-Body Long-Range Solution

In this section, we develop a new technique to solve the three-magnon eigenvalue problem given in (3.2.21). As demonstrated in the previous section, CBA is not sufficient to diagonalize the Hamiltonian in the three-magnon sector. We therefore start from the most general ansatz for the wave function, including infinitely many long-range corrections, and progressively constrain this ansatz using the symmetries of the spin chain under study.

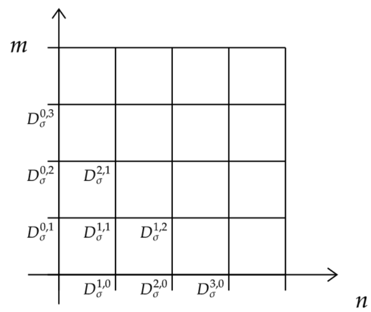

Figure 3.2: *The position-dependent corrections $D_\sigma^{n,m}$ are labeled by two integers, the distances between the three magnons, and thus naturally live on a two-dimensional lattice. They are also labeled by the permutations σ.*

Generalizing the CBA with position-dependent terms, we introduce an ansatz with an infinite number of corrections,

$$|\Psi(p_1,p_2,p_3)\rangle_{12} = \sum_{l_1<l_2<l_3} \Psi(p_1,p_2,p_3;l_1,l_2,l_3)\,|l_1,l_2,l_3\rangle_{12} \ , \tag{3.3.1}$$

with

$$\Psi(p_1,p_2,p_3;l_1,l_2,l_3) = \left(\sum_{\sigma\in S_3}\left(A_\sigma + D_\sigma^{l_2-l_1-1,l_3-l_2-1}\right)e^{i\vec{p}_\sigma\cdot\vec{l}}\right) \ . \tag{3.3.2}$$

We label all the scattering coefficients and the position-dependent corrections by permutations, σ, according to the order of the momentum variables that appear in the plane wave contributions. In this ansatz, we require the position-dependent corrections to be functions of the momenta, the parameter κ, and the distance between the excitations. Therefore, our ansatz includes infinitely many undetermined coefficients for each permutation which can be enumerated on a two-dimensional lattice for each permutation, together with six scattering coefficients A_σ. Since we consider infinite open spin chains without specifying boundary conditions, the corresponding two-dimensional lattice is $\mathbb{Z}^{\geq 0}\times\mathbb{Z}^{\geq 0}$, which is depicted in Figure 3.2. Notice also that the scattering coefficients can always be absorbed into the definition of the position-dependent corrections. We have instead decided to separate them and set the coefficients $D_\sigma^{0,0}=0$ to make the connection with the case of two magnons clearer. Additionally, the translational invariance of the wave function is equivalent to vanishing total momenta as it happens for the usual CBA, since the position-dependent corrections only depend on the relative distance.

When we substitute the ansatz (3.3.2) into the eigenvalue problem (3.2.21), we find three distinct classes of equations based on the relative positions of the excitations. As discussed in Section 3.2, these correspond to the cases where all the magnons are well separated, where only two magnons are interacting, and where all three magnons are interacting simultaneously. Unlike the usual CBA equations, the configurations where the magnons are well separated do not vanish immediately but instead provide an important constraint on the position-dependent coefficients, $D_\sigma^{n,m}$. Consequently, the separation of the three-magnon dispersion relation into the sum of three independent one-magnon dispersion relations (3.2.22) does not naturally arise from this particular ansatz. We therefore demand the eigenvalue to have an additive form and obtain a family of solutions for the eigenvector with the position-dependent corrections.

When the magnons are well separated, the eigenvalue problem is given as

$$\gamma(n,m) = \langle l_1, l_2, l_3 | \mathcal{H} - E_3 | \Psi(p) \rangle_{12} = 0 \,, \tag{3.3.3}$$

where $n = l_2 - l_1 - 1 > 0$ and $m = l_3 - l_2 - 1 > 0$. The explicit form of these *non-interacting equations* given by the wave function is, (3.3.2),

$$\begin{aligned}\gamma(n,m) = \left(3\kappa + \frac{3}{\kappa} - E_3\right) \Psi(p_1,p_2,p_3;l_1,l_2,l_3) - \Psi(p_1,p_2,p_3;l_1 \pm 1,l_2,l_3) \\ - \Psi(p_1,p_2,p_3;l_1,l_2 \pm 1,l_3) - \Psi(p_1,p_2,p_3;l_1,l_2,l_3 \pm 1) \,. \end{aligned} \tag{3.3.4}$$

It is useful to separate the coefficients that accompany the plane waves to distinguish the position dependence arising from the position-dependent corrections from that of the plane waves. Thus, the non-interacting equations (3.3.4) split as

$$\gamma(n,m) = \sum_{\sigma \in \mathcal{S}_3} \gamma_\sigma(p_1,p_2,p_3,n,m)\; e^{i(n+1)(p_{\sigma(2)}+p_{\sigma(3)}) + i(m+1)p_{\sigma(3)}} \,, \tag{3.3.5}$$

where we omit the overall plane wave contribution, $\exp(il_1(p_1+p_2+p_3))$. The term associated with the identity permutation takes the form

$$\begin{aligned}\gamma_{123}(n,m) = -e^{ip_1} D_{123}^{n-1,m} - e^{-ip_1} D_{123}^{n+1,m} - e^{-ip_3} D_{123}^{n,m-1} \\ +\varepsilon_3 D_{123}^{n,m} - e^{ip_3} D_{123}^{n,m+1} - e^{ip_2} D_{123}^{n+1,m-1} - e^{-ip_2} D_{123}^{n-1,m+1} \,. \end{aligned} \tag{3.3.6}$$

The remaining terms can be obtained from this expression by permuting the labels of the position-dependent corrections and momenta. In addition, we have introduced the symbol

$$\varepsilon_3 = 3\left(\kappa + \frac{1}{\kappa}\right) - E_3 = \sum_{j=1}^{3} \left(e^{ip_j} + e^{-ip_j}\right) \,, \tag{3.3.7}$$

which is closely related to the total energy of the three-magnon state, as it will appear at several points in our computations.

Similarly to the eigenvalue equations coming from the CBA, we impose that each γ_σ vanishes independently of the plane wave contributions. Therefore, for each permutation, we obtain a relation between the coefficients $D_\sigma^{n,m}$ with shifted position coordinates. These relations will be the base of the permutation symmetries of our solution.

When only two magnons are interacting, we obtain the *two-magnon interaction* equations. Then we must distinguish whether the interacting pair is positioned to the left or right of the third magnon. For the case where the pair of interacting magnons is on the left of the spin chain, we have

$$\beta_l(m) = \langle l_1, l_1+1, l_3|\mathcal{H} - E_3|\Psi(p_1,p_2,p_3)\rangle_{12} = 0 \;, \tag{3.3.8}$$

for all $m = l_3 - l_2 - 1 > 0$. In terms of the wave functions the projection of the eigenvalue problem to the position space takes the following form,

$$\begin{aligned}\beta_l(m) = \left(\kappa + \frac{3}{\kappa} - E_3\right)\Psi(p_1,p_2,p_3;l_1,l_1+1,l_3) - \Psi(p_1,p_2,p_3;l_1-1,l_1+1,l_3)\\ - \Psi(p_1,p_2,p_3;l_1,l_1+2,l_3) - \Psi(p_1,p_2,p_3;l_1,l_1+1,l_3\pm 1)\;.\end{aligned} \tag{3.3.9}$$

For the case where the pair of interacting magnons is on the right, we have

$$\beta_r(n) = \langle l_1, l_3-1, l_3|\mathcal{H} - E_3|\Psi(p_1,p_2,p_3)\rangle_{12} = 0 \;, \tag{3.3.10}$$

for all $n = l_2 - l_1 - 1 > 0$. Similarly to the previous case, this expression takes the form,

$$\begin{aligned}\beta_r(n) = \left(3\kappa + \frac{1}{\kappa} - E_3\right)\Psi(p_1,p_2,p_3;l_1,l_3-1,l_3) - \Psi(p_1,p_2,p_3;l_1\pm 1,l_3-1,l_3)\\ - \Psi(p_1,p_2,p_3;l_1,l_3-2,l_3) - \Psi(p_1,p_2,p_3;l_1,l_3-1,l_3+1)\;.\end{aligned} \tag{3.3.11}$$

When we compare the left two-magnon interacting equations to the right, we can observe that they are related by the $\mathbb{Z}_2$ symmetry (3.1.20). Recall that the action of $\mathbb{Z}_2$ symmetry exchanges κ with $\frac{1}{\kappa}$ as well as Q_{12} with Q_{21}. Looking at the pair of interacting magnons, the $\mathbb{Z}_2$ action would map the left two-magnon interacting pair to a right pair, but with the third magnon in the wrong position. By combining $\mathbb{Z}_2$ transformation with the action of parity operator, we can explicitly obtain (3.3.10) from (3.3.8) and vice versa. This is closely related to the observation about the restored parity invariance of one-magnon states, (3.2.7). After presenting all the equations, we will come back to this point.

We now follow the same steps as for the non-interacting equations. We substitute the ansatz (3.3.2), decompose these equations into separate terms distinguished by the plane wave factors, and require that each term vanishes independently. In contrast to the non-interacting equations, one of the relative distances between magnons is set to zero, which implies that these equations can be split into three contributions instead of six. In particular, we have

$$\beta_l(m) = \beta_{l,(12)}(m)e^{i(m+2)p_3} + \beta_{l,(13)}(m)e^{i(m+2)p_2} + \beta_{l,(23)}(m)e^{i(m+2)p_1} \ , \tag{3.3.12}$$

where we omit the overall plane wave contribution, $\exp(il_1(p_1+p_2+p_3))$ and the first coefficient in the sum is given as

$$\begin{aligned}\beta_{l,(12)}(m) = & A_{123}\ a(p_2,p_1,\kappa) + A_{213}\ a(p_1,p_2,\kappa) \\ & - e^{-ip_3}\left(e^{ip_1}D_{213}^{0,m-1} + e^{ip_2}D_{123}^{0,m-1}\right) - e^{ip_3}\left(e^{ip_1}D_{213}^{0,m+1} + e^{ip_2}D_{123}^{0,m+1}\right) \\ & - e^{-ip_1-ip_2}\left(e^{2ip_1}D_{213}^{1,m} + e^{2ip_2}D_{123}^{1,m}\right) - \left(e^{2ip_1}D_{213}^{1,m-1} + e^{2ip_2}D_{123}^{1,m-1}\right) \\ & + (\varepsilon_3 - 2\kappa)\left(e^{ip_1}D_{213}^{0,m} + e^{ip_2}D_{123}^{0,m}\right) \ ,\end{aligned} \tag{3.3.13}$$

where the function $a(p_1,p_2,\kappa) = 1 + e^{ip_1+ip_2} - 2\kappa e^{ip_1}$ is defined in equation (3.2.28). Here we label our equations using $(ij) \in \{(12),(13),(23)\}$, as we only have to keep track of these transpositions. The remaining expressions coming from the left two-magnon interacting equation can be obtained by permuting the labels of momentum variables as well as the undetermined coefficients. Concerning these transpositions, both the scattering coefficients and the position-dependent corrections contribute in pairs.

Similarly, the two-magnon interacting equation from the right splits as

$$\beta_r(n) = \beta_{r,(12)}(n)e^{i(p_1+p_2)(n+1)} + \beta_{r,(13)}(n)e^{i(p_1+p_3)(n+1)} + \beta_{r,(23)}(n)e^{i(p_2+p_3)(n+1)} \ , \tag{3.3.14}$$

with

$$\begin{aligned}\beta_{r,(12)}(n) = & A_{312}\ a(p_2,p_1,\kappa^{-1}) + A_{321}\ a(p_1,p_2,\kappa^{-1}) \\ & - e^{ip_3}\left(e^{ip_1}D_{321}^{n-1,0} + e^{ip_2}D_{312}^{n-1,0}\right) - e^{-ip_3}\left(e^{ip_1}D_{321}^{n+1,0} + e^{ip_2}D_{312}^{n+1,0}\right) \\ & - \left(e^{2ip_1}D_{321}^{n,1} + e^{2ip_2}D_{312}^{n,1}\right) - e^{-ip_1-ip_2}\left(e^{2ip_1}D_{321}^{n-1,1} + e^{2ip_2}D_{312}^{n-1,1}\right) \\ & + \left(\varepsilon_3 - 2\kappa^{-1}\right)\left(e^{ip_1}D_{321}^{n,0} + e^{ip_2}D_{312}^{n,0}\right) \ ,\end{aligned} \tag{3.3.15}$$

where we omit the overall plane wave contribution as before. Compared to the two-body interacting equations derived from the usual CBA, given in (3.2.30) and (3.2.31), these equations are corrected by the contributions of the position-dependent corrections. In contrast with the case of the CBA with contact terms, discussed in detail in Appendix A in [1], this infinite tower of corrections cannot be fully washed out. This strongly indicates that the failure of the YBE (3.2.32), which originates from the two-magnon interacting equations of CBA given in (3.2.29), will not be an obstruction to obtaining a solution. Because of the additional degrees of freedom in the form of position-dependent corrections, these two-magnon interacting equations β_r and β_l admit non-trivial solutions for the scattering coefficients and the position-dependent corrections.

In the case where the three magnons are next to each other, we have an expression that is free of position variables,

$$\alpha = \langle l_1, l_1+1, l_1+2|\mathcal{H} - E_3|\Psi(p_1,p_2,p_3)\rangle_{12} = 0 \ , \tag{3.3.16}$$

where

$$\begin{aligned}\langle l_1, l_1+1, l_1+2|\mathcal{H} - E_3|\Psi(p_1,p_2,p_3)\rangle_{12} &= \left(\kappa + \frac{1}{\kappa} - E_3\right)\Psi(p_1,p_2,p_3;l_1,l_1+1,l_1+2) \\ - \Psi(p_1,p_2,p_3;l_1-1,l_1+1,l_1+2) &- \Psi(p_1,p_2,p_3;l_1,l_1+1,l_1+3) \ .\end{aligned} \tag{3.3.17}$$

The explicit form of the *three-magnon interacting equation* up to an overall plane wave contribution, $\exp(il_1(p_1+p_2+p_3))$, is given by

$$\begin{aligned}\alpha(p_1,p_2,p_3) = \sum_{\sigma\in S_3} \Big[&\Big(\kappa + \frac{1}{\kappa} - E_3 - e^{ip_{\sigma(3)}} - e^{-ip_{\sigma(1)}}\Big)A_\sigma \\ &- e^{-ip_{\sigma(1)}}D_\sigma^{1,0} - e^{ip_{\sigma(3)}}D_\sigma^{0,1}\Big]e^{i(p_{\sigma(2)}+2p_{\sigma(3)})} \ .\end{aligned} \tag{3.3.18}$$

This equation completes the list of the equations that are coming from the eigenvalue problem.

Because we are working with open infinitely long spin chains, these three types of equations imply an infinite-dimensional linear system of equations. Since the interacting equations mix the position-dependent corrections with different permutations, we have a single highly interwoven system of equations. To reveal the underlying structure, we pay close attention to the symmetries of the spin chain model. After analyzing the consequences of parity and $\mathbb{Z}_2$ symmetry, we solve the eigenvalue problem in a specific order to capture the residual permutation symmetry of our long-range ansatz.

Parity and $\mathbb{Z}_2$ symmetry. We study the conditions imposed on the long-range ansatz for it to satisfy the analogous parity relation with the one-magnon eigenstate

(3.2.7). Although we only discuss the equations coming from the eigenvalue problem for one of the two possible three-magnon states, $|\Psi(p_1, p_2, p_3)\rangle_{12}$, the $\mathbb{Z}_2$ conjugate of this state exists, and it satisfies the eigenvalue equation (3.2.21),

$$\mathbb{Z}_2 \, |\Psi(p_1, p_2, p_3)\rangle_{12} = |\Psi(p_1, p_2, p_3)\rangle_{21} \ . \tag{3.3.19}$$

This implies that the entire wave function of the eigenvector, $|\Psi(p_1, p_2, p_3)\rangle_{21}$ should be the $\kappa \to 1/\kappa$ version of the wave functions of the state, $|\Psi(p_1, p_2, p_3)\rangle_{12}$, as given in (3.3.1). Indeed, this can be realized by looking at the eigenvalue problem for the three-magnon state whose magnons appear in the order $Q_{21}Q_{12}Q_{21}$. We observe that the form of the non-interacting equations is the same for both sets of position-dependent corrections because the expressions given in (3.3.6) do not include explicit dependence on the κ parameter. Additionally, the three-magnon interacting equation given in (3.3.18) is invariant under the $\kappa \to 1/\kappa$ transformation, therefore the coefficients of the eigenstate $|\Psi(p_1, p_2, p_3)\rangle_{21}$ also satisfy the same three-magnon interacting equation. However, the two-magnon interacting equations (3.3.13) and (3.3.15) significantly change under the $\mathbb{Z}_2$ transformation. Hence, both scattering coefficients and the position-dependent corrections of the $\mathbb{Z}_2$ pair state have the form,

$$\langle l_1, l_2, l_3 | \Psi(p_1, p_2, p_3)\rangle_{21} = \sum_{\sigma \in S_3} \left(A_\sigma(p, 1/\kappa) + D_\sigma^{l_2 - l_1 - 1, l_3 - l_2 - 1}(p, 1/\kappa) \right) e^{i \vec{p}_\sigma \cdot \vec{l}} \ . \tag{3.3.20}$$

Therefore, finding a solution for the $|\Psi\rangle_{12}$ state automatically gives a solution for the $|\Psi\rangle_{21}$ state. Moreover, when we consider the action of the parity, we obtain

$$\begin{aligned} &\mathcal{P} \, |\Psi(p_1, p_2, p_3)\rangle_{12} \\ &\quad = \sum_{-l_3 < -l_2 < -l_1} \left(\sum_{\sigma \in S_3} \left(A_\sigma(p, \kappa) + D_\sigma^{l_2 - l_1 - 1, l_3 - l_2 - 1}(p, \kappa) \right) e^{i \vec{p}_\sigma \cdot \vec{l}} \right) |{-l_3}, -l_2, -l_1\rangle_{21} \ . \end{aligned} \tag{3.3.21}$$

Although the state that is obtained by the action of the parity operator is not necessarily an eigenvector of the Hamiltonian, we can consider a parity-like operator as for the one-magnon state, (3.2.7) using the action of $\mathbb{Z}_2$. The $\mathbb{Z}_2\mathcal{P}$ symmetry only maps momentum variables $p \to -p$ while leaving the color indices invariant as in (3.2.7) if there exists a three-magnon eigenstate whose wave function includes the scattering coefficients $\hat{A}_\sigma(p, \kappa)$ and position-dependent corrections $\hat{D}_\sigma^{n,m}(p, \kappa)$ such that the coefficients of the initial eigenstate $|\Psi\rangle_{12}$ satisfy the following relations,

$$A_\sigma(p, \kappa) = e^{i\varphi(p,\kappa)} \hat{A}_{\sigma^r}(-p, 1/\kappa) \ , \qquad D_\sigma^{n,m}(p, \kappa) = e^{i\varphi(p,\kappa)} \hat{D}_{\sigma^r}^{m,n}(-p, 1/\kappa) \ , \tag{3.3.22}$$

	Equations	Undetermined coefficients
Minimum Separation	$\alpha=0,\ \beta_{l,(ij)}(1)=0,\ \beta_{r,(ij)}(1)=0$	$A_\sigma,\ D_\sigma^{1,0},\ D_\sigma^{0,1},\ D_\sigma^{2,0},\ D_\sigma^{1,1},\ D_\sigma^{0,2}$
All Separation	$\gamma_\sigma(n,m)=0$ $\beta_{l,(ij)}(m+1)-\beta_{l,(ij)}(m)=0$ $\beta_{r,(ij)}(n+1)-\beta_{r,(ij)}(n)=0$	$D_\sigma^{n,m}$ for $n,m\geq 2$ $D_\sigma^{n,m}$ for $m\geq 2$ and $n=0,1$ $D_\sigma^{n,m}$ for $m=0,1$ and $n\geq 2$

Table 3.1: *Summary of the method, we list the equations coming from the eigenvalue problem and the undetermined coefficients that appear in these equations.*

where for $\sigma=(ijk)$ the reflection of the permutation index is denoted by $\sigma^r=(kji)$. We explicitly show the existence of two eigenvectors that satisfy these relations in Section 3.3.2. The overall phase factor $e^{i\varphi(p,\kappa)}$ is incorporated into these relations to avoid over-restricting the solution space for the coefficients of the three-magnon state. If the two eigenvectors whose coefficients satisfy the given relations (3.3.22) coincide, then we obtain,

$$\mathbb{Z}_2\mathcal{P}\,|\Psi(p_1,p_2,p_3)\rangle_{12}=e^{i\varphi(p,\kappa)}\,|\Psi(-p_1,-p_2,-p_3)\rangle_{12}\ . \tag{3.3.23}$$

Furthermore, applying parity twice should give us back the original state, so the phase has to satisfy $e^{i\varphi(p,\kappa)}e^{i\varphi(-p,\kappa^{-1})}=1$. We conclude the discussion on the symmetries of the model by emphasizing that the operator $(\mathbb{Z}_2)^M\mathcal{P}$ successfully replaces the role of the parity operator for any number M of Q's on a spin chain. Under the conditions given in (3.3.22), the solution of the long-range three-magnon state is consistent with the symmetry which was given in (3.2.7).

3.3.1 The Most General Solution

Our strategy to solve these equations is depicted in Table 3.1 and is as follows. We separate the expressions coming from the eigenvalue problem into two classes. The first class of equations consists of the minimum separation equations and does not involve any free position variables, and we use them to obtain the scattering coefficients of the model. Therefore, the first class includes the interacting equations with minimum separation, listed as

$$\alpha(p_1,p_2,p_3)=0\ ,\qquad \beta_{l,(ij)}(1)=0\ ,\qquad \beta_{r,(ij)}(1)=0\ , \tag{3.3.24}$$

for all transpositions of $\mathcal{S}_3$, denoted as (ij), which are referring to the pieces of the two-magnon interacting equations as presented in (3.3.12) and (3.3.14). These seven equations are mainly used to determine the scattering coefficients, A_σ, up to an overall normalization which is unspecified in the form of the coefficient A_{123}. Together with the five scattering coefficients, we should fix at least two of the position-dependent corrections to ensure that all seven equations are solved.

The remaining equations constitute the second class of equations. They give us recurrence relations for the position-dependent corrections, $D_\sigma^{n,m}$. We can separate the eigenvalue problem for position-dependent corrections from the scattering coefficients by considering the difference of two successive two-body equations. Thus, for $n, m \geq 1$, we will solve the equations

$$\gamma_\sigma(n,m) = 0 \ , \qquad \beta_{l,(ij)}(n+1) - \beta_{l,(ij)}(n) = 0 \ , \qquad \beta_{r,(ij)}(n+1) - \beta_{r,(ij)}(n) = 0 \ , \tag{3.3.25}$$

such that $\sigma \in \mathcal{S}_3$ and (ij) are the distinct permutations. These equations, together with (3.3.24), span the infinite linear system of equations for the scattering coefficients and the corrections. By dividing the set of two-magnon interacting equations into two subsets, which we refer to as the first and second class, we achieve an upper-triangular form for the infinite-dimensional system of equations which include all the two-magnon interacting eigenvalue equations and this will simplify the process of solving the two-magnon interacting equations drastically.

In the following we show that the solution of the position-dependent corrections coming from the minimum separation expressions is the initial conditions for the recursion relations in the second class. Furthermore, the relations coming from the two-body interacting equations are the initial conditions of the non-interacting type equations. Therefore, we start solving the eigenvalue problem from the non-interacting equations. After acquiring the most general set of position-dependent corrections that solve the non-interacting equations, we move on to the two-body interacting recurrence relations and incorporate these relations into the non-interacting ones. Finally, we present the most general way to solve the minimum separation equations before taking advantage of the large set of undetermined coefficients and obtaining distinct subfamilies of the three-magnon eigenvectors, which admit interesting physical interpretations.

Solving the non-interacting equations. We start from the non-interacting equations, which we solve via the generating function method. We introduce a complex two-variable function whose Taylor expansion around $(0,0)$ gives us the position-dependent corrections for each permutation,

$$G_\sigma(x,y) = \sum_{n,m=0}^{\infty} D_\sigma^{n,m}(p_1,p_2,p_3;\kappa) x^n y^m \ . \tag{3.3.26}$$

The non-interacting equations, $\gamma_\sigma(n,m)=0$, can then be used to manipulate the initial form of the generating function. First, we refine the position-dependent corrections to get rid of a universal factor in all eigenvalue problem expressions,

$$\tilde{D}^{n,m}_\sigma = e^{-inp_{\sigma(1)}+imp_{\sigma(3)}} D^{n,m}_\sigma \ . \tag{3.3.27}$$

The solution of the non-interacting equations for each permutation is encoded in the closed form of the generating function,

$$\begin{aligned} G_\sigma(e^{-ip_{\sigma(1)}}x, e^{ip_{\sigma(3)}}y) = g_{1,\sigma}(x) + g_{3,\sigma}(y) - \frac{e^{-i\mathcal{P}}x^2y\tilde{D}^{0,1}_\sigma + e^{i\mathcal{P}}xy^2\tilde{D}^{1,0}_\sigma}{Q_3(x,y)} \\ + \frac{e^{i\mathcal{P}}y^2\left(1+e^{-i\mathcal{P}}x\right)}{Q_3(x,y)}g_{1,\sigma}(x) + \frac{e^{-i\mathcal{P}}x^2\left(1+e^{i\mathcal{P}}y\right)}{Q_3(x,y)}g_{3,\sigma}(y) \\ - \frac{xy\left(1+e^{-i\mathcal{P}}x\right)}{Q_3(x,y)}g_{2,\sigma}(x) - \frac{xy\left(1+e^{i\mathcal{P}}y\right)}{Q_3(x,y)}g_{4,\sigma}(y) \ , \end{aligned} \tag{3.3.28}$$

The scaled variables transform the coefficients of generating function from D_σ into $\tilde{D}_\sigma$. Additionally, after the scaling, the denominator $Q_3(x,y)$ which is a third-order polynomial of two variables includes only two coefficients, ε_3 as given in (3.3.7) and exponential of total momentum, $e^{i\mathcal{P}}$,

$$Q_3(x,y) = \varepsilon_3 xy - e^{-i\mathcal{P}}x^2 - e^{i\mathcal{P}}y^2 - x - y - x^2y - y^2x \ . \tag{3.3.29}$$

Vanishing of this polynomial defines an elliptic curve which we use to understand the solution of the non-interacting equations better.[7] The functions $g_{i,\sigma}$ are generating functions that consist of a particular subset of position-dependent corrections. These are not fixed by the non-interacting equations and they are defined as follows,

$$g_{1,\sigma}(x) = \sum_{n=1}^{\infty} \tilde{D}^{n,0}_\sigma x^n \ , \tag{3.3.30}$$

$$g_{2,\sigma}(x) = \sum_{n=1}^{\infty} \tilde{D}^{n,1}_\sigma x^n \ , \tag{3.3.31}$$

$$g_{3,\sigma}(y) = \sum_{m=1}^{\infty} \tilde{D}^{0,m}_\sigma y^m \ , \tag{3.3.32}$$

$$g_{4,\sigma}(y) = \sum_{m=1}^{\infty} \tilde{D}^{1,m}_\sigma y^m \ . \tag{3.3.33}$$

[7] This can be checked by bringing it into its Weierstrass form, which has non-vanishing discriminant and J-invariant for generic values of ε_3 and $e^{i\mathcal{P}}$.

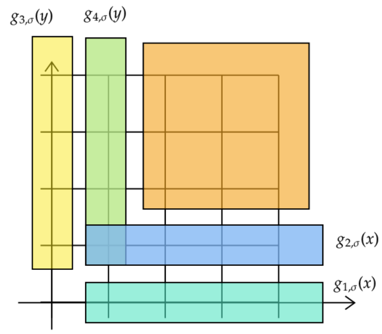

Figure 3.3: *Imposing non-interacting recurrence relations gives us all position-dependent corrections colored with orange, in terms of the rest. The analyticity condition further gives the solution of the position-dependent corrections. Depending on the choice of parametrization either $g_{2,\sigma}$ or $g_{4,\sigma}$, colored in blue and green respectively, is given by analyticity.*

Thus, solving the non-interacting equations reduces the number of undetermined coefficients from a two-dimensional lattice parameterized by positive integers $\mathbb{Z}^{>0} \times \mathbb{Z}^{>0}$, to the boundaries $\{0,1\} \times \mathbb{Z}^{>0}$ and $\mathbb{Z}^{>0} \times \{0,1\}$ of that lattice for each permutation. This is depicted in Figure 3.3. We should also stress that the scaling of the position-dependent corrections, given in (3.3.27), together with the re-scaling of the variables x and y, allows us to write the generating functions G_σ only in terms of energy ε_3 and total momentum $e^{i\mathcal{P}}$. Consequently, the resulting form of the generating function (3.5.33) is exactly the same for each permutation, up to the four undetermined one-variable generating functions, $g_{i,\sigma}$. This implies that it is symmetric in terms of permutations of the indices.

At first glance, the form of the generating function (3.5.33) implies that all one-variable generating functions defined in (3.3.30)-(3.3.33) are undetermined. The rest of the position-dependent corrections for $n, m \geq 2$ can be obtained by taking the derivatives with respect to the generating function,

$$\tilde{D}_\sigma^{n,m} = \lim_{x,y \to 0} \frac{1}{n!m!} \partial_x^{(n)} \partial_y^{(m)} G_\sigma(e^{-ip_{\sigma(1)}}x, e^{ip_{\sigma(3)}}y) \ . \tag{3.3.34}$$

After closer inspection, we observe that the functions (3.3.30)-(3.3.33) cannot be completely independent. The analyticity of the generating function (3.5.33) is not guaranteed for four independent functions, $g_{i,\sigma}$. Equivalently, we observe that the limit that appears in equation (3.3.34) does not exist from every direction on the complex plane for four independent one-variable generating functions. As a consequence, we must require that the numerator of the generating function given in (3.5.33) vanishes on the algebraic curve defined by $Q_3(x,y) = 0$; that is[8]

$$\begin{aligned}\Big[& y(1+e^{-i\mathcal{P}}x)\left(e^{i\mathcal{P}}y g_{1,\sigma}(x) - x g_{2,\sigma}(x)\right) \\ & \quad + x(1+e^{i\mathcal{P}}y)\left(e^{-i\mathcal{P}}x g_{3,\sigma}(y) - y g_{4,\sigma}(y)\right) \\ & \qquad\qquad - xy\left(e^{-i\mathcal{P}}x\tilde{D}^{0,1}_{\sigma} + e^{i\mathcal{P}}y\tilde{D}^{1,0}_{\sigma}\right)\Big]_{Q_3(x,y)=0} = 0\ . \end{aligned} \tag{3.3.35}$$

Once we ensure that this condition of the elliptic curve that includes the origin, $(x,y) = (0,0)$ is satisfied, under the assumption that one-variable generating functions also have positive radius of convergence, the limit (3.3.34) exists on a disc around $(0,0)$ and we can extract the position-dependent corrections. The convergence of the one-variable generating functions is an independent discussion, since they are not determined at this point. To explicitly state the analyticity condition over the four one-variable generating functions given in (3.3.30)-(3.3.33) we factorize the elliptic curve as follows. Here, p denotes the dependence on the momentum variables, p_i all together. The functions $\rho_\pm$ parametrize the two different sheets of the elliptic curve on the complex plane. We explicitly show the dependence of $\rho_\pm$ on the momentum variables because we want to make use of the property,

$$Q_3(x,y) = (x-\rho_+(y,p))(x-\rho_-(y,p)) = (y-\rho_+(x,-p))(y-\rho_-(x,-p))\ , \tag{3.3.36}$$

which is the consequence of the relation, $Q_3(x,y) = \Big[Q(y,x)\Big]_{p_i\to -p_i}$ for all momentum variables. Employing the symmetric form of the non-interacting equations, we will obtain a highly symmetric solution of the two-magnon interacting equations. Since we are only interested in the Taylor expansion around the origin, we only consider the relation coming from the curve ρ_+, as the curve $(\rho_-(y,p),y)$ does not contain the origin.[9] Hence, we can derive an explicit relation from the analyticity condition, (3.3.35),[10]

$$g_{4,\sigma}(y) = \frac{\rho_+(y,p)}{e^{i\mathcal{P}}y} g_{3,\sigma}(y) + \frac{1+e^{-i\mathcal{P}}\rho_+(y,p)}{1+e^{i\mathcal{P}}y}\left[\frac{e^{i\mathcal{P}}y}{\rho_+(y,p)} g_{1,\sigma}(\rho_+(y,p)) - g_{2,\sigma}(\rho_+(y,p))\right]$$

[8] We do not need to impose a stronger condition on the numerator because the denominator $Q_3(x,y)$ only generates a simple pole at $(0,0)$.

[9] This statement is highly dependent on which branch we choose. For $-\pi < \sum_i p_i < \pi$ we use the positive branch of the square root. Essentially, it is sufficient to consider one of the curves $(\rho_\pm(y,p),y)$ depending on the choice of the branch and this can be checked by comparing the analyticity relation, (3.3.35) to the existence of the limit conditions for any n,m given in (3.3.34).

[10] When we restate this equation in terms of position-dependent corrections, we can see that each coefficient of the Taylor expansion in y is a linear combination of the non-interacting equations $\gamma_\sigma(n,m)$. Thus, the analyticity condition (3.3.35) is not a spurious equation, but it captures a linear combination of the non-interacting equations that are not naively captured in $G_\sigma(x,y)$.

$$-\frac{e^{-i\mathcal{P}}\rho_+(y,p)}{1+e^{i\mathcal{P}}y}\tilde{D}^{0,1}_\sigma - \frac{e^{i\mathcal{P}}y}{1+e^{i\mathcal{P}}y}\tilde{D}^{1,0}_\sigma \ . \tag{3.3.37}$$

This expression reduces the number of undetermined position-dependent corrections given in the form of four one-variable generating functions, (3.3.30)-(3.3.33) by one for each permutation. Provided the one-variable generating functions are holomorphic, the final form of the generating function is holomorphic around $(0,0)$, given as

$$\begin{aligned}
G^\gamma_\sigma(e^{-ip_{\sigma(1)}}x, e^{ip_{\sigma(3)}}y) =& -\frac{e^{-i\mathcal{P}}xy(x-\rho_+(y,p))\tilde{D}^{0,1}_\sigma}{Q_3(x,y)} \\
&+ \frac{\varepsilon_3 xy - e^{-i\mathcal{P}}x^2 - x - y - x^2 y}{Q_3(x,y)} g_{1,\sigma}(x) - \frac{xy^2\left(1+e^{i\mathcal{P}}\rho_+(y,p)^{-1}\right)}{Q_3(x,y)} g_{1,\sigma}(\rho_+(y,p)) \\
&+ \frac{\varepsilon_3 xy - e^{i\mathcal{P}}y^2 - x - y - y^2 x - e^{-i\mathcal{P}}x\rho_+(y,p)\left(1+e^{i\mathcal{P}}y\right)}{Q_3(x,y)} g_{3,\sigma}(y) \\
&- \frac{xy\left(1+e^{-i\mathcal{P}}x\right)}{Q_3(x,y)} g_{2,\sigma}(x) + \frac{xy\left(1+e^{-i\mathcal{P}}\rho_+(y,p)\right)}{Q_3(x,y)} g_{2,\sigma}(\rho_+(y,p)) \ .
\end{aligned} \tag{3.3.38}$$

Here we use the superscript γ to distinguish the generating function which satisfies the analyticity condition, and therefore solves all the non-interacting equations coming from the eigenvalue problem. On the other hand, by using the second parametrization given in (3.3.36), we could write the analyticity relation as

$$\begin{aligned}
g_{2,\sigma}(x) =& \frac{\rho_+(x,-p)}{e^{-i\mathcal{P}}x} g_{1,\sigma}(x) + \frac{1+e^{i\mathcal{P}}\rho_+(x,-p)}{1+e^{-i\mathcal{P}}x}\left[\frac{e^{-i\mathcal{P}}x}{\rho_+(x,-p)} g_{3,\sigma}(\rho_+(x,-p)) - g_{4,\sigma}(\rho_+(x,-p))\right] \\
&- \frac{e^{-i\mathcal{P}}x}{1+e^{-i\mathcal{P}}x}\tilde{D}^{0,1}_\sigma - \frac{e^{i\mathcal{P}}\rho_+(x,-p)}{(1+e^{-i\mathcal{P}}x)}\tilde{D}^{1,0}_\sigma \ .
\end{aligned} \tag{3.3.39}$$

Then, the form of the generating function after imposing the analyticity condition would slightly differ, but it is equivalent to the one presented in (3.3.38),

$$\begin{aligned}
G^\gamma_\sigma(e^{-ip_{\sigma(1)}}x, e^{ip_{\sigma(3)}}y) =& -\frac{e^{i\mathcal{P}}xy\left(y-\rho_+(x,-p)\right)\tilde{D}^{1,0}_\sigma}{Q_3(x,y)} \\
&+ \frac{\varepsilon_3 xy - e^{-i\mathcal{P}}x^2 - x - y - x^2 y - e^{i\mathcal{P}}\rho_+(x,-p)y\left(1+e^{-i\mathcal{P}}x\right)}{Q_3(x,y)} g_{1,\sigma}(x) \\
&+ \frac{\varepsilon_3 xy - e^{i\mathcal{P}}y^2 - x - y - y^2 x}{Q_3(x,y)} g_{3,\sigma}(y) - \frac{x^2 y\left(1+e^{-i\mathcal{P}}\rho_+(x,-p)^{-1}\right)}{Q_3(x,y)} g_{3,\sigma}(\rho_+(x,-p)) \\
&- \frac{xy\left(1+e^{i\mathcal{P}}y\right)}{Q_3(x,y)} g_{4,\sigma}(y) + \frac{xy\left(1+e^{i\mathcal{P}}\rho_+(x,-p)\right)}{Q_3(x,y)} g_{4,\sigma}(\rho_+(x,-p)) \ ,
\end{aligned} \tag{3.3.40}$$

This is exactly the parity transform of the (3.3.38). Since we are only solving the non-interacting equations which do not have any explicit κ dependence, the action of parity, as given in (3.3.21), transforms to the following map at the level of generating functions, $\{D_\sigma^{n,m}, x, y, p\} \leftrightarrow \{D_\sigma^{m,n}, y, x, -p\}$. However, solving the interacting equations breaks this property, resulting in the overall solution of the long-range Bethe ansatz lacking parity symmetry. Similarly, the two parametrizations of the elliptic curve given in (3.3.36) are a result of this relation. Furthermore, this is a subset of the operations in which we need to map the left two-magnon interacting equations to the right two-magnon interacting equations. This is given in (3.3.48). In addition to the $\kappa \to 1/\kappa$ transformation, we also do not see the reflection of the permutations, as the generating functions that solve the non-interacting equations are invariant under the permutation of momentum indices.

The resulting form of the generating function, (3.3.38) and (3.3.40) will be altered once more when we solve the two-magnon interacting equations. At this point, the solution of any position-dependent corrections, $D_\sigma^{n,m}$ for $n, m \geq 2$ are given as a linear combination of undetermined coefficients, encoded in $g_{i,\sigma}$ for $i = 1, 2, 3$ or $i = 1, 3, 4$ and the factors in front of the undetermined position-dependent corrections are only powers and linear combinations of $e^{i\mathcal{P}}$ and ε_3. Furthermore, the generating function satisfies a very simple partial differential equation which remains to be explored

$$\partial_x^2 \partial_y^2 \left(Q_3(x, y) G_\sigma^\gamma(x, y) \right) = 0 \; . \tag{3.3.41}$$

for each permutation, σ.

Solving the two-magnon interacting equations. We move on to solve the two-body interacting equations given in the form of difference equations,

$$\beta_{l,(ij)}(m+1) - \beta_{l,(ij)}(m) = 0 \; , \tag{3.3.42}$$

$$\beta_{r,(ij)}(n+1) - \beta_{r,(ij)}(n) = 0 \; , \tag{3.3.43}$$

for all $n, m \geq 1$ and all transpositions of $\mathcal{S}_3$. Using the method of generating functions, these difference equations are transformed into equations involving the generating functions for the undetermined position-dependent coefficients encoded in $g_{i,\sigma}$. We can recast all three of the two-magnon interacting recursion relations from the left, (3.3.42), into the following expression

$$\begin{aligned}\left(e^{ip_1} g_{3,213}(y) + e^{ip_2} g_{3,123}(y)\right) \left(2\kappa - \varepsilon_3 + \frac{1}{y} + y\right) \\ + \left(e^{ip_1} g_{4,213}(y) + e^{ip_2} g_{4,123}(y)\right) \left(1 + e^{i\mathcal{P}} y\right) = C_{12}(y) \; ,\end{aligned} \tag{3.3.44}$$

such that the position-dependent corrections that are left out of the one-variable generating functions are absorbed into the following function

$$
\begin{aligned}
C_{12}(y) = &\left(e^{ip_1}\tilde{D}^{0,1}_{213} + e^{ip_2}\tilde{D}^{0,1}_{123}\right) - y e^{i\mathcal{P}}\left(e^{ip_1}\tilde{D}^{1,0}_{213} + e^{ip_2}\tilde{D}^{1,0}_{123}\right) \\
&+ \frac{y}{1-e^{ip_3}y}\Big[\left(e^{ip_1}\tilde{D}^{0,2}_{213} + e^{ip_2}\tilde{D}^{0,2}_{123}\right) + \left(e^{ip_1}\tilde{D}^{1,1}_{213} + e^{ip_2}\tilde{D}^{1,1}_{123}\right) \\
&+ e^{i\mathcal{P}}\left(e^{ip_1}\tilde{D}^{1,0}_{213} + e^{ip_2}\tilde{D}^{1,0}_{123}\right) - (\varepsilon_3 - 2\kappa)\left(e^{ip_1}\tilde{D}^{0,1}_{213} + e^{ip_2}\tilde{D}^{0,1}_{123}\right)\Big] \ .
\end{aligned}
\tag{3.3.45}
$$

These terms will be determined by the minimum separation equations, (3.3.24). The rest of the relations coming from (3.3.42) can be obtained by permuting the indices of this expression.

Similarly, the two-body interacting equations from the right (3.3.43), give us the following relation between the generating functions

$$
\begin{aligned}
&\left(e^{ip_1}g_{1,321}(x) + e^{ip_2}g_{1,312}(x)\right)\left(\frac{2}{\kappa} - \varepsilon_3 + \frac{1}{x} + x\right) \\
&\quad + \left(e^{ip_1}g_{2,321}(x) + e^{ip_2}g_{2,312}(x)\right)\left(1 + e^{-i\mathcal{P}}x\right) = \tilde{C}_{12}(x) \ .
\end{aligned}
\tag{3.3.46}
$$

Here, we absorbed the position-dependent coefficients which do not fit into one of the one-variable generating functions into the following functions,

$$
\begin{aligned}
\tilde{C}_{12}(x) = &\left(e^{ip_1}\tilde{D}^{1,0}_{321} + e^{ip_2}\tilde{D}^{1,0}_{312}\right) - x e^{-i\mathcal{P}}\left(e^{ip_1}\tilde{D}^{0,1}_{321} + e^{ip_2}\tilde{D}^{0,1}_{312}\right) \\
&+ \frac{x}{1-e^{-ip_3}x}\Big[\left(e^{ip_1}\tilde{D}^{2,0}_{321} + e^{ip_2}\tilde{D}^{2,0}_{312}\right) - (\varepsilon_3 - \frac{2}{\kappa})\left(e^{ip_1}\tilde{D}^{1,0}_{321} + e^{ip_2}\tilde{D}^{1,0}_{312}\right) \\
&+ \left(e^{ip_1}\tilde{D}^{1,1}_{321} + e^{ip_2}\tilde{D}^{1,1}_{312}\right) + e^{-i\mathcal{P}}\left(e^{ip_1}\tilde{D}^{0,1}_{321} + e^{ip_2}\tilde{D}^{0,1}_{312}\right)\Big] \ .
\end{aligned}
\tag{3.3.47}
$$

From (3.3.46) and (3.3.47), the remaining expressions can be easily obtained by permuting the indices as usual. The functions given in (3.3.45) and (3.3.47) contain the position-dependent corrections that appear in the minimum separation equations, (3.3.24). In particular, the expressions inside the square brackets in (3.3.45) and (3.3.47) include exactly the same linear combination of position dependent corrections as $\beta_{l,(12)}(1)$ and $\beta_{r,(12)}(1)$ respectively, except for the contributions coming from the scattering coefficients. Consequently, we interpret the minimum separation equations as specifying the initial conditions for the two-magnon interacting equations.

Note that we can map the two-body interacting equations from the left configuration to the right, and vice versa, using the given transformation

$$
\{p, x, y, \kappa, D^{n,m}_{ijk}\} \leftrightarrow \{-p, y, x, \kappa^{-1}, D^{m,n}_{kji}\} \ . \tag{3.3.48}
$$

This is reminiscent of the symmetry $\mathbb{Z}_2\mathcal{P}$ as discussed in the beginning of this section. As we pointed out in this section, under this set of transformations the non-interacting equations and the three-magnon equations stay invariant and the left and right two-magnon interacting equations transform to each other.

Combining the analyticity condition with the two-magnon interacting equations allows us to obtain half of the one-variable generating functions, which were introduced in (3.3.30)-(3.3.33). The expressions of these generating functions capture the underlying permutation symmetry structure of the spin chain model. After considering the symmetry relations of the two-magnon interacting equations given in (3.3.48), we conclude the right two-magnon equation which is presented in (3.3.46) should be combined with the analyticity condition for the generating function G_{312} with the $(x, \rho_+(x,-p))$ parametrization of the elliptic curve. This particular choice of parametrization gives us the analyticity condition as written in (3.3.39). The solutions are given as,

$$\begin{aligned} g_{1,312}(x) = {} & \frac{x\left(e^{-ip_2}\tilde{C}_{12}(x) + e^{-i\mathcal{P}}x\tilde{D}^{0,1}_{312} + e^{i\mathcal{P}}\rho_+(x,-p)\tilde{D}^{1,0}_{312}\right)}{\tilde{h}_{12}(x,p)} \\ & - \frac{e^{ip_1-ip_2}(1+2x/\kappa-\varepsilon_3 x+x^2)}{\tilde{h}_{12}(x,p)}g_{1,321}(x) - \frac{e^{ip_1-ip_2}x(1+e^{-i\mathcal{P}}x)}{\tilde{h}_{12}(x,p)}g_{2,321}(x) \\ & - \frac{x^2(1+e^{-i\mathcal{P}}/\rho_+(x,-p))}{\tilde{h}_{12}(x,p)}g_{3,312}(\rho_+(x,-p)) + \frac{x(1+e^{i\mathcal{P}}\rho_+(x,-p))}{\tilde{h}_{12}(x,p)}g_{4,312}(\rho_+(x,-p))\,, \end{aligned} \tag{3.3.49}$$

and,[11]

$$\begin{aligned} g_{2,312}(x) = {} & \frac{e^{-ip_2}e^{i\mathcal{P}}\rho_+(x,-p)\tilde{C}_{12}(x)}{\tilde{h}_{12}(x,-p)} - \frac{e^{ip_1-ip_2}(e^{i\mathcal{P}}+x)\rho_+(x,-p)}{\tilde{h}_{12}(x,p)}g_{2,321}(x) \\ & - \frac{(1+x^2+2x/\kappa-\varepsilon_3 x)}{\tilde{h}_{12}(x,-p)}\Bigg(\frac{x\tilde{D}^{0,1}_{312}+e^{2i\mathcal{P}}\rho_+(x,-p)\tilde{D}^{1,0}_{312}}{(e^{i\mathcal{P}}+x)} + \frac{e^{ip_1-ip_2}e^{i\mathcal{P}}\rho_+(x,-p)}{x}g_{1,321}(x) \\ & - \frac{1+e^{i\mathcal{P}}\rho_+(x,-p)}{1+e^{-i\mathcal{P}}x}\left(\frac{e^{-i\mathcal{P}}x}{\rho_+(x,-p)}g_{3,312}(\rho_+(x,-p)) - g_{4,312}(\rho_+(x,-p))\right)\Bigg)\,. \end{aligned} \tag{3.3.50}$$

Although the expressions look complicated, it is remarkable that they admit a compact form in terms of the one-variable generating functions. These expressions are given in terms of relatively simple functions and they are analytic around the origin, under

[11] Note that $\rho_+(x,-p)$ factor which appears in the denominator always cancels with an overall factor $\rho_+(x,-p)$ coming from $g_{3,\sigma}$ as well as $\frac{1}{x}$ factor in front of $g_{1,\sigma}$. This is a consequence of taking $\tilde{D}^{0,0}_{\sigma}$ equal to zero. Therefore, the expression given in (3.3.50) is analytic around $x=0$.

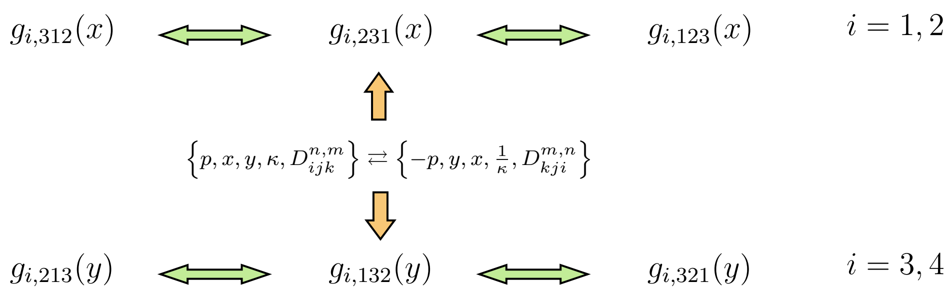

Figure 3.4: *We collect the solutions of the one-variable generating functions coming from the analyticity conditions and two-magnon interacting equations for each permutation. The ones that appear on the same horizontal line are related to each other under the permutation of position-dependent corrections and momentum variables. The ones which appear on the same vertical line are related to each other by changing the labels of position-dependent corrections and changing the parameters according to the prescription in the middle. These relations are also given in Figure 3.5.*

the assumption that the undetermined functions $g_{3,312}$ and $g_{4,312}$ are also analytic. The function which appears in the denominator is given as

$$\tilde{h}_{12}(x,p) = 1 + 2x/\kappa - \varepsilon_3 x + x\rho_+(x,-p) + e^{i\mathcal{P}}\rho_+(x,-p) + x^2 \, . \tag{3.3.51}$$

The rest of the right two-magnon interacting equations can be obtained by permuting the indices to the right,

$$g_{i,312}(x) \longrightarrow g_{i,231}(x) \longrightarrow g_{i,123}(x) \, , \qquad \text{for} \quad i = 1, 2 \, . \tag{3.3.52}$$

The relationship between the generating functions, connected through index rotation, reveals how the components of permutation symmetry manifest. For each one of these one-variable generating functions $g_{i,\sigma}$, obtaining the solution from the equations (3.3.49) and (3.3.50) requires mapping the indices of momentum variables and the position-dependent corrections accordingly, $(312) \to \sigma$.[12]

Similarly, we combine the left two-magnon interacting equations with the analyticity condition for the remaining set of permutations. We choose to use the second parametrization of the elliptic curve given as $(\rho_+(y,p), y)$ together with the equation for the one-variable generating function (3.3.37). This will allow us to organize the solutions of the remaining two-magnon interacting equations in terms of $\mathbb{Z}_2\mathcal{P}$ transformation of the ones which appear in (3.3.52), as depicted in Figure 3.4. From those, we

[12] If we encounter C_{ij} or $\tilde{C}_{ij}$ for $i > j$ after mapping the indices, then we have to exchange the order of indices just for those functions.

obtain,

$$
\begin{aligned}
g_{3,213}(y) = & \frac{y\left(e^{-ip_1}C_{12}(y) + e^{i\mathcal{P}}y\tilde{D}^{1,0}_{213} + e^{-i\mathcal{P}}\rho_+(y,p)\tilde{D}^{0,1}_{213}\right)}{h_{12}(y,p)} \\
& - \frac{e^{ip_2-ip_1}(1+2y\kappa-\varepsilon_3 y+y^2)}{h_{12}(y,p)}g_{3,123}(y) - \frac{e^{ip_2-ip_1}y(1+e^{i\mathcal{P}}y)}{h_{12}(y,p)}g_{4,123}(y) \\
& - \frac{y^2(1+e^{i\mathcal{P}}/\rho_+(y,p))}{h_{12}(y,p)}g_{1,213}(\rho_+(y,p)) + \frac{y(1+e^{-i\mathcal{P}}\rho_+(y,p))}{h_{12}(y,p)}g_{2,213}(\rho_+(y,p))\ ,
\end{aligned}
\tag{3.3.53}
$$

and

$$
\begin{aligned}
g_{4,213}(y) = & \frac{e^{-ip_1}e^{-i\mathcal{P}}\rho_+(y,p)C_{12}(y)}{h_{12}(y,p)} - \frac{e^{ip_2-ip_1}(e^{-i\mathcal{P}}+y)\rho_+(y,p)}{h_{12}(y,p)}g_{4,123}(y) \\
& - \frac{1+y^2+2y\kappa-\varepsilon_3 y}{h_{12}(y,p)}\left(\frac{y\tilde{D}^{1,0}_{213}+e^{-2i\mathcal{P}}\rho_+(y,p)\tilde{D}^{0,1}_{213}}{e^{-i\mathcal{P}}+y} + \frac{e^{ip_2-ip_1}e^{-i\mathcal{P}}\rho_+(y,p)}{y}g_{3,123}(y)\right. \\
& \left. - \frac{1+e^{-i\mathcal{P}}\rho_+(y,p)}{1+e^{i\mathcal{P}}y}\left(\frac{e^{i\mathcal{P}}y}{\rho_+(y,p)}g_{1,213}(\rho_+(y,p)) - g_{2,213}(\rho_+(y,p))\right)\right)\ ,
\end{aligned}
\tag{3.3.54}
$$

such that the denominator is given as

$$
h_{12}(y,p) = 1 + 2\kappa y - \varepsilon_3 y + y^2 + \rho_+(y,p)\left(e^{-i\mathcal{P}}+y\right)\ . \tag{3.3.55}
$$

And we can get the expressions for the solution of one-variable generating functions by permuting the indices of the expressions, (3.3.53) and (3.3.54),

$$
g_{i,213}(y) \longrightarrow g_{i,132}(y) \longrightarrow g_{i,321}(y)\ , \qquad \text{for} \quad i=3,4\ . \tag{3.3.56}
$$

Note that the expressions for the functions $g_{i,\sigma}$ do not spoil the analytical properties of the overall generating function (3.3.38) at the origin because the denominator does not vanish for the chosen ranges of the momentum parameters. Therefore, we can insert the solution of the one-variable generating functions which are listed in (3.3.52) and (3.3.56) into the corresponding generating functions of the form (3.5.33) and obtain a final form of the generating functions for each permutation which solve the second class of equations. As depicted in Figure 3.4, the final form of the solution of the second class of equations coming from the eigenvalue problem, (3.3.25), admits a symmetric solution which is exactly the relation observed between the right and the left two-magnon interacting functions, (3.3.48). However, this means that the particular relations between the coefficients $(A_\sigma + D_\sigma)$ which are labeled by the different permutations are not as straightforward as the usual CBA solution of rational or trigonometric models. Instead, we observe that the six permutations are divided into two sets. Each of the even (odd) permutations can be described by a common form for the one-variable generating functions, and the odd (even) permutations are obtained from reflections together with the transformations given in (3.3.48)[13]. Hence, this division can be described in a unique way, such that knowing the solution of the one-variable generating function for one permutation is enough to generate all. The resulting form of the underlying permutation symmetry can be seen in Figure 3.5.

At this point, we can count the number of unknown coefficients in terms of the one-variable generating functions. After solving the non-interacting equations we obtain the generating function, (3.5.33) which has four undetermined one-variable functions for each of the six permutations. Furthermore, the analyticity condition given in (3.3.37) brings six relations. Finally, the recurrence relations coming from the two-body interacting equations, (3.3.42) and (3.3.43) bring six more relations. Combining all these relations reduces the number of one-variable functions from twenty-four to twelve.

After solving the minimum separation equations and using them as the initial conditions that determine the functions, C_{ij} and $\tilde{C}_{ij}$ from equations (3.3.45) and (3.3.47) we end up with a generating function which encodes all the position-dependent corrections that solve the three-magnon eigenvalue problem. The position-dependent corrections can be extracted from the final form of the generating functions either by expanding them in series or using Cauchy's integral formula,

$$D_{\sigma}^{n,m} = -\oint \frac{dxdy}{4\pi^2} \frac{G_{\sigma}(x,y)}{x^{n+1}y^{m+1}} \,. \tag{3.3.57}$$

We proceed to discuss the solution of the minimum separation equations which completes the solution of the three-magnon relation.

Solving the equations for minimum separation. The last piece of the solution of the three-magnon eigenvalue problem is obtained by solving the equations given in (3.3.24). These expressions contain the scattering coefficients as well as the position-dependent corrections with the shortest separation of magnons. The two-body interacting equations, when the third magnon is just one ϕ state away, are given by the following expressions and their permutations. We write the equations,

$$\beta_{l,(ij)}(1) = 0 \,, \quad \text{and} \quad \beta_{r,(ij)}(1) = 0 \,, \tag{3.3.58}$$

[13]The terms even and odd permutations refer to the number of non-trivial transpositions we need to map (123) to any permutation (ijk). For example we map (123) to (213) by only one transposition (12) therefore (213) is an odd permutation.

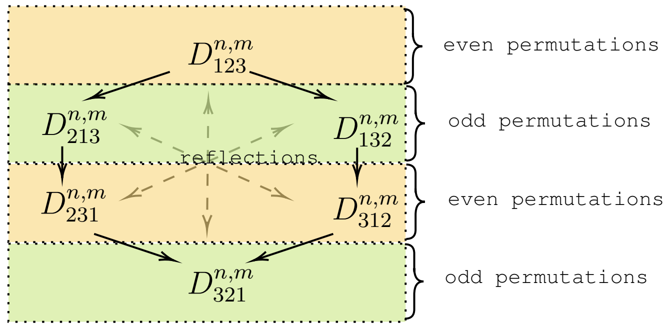

Figure 3.5: *We organize the permutations of position-dependent corrections according to the order of scattering events. Starting from the identity permutation,* (123) *we permute the indices by transpositions and we represent these transpositions by black arrows. In this case the relations between the position-dependent corrections as organized in* (3.3.56) *and* (3.3.52) *come together and the distinction between two sets is separated by colors. These particular transformations also appear in Figure 3.4.*

by isolating one of the scattering coefficients. The following equations correspond to the solution of the two-body interacting equations for which the interacting pair of magnons are on the left of the third magnon, separated by one ϕ. Already from the first set of equations we can explicitly observe how the relations (3.2.30) coming from the CBA are corrected,

$$\begin{aligned} A_{213} &= S_\kappa(p_1,p_2)A_{123} + \frac{1}{a(p_1,p_2,\kappa)}\left[\left(e^{ip_1}\tilde{D}^{0,2}_{213} + e^{ip_2}\tilde{D}^{0,2}_{123}\right) + \left(e^{ip_1}\tilde{D}^{1,1}_{213} + e^{ip_2}\tilde{D}^{1,1}_{123}\right)\right. \\ &\quad \left. -(\varepsilon_3 - 2\kappa)\left(e^{ip_1}\tilde{D}^{0,1}_{213} + e^{ip_2}\tilde{D}^{0,1}_{123}\right) + e^{i\mathcal{P}}\left(e^{ip_1}\tilde{D}^{1,0}_{213} + \tilde{D}^{1,0}_{123}\right)\right], \end{aligned} \tag{3.3.59}$$

$$\begin{aligned} A_{312} &= S_\kappa(p_1,p_3)A_{132} + \frac{1}{a(p_1,p_3,\kappa)}\left[\left(e^{ip_1}\tilde{D}^{0,2}_{312} + e^{ip_3}\tilde{D}^{0,2}_{132}\right) + \left(e^{ip_1}\tilde{D}^{1,1}_{312} + e^{ip_3}\tilde{D}^{1,1}_{132}\right)\right. \\ &\quad \left. -(\varepsilon_3 - 2\kappa)\left(e^{ip_1}\tilde{D}^{0,1}_{312} + e^{ip_3}\tilde{D}^{0,1}_{132}\right) + e^{i\mathcal{P}}\left(e^{ip_1}\tilde{D}^{1,0}_{312} + \tilde{D}^{1,0}_{132}\right)\right], \end{aligned} \tag{3.3.60}$$

$$\begin{aligned} A^L_{321} &= S_\kappa(p_2,p_3)A_{231} + \frac{1}{a(p_2,p_3,\kappa)}\left[\left(e^{ip_2}\tilde{D}^{0,2}_{321} + e^{ip_3}\tilde{D}^{0,2}_{231}\right) + \left(e^{ip_2}\tilde{D}^{1,1}_{321} + e^{ip_3}\tilde{D}^{1,1}_{231}\right)\right. \\ &\quad \left. -(\varepsilon_3 - 2\kappa)\left(e^{ip_2}\tilde{D}^{0,1}_{321} + e^{ip_3}\tilde{D}^{0,1}_{231}\right) + e^{i\mathcal{P}}\left(e^{ip_2}\tilde{D}^{1,0}_{321} + \tilde{D}^{1,0}_{231}\right)\right]. \end{aligned} \tag{3.3.61}$$

Here, the function, $a(p_1,p_2,\kappa) = 1 + e^{ip_1+ip_2} - 2\kappa e^{ip_1}$ is the denominator of the scattering coefficient given in (3.2.13). Furthermore, independently, we also solve the right two-body interacting equations. Notice that these two sets of equations include the same scattering coefficients and position-dependent corrections but paired in two different ways. Under the assumption that A^L_{321} is different from A^R_{321} we obtain,

$$A_{132} = S_{1/\kappa}(p_2,p_3)A_{123} + \frac{1}{a(p_2,p_3,\kappa^{-1})}\left[\left(e^{ip_2}\tilde{D}^{2,0}_{132} + e^{ip_3}\tilde{D}^{2,0}_{123}\right) + \left(e^{ip_2}\tilde{D}^{1,1}_{132} + e^{ip_3}\tilde{D}^{1,1}_{123}\right)\right.$$

$$- \left(\varepsilon_3 - 2\kappa^{-1}\right)\left(e^{ip_2}\tilde{D}^{1,0}_{132} + e^{ip_3}\tilde{D}^{1,0}_{123}\right) + e^{-i\mathcal{P}}\left(e^{ip_2}\tilde{D}^{0,1}_{132} + e^{ip_3}\tilde{D}^{0,1}_{123}\right)\Big] \,, \tag{3.3.62}$$

$$A_{231} = S_{1/\kappa}(p_1,p_3)A_{213} + \frac{1}{a(p_1,p_3,\kappa^{-1})}\Big[\left(e^{ip_1}\tilde{D}^{2,0}_{231} + e^{ip_3}\tilde{D}^{2,0}_{213}\right) + \left(e^{ip_1}\tilde{D}^{1,1}_{231} + e^{ip_3}\tilde{D}^{1,1}_{213}\right)$$

$$- \left(\varepsilon_3 - 2\kappa^{-1}\right)\left(e^{ip_1}\tilde{D}^{1,0}_{231} + e^{ip_3}\tilde{D}^{1,0}_{213}\right) + e^{-i\mathcal{P}}\left(e^{ip_1}\tilde{D}^{0,1}_{231} + e^{ip_3}\tilde{D}^{0,1}_{213}\right)\Big] \,, \tag{3.3.63}$$

$$A^R_{321} = S_{1/\kappa}(p_1,p_2)A_{312} + \frac{1}{a(p_1,p_2,\kappa^{-1})}\Big[\left(e^{ip_1}\tilde{D}^{2,0}_{321} + e^{ip_2}\tilde{D}^{2,0}_{312}\right) + \left(e^{ip_1}\tilde{D}^{1,1}_{321} + e^{ip_2}\tilde{D}^{1,1}_{312}\right)$$

$$- \left(\varepsilon_3 - 2\kappa^{-1}\right)\left(e^{ip_1}\tilde{D}^{1,0}_{321} + e^{ip_2}\tilde{D}^{1,0}_{312}\right) + e^{-i\mathcal{P}}\left(e^{ip_1}\tilde{D}^{0,1}_{321} + e^{ip_2}\tilde{D}^{0,1}_{312}\right)\Big] \,. \tag{3.3.64}$$

We specifically labeled the scattering coefficients A_{321} coming from the left and the right equations as A^L_{321} and A^R_{321} to emphasize that at least one of the position-dependent corrections in these equations must solve the equation,

$$A^L_{321} = A^R_{321} \,, \tag{3.3.65}$$

for the two sets of equations to become compatible. It is important to realize that a YBE is hidden in this particular equation. More explicitly, the above equation can be brought into the form,

$$\frac{A^L_{321}}{A_{231}}\frac{A_{231}}{A_{213}}\frac{A_{213}}{A_{123}}A_{123} = \frac{A^R_{321}}{A_{312}}\frac{A_{312}}{A_{132}}\frac{A_{132}}{A_{123}}A_{123} \,. \tag{3.3.66}$$

Since the two-magnon interacting equations are deformed in a non-trivial way, we can find solutions to this equation. However, this is not the only YBE that arises in the solution of the long-range ansatz. We obtain a tower of modified YBEs for the position-dependent corrections for any configuration once we impose special conditions and reduce to more constrained subclasses of the solution. We will postpone the discussion on this topic until we revisit the three-magnon state from the context of Yang operators in Section 3.7.

Finally, the three-body interacting equation brings one more constraint on the closest position-dependent corrections,

$$\alpha(p_1,p_2,p_3) = 0 \,. \tag{3.3.67}$$

In the usual integrable spin chains which admit CBA, solving the two-magnon interacting equations automatically solves the three-magnon equation. However, after substituting the solutions (3.3.59)-(3.3.65) into $\alpha(p_1,p_2,p_3)$, it does not vanish in our case. Since in both equations (3.3.65) and (3.3.67) the position-dependent corrections $D^{1,0}_\sigma$, $D^{0,1}_\sigma$, $D^{2,0}_\sigma$, $D^{0,2}_\sigma$, $D^{1,1}_\sigma$, for all $\sigma \in \mathcal{S}_3$, appear, we can just use them to solve for any two of these coefficients. This would be a highly non-symmetric way of solving these equations, but it would also be the most general way to obtain a solution of the long-range ansatz. Here, we avoid giving the most general solution explicitly because we think that it does not offer any particular insight. Solving these equations in a $\mathcal{S}_3$-symmetric way in its whole generality is beyond our reach. Even more importantly, we do not want to restrict ourselves by looking for a fully manifest permutation symmetry, as it might be broken, twisted, or deformed. Instead, in the next section we present a special subset of three-magnon solutions for which we impose extra conditions to solve the eigenvalue problem fully and symmetrically.

3.3.2 Special Solution for the Three-Body Problem

In this section, we present an example of a special solution to the three-magnon problem contained in the general solution presented in the previous section. Rather than determining the scattering coefficients A_σ through the equations (3.3.24), we fix the scattering coefficients of the long-range ansatz according to the scattering coefficients that arise from the usual CBA, in particular, we use either (3.2.30) or (3.2.31), and use the position-dependent corrections to compensate for our choices. Starting from the form of the generating function (3.5.33), we ensure that the position-dependent corrections obtained in this section already satisfy the non-interacting equations provided the one-variable generating functions fulfill the analyticity condition (3.3.35). Furthermore, all undetermined position-dependent corrections in the previous section, are fixed to achieve solutions with factorized scattering coefficients. The existence of this solution and similar special solutions discussed in [1], makes the connection between the Temperley-Lieb model and our dynamical spin chain clearer, as it allows us to explicitly identify the corrections required for the scattering coefficients for each magnon configuration.

We also consider starting from the scattering coefficients of the XXX model and compute the explicit corrections needed to solve this model. This particular solution not only indicates yet another direct connection between our model and the XXX model, but also enables comparison between two possible ways to obtain the dynamical spin chain model. Furthermore, in all of these special solutions, it is easy to see that the corrections always come with overall $(\kappa - \kappa^{-1})$ factors which imply that the orbifold point limit, $\kappa \to 1$ takes us back to the CBA for the $\mathbb{Z}_2$ orbifold of $\mathcal{N} = 4$ SYM. Although these particular choices we present in the next three subsections, explicitly break the combination of parity and $\mathbb{Z}_2$ symmetry, we can easily obtain a solution that is invariant under the $\mathbb{Z}_2\mathcal{P}$ operator by combining these solutions we present.

Motivation Coming from Felder's Dynamical R-matrix:

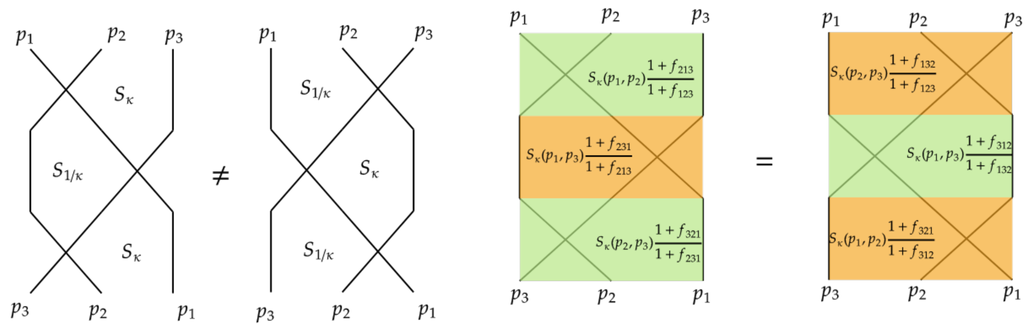

Figure 3.6: *We demonstrate the idea behind inserting position-dependent corrections and 'correcting' the YBE. While doing so we still want to explicitly have the scattering coefficients of the two-magnon eigenstates. Additionally, change in the color from one scattering event to the other reminds us of the action of the coassociators given in* (3.7.37).

Apart from choosing the scattering coefficients that factorize, the additional conditions we present in the section to constrain the solution for the position-dependent corrections are motivated by obtaining a generalized form of factorized scattering coefficients which are modified by the position-dependent corrections. To achieve this we are inspired by the R-matrix that satisfies DYBE and admits a non-trivial coassociator in its quantum group [139]. If we lift the co-associativity of the underlying Hopf algebra structure, some or all of the scattering processes would be affected by the existence of a coassociator. Schematically, we expect the scattering processes to have a form like

$$S_{12}(p,\lambda)((p_1 \otimes p_2) \otimes p_3) = S_\kappa(p_1,p_2)((p_2 \otimes p_1) \otimes p_3) \;, \tag{3.3.68}$$

such that S_{ij} is representing a scattering operator and $S_\kappa(p_1,p_2)$ is the scattering coefficient, moreover for exchanging the last two momenta we expect to have,

$$\begin{aligned} &\Phi^{-1}_{123} S_{23}(p,\lambda)\Phi_{123}((p_1 \otimes p_2) \otimes p_3) \\ &\quad = S_{23}(p,\lambda - 2\eta h^{(1)})(p_1 \otimes (p_2 \otimes p_3)) = S_{1/\kappa}(p_2,p_3)(p_1 \otimes (p_2 \otimes p_3)) \;. \end{aligned} \tag{3.3.69}$$

Although we have not yet been able to define a scattering operator (or a R-matrix) which demonstrated exactly these properties, we impose the factorization of scattering coefficients and partial factorization of the position-dependent corrections to achieve a similar structure to (3.7.38) and (3.3.69) as also depicted in Figure 3.6.

S_κ solution. For the first special solution, we consider scattering coefficients that are factorized in terms of $S_\kappa(p_1,p_2)$, given in (3.2.14). Choosing this form for the scattering coefficients implies a preference for the left-interacting equations of the naive CBA, as given in (3.2.30),

$$\frac{A_{213}}{A_{123}} = S_\kappa(p_1,p_2)\ , \quad \frac{A_{312}}{A_{132}} = S_\kappa(p_1,p_3)\ , \quad \frac{A_{321}}{A_{231}} = S_\kappa(p_2,p_3)\ , \tag{3.3.70}$$

$$\frac{A_{132}}{A_{123}} = S_\kappa(p_2,p_3)\ , \quad \frac{A_{231}}{A_{213}} = S_\kappa(p_1,p_3)\ , \quad \frac{A_{321}}{A_{312}} = S_\kappa(p_1,p_2)\ . \tag{3.3.71}$$

The scattering coefficients (3.3.70) make the scattering factors disappear from the left two-magnon interacting equations, $\beta_l(1)$, but the scattering coefficients (3.3.71) do not simplify the ones from the right, $\beta_r(1)$.

Before solving the equations (3.3.24), we impose additional relations between the position-dependent corrections inspired by the CBA. In particular, for any $n,m \geq 0$, we fix

$$\tilde{D}^{n,m}_{213} = S_\kappa(p_1,p_2)\tilde{D}^{n,m}_{123}\ , \tag{3.3.72}$$

$$\tilde{D}^{n,m}_{312} = S_\kappa(p_1,p_3)\tilde{D}^{n,m}_{132}\ , \tag{3.3.73}$$

$$\tilde{D}^{n,m}_{321} = S_\kappa(p_2,p_3)\tilde{D}^{n,m}_{231}\ . \tag{3.3.74}$$

This implies that the position-dependent corrections are related by the appropriate scattering coefficients, S_κ, if their indices are related by a transposition of the first two indices, ijk and jik. The fact that now the position-dependent corrections are *partially-factorized* helps uncover the physics of this problem. In addition, we also fix the normalization of the state by setting

$$A_{123} = 1\ . \tag{3.3.75}$$

Then, we first consider the three-magnon interacting equation, given in (3.3.18). We take advantage of the observation that the scattering coefficients and the position-dependent corrections share the same label and thus have a common exponential of momenta factor, such as $e^{ip_i+2ip_j}$. This allows us to choose the following expressions for the position-dependent corrections in (3.3.18),

$$\left(\tilde{D}^{0,1}_{123} + \tilde{D}^{1,0}_{123}\right) = 2\left(\kappa - \frac{1}{\kappa}\right)\ , \tag{3.3.76}$$

$$\left(\tilde{D}^{0,1}_{132} + \tilde{D}^{1,0}_{132}\right) = 2\left(\kappa - \frac{1}{\kappa}\right) S_\kappa(p_2,p_3)\ , \tag{3.3.77}$$

$$\left(\tilde{D}^{0,1}_{231} + \tilde{D}^{1,0}_{231}\right) = 2\left(\kappa - \frac{1}{\kappa}\right) S_\kappa(p_1,p_3)S_\kappa(p_1,p_2)\ , \tag{3.3.78}$$

which gives us the solution of the three-magnon interacting equation. We obtain the same structure of scattering coefficients as one might infer from the naive CBA. However, it is important to emphasize that there is no intrinsic reason to justify this choice of coefficients beyond inspiration from the CBA and the fact that they satisfy the three-magnon interacting equation (3.3.18). Before moving to the two-magnon interacting equations for the shortest separation, we fix all the remaining freedom unconstrained by (3.3.18) by choosing

$$\tilde{D}_{\sigma}^{1,1} = 0 \ , \qquad \tilde{D}_{\sigma}^{1,0} = \tilde{D}_{\sigma}^{0,1} \ . \tag{3.3.79}$$

The two-body interacting equations from the left can be used to fix the coefficients $D_{\sigma}^{0,2}$,

$$\tilde{D}_{123}^{0,2} = \left(\kappa - \frac{1}{\kappa}\right)\left(\varepsilon_3 - e^{i\mathcal{P}} - 2\kappa\right) \ , \tag{3.3.80}$$

$$\tilde{D}_{132}^{0,2} = S_{\kappa}(p_2, p_3)\left(\kappa - \frac{1}{\kappa}\right)\left(\varepsilon_3 - e^{i\mathcal{P}} - 2\kappa\right) \ , \tag{3.3.81}$$

$$\tilde{D}_{231}^{0,2} = S_{\kappa}(p_1, p_3)S_{\kappa}(p_1, p_2)\left(\kappa - \frac{1}{\kappa}\right)\left(\varepsilon_3 - e^{i\mathcal{P}} - 2\kappa\right) \ . \tag{3.3.82}$$

Similarly, the two-body interacting equations from the right can be used to fix the coefficients $D_{\sigma}^{2,0}$. These equations give us the same structure with scattering coefficients as in $D_{\sigma}^{0,2}$, but with a more involved overall factor.

$$\tilde{D}_{123}^{2,0} = \frac{1-\kappa^2}{\kappa^2} f_{20}(p_3) \ , \tag{3.3.83}$$

$$\tilde{D}_{132}^{2,0} = \frac{1-\kappa^2}{\kappa^2} S_{\kappa}(p_2, p_3) f_{20}(p_2) \ , \tag{3.3.84}$$

$$\tilde{D}_{231}^{2,0} = \frac{1-\kappa^2}{\kappa^2} S_{\kappa}(p_1, p_3)S_{\kappa}(p_1, p_2) f_{20}(p_1) \ , \tag{3.3.85}$$

such that

$$f_{20}(p_3) = \left[e^{-ip_3}\left(\varepsilon_3 + e^{i\mathcal{P}} + e^{-i\mathcal{P}} - 2\kappa\right) - \kappa\left(3\varepsilon_3 - 2e^{ip_3} + e^{-i\mathcal{P}} - 4\kappa - \frac{2}{\kappa}\right)\right] \ . \tag{3.3.86}$$

The reason why the solutions for the two-body interacting equations from the right are more complicated is that we fix the freedom of our coefficients using S_{κ} factors, which are suited for solving the structure of the two-body interacting equations from the left but not for the two-body interacting equations from the right.

We have now extracted all the information we can from the minimum separation equations, and we proceed to consider the second class of equations. As in the previous section, they are solved by imposing all the recurrence relations to the generating function (3.5.33) and ensuring analyticity. This last step can be performed by computing the resulting form of the functions, (3.3.45) and (3.3.47) under the special choices we made in this subsection. Using (3.3.72), we get

$$\left(e^{ip_1}\tilde{D}^{n,m}_{213}+e^{ip_2}\tilde{D}^{n,m}_{123}\right)=\omega(p_1,p_2,\kappa)\tilde{D}^{n,m}_{123}\ , \tag{3.3.87}$$

where we define

$$\omega(p_1,p_2,\kappa)=\frac{(e^{ip_2}-e^{ip_1})(1+e^{ip_1+ip_2})}{1+e^{ip_1+ip_2}-2\kappa e^{ip_1}}\ . \tag{3.3.88}$$

We combine this piece of observation with the resulting form of the functions which are defined in (3.3.45),

$$C_{12}(y)=\left(\kappa-\frac{1}{\kappa}\right)\left(1-ye^{i\mathcal{P}}\right)\omega(p_1,p_2,\kappa)\ , \tag{3.3.89}$$

and (3.3.47),

$$\tilde{C}_{12}(x)=\left(\kappa-\frac{1}{\kappa}\right)\left(1-\frac{x(\varepsilon_3-\frac{2}{\kappa}-xe^{-ip_3}e^{-i\mathcal{P}}+\frac{f_{20}(p_3)}{\kappa})}{1-e^{-ip_3}x}\right)S_\kappa(p_2,p_3)S_\kappa(p_1,p_3)\omega(p_1,p_2,\kappa)\ . \tag{3.3.90}$$

The common form of these expressions including factorized scattering coefficients and the permutation relations derived in Section 3.3 and depicted in Figure 3.4 are enough to show that the factorization will continue to hold for higher position-dependent corrections. In addition to the factorized scattering coefficients, we will observe the corrections which are related to each other as observed in Section 3.3. Hence, for any $n,m\geq 1$, we have

$$D^{n,m}_{123}=f(p_1,p_2,p_3;n,m;\kappa)\ , \tag{3.3.91}$$
$$D^{n,m}_{132}=S_\kappa(p_2,p_3)f(p_1,p_3,p_2;n,m;\kappa)\ , \tag{3.3.92}$$
$$D^{n,m}_{213}=S_\kappa(p_1,p_2)f(p_2,p_1,p_3;n,m;\kappa)\ , \tag{3.3.93}$$
$$D^{n,m}_{231}=S_\kappa(p_1,p_3)S_\kappa(p_1,p_2)f(p_2,p_3,p_1;n,m;\kappa)\ , \tag{3.3.94}$$
$$D^{n,m}_{312}=S_\kappa(p_1,p_3)S_\kappa(p_2,p_3)f(p_3,p_1,p_2;n,m;\kappa)\ , \tag{3.3.95}$$
$$D^{n,m}_{321}=S_\kappa(p_2,p_3)S_\kappa(p_1,p_3)S_\kappa(p_1,p_2)f(p_3,p_2,p_1;n,m;\kappa)\ , \tag{3.3.96}$$

such that $f(p_1,p_2,p_3;n,m;\kappa)$ is defined from the final form of the generating function $G_{123}(x,y)$,

$$f(p_1,p_2,p_3;n,m,\kappa)=-\oint_\Sigma\frac{dxdy}{4\pi^2}\frac{G_{123}(x,y)}{x^{n+1}y^{m+1}}\ , \tag{3.3.97}$$

where Σ is a small ball around the origin. The function $G_{123}(x, y)$ evaluated for the special solution is given in Appendix B in [1]. By introducing this function f we want to emphasize that the position-dependent coefficients are related by an appropriate permutation of the momentum labels and an appropriate scattering coefficient, which is neither assumed on the ansatz (3.3.2) nor expected from the lack of permutation symmetry between the excitations. More importantly, we observe that the special choices we made starting from (3.3.70) to (3.3.74) enhanced the permutation symmetry which is depicted in Figure 3.5 to the full $\mathcal{S}_3$, which we will analyze using Yang operators in the next section. Under these choices of scattering coefficients and the position-dependent corrections for the shortest separation, we obtain a solution of the three-magnon state that satisfies the eigenvalue problem (3.2.21). We are still left with three one-variable generating functions that codify many undetermined coefficients. We can absorb undetermined coefficients into $g_{2,123}$, $g_{2,132}$ and $g_{2,231}$, then setting all these coefficients to zero would give us a non-trivial solution with the structure laid down in equations (3.3.91)-(3.3.96). In Appendix B in [1], we elaborate on the details of combining the special solution of the minimum separation equations with the second class of equations. We label this solution as $|\xi(p_1, p_2, p_3)\rangle_\kappa$ and it has the following form,

$$|\xi(p_1, p_2, p_3)\rangle_\kappa = \sum_{l_1<l_2<l_3} \left(\sum_{\sigma\in\mathcal{S}_3} A_\sigma \, \left(1 + f(p_{\sigma(1)}, p_{\sigma(2)}, p_{\sigma(3)}; n, m; \kappa)\right) e^{i\vec{p}_\sigma\cdot\vec{l}} \right) |l_1, l_2, l_3\rangle \tag{3.3.98}$$

Here, the separation between the scattering coefficients and position-dependent corrections becomes clearer. We can interpret the terms accompanying the plane wave corrections as explicit modifications to the plane wave basis. It is important to note that this eigenvector, by itself, does not remain invariant under the operator $\mathbb{Z}_2\mathcal{P}$. However, by combining it with the special solution presented in the next section, we obtain states that satisfy the relations given in (3.3.22).

Similarly, special solutions with factorized scattering coefficients in terms of $S_{1/\kappa}$ or $S_{\kappa=1}$ were discussed in detail in [1].

3.4 Four-Body Long-Range Solution

In this section, we apply the long-range Bethe ansatz technique developed in Section 3.3 to the four-magnon problem. We begin by identifying the recursion relations arising from the eigenvalue equation and encoding them in generating functions. The details of this procedure are presented in [2] and are omitted here in order to keep the discussion concise. Following the steps outlined in the previous section, we then analyse the specific features of the four-magnon case and further develop the long-range Bethe ansatz formalism in light of the insights obtained.

The four-magnon eigenvalue problem is given by

$$\mathcal{H}\,|\Psi(p_1,p_2,p_3,p_4)\rangle_{ii} = E_4(p_1,p_2,p_3,p_4)\,|\Psi(p_1,p_2,p_3,p_4)\rangle_{ii}\ , \tag{3.4.1}$$

for two configurations labeled by $i \in \{1,2\}$, which denote the color indices of the ϕ's in the left and right of the spin chain states. We restrict our search to solutions with the additive energy property,

$$E_4(p_1,p_2,p_3,p_4) = \sum_{i=1}^{4} E(p_i)\ , \tag{3.4.2}$$

with the dispersion relation given in (3.2.4). For the open infinitely long spin chains, the long-range Bethe ansatz is given as

$$|\Psi(p_1,p_2,p_3,p_4)\rangle_{11} = \sum_{l_1<l_2<l_3<l_4} \Psi(l_1,l_2,l_3,l_4)\,|Q_{12}(l_1),Q_{21}(l_2),Q_{12}(l_3),Q_{21}(l_4)\rangle\ , \tag{3.4.3}$$

$$\Psi(l_1,l_2,l_3,l_4) = \sum_{\sigma\in\mathcal{S}_4}\left(A_\sigma + D_\sigma^{l_2-l_1-1,l_3-l_2-1,l_4-l_3-1}\right)e^{i\vec{p}_\sigma\cdot\vec{l}}\,, \tag{3.4.4}$$

such that

$$e^{i\vec{p}_\sigma\cdot\vec{l}} = e^{i(p_{\sigma(1)}l_1+p_{\sigma(2)}l_2+p_{\sigma(3)}l_3+p_{\sigma(4)}l_4)}\ , \tag{3.4.5}$$

together with the $\mathbb{Z}_2$ conjugate state, $|\Psi(p_1,p_2,p_3,p_4)\rangle_{22}$, whose wave function is the same up to the $\kappa\to\kappa^{-1}$ transformation. In this setup, each wave function as defined in (3.4.4) consists of a sum over all permutations of four positions $\vec{l}$ and four momenta $\vec{p}$, denoted by using the symmetric group on four elements, $\mathcal{S}_4$.[14] As in the three-magnon problem given in Section 3.3, we separate the scattering coefficients from the position-dependent corrections and adopt a general form that represents the Fourier transform of a function on a lattice. This approach allows us to project the four-magnon eigenvalue problem onto position space and obtain recursion relations for the position-dependent corrections while keeping the contributions from the scattering coefficients distinct.

[14] In this article, when we need to refer to a specific permutation $\sigma\in\mathcal{S}_4$ that maps $\sigma(1)=i$, $\sigma(2)=j$, $\sigma(3)=k$ and $\sigma(4)=l$, we will denote it as the string $(ijkl)$. This notation differs from the cyclic notation, so it is important to avoid any confusion between the two.

We identify five types of equations that require solutions in terms of the scattering coefficients and position-dependent corrections. The shift symmetry of the wave function coming from (3.1.22) makes it convenient to switch from the position coordinates to the distance between the magnons to simplify the notation,

$$n = l_2 - l_1 - 1\;, \quad m = l_3 - l_2 - 1\;, \quad r = l_4 - l_3 - 1\;. \tag{3.4.6}$$

These five types of equations correspond to all possible configurations of four magnons relative to each other. When all magnons are well separated, we obtain the *non-interacting equations*. If two magnons are adjacent and the remaining two are far apart, we get *two-magnon interacting equations*, this category includes three distinct cases depending on which pair is interacting. When there are two adjacent pairs that are separated from each other, we refer to them as *two two-magnon interacting equations*. If three magnons are clustered together and the fourth is far apart, the result is *three-magnon interacting equations*. Finally, when all four magnons are adjacent, we have *four-magnon interacting equations*. These are listed as:

non-interacting	$n, m, r > 0$	$\delta_{ijkl}(n, m, r)$
two-magnon interaction	$n, m > 0, r = 0$	$\gamma_{r,ij}(n, m)$
	$m, r > 0, n = 0$	$\gamma_{l,ij}(m, r)$
	$n, r > 0, m = 0$	$\gamma_{m,ij}(n, r)$
two two-magnon interaction	$m > 0, n, r = 0$	$\gamma_{rl,ij}(m)$
three-magnon interaction	$n > 0, m, r = 0$	$\beta_{r,i}(n)$
	$r > 0, m, n = 0$	$\beta_{l,i}(r)$
four-magnon interaction	$n, m, r = 0$	α

Here, we explicitly compute the eigenvalue equation for the non-interacting case and define the necessary quantities during the process.

Non-interacting equations. We start by looking at the non-interacting equations, resulting from the well-separated magnons,

$$\begin{aligned}\delta(n, m, r) =& e^{-il_1\mathcal{P}_4}\, \langle l_1, l_2, l_3, l_4|\mathcal{H} - E_4|\Psi(p_1, p_2, p_3, p_4)\rangle_{12} \\ =& e^{-il_1\mathcal{P}_4}\Bigg[\left(4\kappa + 4\kappa^{-1} - E_4\right)\Psi(l_1, l_2, l_3, l_4) - \Psi(l_1 \pm 1, l_2, l_3, l_4) \\ & -\Psi(l_1, l_2 \pm 1, l_3, l_4) - \Psi(l_1, l_2, l_3 \pm 1, l_4) - \Psi(l_1, l_2, l_3, l_4 \pm 1)\Bigg]\;,\end{aligned} \tag{3.4.7}$$

such that all the relative distances are positive integers $n, m, r > 0$ and total momentum is given in (3.4.11). The notation ± 1 indicates that we have to include the term with $+1$ and -1 shifts of the position, as writing all the terms will clutter our equations. After substituting (3.4.4), we distinguish the plane wave contributions from the position-dependent corrections to keep track of the permutations of momenta,

$$\delta(n,m,r) = \sum_{\sigma \in \mathcal{S}_4} \delta_\sigma(n,m,r) e^{in(p_{\sigma(2)}+p_{\sigma(3)}+p_{\sigma(4)})+im(p_{\sigma(3)}+p_{\sigma(4)})+irp_{\sigma(4)}} \,. \tag{3.4.8}$$

Then, to solve the non-interacting equations coming from the four-magnon eigenvalue problem, we require each δ_σ to vanish separately for any $n, m, r > 0$. We explicitly give one of these expressions, as the rest can be obtained by permuting the indices of the momentum variables.

$$\begin{aligned}\delta_{1234}(n,m,r) = e^{i(3p_4+2p_3+p_2)}\Big(&\varepsilon_4 D_{1234}^{n,m,r} - e^{-ip_4} D_{1234}^{n,m,r-1} - e^{ip_4} D_{1234}^{n,m,r+1} - e^{-ip_3} D_{1234}^{n,m-1,r+1} \\ &-e^{ip_3} D_{1234}^{n,m+1,r-1} - e^{-ip_2} D_{1234}^{n-1,m+1,r} - e^{ip_2} D_{1234}^{n+1,m-1,r} - e^{-ip_1} D_{1234}^{n+1,m,r} - e^{ip_1} D_{1234}^{n-1,m,r}\Big) \,,\end{aligned} \tag{3.4.9}$$

where we introduced a parameter which is related to the total energy as

$$\varepsilon_4 = 4\kappa^{-1} + 4\kappa - E_4 = \sum_{i=1}^{4} e^{ip_i} + e^{-ip_i} \,, \tag{3.4.10}$$

and we denote the total momentum as

$$e^{i\mathcal{P}_4} = \exp\left(i \sum_{i=1}^{4} p_i\right) \,. \tag{3.4.11}$$

By scaling the position-dependent corrections, we can acquire a form of the non-interacting equations that only depends on the parameters ε_4 and the exponential of the total momentum.

$$\tilde{D}_\sigma^{n,m,r} = e^{-inp_{\sigma(1)}+im(p_{\sigma(3)}+p_{\sigma(4)})+irp_{\sigma(4)}} D_\sigma^{n,m,r} \,. \tag{3.4.12}$$

Under this transformation, we obtain,

$$\begin{aligned}\delta_{1234}(n,m,r) = e^{i(p_2+2p_3+3p_4)}\Big(&\varepsilon_4 \tilde{D}_{1234}^{n,m,r} - \tilde{D}_{1234}^{n,m,r-1} - \tilde{D}_{1234}^{n,m,r+1} - \tilde{D}_{1234}^{n,m-1,r+1} \\ &-\tilde{D}_{1234}^{n,m+1,r-1} - e^{-i\mathcal{P}_4} \tilde{D}_{1234}^{n-1,m+1,r} - e^{i\mathcal{P}_4} \tilde{D}_{1234}^{n+1,m-1,r} - \tilde{D}_{1234}^{n+1,m,r} - \tilde{D}_{1234}^{n-1,m,r}\Big) \,.\end{aligned} \tag{3.4.13}$$

It is crucial to keep in mind that there are other ways to scale position-dependent corrections which would still reduce the momentum-dependent coefficients of the eigenvalue problem to depend only on the total momentum and the total energy. As these other scalings are of the form $\tilde{E}_\sigma^{n,m,r} = e^{-\alpha i m \mathcal{P}_4}\tilde{D}_\sigma^{n,m,r}$, for $\alpha \in \mathbb{R}$, these scaled position-dependent corrections would change the position of the $e^{i\mathcal{P}_4}$ and $e^{-i\mathcal{P}_4}$ factors in the non-interacting eigenvalue equations but this would still give us a similar solution. A similar scaling transformation was used in the long-range Bethe ansatz for three-magnon states. In that case, there is only one way to reduce the coefficients of the non-interacting expression, which is to depend solely on the total momentum and total energy. For four-magnon states, it is not surprising to find distinct ways to perform this scaling, reflecting the increased complexity of the system. These scaling choices are reminiscent of the isometries of the three-dimensional lattice that encodes the position-dependent corrections for each permutation, σ. Furthermore, each scaling transforms the wave function into two distinct pieces. Under the scaling of the position-dependent correction given in (3.4.12) the general structure of the wave function transforms to

$$\begin{aligned}|\Psi(p_1,p_2,p_3,p_4)\rangle_{11} = \sum_{l_1<l_2<l_3<l_4}\sum_{\sigma\in\mathcal{S}_4}\Big(&A_\sigma e^{i\vec{p}_\sigma\cdot\vec{l}}\\ &+ e^{ip_{\sigma(2)}+2ip_{\sigma(3)}+3ip_{\sigma(4)}}\tilde{D}_\sigma^{n,m,r}e^{il_2\mathcal{P}_4}\Big)\,|l_1,l_2,l_3,l_4\rangle_{11}\ .\end{aligned}$$

The scaling $\tilde{E}_\sigma$ also transforms the wave function into a similar form. In particular, the scaling from D_σ to $\tilde{D}_\sigma$ isolates all position-dependent corrections into a separate wave function in the center-of-mass limit, along with the scattering coefficient contributions, which remain in the CBA form. This approach significantly simplifies the long-range Bethe ansatz. Therefore, after presenting the eigenvalue equations, we consistently use the scaled position-dependent corrections $\tilde{D}_\sigma$ throughout the following sections as was the case for three-magnon position-dependent corrections in the previous section.

The rest of the equations can be derived in a similar way. By exploring the relationships between these equations, shaped by the symmetries of the model, we will uncover special families of solutions.

Parity and $\mathbb{Z}_2$ symmetry. The two discrete symmetries of the Hamiltonian (3.1.19), $\mathbb{Z}_2$ and parity,[15] given in (3.1.21) and (3.1.26) play a crucial role in characterizing the spectrum of the model. Here we analyze the action of these two operators on the four-magnon long-range Bethe ansatz states and present the effect of these operators on the eigenvalue equations presented in this section.

[15] Since we are considering the four-magnon problem ($M = 4$), the operator $\mathbb{Z}_2^M\mathbb{P}$ given in (3.1.26) reduces to the parity operator.

As given in (3.1.20), the $\mathbb{Z}_2$ operator maps two distinct momentum states to each other,

$$\mathbb{Z}_2 \left|\Psi(p_1,p_2,p_3,p_4)\right\rangle_{11} = \left|\Psi(p_1,p_2,p_3,p_4)\right\rangle_{22} \ . \tag{3.4.14}$$

This implies that the wave function of the state $|\Psi\rangle_{22}$ should be the $\kappa \to \kappa^{-1}$ version of the state $|\Psi\rangle_{11}$ and, more explicitly, we obtain the following relations on the scattering coefficients and the position-dependent corrections,

$$A_\sigma(p,\kappa^{-1}) = \hat{A}_\sigma(p,\kappa) \ , \qquad D_\sigma^{n,m,r}(p,\kappa^{-1}) = \hat{D}_\sigma^{n,m,r}(p,\kappa) \ , \tag{3.4.15}$$

where $A_\sigma(p,\kappa)$ and $D_\sigma^{n,m,r}(p,\kappa)$ are the coefficients associated with the state $|\Psi\rangle_{11}$ and $\hat{A}_\sigma(p,\kappa)$ and $\hat{D}_\sigma^{n,m,r}(p,\kappa)$ are the coefficients of state $|\Psi\rangle_{22}$. We observe that the transformation $\kappa \to \kappa^{-1}$ leaves the form of the non-interacting equations (3.4.9) and the three-magnon interacting equations, invariant

$$\delta(n,m,r) \xrightarrow{\kappa\to\kappa^{-1}} \delta(n,m,r)_{\text{with } D_\sigma(p,\kappa^{-1})} \tag{3.4.16}$$

$$\beta_{l(r)}(n) \xrightarrow{\kappa\to\kappa^{-1}} \beta_{l(r)}(n)_{\text{with } D_\sigma(p,\kappa^{-1})} \tag{3.4.17}$$

which was also the case for the three-magnon problem. On the other hand, the coefficients of the two-magnon interacting equations, and the four-magnon interacting equation depend on κ in a way which is not symmetric under $\kappa \to \kappa^{-1}$, therefore they change under the $\mathbb{Z}_2$ transformation.

The action of parity cannot only reverse the order of the states by $l_i \to -l_i$. To follow the color contraction rules, additionally, we replace Q_{12} with Q_{21} while preserving the color indices of ϕ's in the reflection process. This is a particular definition of the parity, as preserving the color indices of Q_{12} and Q_{21} while changing the colors of ϕ's in the reflection process would mix with the action of the $\mathbb{Z}_2$ operator. Then, the action of parity on the momentum states is given by

$$\mathcal{P}\left|\Psi(p_1,p_2,p_3,p_4)\right\rangle_{11} = \sum_{l_1<l_2<l_3<l_4} \Psi(l_1,l_2,l_3,l_4)\left|-l_4,-l_3,-l_2,-l_1\right\rangle_{11} \tag{3.4.18}$$

$$= \sum_{l_1<l_2<l_3<l_4}\sum_{\sigma\in\mathcal{S}_4}\left(A_\sigma(\vec{p},\kappa) + D_\sigma^{l_2-l_1-1,l_3-l_2-1,l_4-l_3-1}(\vec{p},\kappa)\right)e^{i\vec{p}_\sigma\cdot\vec{l}}\left|-l_4,-l_3,-l_2,-l_1\right\rangle_{11} \ , \tag{3.4.19}$$

where $\vec{p}_\sigma = (p_{\sigma(1)},p_{\sigma(2)},p_{\sigma(3)},p_{\sigma(4)})$. If, for every element $\sigma = (ijkl) \in \mathcal{S}_4$, we introduced the reflected element of the symmetric group $\sigma^r = (lkji)$, and we inverted the ordering of the position variables, $-l_i = x_{5-i}$, the parity transform of the four-magnon long-range Bethe ansatz (3.4.4) is written as

$$\mathcal{P}\left|\Psi(p_1,p_2,p_3,p_4)\right\rangle_{11} = \sum_{l_1<l_2<l_3<l_4} \Psi(l_1,l_2,l_3,l_4)\left|-l_4,-l_3,-l_2,-l_1\right\rangle_{11} \tag{3.4.20}$$

$$= \sum_{x_1<x_2<x_3<x_4} \sum_{\sigma\in\mathcal{S}_4} \left(A_\sigma(\vec{p},\kappa) + D_\sigma^{x_4-x_3-1,x_3-x_2-1,x_2-x_1-1}(\vec{p},\kappa)\right) e^{-i\vec{p}_{\sigma^r}\cdot\vec{x}} \left|x_1,x_2,x_3,x_4\right\rangle_{11} \ . \tag{3.4.21}$$

Then, we conclude that the four-magnon eigenstate is parity invariant

$$\mathcal{P}\left|\Psi(p_1,p_2,p_3,p_4)\right\rangle_{11} = e^{i\varphi(p,\kappa)}\left|\Psi(-p_1,-p_2,-p_3,-p_4)\right\rangle_{11} \ . \tag{3.4.22}$$

if the following conditions are satisfied by the scattering coefficients and the position-dependent corrections,

$$e^{i\varphi(\vec{p},\kappa)} A_{\sigma^r}(-\vec{p},\kappa) = A_\sigma(\vec{p},\kappa) \ , \tag{3.4.23}$$

$$e^{i\varphi(p,\kappa)} D_{\sigma^r}^{n,m,r}(-\vec{p},\kappa) = D_\sigma^{r,m,n}(\vec{p},\kappa) \ . \tag{3.4.24}$$

Here, $e^{\varphi(\vec{p},\kappa)}$ is a phase factor that is defined with respect to the scattering coefficients and the position-dependent corrections. The action of parity can be summarized in terms of a map defined by the scattering coefficients and the position-dependent corrections,

$$\{p_1,p_2,p_3,p_4,\kappa,A_\sigma,D_\sigma^{n,m,r}\} \to \{-p_1,-p_2,-p_3,-p_4,\kappa,A_{\sigma^r},D_{\sigma^r}^{r,m,n}\} \ . \tag{3.4.25}$$

This formulation of the parity transformation does not explicitly account for how the dependence of the scattering coefficients and position-dependent corrections on momentum variables changes when the momentum variables are flipped in sign, as it is given in (3.4.23) and (3.4.24). Until we obtain the explicit solution for the position-dependent corrections, we use this transformation as a guiding principle, expecting the generating functions to stay invariant under it. This ensures that the overall solution satisfies (3.4.22), allowing us to determine the eigenvalues of the parity operator from the explicit form of the position-dependent corrections. From the parity transformation map, we observe that the scaled position-dependent corrections transform as follows:

$$\tilde{D}_\sigma^{n,m,r} \to e^{-im\mathcal{P}_4}\tilde{D}_{\sigma^r}^{r,m,n} \ . \tag{3.4.26}$$

Furthermore, under the parity transformation, the left and right two-magnon interacting equations transform to each other, as well as the left and right three-magnon interacting equations,

$$\gamma_{l,34}(m,r) \leftrightarrow \gamma_{r,12}(r,m) \tag{3.4.27}$$

$$\beta_{l,4}(r) \leftrightarrow \beta_{r,1}(r) \tag{3.4.28}$$

Additionally, the four-magnon interacting equation preserves its form, while the two two-magnon interacting equations and the non-interacting equations get mapped to another equation of the same type with altered permutation indices,

$$\delta_\sigma(n,m,r) \leftrightarrow \delta_{\sigma^r}(r,m,n) \tag{3.4.29}$$

$$\gamma_{rl,34}(m) \leftrightarrow \gamma_{rl,12}(m) \tag{3.4.30}$$

$$\alpha \leftrightarrow \alpha \tag{3.4.31}$$

The relations between the scattering coefficients and the position-dependent corrections derived from the action of the $\mathbb{Z}_2$ and parity transformations will help us constrain the generating functions and obtain the special solution for the eigenvectors.

3.4.1 The Most General Solution

After deriving the eigenvalue equations in position space, and highlighting the symmetries of the Hamiltonian underlying these expressions, we proceed to solve the eigenvalue problem. The initial step is to interpret these relations as recursion relations and reformulate the problem within the framework of generating functions. From the outset, it becomes evident that for the states of an open, infinite spin chain, the eigenvalue problem alone does not fully constrain the position-dependent corrections, leaving a significant number of degrees of freedom undetermined. Consequently, the generating functions will inherently encode this freedom. In this section, we systematically reduce these additional degrees of freedom by leveraging the symmetries of the model and insights drawn from the two-magnon CBA eigenstates. Then, in Section 3.8 we further impose periodic boundary conditions.

Solving the non-interacting equations. We define a generating function of three complex variables that encodes the position-dependent corrections for each permutation in its expansion around the origin,

$$G_\sigma(x,y,z) = \sum_{n,m,r=0}^{\infty} D_\sigma^{n,m,r} x^n y^m z^r \ . \tag{3.4.32}$$

We should keep in mind that the position-dependent corrections, $D_\sigma^{n,m,r}$ for all $\sigma \in \mathcal{S}_4$ are functions of momentum variables (p_1, p_2, p_3, p_4) and κ. These position-dependent corrections come from the $|\Psi\rangle_{11}$ states, meaning that the $\mathbb{Z}_2$ conjugate states, $|\Psi\rangle_{22}$, would contain the $\kappa \to \kappa^{-1}$ transformed version of these $D_\sigma^{n,m,r}$. Although we focus on the solution of the former, the latter follows exactly the same procedure and can be obtained by $\kappa \to \kappa^{-1}$. Since the scaling of the position-dependent corrections (3.4.12) simplifies the eigenvalue equations drastically, we use the generating function with the scaled position-dependent corrections. This one is related to the initial definition of the generating function (3.4.32) as

$$\tilde{G}_\sigma(x,y,z) = G_\sigma(e^{-ip_{\sigma(1)}}x, e^{ip_{\sigma(3)}+ip_{\sigma(4)}}y, e^{ip_{\sigma(4)}}z) \ . \tag{3.4.33}$$

Additionally, by combining the parity transformation on the wave function given in (3.4.25) with the parity transformation on the variables of the generating function,

$$\{x,y,z\} \leftrightarrow \{z, e^{i\mathcal{P}_4}y, x\} \ , \tag{3.4.34}$$

where the rescaling of y is a consequence of the observation (3.4.26), the transformation of the generating function under the action of parity becomes,

$$\tilde{G}_\sigma(x,y,z) \to \tilde{G}_{\sigma^r}(z,y,x) \ . \tag{3.4.35}$$

This is consistent with the rest of our formalism. By applying the parity transformation at the level of the generating function, one can verify whether the solution respects parity invariance. Indeed, we demonstrate later that this is the case.

We start solving the eigenvalue problem in terms of generating functions starting from the non-interacting equations given in (3.4.13). We impose the vanishing of the non-interacting equations,

$$\delta_\sigma(n,m,r) = 0 \quad \text{for} \quad n,m,r > 0 \ , \tag{3.4.36}$$

and obtain the following form of the scaled generating function,

$$\tilde{G}_\sigma(x,y,z) = \frac{F_\sigma(x,y,z)}{Q_4(x,y,z)} \ , \tag{3.4.37}$$

where the denominator is given by the polynomial,

$$Q_4(x,y,z) = \varepsilon_4 xyz - e^{-i\mathcal{P}_4}x^2z - e^{i\mathcal{P}_4}y^2z - xy - yz - xy^2 - xz^2 - x^2yz - xyz^2 \ , \tag{3.4.38}$$

and the numerator takes the form,

$$\begin{aligned} F_\sigma(x,y,z) = &\left(Q_4(x,y,z) + xz^2 + xyz^2\right)\tilde{G}_\sigma(x,y,0) - (1+y)xyz\partial_z\tilde{G}_\sigma(x,y,0) \\ &+ \left(Q_4(x,y,z) + e^{i\mathcal{P}_4}y^2z + xy^2\right)\tilde{G}_\sigma(x,0,z) - (z + e^{-i\mathcal{P}_4}x)xyz\partial_y\tilde{G}_\sigma(x,0,z) \\ &+ \left(Q_4(x,y,z) + e^{-i\mathcal{P}_4}x^2z + x^2yz\right)\tilde{G}_\sigma(0,y,z) - (1 + e^{i\mathcal{P}_4}y)xyz\partial_x\tilde{G}_\sigma(0,y,z) \\ &-(\varepsilon_4 xyz - e^{-i\mathcal{P}_4}x^2z - xy - yz - x^2yz)\tilde{G}_\sigma(x,0,0) \end{aligned}$$

$$
\begin{aligned}
&+xyz\partial_z\tilde{G}_\sigma(x,0,0)+e^{-i\mathcal{P}_4}x^2yz\partial_y\tilde{G}_\sigma(x,0,0)\\
&-\left(\varepsilon_4 xyz-e^{i\mathcal{P}_4}y^2z-xy-yz-xy^2\right)\tilde{G}_\sigma(0,y,0)\\
&+(1+y)xyz\partial_z\tilde{G}_\sigma(0,y,0)+(e^{i\mathcal{P}_4}y+1)xyz\partial_x\tilde{G}_\sigma(0,y,0)\\
&-\left(\varepsilon_4 xyz-xy-yz-xz^2-xyz^2\right)\tilde{G}_\sigma(0,0,z)\\
&+xyz^2\partial_y\tilde{G}_\sigma(0,0,z)+xyz\partial_x\tilde{G}_\sigma(0,0,z)+(\varepsilon_4 xyz-xy-yz)\tilde{D}_\sigma^{0,0,0}\\
&-xyz\left(\tilde{D}_\sigma^{0,0,1}+\tilde{D}_\sigma^{1,0,0}\right)\ .
\end{aligned}
\tag{3.4.39}
$$

We keep the contribution of $\tilde{D}^{0,0,0}$ for completeness but we will choose conventions where this vanishes. Here, we use $\partial_z\tilde{G}_\sigma(x,y,0)$ as shorthand notation for $\Big[\partial_z G_\sigma(x,y,z)\Big]_{z=0}$, and similarly for the other derivatives. After imposing the non-interacting equations on the initial form of the generating function (3.4.32), we observe that the number of unknown position-dependent corrections is reduced to those encoded in six two-variable generating functions: $G_\sigma(x,y,0)$, $G_\sigma(x,0,z)$, $G_\sigma(0,y,z)$, $\partial_z G_\sigma(x,y,0)$, $\partial_y G_\sigma(x,0,z)$, and $\partial_x G_\sigma(0,y,z)$ in addition to nine single-variable generating functions such as $G_\sigma(x,0,0)$, $G_\sigma(0,y,0)$, $G_\sigma(0,0,z)$, among others. Because the numerator of the generating function consists of the sum of functions that depend at most on two of the three variables weighted with coefficients that are at most linear in the remaining variables (e.g. $\tilde{G}_\sigma(x,y,0)$ is multiplied by a polynomial that is at most linear in z, while $\partial_x\tilde{G}_\sigma(0,0,z)$ is multiplied by a polynomial that is at most linear in x and y), it fulfills the differential equation

$$
\partial_x^2\partial_y^2\partial_z^2\big(F_\sigma(x,y,z)\big)=0\ , \tag{3.4.40}
$$

and interacting equations can also be interpreted as differential equations. Before deriving the relations between generating functions coming from the interacting equations we point out that a simple counting of the position-dependent corrections which are fixed by the non-interacting equations reveals the number of undetermined two-variable generating functions. It turns out that the undetermined position-dependent corrections counted in terms of two-variable generating functions should be four rather than six. This implies that the generating function given in (3.4.39) does not know about a set of non-interacting equations encoded by two of these two-variable generating functions. Furthermore, we observe that the generating function given in (3.4.37) is not analytic around the origin, contradicting our initial assumption (3.4.32) and undermining the entire purpose of extracting position-dependent corrections from the generating function. These two observations lead us to eliminate the spurious two-variable generating functions by imposing analyticity at the origin, allowing us to obtain the final form of the generating function that incorporates the solution to all non-interacting equations, (3.4.9). At first glance, this may seem somewhat artificial; however, we find that there is a natural way to impose the analyticity constraints, and these additional constraints correspond to the non-interacting eigenvalue equations that are missing from (3.4.39).

Analyticity. To complete the derivation of a generating function that includes the position-dependent corrections solving the non-interacting equations (3.4.9), we impose analyticity at the point $(x, y, z) = (0, 0, 0)$. More precisely, we examine the generating function defined in (3.4.37) and eliminate the poles at the origin by solving a system of equations. The coefficients that accompany inverse powers in the expansion of the generating function are linear combinations of undetermined, position-dependent corrections. They form a system of equations that turns out to be a subset of the original non-interacting equations (3.4.9), which confirms the consistency of the approach and leads to the final form of the non-interacting generating function. Instead of canceling the poles one by one, we impose analyticity conditions altogether as follows. We start by identifying the curve defined by the vanishing of the polynomial in the denominator (3.4.38). As a first step, we factorize the elliptic curve appearing in the denominator,

$$Q_4(x,y,z) = (z - z_+(x,y))(z - z_-(x,y)) \ , \tag{3.4.41}$$

where

$$z_\pm(x,y) = \frac{\varepsilon_4 xy - \left(e^{-i\mathcal{P}_4}x^2 + y\right)\left(1 + e^{i\mathcal{P}_4}y\right)}{2x(1+y)} \mp \sqrt{\left(\frac{\varepsilon_4 xy - \left(e^{-i\mathcal{P}_4}x^2 + y\right)\left(1 + e^{i\mathcal{P}_4}y\right)}{2x(1+y)}\right)^2 - y} \ . \tag{3.4.42}$$

Demanding analyticity of $\tilde{G}_\sigma(x,y,z)$ at the origin is equivalent to demanding the numerator of $\tilde{G}_\sigma(x,y,z)$, (3.4.39), to vanish at the points where the curve $Q_4(x,y,z)$ given in (3.4.38) vanishes around the origin. In contrast to the three-magnon case analyzed in [1], here both the z_+ curve and the z_- curve contain the $(x,y,z) = (0,0,0)$ point, however, this point is a branch point for both of them. When we assume that $-\pi < Arg(x) < \pi$, and similarly for y, z, and the total momentum, $e^{i\mathcal{P}_4}$, then z_+ admits the origin as a limit point and we can expand around the origin.[16] However, demanding analyticity at $z = z_+(x,y)$ alone,

$$F_\sigma(x,y,z_+(x,y)) = 0 \ , \tag{3.4.43}$$

[16] Similarly, the z_+ curve is ill-defined for $x = 0$ when we approach the origin from the outside of the range $-\pi < Arg(x) < \pi$ for complex variables x, y, z and $e^{i\mathcal{P}_4}$. Here we assume that we are in the positive cone of the three-dimensional complex space and $-\pi < \mathcal{P}_4 < \pi$. Note that a similar analysis can be done for the rest of the complex space and we can choose appropriate curves to ensure analyticity as well. For simplicity here we present only one.

is not enough to ensure analyticity around the origin. On the other hand, demanding that the numerator vanishes on the curve $z = z_-(x, y)$ together with the first analyticity condition given above would force all the position-dependent corrections, $D_\sigma^{n,m,r}$ to vanish for $n, m, r \geq 1$ because these two conditions would cancel the entire denominator of the generating function, $Q_4(x, y, z)$ and when incorporating the interacting equations into our solution, this would lead to an inconsistency.

A natural way to complete the analyticity conditions is to demand that the resulting generating function is invariant under parity transformation, (3.4.25) together with (3.4.34). This condition leads us to consider,

$$z_\pm(x, y) \xrightarrow{\mathbb{P}} x_\pm(y, z) \;, \tag{3.4.44}$$

such that $x_\pm$ is coming from another factorization of the elliptic curve,

$$Q_4(x, y, z) = (x - x_+(y, z))(x - x_-(y, z)) \;. \tag{3.4.45}$$

Exactly as in the case of $z_\pm$, the origin is a branch point of $x_\pm$, and only x_+ admits a well-defined limit around it. We observe that together with (3.4.43), imposing

$$F_\sigma(x_+(y, z), y, z) = 0 \;, \tag{3.4.46}$$

determines two of the two-variable generating functions and removes all poles near the origin, while still yielding a non-trivial denominator. The resulting generating function is also parity invariant. To achieve this, we first solve the condition (3.4.43) by fixing the $\partial_z \tilde{G}_\sigma(x, y, 0)$ component of the generating function. Next, we solve the second condition (3.4.46) to obtain the two-variable function $\partial_x \tilde{G}_\sigma(0, y, z)$. Substituting these into the non-interacting ansatz gives the final form of the generating function.

In what follows, we turn to the relations between the generating functions that arise from the interacting eigenvalue equations. When we combine the solutions of the interaction and non-interacting equations given in this section, we choose to first solve the interacting equations and then impose the analyticity conditions given in (3.4.43) and (3.4.46) on the numerator of the generating function, which already includes the solution to the interacting equations. This approach does not alter the final result, and it ensures the analyticity of the full generating function.

Interaction equations in terms of generating functions. The generating function (3.4.37), together with the analyticity conditions (3.4.43) and (3.4.46), codifies the position-dependent corrections that solve the non-interacting equation (3.4.39). As in the three-magnon case, the non-interacting equations fix almost all position-dependent corrections. The remaining undetermined position-dependent corrections lie on the boundaries of the three-dimensional lattice and they are encoded in the two-variable and one-variable generating functions that appear in (3.4.39). This is the analogue of the three-magnon solution which has the boundary position-dependent corrections unfixed after solving the three-magnon non-interacting equations as depicted in Figure 3.3. Therefore, the interacting eigenvalue equations will be constraints on these two-variable generating functions and the nine single-variable generating functions.

As for the non-interacting equations, we first transform the recursion relations coming from the interacting equations to relations between generating functions, and then we solve these relations in the context of the special solution by imposing additional constraints in the next section. Note that the interacting eigenvalue equations for the minimum separation of the magnons,

$$\alpha\ , \qquad \beta_l(1)\ , \qquad \beta_r(1)\ , \qquad \gamma_l(1,1)\ , \qquad \gamma_m(1,1)\ , \qquad \gamma_r(1,1)\ , \qquad \gamma_{lr}(1)\ , \tag{3.4.47}$$

play a key role throughout the solution. Therefore, it is worth noting that they appear as initial conditions for the relations of generating functions, which we present in this section as was also the case for the three-magnon problem. Furthermore, we explicitly solve these equations at the beginning of Section 3.4.2 under additional assumptions on the scattering coefficients and position-dependent corrections. This results in a remarkably simple form of the position-dependent corrections, which remains valid even for configurations with larger magnon separations as we construct the special solution.

To complete the set of relations between the generating functions of the four-magnon problem, we also transform the interacting equations into the generating function formalism. An example of this transformation is given as

$$F^{\gamma_{l,34}}(x,y) = \sum_{n,m=0}^{\infty} \gamma_{l,34}(n+1,m+1)x^n y^m = 0\ . \tag{3.4.48}$$

And similarly we compute all these expressions for all permutations and distinct cases of interacting eigenvalue equations. We denote this set of relations as

$$\{F^{\gamma_{l,ij}}(y,z), F^{\gamma_{m,ij}}(x,z), F^{\gamma_{r,ij}}(x,y), F^{\beta_{l,i}}(z), F^{\gamma_{lr,ij}}(y), F^{\beta_{r,i}}(x)\}. \tag{3.4.49}$$

As discussed in this section, under the action of $\mathbb{Z}_2$ the coefficients in front of the generating functions stay invariant. We conclude that the scattering coefficients and the position-dependent corrections of the $|\Psi\rangle_{22}$ state have to satisfy the same equations. On the other hand, under the parity transformation, the expression for the three-magnon from the left transforms to the three-magnon from the right, and the expression for the two two-magnon interaction stays invariant.

Here, we completed the derivation of the relations between the pieces of the generating function (3.4.37) which are not fixed by the non-interacting equations. Combining all of these equations and obtaining the final form of the generating function is straightforward, as all of these relations are linear in terms of the one- and two-variable generating functions. However, there are infinitely many undetermined position-dependent corrections after combining all the pieces and the final form is not very illuminating. Therefore, instead of blindly trying to simplify our solution, we use this freedom to our advantage and impose additional conditions inspired by the CBA to obtain a simple solution.

3.4.2 Special Solution for the Four-Body Problem

In this section, we present a special solution to the four-magnon eigenvalue problem in the same spirit as Section 3.3.2. As the complexity of the system of linear equations increases from the three-magnons to the four-magnons, solving all the relations derived from the interacting equations leaves a large number of undetermined coefficients behind. Instead, we impose additional conditions, similar to those used in the three-magnon problem in Section 3.3.2, to obtain a solution with significantly fewer undetermined degrees of freedom.[17] However, even with these special conditions, not all position-dependent corrections are fully determined. We will utilize this remaining freedom in Section 3.5 to establish the connection between solutions with different numbers of magnons.

To obtain the special solution, we impose the factorization of scattering coefficients, consistent with the two-magnon solution (3.2.10),

$$\frac{A_{jikl}}{A_{ijkl}} = \frac{A_{kjil}}{A_{kijl}} = \frac{A_{klji}}{A_{klij}} = S_\kappa(p_i, p_j) \ , \tag{3.4.50}$$

for any permutation, A_σ such that $\sigma = (ijkl) \in \mathcal{S}_4$. Additionally, to enforce invariance under a subgroup of the permutation group, we constrain the position-dependent corrections by a partial factorizability condition. For the middle two permutation indices of all position-dependent corrections, we impose the following relation,

$$\tilde{D}^{n,m,r}_{ikjl} = S_\kappa(p_j, p_k) \tilde{D}^{n,m,r}_{ijkl} \ , \tag{3.4.51}$$

[17]We draw inspiration from dynamical Felder-like setups [139] and choose these additional constraints to establish factorizability. Details of the reasoning are given in Section 3.3.2.

for all D_σ, with $\sigma = (ijkl) \in \mathcal{S}_4$. Under these conditions, we first solve the eigenvalue equations with minimum separation as given in (3.4.47) and obtain the position-dependent corrections for the lowest separation explicitly. Then, we move on and solve the rest of the eigenvalue equations in terms of generating functions. We only solve for the pieces of the generating function, (3.4.39) which are not fixed by the non-interacting equations and impose the analyticity condition only at the end to simplify the expressions for the generating functions. Nevertheless, the final form of the solution describes a true eigenstate which can be checked independently.

Special solution for the minimum separation. Among the eigenvalue equations arising from the four-magnon problem, the one corresponding to the minimum separation of magnons, given in (3.4.47), plays a distinctive role. As in the three-magnon case, these equations serve as initial conditions for solving a system of differential equations. We solve the minimum separation equations by making special choices designed to render the remaining equations as permutationally symmetric as possible. These equations effectively determine the behavior of all position-dependent corrections, as they appear in the generating function relations in isolation from other contributions. Moreover, the role of these equations as initial values is not merely an analogy: the eigenvalue equations can be interpreted directly as difference equations and then transformed into differential equations via generating functions. Therefore, we will see that also in Section 3.6 when we are able to write a solution to the four-magnon problem based on the three-magnon solution we will do it by matching that solution to the solution of the minimum separation equations, especially the coefficients $\tilde{D}_\sigma^{1,0,0}$ and $\tilde{D}_\sigma^{0,0,1}$, and this will be enough to fully fix the position-dependent corrections.

Starting with the eigenvalue equations at minimum separation, given in (3.4.47), we impose the special conditions from (3.4.50) and (3.4.51) to identify the position-dependent corrections within these expressions. In doing so, we set some of these corrections to zero, simplifying the solution. As a result, the solution we present is not unique; however, it retains key features of the spin chain model. These properties include the vanishing of position-dependent corrections at the orbifold point ($\kappa = 1$), and the preservation of parity invariance, as specified in (3.4.23), (3.4.24), and (3.4.25).

As a first step, we use the four-magnon interacting equation to illustrate how the expressions can be simplified under the special conditions (3.4.50) and (3.4.51), leading to a special solution. The four-magnon interacting equation is given as

$$\alpha = \sum_{(ijkl)\in\mathcal{S}_4} e^{i(p_j+p_k+3p_l)}\omega(p_j,p_k;\kappa)\Big[\left(\kappa-\kappa^{-1}\right)A_{ijkl}+\left(\varepsilon_4-4\kappa-2\kappa^{-1}\right)\tilde{D}^{0,0,0}_{ijkl}-\tilde{D}^{1,0,0}_{ijkl}-\tilde{D}^{0,0,1}_{ijkl}\Big]\,, \tag{3.4.52}$$

such that

$$\omega(p_j, p_k; \kappa) = \frac{\left(e^{ip_j} - e^{ip_k}\right)\left(1 + e^{ip_j + ip_k}\right)}{1 + e^{ip_j + ip_k} - 2\kappa e^{ip_j}} \; . \tag{3.4.53}$$

To obtain this form, we make use of the following identity for the scattering coefficients which are factorized in terms of S_κs,

$$\sum_{(ijkl)\in\mathcal{S}_4} e^{i(p_j+2p_k+3p_l)}(e^{-ip_j}a(p_j,p_i,\kappa) + e^{-ip_l}a(p_l,p_k,\kappa))A_{ijkl} = 0 \; , \tag{3.4.54}$$

which vanishes because the sum can be re-arranged by using (3.4.50) and the definition of the scattering coefficient S_κ, (3.2.14). Secondly, the partial factorization (3.4.51) can be used to reduce the sum over all the permutations to a sum over only half of them. In this case, the summand, which includes the scattering coefficient, also simplifies and gives us an overall $(\kappa - \kappa^{-1})$ factor,

$$\begin{aligned} &\sum_{i,l\in\{1,2,3,4\}} e^{i(p_j+p_k+3p_l)} \left[a(p_k,p_j,\kappa^{-1})A_{ijkl} + a(p_j,p_k,\kappa^{-1})A_{ikjl}\right] \\ &\qquad = -\sum_{i,l\in\{1,2,3,4\}} e^{i(p_j+p_k+3p_l)} \frac{2\left(\kappa-\kappa^{-1}\right)\left(e^{ip_j} - e^{ip_k}\right)\left(1 + e^{ip_j+ip_k}\right)}{1 + e^{ip_j+ip_k} - 2\kappa e^{ip_j}} A_{i\underline{jk}l} \; , \end{aligned} \tag{3.4.55}$$

where the underlined indices indicate that, between (jk) and (kj), only the terms with $j < k$ are included. The $(\kappa - \kappa^{-1})$ factor plays a crucial role, as it ensures that all position-dependent corrections vanish in the limit $\kappa \to 1$, leaving only the CBA solution at the orbifold point. Similarly, for the rest of the four-magnon interacting equation, we make use of the partial factorizability property (3.4.51) and obtain,

$$\begin{aligned} &-\sum_{i,l\in\{1,2,3,4\}} e^{i(p_j+p_k+3p_l)} \left(e^{ip_k} + S_\kappa(p_j,p_k)e^{ip_j}\right)\left(\tilde{D}^{1,0,0}_{i\underline{jk}l} + \tilde{D}^{0,0,1}_{i\underline{jk}l}\right) \\ &\qquad = \sum_{i,l\in\{1,2,3,4\}} e^{i(p_j+p_k+3p_l)} \frac{\left(e^{ip_j} - e^{ip_k}\right)\left(1 + e^{ip_j+ip_k}\right)}{1 + e^{ip_j+ip_k} - 2\kappa e^{ip_j}} \left(\tilde{D}^{1,0,0}_{i\underline{jk}l} + \tilde{D}^{0,0,1}_{i\underline{jk}l}\right) \; . \end{aligned} \tag{3.4.56}$$

Therefore, we combine the final form of the sum over the permutations of scattering coefficients (3.4.55) with the sum over the position-dependent corrections (3.4.56) and obtain (3.4.52). Finally, we conclude that, for any permutation σ, a simple relation between the scattering coefficients and the position-dependent corrections of the lowest separation makes the four-magnon interacting equation vanish,

$$\tilde{D}^{1,0,0}_\sigma = \tilde{D}^{0,0,1}_\sigma = \left(\kappa - \kappa^{-1}\right) A_\sigma \; , \tag{3.4.57}$$

which is very similar to the special solution of the three magnon problem given in [1]. Note that taking $D^{0,0,0} = 0$ is reasonable for open infinite spin chains, as we can always redefine the position-dependent corrections and the scattering coefficients in the long-range Bethe ansatz (3.4.4) by shifting all of them with an expression that does not depend on position variables.

Moving our attention to solving the three-magnon interaction and two two-magnon interacting equations with minimum separation, imposing our assumptions, gives us the following solution,

$$\tilde{D}^{0,0,2}_{\sigma} = \left(\kappa - \kappa^{-1}\right)\left(2e^{ip_{\sigma(4)}} + \varepsilon_4 - 2\kappa - 2\kappa^{-1}\right) A_{\sigma} \;, \tag{3.4.58}$$

$$\tilde{D}^{2,0,0}_{\sigma} = \left(\kappa - \kappa^{-1}\right)\left(2e^{-ip_{\sigma(1)}} + \varepsilon_4 - 2\kappa - 2\kappa^{-1}\right) A_{\sigma} \;, \tag{3.4.59}$$

$$\tilde{D}^{1,1,0}_{\sigma} = -e^{i\mathcal{P}_4}\left(\kappa - \kappa^{-1}\right) A_{\sigma} \;, \quad \tilde{D}^{0,1,1}_{\sigma} = -\left(\kappa - \kappa^{-1}\right) A_{\sigma} \;, \tag{3.4.60}$$

provided that we fix $\tilde{D}^{0,1,0}_{ijkl} = \tilde{D}^{1,0,1}_{ijkl} = 0$. Finally, the solution of the minimum separation two-magnon interacting equations is given as

$$\tilde{D}^{0,1,2}_{\sigma} = -\left(2e^{ip_{\sigma(4)}} + 2\varepsilon_4 - 4\kappa - 2\kappa^{-1}\right)\left(\kappa - \kappa^{-1}\right) A_{\sigma} \;, \tag{3.4.61}$$

$$\tilde{D}^{1,0,2}_{\sigma} = \tilde{D}^{2,0,1}_{\sigma} = \left(e^{-ip_{\sigma(1)}+ip_{\sigma(4)}} + \frac{e^{-i\mathcal{P}_4}}{2}\left(1 - e^{i\mathcal{P}_4}\right)^2\right)\left(\kappa - \kappa^{-1}\right) A_{\sigma} \;, \tag{3.4.62}$$

$$\tilde{D}^{2,1,0}_{\sigma} = -e^{i\mathcal{P}_4}\left(2e^{-ip_{\sigma(1)}} + 2\varepsilon_4 - 4\kappa - 2\kappa^{-1}\right)\left(\kappa - \kappa^{-1}\right) A_{\sigma} \;, \tag{3.4.63}$$

provided that we fix $\tilde{D}^{0,2,0}_{ijkl} = \tilde{D}^{1,1,1}_{ijkl} = 0$. This completes the solution of the eigenvalue equations with minimum separation. An immediate question we can ask about these position-dependent corrections is whether or not they satisfy the conditions given in (3.4.23) and (3.4.24) for the overall wave function to be parity invariant. The answer is yes, but when we apply the parity transformation map (3.4.25) we should keep in mind that the scaled position-dependent corrections bring extra factors of $e^{i\mathcal{P}_4}$, as emphasized in (3.4.26).

In solving the minimum separation equations, we made specific choices, such as setting $\tilde{D}^{0,1,0}_{\sigma} = 0$. Alternatively, one could choose $\tilde{D}^{0,1,0}_{\sigma} = (\kappa - \kappa^{-1})A_{\sigma}$, analogous to the position-dependent corrections in (3.4.57). This choice would shift the remaining coefficients by a factor of $(\kappa - \kappa^{-1})A_{\sigma}$. For example, instead of (3.4.58), we would obtain, $\tilde{D}^{0,0,2}_{\sigma} = (\kappa - \kappa^{-1})(2e^{ip_{\sigma(4)}} - 1 + \varepsilon_4 - 2\kappa - 2\kappa^{-1})A_{\sigma}$. At this point, we see no compelling reason to prefer one choice over the other, and therefore proceed with a representative option. A more natural prescription for fixing these position-dependent corrections may emerge by refining the solution to the eigenvalue equation with periodic boundary conditions, as discussed in Section 3.8, particularly for long spin chains. We leave this to future work.

Special solution for all position-dependent corrections. After fixing the minimum separation position-dependent coefficients, we focus on fixing the undetermined pieces of the generating functions by substituting the special solution above and using the partial factorization of the position-dependent corrections, (3.4.51) which can be rewritten in terms of the generating function as

$$\tilde{G}_{ikjl}(x,y,z) = S_\kappa(p_j,p_k)\tilde{G}_{ijkl}(x,y,z)\ . \tag{3.4.64}$$

This relation between generating functions reduces the number of distinct generating functions from twenty-four to twelve. Then, we calculate three two-variable generating functions for each permutation $\sigma \in \mathcal{S}_4$ by solving the two-magnon interacting equations $F^{\gamma_{l,ij}}(y,z), F^{\gamma_{m,ij}}(x,z), F^{\gamma_{r,ij}}(x,y)$ as they were listed in (3.4.49). The solution of the two-magnon interacting equations is given as follows,

$$\begin{aligned}&\left(y(1-\varepsilon_4 z+z^2+2\kappa z+y)+z^2\right)\tilde{G}_\sigma(0,y,z) = -yz\left(1+e^{i\mathcal{P}_4}y\right)\partial_x\tilde{G}_\sigma(0,y,z) - 2yz\left(\kappa-\kappa^{-1}\right)A_\sigma\\&\quad + y(1-\varepsilon_4 z+y+2\kappa z)\tilde{G}_\sigma(0,y,0) + yz\left(1+e^{i\mathcal{P}_4}y\right)\partial_x\tilde{G}_\sigma(0,y,0) + yz(1+y)\partial_z\tilde{G}_\sigma(0,y,0)\\&\quad + \left(y\left(1-\varepsilon_4 z+z^2+2\kappa z\right)+z^2\right)\tilde{G}_\sigma(0,0,z) + yz^2\partial_y\tilde{G}_\sigma(0,0,z) + yz\partial_x\tilde{G}_\sigma(0,0,z)\ .\end{aligned} \tag{3.4.65}$$

We choose to express $\tilde{G}(0,y,z)$ in terms of $\partial_x\tilde{G}(0,y,z)$, so that $\tilde{G}(0,y,z)$ is thereby determined, while $\partial_x\tilde{G}(0,y,z)$ remains to be fixed. Here we omit the constraints coming from the analyticity condition (3.4.43) and (3.4.46) to simplify the expressions. At this stage, the solution of the generating function looks like it has poles around the origin, once we divide by the polynomial factor that appears on the left-hand side of (3.4.65). These are again spurious poles coming from the two-magnon interacting equations that are not counted yet. Similar to the non-interacting equations we impose analyticity by fixing one of the single-variable generating functions on the curve, which is coming from the vanishing of the polynomial factor in the denominator of $\tilde{G}_\sigma(0,y,z)$, that passes through the origin. We can impose each of these analyticity conditions at the end when we assemble everything. Similarly, we solve two more two-variable generating functions from the rest of the two-magnon interacting equations,

$$\begin{aligned}&(\kappa(xz(-\varepsilon_4+x+z)+x+z)+2xz)\,\tilde{G}_\sigma(x,0,z) = -\kappa xz(e^{-i\mathcal{P}_4}x+z)\partial_y G_\sigma(x,0,z)\\&+(\kappa(xz(-\varepsilon_4+z)+x+z)+2xz)\,\tilde{G}_\sigma(0,0,z) + \kappa xz^2\partial_y\tilde{G}_\sigma(0,0,z) + \kappa xz\partial_x\tilde{G}_\sigma(0,0,z)\\&+(\kappa(xz(-\varepsilon_4+x)+x+z)+2xz)\,\tilde{G}_\sigma(x,0,0) + e^{-i\mathcal{P}_4}\kappa x^2 z\partial_y\tilde{G}_\sigma(x,0,0) + \kappa xz\partial_z\tilde{G}_\sigma(x,0,0)\\&-\frac{2xz\kappa\left(\kappa-\kappa^{-1}\right)A_\sigma\left(1-e^{-ip_{\sigma(1)}}x-e^{ip_{\sigma(4)}}z\right)}{\left(1-e^{-ip_{\sigma(1)}}x\right)\left(1-e^{ip_{\sigma(4)}}z\right)}\ .\end{aligned} \tag{3.4.66}$$

We highlight these factors because they will play a crucial role in the following sections. The rest of the two-magnon interacting equations are solved,

$$\left((x^2+e^{i\mathcal{P}_4}y)(e^{i\mathcal{P}_4}y+1)-e^{i\mathcal{P}_4}xy(\varepsilon_4-2\kappa)\right)\tilde{G}_\sigma(x,y,0) = -e^{i\mathcal{P}_4}xy(1+y)\partial_z\tilde{G}_\sigma(x,y,0)$$

$$
\begin{aligned}
&- 2e^{i\mathcal{P}_4}xy(\kappa-\kappa^{-1})A_\sigma + e^{i\mathcal{P}_4}y\left(1+e^{i\mathcal{P}_4}y-\varepsilon_4 x+2\kappa x\right)\tilde{G}_\sigma(0,y,0)\\
&+ e^{i\mathcal{P}_4}xy\Big((1+y)\partial_z\tilde{G}_\sigma(0,y,0)+\left(1+e^{i\mathcal{P}_4}y\right)\partial_x\tilde{G}_\sigma(0,y,0)\Big)\\
&+ \left(x^2-e^{i\mathcal{P}_4}xy(\varepsilon_4-2\kappa-x-x^{-1})\right)\tilde{G}_\sigma(x,0,0)+x^2y\partial_y\tilde{G}_\sigma(x,0,0)+e^{i\mathcal{P}_4}xy\partial_z\tilde{G}_\sigma(x,0,0)\,.
\end{aligned}
\tag{3.4.67}
$$

Furthermore, we solve eigenvalue equations coming from the two two-magnon interacting equation $F^{\gamma_{lr,ij}}(y)$ as well as the three-magnon interacting equations $F^{\beta_{l,i}}(z)$ and $F^{\beta_{r,i}}(x)$ in terms of generating functions. In this case, the partial factorization property alone is not enough to get rid of the sum over permutation indices, therefore we choose to solve for each permutation separately to obtain the most symmetric solution. To demonstrate the strategy we focus on the left three-magnon interacting expression,

$$
F^{\beta_{l,a}}(z)=\sum_{(ijk)\in\mathcal{S}_3}F^{\beta_{l,a}}_{ijk}(z)\,,
\tag{3.4.68}
$$

such that $(ijka)\in\mathcal{S}_4$ and, instead of finding the general solution of $F^{\beta_{l,a}}(z)=0$, we find the solution of $F^{\beta_{l,a}}_{ijk}(z)=0$ and check if the resulting solution in terms of the one-variable generating function satisfies the partial factorization (3.4.51). In this case, we obtain,

$$
\tilde{G}_\sigma(0,0,z)=-\frac{z\partial_x\tilde{G}_\sigma(0,0,z)+z^2\partial_y\tilde{G}_\sigma(0,0,z)-2z\left(\kappa-\kappa^{-1}\right)A_\sigma/\left(1-e^{ip_{\sigma(4)}}z\right)}{1-(\varepsilon_4-2\kappa-2\kappa^{-1})z+z^2}\,.
\tag{3.4.69}
$$

Similarly, the solution of the three-magnon interaction from the right and the two-two magnon interacting equations give

$$
\tilde{G}_\sigma(x,0,0)=-\frac{x\partial_z\tilde{G}_\sigma(x,0,0)+x^2e^{-i\mathcal{P}_4}\partial_y\tilde{G}_\sigma(x,0,0)-2x\left(\kappa-\kappa^{-1}\right)A_\sigma/\left(1-e^{-ip_{\sigma(1)}}x\right)}{1-(\varepsilon_4-2\kappa^{-1}-2\kappa)x+x^2}\,,
\tag{3.4.70}
$$

$$
\tilde{G}_\sigma(0,y,0)=\frac{1}{\varepsilon_4-4\kappa}\Big((1+y)\partial_z\tilde{G}_\sigma(0,y,0)+(1+e^{i\mathcal{P}_4}y)\partial_x\tilde{G}_\sigma(0,y,0)-2\left(\kappa-\kappa^{-1}\right)A_\sigma\Big)\,.
\tag{3.4.71}
$$

At this point, we have solved all the interacting equations. The last step remaining is to impose the analyticity conditions (3.4.43) and (3.4.46) and substitute all the two-variable and one-variable generating functions into the generating function (3.4.37). Nevertheless, this final form of the special solution still has undetermined position-dependent corrections. Since the expressions from each of the pieces of the generating function are very involved, we summarize the solution by color coding the pieces of the non-interacting generating function according to the stage we find the solution. When we bring everything together, we obtain

$$\begin{aligned}
Q_4(x,y,z)G_\sigma(x,y,z) = {} & \left(Q_4(x,y,z)+xz^2+xyz^2\right)\tilde{G}_\sigma(x,y,0)-(1+y)xyz\partial_z\tilde{G}_\sigma(x,y,0) \\
& +\left(Q_4(x,y,z)+e^{i\mathcal{P}_4}y^2z+xy^2\right)\tilde{G}_\sigma(x,0,z)-(z+e^{-i\mathcal{P}_4}x)xyz\underline{\partial_y\tilde{G}_\sigma(x,0,z)} \\
& +\left(Q_4(x,y,z)+e^{-i\mathcal{P}_4}x^2z+x^2yz\right)\tilde{G}_\sigma(0,y,z)-(1+e^{i\mathcal{P}_4}y)xyz\partial_x\tilde{G}_\sigma(0,y,z) \\
& -(\varepsilon_4xyz-e^{-i\mathcal{P}_4}x^2z-xy-yz-x^2yz)\tilde{G}_\sigma(x,0,0) \\
& +xyz\partial_z\tilde{G}_\sigma(x,0,0)+e^{-i\mathcal{P}_4}x^2yz\underline{\partial_y\tilde{G}_\sigma(x,0,0)} \\
& -\left(\varepsilon_4xyz-e^{i\mathcal{P}_4}y^2z-xy-yz-xy^2\right)\tilde{G}_\sigma(0,y,0) \\
& +(1+y)xyz\partial_z\tilde{G}_\sigma(0,y,0)+(e^{i\mathcal{P}_4}y+1)xyz\partial_x\tilde{G}_\sigma(0,y,0) \\
& -\left(\varepsilon_4xyz-xy-yz-xz^2-xyz^2\right)\tilde{G}_\sigma(0,0,z) \\
& +xyz^2\underline{\partial_y\tilde{G}_\sigma(0,0,z)}+xyz\partial_x\tilde{G}_\sigma(0,0,z) \\
& -xyz\left(\tilde{D}_\sigma^{0,0,1}+\tilde{D}_\sigma^{1,0,0}\right)\,.
\end{aligned} \tag{3.4.72}$$

For clarity, we color-code the components of the generating function based on how they are fixed. The blue two-variable terms are determined in this section using the two-magnon interacting equations (3.4.65), (3.4.66), and (3.4.67). The purple one-variable terms are fixed by the three-magnon interacting equations (3.4.69), (3.4.70), and (3.4.71). The orange derivative terms are fixed by imposing analyticity on the two-variable generating functions obtained from two-magnon interactions. This is done in a parity-invariant way and is explained in detail in Section 3.6. The green two-variable derivative terms are then fixed by the analyticity conditions (3.4.43) and (3.4.46), as shown in Appendix B in [2], equations B.5 and B.7. The red position-dependent correction is determined from the minimum separation equations and given in (3.4.57). When solved in this order, the remaining undetermined coefficients appear only in the underlined generating functions. These are fully fixed in Section 3.6, although in a different order than presented here.

Counting of undetermined coefficients. After imposing the recursion relations derived from the non-interacting equations (3.4.13), we find that there are six two-variable generating functions and nine one-variable generating functions that are not fixed, the latter being contained in the former. Imposing the analyticity condition reduces the number of undetermined two-variable generating functions to four, which agrees with the counting of the non-interacting equations as recurrence relations.

	Eq. Type	Two-variable	One-variable
Initial Freedom	Non-Interacting	6	9
Constraint	Analy. Non-Int.	2	0
	Two-Magnon Int.	3	0
	Two-M. Analy.+Parity	0	4
	Three-Magnon	0	3
Final Freedom		1	2

Table 3.2: *We list the counting of the position-dependent corrections starting from implementing the non-interacting recursion relations to the generating function* (3.4.32)*. Non-interacting equations give the initial freedom as given in* (3.4.39)*. Then analyticity conditions on this form of the generating function* (3.4.43) *and* (3.4.46) *bring the first set of constraints. Two-magnon interacting equations solved with additional constraints result in* (3.4.65)*,* (3.4.66) *and* (3.4.67)*. Ensuring the analyticity of these expressions in a parity-invariant way brings four more constraints. Finally, solving the three-magnon interacting equations gives* (3.4.69)*,* (3.4.70)*, and* (3.4.71)*. Here, we step-by-step count the constraints coming from the interacting equations and analyticity conditions. In the three-magnon problem, the generating function was a two-variable quantity and the special solution was leaving a one-variable function many freedom, in parallel four-magnon problem is a three-variable function, and after the special solution, we are left with a two-variable function.*

Then, the special solution fixes three out of four two-variable generating functions and leaves us with only one two-variable generating function, $\partial_y \tilde{G}(x, 0, z)$ which we will use to connect the solution of the four-magnon problem with three-magnons. Note that the solution of analyticity conditions given in (3.4.43) and (3.4.46), does not fix the one-variable generating functions which lie on the boundary of these two-variable ones, however the additional analyticity conditions coming from the special two-magnon solution above fix three of the single-variable pieces, additionally imposing parity fixes one more. Then, incorporating the three-magnon interacting equations and two-two magnon interacting equations fixes three one-variable generating functions and we are left with two one-variable generating functions as listed in Table 3.2. Recall that the generating function of the three-magnon problem was a two-variable quantity and the special solution was leaving a one-variable function many freedom, in parallel four-magnon problem is a three-variable function and after the special solution, we are left with a two-variable function. And the two single-variable functions which remain undetermined are the boundaries of this one two-variable function.

After investigating the relation between the eigenvectors with different numbers of excitations we constrain this solution further and get rid of all the leftover freedom.

Permutation symmetry is restored. The main idea behind finding the special solution described in this section is to express the position-dependent corrections solely in terms of permutations of momentum variables, for fixed magnon separations (i.e., fixed values of n, m, r). In other words, we seek a single function that captures all such corrections, where the only difference between them is the ordering of the momentum variables according to the corresponding permutation label:

$$D_{1234}^{n,m,r} \longleftrightarrow f(p_1, p_2, p_3, p_4), \tag{3.4.73}$$

$$D_{2134}^{n,m,r} \longleftrightarrow f(p_2, p_1, p_3, p_4). \tag{3.4.74}$$

To achieve this, we start with the generating functions which include the scaled position-dependent corrections. These forms of generating function only include the factors of total energy, total momentum, and κ which are invariant under the permutation of indices. This way all dependence on permutation of momenta is absorbed into the scaled position-dependent corrections. Then we construct generating functions that depend on a single permutation index, using initial conditions given in (3.4.57) and solutions to the two-variable components such as those in (3.4.65). By either setting all undetermined parts of the generating function to zero or assuming they are analytic functions around the origin, which have the same permutational symmetry, we reduce the full set of twenty-four generating functions $\tilde{G}_\sigma(x, y, z)$, each encoding a distinct position-dependent correction, to a single unified generating function,

$$\tilde{G}_\sigma(x, y, z) \longrightarrow \tilde{G}(p_{\sigma(1)}, p_{\sigma(2)}, p_{\sigma(3)}, p_{\sigma(4)}, \kappa; x, y, z)\ . \tag{3.4.75}$$

This way by permuting the order of momentum variables that we input to the generating function we are able to obtain the position-dependent corrections for distinct permutation labels σ. This implies that the position-dependent corrections admit a unifying description among the permutations of the indices,

$$D_\sigma^{n,m,r} = (\kappa - \kappa^{-1}) A_\sigma f(\vec{p}_\sigma; n, m, r, \kappa) = \oint_B \frac{dxdydz}{(2\pi i)^3} \frac{G(\vec{p}_\sigma, \kappa; x, y, z)}{x^{n+1} y^{m+1} z^{r+1}}\ . \tag{3.4.76}$$

To emphasize this point better we use the Yang operator formalism and analyze the coefficients that accompany the plane waves with respect to the permutation indices after fully constraining the solution.

3.5 From $M+1$-Magnons to M-Magnons

In this section, we investigate the relation between eigenstates of the Hamiltonian with different numbers of excitations. Our goal is to develop a systematic method that starts from an $M+1$-magnon eigenstate and yields the corresponding M-magnon eigenstate. This method must operate directly on the CBA and its long-range generalization, while also accommodating the structure of our model—where the $M = 1, 2$ magnon problems are solved by the CBA, and the $M \geq 3$ magnon problems require the long-range Bethe ansatz.

In conventional integrable models solvable by the CBA, the factorization in terms of two-magnon scattering amplitudes provides strong evidence for underlying integrability. However, in the case of the Hamiltonian (3.1.19), only the $M = 1, 2$ magnon sectors admit standard CBA solutions; for $M \geq 3$, position-dependent corrections must be incorporated. To bridge the gap between these cases, we introduce a limiting procedure that averages over all possible positions of a chosen magnon in an $(M+1)$-magnon eigenstate. Physically, this amounts to 'smearing' one magnon, which we show yields the corresponding M-magnon eigenstate.

We demonstrate that, under suitable assumptions detailed below, this limit establishes a concrete relation between eigenstates with successive magnon numbers. As we will see, this approach not only clarifies the recursive structure of the wave functions but also allows us to constrain all previously undetermined position-dependent corrections in the solution constructed in Section 3.4.2.

3.5.1 The Case of the Coordinate Bethe Ansatz

To explain the method, we begin by applying it to a generic three-magnon eigenstate expressed in standard CBA form. For an integrable model such as the Heisenberg XXX or XXZ spin chain, the two-magnon wave function takes the form

$$\Psi(p_1, p_2, l_1, l_2) = A^{(2)}_{12} e^{ip_1 l_1 + ip_2 l_2} + A^{(2)}_{21} e^{ip_2 l_1 + ip_1 l_2} \ , \tag{3.5.1}$$

defined up to an overall normalization,

$$|\Psi(p_1, p_2)\rangle = C \sum_{l_1 < l_2} \Psi(p_1, p_2, l_1, l_2) |l_1, l_2\rangle \ , \tag{3.5.2}$$

that can be chosen such that $A^{(2)}_{12} = 1$. Similarly, the three-magnon wave function takes the form,

$$\Psi(p_1, p_2, p_3, l_1, l_2, l_3) = \sum_{\sigma \in \mathcal{S}_3} A^{(3)}_{\sigma} e^{ip_{\sigma(1)} l_1 + ip_{\sigma(2)} l_2 + ip_{\sigma(3)} l_3} \ . \tag{3.5.3}$$

In integrable models, the three-magnon scattering coefficients $A_\alpha^{(3)}$ factorize into products of two-magnon coefficients $A_\sigma^{(2)}$ as

$$A_\sigma^{(3)} = \prod_{\alpha_i} A_{\alpha_i}^{(2)} \ , \tag{3.5.4}$$

where we have decomposed the permutation σ into a product of transpositions $\sigma = \alpha_1\alpha_2\alpha_3$. Although this decomposition is not unique, the YBE guarantees consistency among the possible decompositions.

To smear the magnon at position l_3, we average the wave function over all possible positions it can occupy, normalized by the total number of positions:

$$\lim_{N\to\infty} \frac{1}{N} \sum_{m=0}^{N} \Psi(p_1, p_2, p_3; n, m) = \lim_{N\to\infty} \left(\sum_{\sigma\in\mathcal{S}_3} A_\sigma^{(3)} e^{i(n+1)(p_{\sigma(2)}+p_{\sigma(3)})+ip_{\sigma(3)}} \frac{1}{N} \sum_{m=0}^{N} e^{ip_{\sigma(3)}m} \right) . \tag{3.5.5}$$

To 'localize' the smeared magnon, we scale its momentum as $p_3 = 2\pi\frac{\bar{p}_3}{N}$. In this limit, the magnon becomes stationary at $\bar{p}_3 = 0$, and the summation yields:

$$\lim_{N\to\infty} \frac{1}{N} \sum_{m=0}^{N} \Psi(p_1, p_2, p_3; n, m) = \frac{i}{2\pi} \left(A_{123}^{(3)} e^{i(n+1)p_2} + A_{213}^{(3)} e^{i(n+1)p_1} \right) \frac{1 - e^{2\pi i \bar{p}_3}}{\bar{p}_3} \ . \tag{3.5.6}$$

Here, the exponential factor $e^{i(n+2)p_{\sigma(3)}}$ appearing in front of the scattering coefficients $A_\sigma^{(3)}$ simplifies to unity when $\sigma(3) = 3$, and vanishes for $\sigma(3) = 1, 2$ as we take $N \to \infty$ limit due to

$$\lim_{N\to\infty} \frac{1}{N} \frac{1 - e^{ip_{\sigma(3)}N}}{1 - e^{ip_{\sigma(3)}}} = 0 \ , \qquad \text{for} \quad \sigma(3) = 1, 2 \ , \tag{3.5.7}$$

as neither p_1 nor p_2 is localized at zero. Thus, by subsequently taking the limit $\bar{p}_3 \to 0$, we recover the two-magnon wave function (after removing the center-of-mass phase):

$$\lim_{\bar{p}_3\to 0} \lim_{N\to\infty} \frac{1}{N} \sum_{m=0}^{N} \tilde{\Psi}(p_1, p_2, p_3; n, m) = A_{123}^{(3)} e^{i(n+1)p_2} + A_{213}^{(3)} e^{i(n+1)p_1} \ . \tag{3.5.8}$$

This demonstrates that the two-magnon eigenstate can be recovered from the three-magnon eigenstate via the smearing limit. Crucially, this construction relies on the integrability of the model, which ensures that the three-magnon scattering coefficients factorize according to (3.5.4). For instance, assuming the normalization $A_{123} = 1$, we obtain:

$$A_{123}^{(3)} = A_{12}^{(2)} = 1 \ , \qquad A_{213}^{(3)} = A_{21}^{(2)} \ . \tag{3.5.9}$$

We emphasize that this smearing procedure applies to any CBA solution with $M+1$ magnons (for $M \geq 1$), and yields the corresponding M-magnon solution. In particular, smearing a magnon in the two-magnon eigenstate recovers the corresponding one-magnon eigenstate, up to a normalization factor determined by the original wave function. In the following, we apply the same strategy to the long-range Bethe ansatz.

3.5.2 From Three-Magnon to Two-Magnon in Long-Range Bethe Ansatz

In this section, we test the relation between the two-magnon CBA solution and the three-magnon long-range Bethe ansatz solution of our Hamiltonian. We particularly focus on the special solution with factorized S_κ scattering coefficients given in Section 3.3.2 for the states with the magnons in the $Q_{12}Q_{21}Q_{12}$ order. We refer to the particular wave function coming from that special solution $\Psi(p_1, p_2, p_3; l_1, l_2, l_3)$. Recall that the long-range Bethe ansatz is given as

$$\Psi(p_1, p_2, p_3; l_1, l_2, l_3) = \sum_{\sigma \in \mathcal{S}_3} \left(A_\sigma + D_\sigma^{l_2-l_1-1, l_3-l_2-1} \right) e^{i\vec{p}_\sigma^3 \cdot \vec{l}^3} \tag{3.5.10}$$

$$= e^{il_1 \sum_i^3 p_i} \sum_{\sigma \in \mathcal{S}_3} \left(A_\sigma + D_\sigma^{n,m} \right) e^{i(n+1)(p_{\sigma(2)}+p_{\sigma(3)})+i(m+1)p_{\sigma(3)}} \ , \tag{3.5.11}$$

for simplicity, we replace the position of magnons with the separation between them, $n = l_2 - l_1 - 1$ and $m = l_3 - l_2 - 1$. Following the same steps given for the CBA, we sum over all possible positions that the magnon at l_3 can take

$$\lim_{N\to\infty} \frac{1}{N} \sum_{l_3=l_2+1}^{N} \Psi(p_1, p_2, p_3, l_1, l_2, l_3)$$
$$= e^{il_1 \mathcal{P}_3} \lim_{N\to\infty} \sum_{\sigma \in \mathcal{S}_3} e^{i(n+1)(p_{\sigma(2)}+p_{\sigma(3)})} \frac{1}{N} \sum_{m=0}^{N} \left(A_\sigma + D_\sigma^{n,m} \right) e^{i(m+1)p_{\sigma(3)}} \ . \tag{3.5.12}$$

After scaling one of the momentum variables as $p_3 = \bar{p}_3/N$ and localizing the limit of the sum of the wave functions at $\bar{p}_3 \to 0$, we obtain,

$$\lim_{\bar{p}_3\to 0} \lim_{N\to\infty} \frac{1}{N} \sum_{l_3=l_2+1}^{N} \Psi(p_1, p_2, p_3, l_1, l_2, l_3) = \Psi_{11}(p_1, p_2, l_1, l_2)$$
$$+ \lim_{\bar{p}_3\to 0} \lim_{N\to\infty} \frac{1}{N} e^{il_2 \mathcal{P}_3} \sum_{\sigma \in \mathcal{S}_3} e^{i(p_{\sigma(3)}-p_{\sigma(1)})} \sum_{m=0}^{N} \tilde{D}_\sigma^{n,m} \ , \tag{3.5.13}$$

by using the result (3.5.8), such that the two-magnon wave function, $\Psi_{11}(p_1,p_2,l_1,l_2)$ is the two-magnon eigenstate of our model with S_κ scattering coefficients given in (3.2.13) and $\tilde{D}$ is the scaled position-dependent correction for three magnons as defined in (3.3.27). Since the contribution of the scattering coefficients after smearing directly gives the wave function of the two-magnon CBA solution $\Psi_{11}(p_1,p_2,l_1,l_2)$, we expect the contribution with the position-dependent corrections to vanish. To show this, we strictly focus on that part of the computation. Crucially, we know the $N\to\infty$ limit for the sum of the position-dependent corrections can be written as

$$\lim_{N\to\infty}\sum_{m=0}^{N}\tilde{D}_\sigma^{n,m}=\sum_{m=0}^{\infty}\tilde{D}_\sigma^{n,m}=\frac{1}{n!}\frac{\partial^n\tilde{G}_\sigma(x,1)}{\partial x^n}\bigg|_{x=0}\,, \tag{3.5.14}$$

such that $\tilde{G}_\sigma(x,y)=G_\sigma\left(e^{-ip_{\sigma(1)}}x,e^{ip_{\sigma(3)}}y\right)$ is the three-magnon generating function which encodes the S_κ special solution of the three-magnon problem as it is given in Appendix B of [1] and it is summarized in Appendix A of [2] here. For each integer n, the coefficients $\frac{\partial^n\tilde{G}_\sigma(x,1)}{\partial x^n}\Big|_{x=0}$ are a function of total energy, ε_3 and total momentum, $\mathcal{P}_3$ as well as κ,

$$\begin{aligned}\tilde{G}_\sigma(x,1)=[F_\sigma(x)+H_\sigma(x)]\,/\big[&\kappa e^{ip_3}\left(-\varepsilon_3\,e^{i\mathcal{P}_3}x+e^{2i\mathcal{P}_3}+e^{i\mathcal{P}_3}x^2+2e^{i\mathcal{P}_3}x+e^{i\mathcal{P}_3}+x^2\right)\\&\left(-\varepsilon_3\,\kappa x+\kappa+\kappa x^2+2x\right)\left(-\varepsilon_3\,\kappa\rho_++\kappa+\kappa\rho_+^2+2\rho_+\right)\left(e^{i\mathcal{P}_3}-2\kappa\rho_++1\right)\\&\left(e^{ip_1}S_\kappa(p_1,p_2)+e^{ip_2}\right)\left(S_\kappa(p_1,p_2)S_\kappa(p_2,p_3)+S_\kappa(p_1,p_3)\right)\big]\,,\end{aligned} \tag{3.5.15}$$

such that the function $H_\sigma(x)$ includes only part of the generating function which is not fixed by the initial assumptions of the three-magnon special solution and we set it to zero previously,

$$\begin{aligned}H_\sigma(x)=&-\kappa e^{ip_3}x^2(1+e^{-i\mathcal{P}_3}x)\left(\rho_+(2-\varepsilon_3\,\kappa)+\kappa+\kappa\rho_+^2\right)\left(e^{ip_1}S_\kappa(p_1,p_2)+e^{ip_2}\right)\\&(S_\kappa(p_1,p_2)S_\kappa(p_2,p_3)+S_\kappa(p_1,p_3))(e^{i\mathcal{P}_3}(\kappa-2y)+\kappa x)(e^{i\mathcal{P}_3}y-2\kappa\rho_++1)\partial_yG_\sigma(x,0)\\&+\kappa e^{ip_3}\rho_+^2(1+e^{-i\mathcal{P}_3}\rho_+)\left(x(2-\varepsilon_3\,\kappa)+\kappa+\kappa x^2\right)\left(e^{ip_1}S_\kappa(p_1,p_2)+e^{ip_2}\right)\\&(S_\kappa(p_1,p_2)S_\kappa(p_2,p_3)+S_\kappa(p_1,p_3))(e^{i\mathcal{P}_3}y-2\kappa x+1)(e^{i\mathcal{P}_3}(\kappa-2y)+\kappa\rho_+)\partial_yG_\sigma(\rho_+,0)\,,\end{aligned} \tag{3.5.16}$$

and $F_\sigma(x)$ represents the rest of the numerator of the three-magnon special solution of the generating function which is a polynomial in variable x and its coefficients are parametrized by momentum variables and κ. It is explicitly given in the Mathematica file `fourmagnon.np` attached to [2]. Additionally, we adopt the shorthand notation for the expression,

$$\rho_+=\rho_+(1)=\frac{\sqrt{-e^{i\mathcal{P}_3}\left(e^{i\mathcal{P}_3}\left(-\varepsilon_3{}^2+4\varepsilon_3+4e^{i\mathcal{P}_3}+4\right)+4\right)}+(\varepsilon_3-2)e^{i\mathcal{P}_3}}{2(e^{i\mathcal{P}_3}+1)}\,, \tag{3.5.17}$$

which is coming from the factorization of the three-magnon curve that we used to ensure the analyticity of the generating function. If we assume that $G_\sigma^{(0,1)}(x,0)$ is an analytic function around $x=0$ and does not have a pole at $x=\rho_+$ then $\frac{\partial^n \tilde{G}_\sigma(x,1)}{\partial x^n}\Big|_{x=0}$ exists for each positive integer, and it is parametrized by nothing but momentum variables and κ. This is not affected by scaling one of the momentum variables as $p_3 = \frac{\tilde{p}_3}{N}$. Therefore we conclude that for any positive integer n

$$\lim_{N\to\infty} \sum_{m=0}^{N} \tilde{D}_\sigma^{n,m} = \textit{finite} \tag{3.5.18}$$

and since scaling the finite sum $\sum_{m=0}^{N} \tilde{D}_\sigma^{n,m}$ with a positive integer cannot cause a blow-up in the limit,

$$\lim_{N\to\infty} \frac{1}{N} \sum_{m=0}^{N} \tilde{D}_\sigma^{n,m} = 0 \ . \tag{3.5.19}$$

Thus, when the third magnon is smeared, the effect of position-dependent corrections is washed off. Similarly, when we smear the first magnon instead of the last one, meaning the Q_{12} magnon at l_1, we should start from the special solution of the three-magnon problem with the scattering coefficients factorized in terms of $S_{1/\kappa}$ factors that were also computed in Section 5.2 of [1]. Then, the smearing process gives us the wave function of the eigenstate of the two-magnon problem with the magnons $Q_{21}Q_{12}$ and $S_{1/\kappa}$ as its scattering coefficient.

The case of the four-magnon long-range Bethe ansatz is more intricate. Unlike in the three-to-two magnon reduction, where the position-dependent corrections vanish in the smearing limit, here we require that they do not vanish. Instead, they must reduce consistently to the position-dependent corrections of the three-magnon problem. This will ensure compatibility of the long-range structure across different magnon sectors and provide a stringent consistency check of our results.

3.5.3 From Four-Magnon to Three-Magnon in Long-Range Bethe Ansatz

We now turn to the smearing procedure applied to the special solution of the four-magnon problem, as presented in Section 3.4.2. Here we derive the requirements of smearing a magnon in a four-magnon eigenstate and recovering the corresponding special solution of the three-magnon problem with the correct factorized scattering coefficients. For all $M \geq 3$, the construction of eigenstates in our model necessarily involves position-dependent corrections. It is therefore essential to show that these corrections do not generically vanish under smearing—contrary to the behavior observed in the reduction from three-to-two magnons. Establishing this point further supports the existence of a family of M-magnon eigenstate solutions connected via smearing. This transition from the four- to the three-magnon state completes the web of relations among eigenstates in our model.

Moreover, we will demonstrate that these relations among eigenstates with differing numbers of excitations impose nontrivial constraints on the position-dependent corrections—constraints that are not manifest in either the general or special solutions of the eigenvalue problem alone. These additional conditions refine the structure of the allowed solutions and enhance our understanding of the solution space. Importantly, they lay the groundwork for a systematic extension of the long-range Bethe ansatz to an arbitrary number of magnons—a direction we pursue in forthcoming work.

We now focus on the special solution of the four-magnon long-range Bethe ansatz introduced in Section 3.4.2. The corresponding wave function for an open infinite spin chain is conveniently expressed in terms of the coordinate l_1 and the relative separations (n, m, r) and takes the following form:

$$\begin{aligned}
&\Psi(p_1, p_2, p_3, p_4; l_1, l_2, l_3, l_4) \\
&\quad = e^{il_1 \mathcal{P}_4} \sum_{\sigma \in \mathcal{S}4} \left(A_\sigma + D_\sigma^{n,m,r}\right) e^{i(n+1)(p_{\sigma(2)}+p_{\sigma(3)}+p_{\sigma(4)})+i(m+1)(p_{\sigma(3)}+p_{\sigma(4)})+i(r+1)p_{\sigma(4)}} \, .
\end{aligned} \tag{3.5.20}$$

To implement the smearing of the fourth magnon, located at l_4, we sum over all possible values it can take while keeping the remaining coordinates fixed. This results in the following expression:

$$\begin{aligned}
&\lim_{N\to\infty} \frac{1}{N} \sum_{l_4=l_3+1}^{N} \Psi(p_1, p_2, p_3, p_4; l_1, l_2, l_3, l_4) \\
&\qquad = e^{il_1 \mathcal{P}_4} \lim_{N\to\infty} \frac{1}{N} \sum_{\sigma \in \mathcal{S}4} e^{i\vec{p}\cdot\vec{n}} \left(\sum_{r=0}^{N} A_\sigma \, e^{i(r+1)p_{\sigma(4)}} + \sum_{r=0}^{N} D_\sigma^{n,m,r} \, e^{i(r+1)p_{\sigma(4)}} \right) .
\end{aligned} \tag{3.5.21}$$

Here, $\vec{p}\cdot\vec{n}$ denotes the plane wave contributions which are not directly related to smearing, $\vec{p}\cdot\vec{n} = (n+1)(p_{\sigma(2)} + p_{\sigma(3)} + p_{\sigma(4)}) + (m+1)(p_{\sigma(3)} + p_{\sigma(4)})$. Using the generalized version of the result in (3.5.8), we extend the smearing procedure from the four-magnon wave function to the three-magnon wave function, where the scattering coefficients factorize in terms of S_κ. This allows us to derive the scattering coefficients for the three-magnon long-range Bethe ansatz special solution directly from those of the four-magnon case. To obtain the special solution for the three-magnon problem, we take the following limit

$$\lim_{\bar{p}_4\to 0}\lim_{N\to\infty}\frac{1}{N}\sum_{l_4=l_3+1}^{N}\Psi_{11}(p_1,p_2,p_3,p_4,l_1,l_2,l_3,l_4)\stackrel{!}{=}\Psi_{12}(p_1,p_2,p_3,l_1,l_2,l_3)\ , \tag{3.5.22}$$

for $\bar{p}_4 = p_4/N$. This implies a corresponding matching condition between the position-dependent corrections of the four- and three-magnon solutions:

$$\lim_{\bar{p}_4\to 0} e^{il_1\sum_i^4 p_i}\lim_{N\to\infty}\frac{1}{N}\sum_{\sigma\in\mathcal{S}_4}e^{i\vec{p}\cdot\vec{n}}\sum_{r=0}^{N}D_\sigma^{n,m,r}e^{i(r+1)p_{\sigma(4)}} = e^{il_1\sum_i^3 p_i}\sum_{\sigma\in\mathcal{S}_3}e^{i\vec{p}\cdot\vec{n}}D_\sigma^{n,m}\ . \tag{3.5.23}$$

Since both the three- and four-magnon position-dependent corrections admit factorized representations—see equation (3.4.76)—we expect this limit to hold separately for each permutation. Therefore, similarly to the three-magnon case given in the previous section, first we focus on the infinite sum of position-dependent corrections, and we express this in terms of the four-magnon generating function which encodes the special solution of the four-magnon eigenvalue problem as in (3.4.72),

$$\lim_{N\to\infty}\sum_{r=0}^{N}\tilde{D}_\sigma^{n,m,r} = \sum_{r=0}^{\infty}\tilde{D}_\sigma^{n,m,r} = \frac{1}{n!\ m!}\frac{\partial^n\partial^m\tilde{G}_\sigma^{(4)}(x,y,1)}{\partial x^n\partial y^m}\Bigg|_{x,y=0}\ . \tag{3.5.24}$$

To avoid confusion, we label the generating functions $\tilde{G}^{(M)}$ to indicate the total number M of magnons in the corresponding spin chain. A crucial observation is that taking the limit $z\to 1$ at the level of the generating function corresponds exactly to performing the infinite sum over the relative position r. This connection will play a key role in the forthcoming analysis.

Since analyticity around the origin was ensured in Section 3.4 by imposing the conditions (3.4.43) and (3.4.46), the generating function encoding the four-magnon eigenvalue problem (3.4.1) admits a convergent Taylor expansion around $z = 0$. Consequently, if the limit $z\to 1$ were nonsingular, the situation would mirror that of the three-magnon case described in the previous section, and the left-hand side of (3.5.23) would vanish. However, this would result in a CBA-type three-magnon wave function that fails to solve the three-magnon eigenvalue problem.

Consequently, the four-magnon generating function must necessarily develop poles at $z = 1$ as the momentum variable localizes at $\bar{p} = 0$. More precisely, we expect the total smearing process to diverge in the absence of the $1/N$ prefactor,

$$\tilde{G}^{(4)}_{\sigma}(x,y,z) \to \infty \qquad \text{as} \qquad z \to 1, \quad \bar{p}_4 \to 0 \, . \tag{3.5.25}$$

We expect this divergence to occur in a controlled way: when we scale the partial sum by the factor $\frac{1}{N}$ and smear the magnon, this cancels the divergence and allows us to recover the correct three-magnon position-dependent coefficients. An asymptotic behavior consistent with this expectation is given by

$$\tilde{G}^{(4)}_{\sigma}(x,y,z) \sim \frac{1}{1-e^{ip_{\sigma(4)}}z}\tilde{G}^{(3)}_{\sigma}(x,y) \, , \qquad z \to 1 \, , \tag{3.5.26}$$

which produces the desired divergence for permutations with $\sigma(4) = 4$ when we localize $p_4 \to 0$. For permutations with $\sigma(4) \neq 4$, no divergence occurs as $z \to 1$ unless $p_{\sigma(4)} = 2n\pi$ for some integer n.

This structure ensures that, during the smearing and localization process, a large subset of permutations is suppressed, leaving only those of the form $\sigma = (ijk4)$, which correspond precisely to the permutations relevant for the three-magnon problem.

If we assume that the four-magnon generating function has the form given above, indeed

$$\begin{aligned} \lim_{N\to\infty}\frac{1}{N}\sum_{r=0}^{N}\tilde{D}^{n,m,r}_{\sigma} &= \lim_{N\to\infty}\frac{1}{N}\sum_{r=0}^{N}\frac{1}{n!m!r!}\left.\frac{\partial^n\partial^m\partial^r\tilde{G}^{(4)}_{\sigma}(x,y,z)}{\partial x^n\partial y^m\partial z^r}\right|_{x,y,z=0} \\ &\sim \frac{1}{n!m!}\left.\frac{\partial^n\partial^m\tilde{G}^{(3)}_{\sigma}(x,y)}{\partial x^n\partial y^m}\right|_{x,y=0}\lim_{N\to\infty}\frac{1}{N}\sum_{r=0}^{N}\frac{1}{r!}\left.\frac{\partial^r(z^r)}{\partial z^r}\right|_{z=0} = \frac{1}{n!m!}\frac{\partial^n\partial^m\tilde{G}^{(3)}_{\sigma}(x,y)}{\partial x^n\partial y^m} \, . \end{aligned} \tag{3.5.27}$$

In the remainder of this section, we analyze the special solution of the four-magnon eigenvalue problem and demonstrate, step by step, how the three-magnon position-dependent corrections emerge. We begin by examining the transition between the total energy and total momentum coefficients. Next, we show that the characteristic polynomial appearing in the denominator of the generating function—arising from the solution of the non-interacting equations (3.4.38)—reduces to its three-magnon counterpart. This allows us to identify the precise relations between the four-magnon and three-magnon special solutions which solve the non-interacting equations. After that, we refine relations between the solutions that also solve the two-magnon interacting equations. Finally, we show that the analyticity conditions and the solution of the lowest separation position-dependent corrections are compatible.

Under the scaling $p_4 = \frac{\bar{p}_4}{N}$, the total energy (3.4.10) and total momentum become

$$\varepsilon_4 = \varepsilon_3 + e^{i\frac{\bar{p}_4}{N}} + e^{-i\frac{\bar{p}_4}{N}} \, , \tag{3.5.28}$$

$$e^{i\mathcal{P}_4} = e^{i\mathcal{P}_3} e^{i\frac{\bar{p}_4}{N}} \;, \tag{3.5.29}$$

such that the four-magnon total energy and total momentum reduce to their three-magnon subtotals in the limit $N \to \infty$. This is enough to show that the denominator of the four-magnon generating function reduces to the three-magnon expression as $N \to \infty$,

$$\lim_{N\to\infty} Q_4(x, y, 1) = Q_3(x, y) \;, \tag{3.5.30}$$

where $Q_3(x, y)$ is given in (3.3.29). Then, to show that the special solution of the four-magnon problem has the form given in (3.5.26), first we point out that the pieces of the special solution coming from the middle two-magnon interacting equations as given in (3.4.66) and the three-magnon interacting equations from the left as they are given in (3.4.69), explicitly contain factors of the form $\left(1 - e^{ip_{\sigma(4)}} z\right)^{-1}$. In the limit $p_4 = \bar{p}_4/N \to 0$ as $N \to \infty$, these factors reduce precisely to the expected $(1 - z)^{-1}$ form for permutations of the type $\sigma = (ijk4)$. After identifying evidence for a potential divergence in the four-magnon generating function, we explicitly construct the additional conditions necessary to recover, exactly, the three-magnon generating function that encodes the special solution of the three-magnon problem. We begin by recalling the form of the generating function that satisfies the four-magnon non-interacting equations, as given in (3.4.37) and (3.4.39). We then substitute the contributions from the special solution, specifically the expressions in (3.4.67), (3.4.66), and (3.4.65), along with the remaining components in (3.4.69), (3.4.70), and (3.4.71). Finally, we impose the analyticity conditions given in (3.4.43) and (3.4.46) to arrive at the final form of the generating function, implicitly defined in (3.4.72).

To simplify the comparison between the four-magnon and three-magnon solutions, we focus on the structure of the generating function $G^{(4)}_\sigma(x, y, z)$. If we disregard the terms independent of the variable z in (3.4.39), we can write

$$\begin{aligned}
F^{(4)}_\sigma(x, y, z) \supset{}& \left(Q_4(x, y, z) + e^{i\mathcal{P}_4} y^2 z + xy^2\right) \tilde{G}_\sigma(x, 0, z) - (z + e^{-i\mathcal{P}_4} x) xyz \partial_y \tilde{G}_\sigma(x, 0, z) \\
&+ \left(Q_4(x, y, z) + e^{-i\mathcal{P}_4} x^2 z + x^2 yz\right) \tilde{G}_\sigma(0, y, z) - (1 + e^{i\mathcal{P}_4} y) xyz \partial_x \tilde{G}_\sigma(0, y, z) \\
&- \left(\varepsilon_4 xyz - xy - yz - xz^2 - xyz^2\right) \tilde{G}_\sigma(0, 0, z) + xyz^2 \partial_y \tilde{G}_\sigma(0, 0, z) + xyz \partial_x \tilde{G}_\sigma(0, 0, z) \;.
\end{aligned} \tag{3.5.31}$$

where $\supset$ indicates the terms contained in F except for those independent of the variable z, and we have added a label to F to indicate the number of magnons. We are not interested in the terms independent of the variable z because they contribute only finite coefficients to the infinite sum over position-dependent terms, and thus will disappear in the $N \to \infty$ limit due to the $1/N$ factor. The terms that depend on the variable z are potentially divergent in the limit $p_4 = \bar{p}_4/N \to 0$ and $z \to 1$, and thus play a crucial role in recovering the position-dependent corrections of the three-magnon special solution.

Since we know the exact transformation of the denominator, as given in (3.5.30), we refine our expectation given in (3.5.26) to

$$F^{(4)}_{ijk4}(x,y,z) \sim \left(1 - e^{ip_4} z\right)^{-1} F^{(3)}_{ijk}(x,y) \;, \tag{3.5.32}$$

for $(ijk) \in \mathcal{S}_3$ and we compare with the three-magnon generating function which includes the position-dependent corrections that solve the three-magnon non-interacting equations as given in (3.3.40). Although the three-magnon special solution is presented in Section 3.3.2 and even more in detail in [1], to easily discuss the asymptotic relation given in (3.5.32) we look at the numerator of the three-magnon generating function which solves the non-interacting equations,

$$\begin{aligned} F^{(3)}_{ijk}(x,y) &= \left(Q_3(x,y) + e^{i\mathcal{P}} y^2 \left(1 + e^{-i\mathcal{P}} x\right)\right) \tilde{G}^{(3)}_{ijk}(x,0) + \left(Q_3(x,y) + e^{-i\mathcal{P}} x^2 \left(1 + e^{i\mathcal{P}} y\right)\right) \tilde{G}^{(3)}_{ijk}(0,y) \\ &\quad - xy \left(1 + e^{-i\mathcal{P}} x\right) \partial_y \tilde{G}^{(3)}_{ijk}(x,0) - xy \left(1 + e^{i\mathcal{P}} y\right) \partial_x \tilde{G}^{(3)}_{ijk}(0,y) + xy \left(\tilde{D}^{0,1}_{ijk} + \tilde{D}^{1,0}_{ijk}\right) \;. \end{aligned} \tag{3.5.33}$$

By using the transitions between the total energy and total momentum variables and the transition between the denominators of the generating function, we observe that the factors that accompany the distinct pieces of the generating function in the above expressions one-to-one match under the $\bar{p}_4 \to 0$ as $N \to \infty$ limit. Therefore, we can refine our expectation from the connection between the generating function even further than (3.5.32) and get the following relations under the smearing limit,

$$\tilde{G}^{(4)}_{ijk4}(x,0,z) \sim \left(1 - e^{ip_4} z\right)^{-1} \tilde{G}^{(3)}_{ijk}(x,0) \;, \tag{3.5.34}$$

$$\tilde{G}^{(4)}_{ijk4}(0,y,z) \sim \left(1 - e^{ip_4} z\right)^{-1} \tilde{G}^{(3)}_{ijk}(0,y) \;, \tag{3.5.35}$$

$$\partial_y \tilde{G}^{(4)}_{ijk4}(x,0,z) \sim \left(1 - e^{ip_4} z\right)^{-1} \partial_y \tilde{G}^{(3)}_{ijk}(x,0) \;, \tag{3.5.36}$$

$$\partial_x \tilde{G}^{(4)}_{ijk4}(0,y,z) \sim \left(1 - e^{ip_4} z\right)^{-1} \partial_x \tilde{G}^{(3)}_{ijk}(0,y) \;, \tag{3.5.37}$$

furthermore, to be consistent with the asymptotic behavior given above, we expect,

$$\begin{aligned} &- \left(\varepsilon_4 xyz - xy - yz - xz^2 - xyz^2\right) \tilde{G}^{(4)}_{ijk4}(0,0,z) \\ &\quad + xyz \left(\partial_x \tilde{G}^{(4)}_{ijk4}(0,0,z) + z \partial_y \tilde{G}^{(4)}_{ijk4}(0,0,z)\right) \sim \left(1 - e^{ip_4} z\right)^{-1} 2xy(\kappa - \kappa^{-1}) A^{(3)}_{ijk} \;, \end{aligned} \tag{3.5.38}$$

which we can deduce only by comparing the four-magnon generating function (3.5.31) to the three-magnon one (3.5.33). Intuitively, this implies the following relation between the single-variable generating functions coming from the four-magnon problem and the single position-dependent corrections of the three-magnon problem,

$$\tilde{G}^{(4)}_{ijk4}(0,0,z) \sim \textit{finite} \,, \tag{3.5.39}$$

$$\partial_x \tilde{G}^{(4)}_{ijk4}(0,0,z) \sim \left(1 - e^{ip_4} z\right)^{-1} D^{1,0}_{\sigma} \,, \tag{3.5.40}$$

$$\partial_y \tilde{G}^{(4)}_{ijk4}(0,0,z) \sim \left(1 - e^{ip_4} z\right)^{-1} D^{0,1}_{\sigma} \,, \tag{3.5.41}$$

as $z \to 1$ such that $\tilde{G}^{(4)}_{ijk4}(0,0,z)$ does not blow up as $z \to 1$ and once we combine it with $1/N$ we observe that under the smearing limit, this piece vanishes. This is in complete agreement with the fact that $\tilde{D}^{0,0} = 0$ in our conventions. Up to this point, we have only considered the conditions imposed by the non-interacting equations. Now we take the special solution of the pieces of the generating function given in Section 3.3.2 and explicitly show what happens to these pieces of the generating function under the smearing procedure to match the special solution of the pieces of the three-magnon special solution. We will show that obtaining the three-magnon special solution under smearing imposes additional constraints on the special solution of the four-magnon problem. First, we focus on the special solution given in (3.4.65) and (3.4.66) and isolate the pieces that may diverge under the smearing

$$\begin{aligned}\tilde{G}^{(4)}_{ijk4}(0,y,z) \supset & -\frac{yz\left(1+e^{i\mathcal{P}_4}y\right)\partial_x \tilde{G}^{(4)}_{ijk4}(0,y,z)}{y(1-\varepsilon_4 z + z^2 + 2\kappa z + y) + z^2} \\ & + \frac{\left(y\left(1-\varepsilon_4 z + z^2 + 2\kappa z\right) + z^2\right)\tilde{G}^{(4)}_{ijk4}(0,0,z) + yz^2 \partial_y \tilde{G}^{(4)}_{ijk4}(0,0,z) + yz\partial_x \tilde{G}^{(4)}_{ijk4}(0,0,z)}{y(1-\varepsilon_4 z + z^2 + 2\kappa z + y) + z^2} \,.\end{aligned} \tag{3.5.42}$$

$$\begin{aligned}\tilde{G}^{(4)}_{ijk4}(x,0,z) \supset & -\frac{\kappa xz(e^{-i\mathcal{P}_4}x + z)\partial_y G^{(4)}_{ijk4}(x,0,z)}{\kappa(xz(-\varepsilon_4 + x + z) + x + z) + 2xz} - \frac{2xz\left(\kappa^2-1\right)A^{(4)}_{ijk4}\left(1 - e^{-ip_i}x - e^{ip_4}z\right)h(x,z)}{\kappa(xz(-\varepsilon_4 + x + z) + x + z) + 2xz} \\ & + \frac{\left(\kappa(xz(-\varepsilon_4 + z) + x + z) + 2xz\right)\tilde{G}^{(4)}_{ijk4}(0,0,z) + \kappa xz^2 \partial_y \tilde{G}^{(4)}_{ijk4}(0,0,z) + \kappa xz\partial_x \tilde{G}^{(4)}_{ijk4}(0,0,z)}{\kappa(xz(-\varepsilon_4 + x + z) + x + z) + 2xz} \,,\end{aligned} \tag{3.5.43}$$

The condition (3.5.38) is satisfied, by taking into account the special solution of the $\tilde{G}_{\sigma}(0,0,z)$ given in (3.4.69) in the following way,

$$\partial_x \tilde{G}^{(4)}_{ijk4}(0,0,z) + z\partial_y \tilde{G}^{(4)}_{ijk4}(0,0,z) \sim \frac{2\left(\kappa - \kappa^{-1}\right)A^{(4)}_{ijk4}}{1 - e^{ip_4}z} \tag{3.5.44}$$

which implies that in the smearing procedure $\tilde{G}_{\sigma}(0,0,z) \sim 0$ as $z \to 1$ and $N \to \infty$. The asymptotic behavior above is absolutely necessary to establish the connection between the four-magnon and three-magnon solutions, and therefore it is the first extra condition we derived between the pieces of the generating function in addition to the special solution. Note that this asymptotic relation suggests,

$$\partial_x \tilde{G}^{(4)}_{ijk4}(0,0,z) + z\partial_y \tilde{G}^{(4)}_{ijk4}(0,0,z) = \frac{2\left(\kappa-\kappa^{-1}\right) A^{(4)}_{ijk4} f_1(z)}{1-e^{ip_4}z} + f_2(z) \tag{3.5.45}$$

such that as $z \to 1$ these two unknown functions should behave as $f_1(z) \to 1$ and $f_2(z)$ stays finite. Then, we use this to refine the special solution of two-magnon interacting equations under the smearing limit and obtain the following behavior,

$$\tilde{G}^{(4)}_{ijk4}(0,y,z) \sim -\frac{\left(1+e^{i\mathcal{P}_4}y\right)\partial_x \tilde{G}^{(4)}_{ijk4}(0,y,z)}{2\kappa-\varepsilon_3\ +y+y^{-1}} + \frac{2\left(\kappa-\kappa^{-1}\right) A^{(4)}_{ijkl}}{2\kappa-\varepsilon_3\ +y+y^{-1}}\ . \tag{3.5.46}$$

Similarly, we obtain,

$$\tilde{G}^{(4)}_{ijk4}(x,0,z) \sim -\frac{(1+e^{-i\mathcal{P}_4}x)\partial_y G^{(4)}_{ijk4}(x,0,z)}{2\kappa^{-1}-\varepsilon_3\ +x+x^{-1}} + \frac{2\left(\kappa-\kappa^{-1}\right) A^{(4)}_{ijk4}}{\left(2\kappa^{-1}-\varepsilon_3\ +x+x^{-1}\right)(1-e^{-ip_i}x)(1-e^{ip_4}z)}\ . \tag{3.5.47}$$

Comparing these asymptotic expressions to the special solution of the three-magnon interacting equations, we conclude that the initial expectation given in (3.5.36) should be refined as

$$\partial_y \tilde{G}^{(4)}_{ijk4}(x,0,z) \sim \left(1-e^{ip_4}z\right)^{-1}\partial_y \tilde{G}^{(3)}_{ijk}(x,0) + \frac{2\left(\kappa-\kappa^{-1}\right) A^{(4)}_{ijk4} + (1-e^{-ip_i}x)c_{ijk}(x)}{\left(1+e^{-i\mathcal{P}}x\right)(1-e^{-ip_i}x)(1-e^{ip_4}z)} \tag{3.5.48}$$

Remarkably, once this piece of generating function behaves as given above, in addition to the behavior assumed in (3.5.44), we conclude by the two-magnon interacting equations that the rest of the two-variable generating functions should indeed behave as

$$\tilde{G}^{(4)}_{ijk4}(x,0,z) \sim \left(1-e^{ip_4}z\right)^{-1}\tilde{G}^{(3)}_{ijk}(x,0) \tag{3.5.49}$$

$$\tilde{G}^{(4)}_{ijk4}(0,y,z) \sim \left(1-e^{ip_4}z\right)^{-1}\tilde{G}^{(3)}_{ijk}(0,y) \tag{3.5.50}$$

$$\partial_x \tilde{G}^{(4)}_{ijk4}(0,y,z) \sim \left(1-e^{ip_4}z\right)^{-1}\partial_x \tilde{G}^{(3)}_{ijk}(0,y) \tag{3.5.51}$$

Since the three-magnon special solution does not fix the piece of the generating function $\partial_y \tilde{G}^{(3)}_{ijk}(x,0)$ and four-magnon special solution also does not fix $\partial_y \tilde{G}^{(4)}_{ijkl}(x,0,z)$, the extra factor that appears in the asymptotic relation between these pieces does not contradict the initial expectation.

The only thing left to complete the comparison and establish the limit given in (3.5.22) is to show that the analyticity conditions are compatible and the solution of the lowest separation scattering coefficients is compatible. As we explained in Section 3.3 and at the end of the special solution given in Section 3.4, we can impose the analyticity conditions (3.4.43) and (3.4.46) after inserting the solution of the two-magnon interacting equations into the generating function which includes the solution of non-interacting equations as in (3.4.39). Additionally, the same strategy was followed to obtain the special solution of the three-magnon solution which was presented in Appendix B of [1]. Then, the comparison between the analyticity conditions boils down to pointing out that the first analyticity condition given in (3.4.43) does not depend on the variable z. Therefore, even if we impose it on the generating function, under the smearing limit it will not have any effect on the result for smearing the magnon from the right. At this point, we are left with the second analyticity condition as given in (3.4.46), where we observe that

$$\lim_{N\to\infty} x_{\pm}^{(4)}(y,z) = \rho_{\pm}^{(3)}(y) \tag{3.5.52}$$

for $\rho_{\pm}^{(3)}(y)$ given in (3.3.36). This shows that the analyticity condition is consistent under the smearing limit and the relation we obtain about pieces of generating function by solving (3.4.46) will boil down to the relation coming from the analyticity condition of three-magnon solution. Finally, due to the factorized form of the scattering coefficients, we immediately see

$$A_{ijk4}^{(4)} = A_{ijk}^{(3)} \tag{3.5.53}$$

which implies that

$$D_{ijk4}^{1,0,0} = D_{ijk4}^{0,0,1} = D_{ijk}^{1,0} = D_{ijk}^{0,1}\,. \tag{3.5.54}$$

Even inside the set of position-dependent corrections that are involved in minimum separation equations, these two pairs of position-dependent corrections play a distinguished role. Since the pair, $\tilde{D}_{\sigma}^{1,0,0}$ and $\tilde{D}_{\sigma}^{0,0,1}$ is the only position-dependent corrections involved in four-magnon interacting equations and the pair $\tilde{D}_{\sigma}^{1,0}$ and $\tilde{D}_{\sigma}^{0,1}$ is involved in three-magnon interacting equations, we are able to solve them in the most symmetric way possible while setting the initial values of the eigenvalue problem. Since they are also the only pair independently appearing in the generating function which solves the non-interacting equations such as (3.4.39), their symmetric solution plays a crucial role in the solution of the rest of the position-dependent corrections. Therefore it makes sense to have such a connection between the four and three-magnon solutions, more precisely it makes sense to be able to connect a four-magnon solution to another special three-magnon solution and equations (3.5.53) and (3.5.54) are the necessary conditions which ensure that the initial conditions of these two eigenvalue problems match. It is certainly not a sufficient condition for smearing limit to work. For the rest of the position-dependent corrections, we can only write a direct relation under the smearing limit, once the conditions given above are satisfied,

$$\lim_{\bar{p}_4 \to 0} \lim_{N \to \infty} \frac{1}{N} \sum_{r=0}^{N} \tilde{D}^{n,m,r}_{ijk4} = \tilde{D}^{n,m}_{ijk} \tag{3.5.55}$$

and

$$\lim_{\bar{p}_4 \to 0} \lim_{N \to \infty} \frac{1}{N} \sum_{r=0}^{N} \tilde{D}^{n,m,r}_{ijkl} = 0 \qquad \text{for} \qquad l \neq 4 \tag{3.5.56}$$

which leads us to conclude (3.5.22).

Additionally, we can perform the smearing limit from the four-magnon solution to the three-magnon solution from the left as well. In this case, the limit would take the following form,

$$\lim_{\bar{p}_1 \to 0} \lim_{N \to \infty} \frac{1}{N} \sum_{l_1=-N}^{l_2-1} \Psi_{11}(p_1, p_2, p_3, p_4, l_1, l_2, l_3, l_4) = \Psi_{21}(p_2, p_3, p_4, l_2, l_3, l_4) \;, \tag{3.5.57}$$

which would correspond to the asymptotic behaviour,

$$\tilde{G}^{(4)}_{\sigma}(x, y, z) \sim \frac{1}{1 - e^{-ip_{\sigma(1)}} x} \tilde{H}^{(3)}_{\sigma}(y, z) \;, \qquad x \to 1 \;, \tag{3.5.58}$$

for the solution of the three-magnon problem for the configuration $Q_{21}Q_{12}Q_{21}$ given in Appendix A.2 of [2]. This limit would correspond to looking at asymptotics of the generating function as $x \to 1$ together with $N \to \infty$ and we would pick up the poles of the type $\left(1 - e^{ip_{\sigma(1)}} x\right)^{-1}$ as it can be seen from the special solution given in Section 3.3.2. Note that the three-magnon solution we obtain under the smearing limit would correspond to an eigenstate with overall color indices, $|\Psi\rangle_{21}$ and the position states would be the $\mathbb{Z}_2$ conjugates of the ones we obtain for smearing limit from the right in this section. However, scattering coefficients would still factorize in terms of S_κ since we started with the four-magnon solution which only has S_κs. Nevertheless, we know that this is another special solution which is the $\mathbb{Z}_2$ conjugate of the solution given in Section 5.2 of [1].

Moreover, we could also perform a 'double' smearing limit by taking the separation between the second and the third magnon to infinity,

$$\lim_{\bar{p}_4 \to 0} \lim_{\bar{p}_3 \to 0} \lim_{N \to \infty} \frac{1}{N} \sum_{l_3=l_2+1}^{N} \Psi_{11}(p_1, p_2, p_3, p_4, l_1, l_2, l_3, l_3+1) = \Psi_{11}(p_1, p_2, l_1, l_2) \;. \tag{3.5.59}$$

Then, we are left with the two-magnon solution since we do not have any poles of type $(1-y)^{-1}$ in the special solution as $y \to 1$. This observation makes the $y \to 1$ limit very similar to the case of smearing the three-magnon to the two-magnon solution and the position-dependent corrections vanish under this limit and we are left with the two-magnon solution.

3.6 Further Constraining the Four-Magnon Solution

In this section, inspired by the smearing limit, we further constrain the solution we constructed in Section 3.4.2 using the special three-magnon solution obtained in Section 3.3.2. The final form of the four-magnon solution we obtain here both solves the eigenvalue equations obtained in Section 3.4 and reduces to the three-magnon solution under the smearing procedure, but we do not claim this solution to be unique because it depends on the particular solution we chose for minimum separation equations given in Section 3.4.2.

In Section 3.4.2, we followed a specific order to solve the eigenvalue equations and analyticity conditions. However, for the purposes of this section, it is more convenient to change this order. This allows us to construct a solution that both satisfies the relations between generating functions—derived in Section 3.4.2—and explicitly depends on the three-magnon solution. Our strategy begins with the two-magnon interacting equations, starting from (3.4.71). We incorporate the asymptotic behavior introduced in (3.5.59), and use the remaining freedom from Section 3.4.2 to fix certain single-variable functions. We then verify that the resulting solution agrees with the one in Section 3.4.2, at leading orders in the Taylor expansion.

Next, we express the two-variable generating functions in terms of the single-variable generating functions obtained from the three-magnon solution. In this construction, we ensure that all interacting equations of the four-magnon problem are satisfied: (3.4.69), (3.4.70), (3.4.71), as well as (3.4.65), (3.4.66), and (3.4.67). We also impose analyticity on the two-magnon interacting equations to determine the remaining single-variable generating functions. Finally, we complete the solution by imposing analyticity conditions on the full three-variable generating function.

Let us start by considering the smearing of two magnons in a four-magnon eigenstate. From (3.5.59), we know that the generating functions do not have any poles at $y \to 1$. Also, the initial conditions discussed in Section 3.4.2 are compatible with setting

$\tilde{D}^{0,1,0}_{ijkl} = 0$. Thus, we have the freedom to fix the single-variable generating function,

$$G^{(4)}_{ijkl}(0, y, 0) = 0 \ . \tag{3.6.1}$$

Then, the two two-magnon interacting equation (3.4.71) implies,

$$(1+y)\partial_z \tilde{G}^{(4)}_{ijkl}(0,y,0) + (1+e^{i\mathcal{P}_4}y)\partial_x \tilde{G}^{(4)}_{ijkl}(0,y,0) = 2\left(\kappa - \kappa^{-1}\right) A_{ijkl} \ , \tag{3.6.2}$$

which can be solved by taking

$$\partial_z \tilde{G}^{(4)}_{ijkl}(0,y,0) = \frac{\left(\kappa-\kappa^{-1}\right) A_{ijkl}}{1+y} \ , \quad \partial_x \tilde{G}^{(4)}_{ijkl}(0,y,0) = \frac{\left(\kappa-\kappa^{-1}\right) A_{ijkl}}{1+e^{i\mathcal{P}_4}y} \ . \tag{3.6.3}$$

This is a simple and parity invariant (under the maps (3.4.25) and (3.4.34)) solution of the single-variable generating functions which depend on y. In addition, if we expand these expressions around the origin, we get

$$\partial_z \tilde{G}^{(4)}_{ijkl}(0,y,0) = \tilde{D}^{0,0,1}_{ijkl} + \tilde{D}^{0,1,1}_{ijkl} y + \mathcal{O}(y^2) = (\kappa-\kappa^{-1})A_{ijkl} - (\kappa-\kappa^{-1})A_{ijkl}\, y + \mathcal{O}(y^2) \ , \tag{3.6.4}$$

$$\partial_x \tilde{G}^{(4)}_{ijkl}(0,y,0) = \tilde{D}^{1,0,0}_{ijkl} + \tilde{D}^{1,1,0}_{ijkl}\, y + \mathcal{O}(y^2) = (\kappa-\kappa^{-1})A_{ijkl} - e^{i\mathcal{P}_4}(\kappa-\kappa^{-1})A_{ijkl}\, y + \mathcal{O}(y^2) \ , \tag{3.6.5}$$

which exactly match the position-dependent coefficients computed using the minimum separation equations, see equations (3.4.57) and (3.4.60). We use this solution and combine it with the one-variable generating functions given in (3.4.69) and (3.4.70) and consider refining the solution of the generating functions $\tilde{G}_{ijkl}(0,y,z)$ and $\partial_x \tilde{G}_{ijkl}(0,y,z)$. From the asymptotic behavior of these generating functions under the smearing limit, given in (3.5.50) and (3.5.51), we expect to have

$$\tilde{G}^{(4)}_{ijkl}(0,y,z) = \frac{\tilde{G}^{(3)}_{ijk}(0,y) f_1(y)}{(1-e^{ip_l}z)\, f_2(y,z)} + f_3(y,z) \ , \tag{3.6.6}$$

$$\partial_x \tilde{G}^{(4)}_{ijkl}(0,y,z) = \frac{\partial_x \tilde{G}^{(3)}_{ijk}(0,y)}{(1-e^{ip_l}z)} + f_4(y,z) \ . \tag{3.6.7}$$

Using the solution of the single-variable generating functions obtained in the previous step, we can substitute this ansatz into the special solution of the two-magnon interacting equation given in (3.4.65) and observe,

$$\frac{\tilde{G}^{(3)}_{ijk}(0,y) f_1(y)}{(1-e^{ip_l}z)\, f_2(y,z)} + f_3(y,z)$$

$$= -\frac{yz\left(1+e^{i\mathcal{P}_4}y\right)}{(y(1-\varepsilon_4 z+z^2+2\kappa z+y)+z^2)}\left(\frac{\partial_x\tilde{G}^{(3)}_{ijk}(0,y)}{(1-e^{ip_l}z)}+f_4(y,z)\right)$$
$$+\frac{z\,(1-e^{ip_l}z)\,(z-2\kappa^{-1}y)\,\tilde{G}^{(4)}_{ijkl}(0,0,z)+2yz(\kappa-\kappa^{-1})A_{ijkl}}{(1-e^{ip_l}z)\,(y(1-\varepsilon_4 z+z^2+2\kappa z+y)+z^2)}\,, \tag{3.6.8}$$

where we reduce the one-variable dependence on z to $\tilde{G}^{(4)}_{ijkl}(0,0,z)$ by using (3.4.69). The fact that the pieces of the three-magnon generating function $G^{(3)}$ have to satisfy the two-magnon eigenvalue equations of the three-magnon problem, given in (3.3.44) ensures that (3.6.8) is satisfied by taking

$$f_1(y) = 2\kappa-\varepsilon_3\;+y+y^{-1}\,, \tag{3.6.9}$$
$$f_2(y,z) = z+z^{-1}+yz^{-1}+zy^{-1}+2\kappa-\varepsilon_4\,, \tag{3.6.10}$$
$$f_3(y,z) = \frac{(zy^{-1}-2\kappa^{-1})\,\tilde{G}^{(4)}_{ijkl}(0,0,z)+\tilde{f}_3(y,z)}{z+z^{-1}+yz^{-1}+zy^{-1}+2\kappa-\varepsilon_4}\,, \tag{3.6.11}$$

also,

$$f_4(y,z) = -\frac{\tilde{f}_3(y,z)}{1+e^{i\mathcal{P}_4}y}\,. \tag{3.6.12}$$

Note that for both two-variable generating functions given above, there is a common two-variable function, $\tilde{f}_3(y,z)$ which cancels inside the two-magnon interacting equation (3.6.8). Therefore, this function does not play a role in two-magnon interacting equations, but it contributes to the non-interacting generating function (3.4.39). We will use this extra freedom at the end of this section to fix the analyticity of the non-interacting generating function. To explicitly show the effect of the expressions given in equations (3.6.9)-(3.6.12), we plug these solutions into (3.6.8) and observe that thanks to the three-magnon solution which satisfies (3.3.44), the two-magnon interacting equations of the four-magnon problem are also satisfied. This implies that the two-variable generating functions can be written in terms of the initial conditions and the three-magnon solution,

$$\tilde{G}^{(4)}_{ijkl}(0,y,z) = \frac{\tilde{G}^{(3)}_{ijk}(0,y)yz\,(2\kappa-\varepsilon_3\;+y+y^{-1})}{(1-e^{ip_l}z)\,(y(1-\varepsilon_4 z+z^2+2\kappa z+y)+z^2)}$$
$$+\frac{z\,(z-2\kappa^{-1}y)\,\tilde{G}^{(4)}_{ijkl}(0,0,z)+\tilde{f}_3(y,z)}{y(1-\varepsilon_4 z+z^2+2\kappa z+y)+z^2}\,, \tag{3.6.13}$$
$$\partial_x\tilde{G}^{(4)}_{ijkl}(0,y,z) = \frac{\partial_x\tilde{G}^{(3)}_{ijk}(0,y)}{1-e^{ip_l}z}-\frac{\tilde{f}_3(y,z)}{1+e^{i\mathcal{P}_4}y}\,, \tag{3.6.14}$$

which is a consistent solution of the four-magnon eigenvalue equations. At this point we can impose the analyticity condition on $\tilde{G}^{(4)}_{ijkl}(0,y,z)$ by demanding that the numerator of this two-variable function vanish at the curve, coming from one of the two factors in $f_2(y,z)=0$.[18] This way we ensure that the two-variable generating function $\tilde{G}^{(4)}_{ijkl}(0,y,z)$ is analytic and we can expand it around the origin to extract the position-dependent corrections. This step should not be confused with the analyticity of the whole generating function $\tilde{G}^{(4)}_{ijkl}(x,y,z)$ as discussed in Section 3.4 which we will impose in Appendix B in [2]. We demonstrate how to impose the analyticity condition for a two-variable function in the following way. The curve, we obtain from $f_2(y,z)=0$ that passes through the origin is given as

$$y_+(z)=\frac{1}{2}\left(\varepsilon_4 z-z^2-2\kappa z-1+\sqrt{(-\varepsilon_4 z+z^2+2\kappa z+1)^2-4z^2}\right)\,, \tag{3.6.15}$$

then we ensure analyticity by solving

$$\Big[\left(y(1-\varepsilon_4 z+z^2+2\kappa z+y)+z^2\right)\tilde{G}^{(4)}_{ijkl}(0,y,z)\Big]_{y\to y_+(z)}=0\,, \tag{3.6.16}$$

which gives us

$$\tilde{G}_{ijkl}(0,0,z)=-\frac{y_+(z)G^{(3)}_{ijk}(0,y_+(z))\left(-\varepsilon_3+y_+(z)+2\kappa+y_+(z)^{-1}\right)-\left(1-e^{ip_l}z\right)\tilde{f}_3(y_+(z),z)}{\left(1-ze^{ip_l}\right)\left(z-2\kappa^{-1}y_+(z)\right)}\,. \tag{3.6.17}$$

In this case, the asymptotic relations given in (3.5.39)-(3.5.41) are satisfied because, as $z\to 1$ and $N\to\infty$, the $f_2(y,z)$ given in (3.6.10) reduces to $(2\kappa-\varepsilon_3+y+y^{-1})$. Therefore, although the $(1-ze^{ip_l})$ in the denominator goes to zero under the smearing limit, the numerator of the final expression (3.6.17) has a zero in the smearing limit and these two factors cancel, and we are left with a finite quantity, as predicted in (3.5.39).

Furthermore, we can now repeat this process for the smearing from the left, given in (3.5.57). In that case, smearing a magnon from left starting from the state $Q_{12}Q_{21}Q_{12}Q_{21}$ results in the three-magnon special solution with S_κ scattering coefficients with the ordering $Q_{21}Q_{12}Q_{21}$. This solution is given in [1] and it has the same form as the solution given in Appendix B in [2] apart from the swapped constant functions between two-magnon interacting equations. Repeating the same steps as before, we find

$$\tilde{G}^{(4)}_{ijkl}(x,y,0)=\frac{\tilde{H}^{(3)}_{jkl}(y,0)e^{i\mathcal{P}_4}xy\left(2\kappa-\varepsilon_3+y^{-1}+y\right)}{\left(1-e^{-ip_i}x\right)g(x,y)}+\frac{x\left(x-2e^{i\mathcal{P}_4}\kappa^{-1}y\right)\tilde{G}^{(4)}_{ijkl}(x,0,0)+\tilde{g}_3(x,y)}{g(x,y)}\,, \tag{3.6.18}$$

[18] How to impose analyticity condition on two-variable generating functions also detailly explained in Part I, [1].

$$\partial_z \tilde{G}^{(4)}_{ijkl}(x,y,0) = \frac{(1+e^{-i\mathcal{P}_4}y)\partial_z \tilde{H}^{(3)}_{jkl}(y,0)}{(1+y)\,(1-e^{-ip_i}x)} - \frac{\tilde{g}_3(x,y)}{e^{i\mathcal{P}_4}xy(1+y)} \ , \tag{3.6.19}$$

where

$$g(x,y) = (x^2 + e^{i\mathcal{P}_4}y)(e^{i\mathcal{P}_4}y+1) - e^{i\mathcal{P}_4}xy(\varepsilon_4 - 2\kappa) \ . \tag{3.6.20}$$

Additionally, we use $\tilde{G}^{(4)}_{ijkl}(x,0,0)$ to insert the unfixed single-variable equations and demand analyticity of the two-variable generating function $\tilde{G}^{(4)}_{ijkl}(x,y,0)$. For the curve, $\tilde{y}_+(x)$ that passes through the origin defined by $g(x,y)=0$,

$$\tilde{y}_+(x) = e^{-i\mathcal{P}_4}y_+(x) \tag{3.6.21}$$

as it is given in (3.6.15), we obtain,

$$\tilde{G}^{(4)}_{ijkl}(x,0,0) = -\frac{\tilde{H}^{(3)}_{jkl}(\tilde{y}_+(x),0)e^{i\mathcal{P}_4}\tilde{y}_+(x)\,(2\kappa - \varepsilon_3 + \tilde{y}_+(x)^{-1} + \tilde{y}_+(x)) - (1-e^{-ip_i}x)\,\tilde{g}_3(x,y_+(x))}{(1-e^{-ip_i}x)\,(x - 2e^{i\mathcal{P}_4}\kappa^{-1}\tilde{y}_+(x))} \ . \tag{3.6.22}$$

Similar to the previous case, we leave $\tilde{g}_3(x,y)$ free to use it to ensure the analyticity of the non-interacting generating function. The final step is to repeat this process for $G^{(4)}_{ijkl}(x,0,z)$. Since this piece plays a role in both smearing from the left and smearing from the right, we use an ansatz that would accommodate both of these cases and we start with

$$\tilde{G}^{(4)}_{ijkl}(x,0,z) = \frac{\tilde{G}^{(3)}_{ijk}(x,0)h_1(x)}{(1-e^{ip_l}z)\,h_2(x,z)} + \frac{\tilde{H}^{(3)}_{jkl}(0,z)h_1(z)}{(1-e^{-ip_i}x)\,h_2(x,z)} + h_3(x,z) \ , \tag{3.6.23}$$

$$\partial_y \tilde{G}^{(4)}_{ijkl}(x,0,z) = \frac{(1+e^{-i\mathcal{P}_4}x)\partial_y \tilde{G}^{(3)}_{ijk}(x,0)}{(1-e^{ip_l}z)\,(z+e^{-i\mathcal{P}_4}x)} + \frac{(1+e^{i\mathcal{P}_4}z)\partial_y \tilde{H}^{(3)}_{jkl}(0,z)}{(1-e^{-ip_i}x)\,(z+e^{-i\mathcal{P}_4}x)} + h_4(x,z) \ . \tag{3.6.24}$$

Imposing what we know about three-magnon interacting equations reduces the solution of the two-magnon special solution to a combination of two, two-magnon interacting equations of the three-magnon problem. We conclude that we can fix the undetermined expressions in (3.6.23) and (3.6.24) to the following forms

$$h_1(x) = 2\kappa^{-1} - \varepsilon_3 + x + x^{-1} \ , \tag{3.6.25}$$

$$h_2(x,z) = x + z + x^{-1} + z^{-1} + 2\kappa^{-1} - \varepsilon_4 \ , \tag{3.6.26}$$

$$h_3(x,z) = \frac{x^{-1}-2\kappa}{h_2(x,z)}\tilde{G}^{(4)}_{ijkl}(0,0,z) + \frac{z^{-1}-2\kappa}{h_2(x,z)}\tilde{G}^{(4)}_{ijkl}(x,0,0)\ , \tag{3.6.27}$$

where both $\tilde{G}^{(4)}_{ijkl}(x,0,0)$ and $\tilde{G}^{(4)}_{ijkl}(0,0,z)$ are given in terms of the initial conditions $\tilde{D}^{1,0}$ and $\tilde{D}^{0,1}$ of the three magnon problem in (3.6.17) and (3.6.22) and analyticity conditions. Consequently, we obtain

$$h_4(x,z) = -\frac{c_{ijk}(x)\,(1-e^{-ip_i}x) + c_{jkl}(z)\,(1-e^{ip_l}z) - 2A_{ijkl}\,(\kappa-\kappa^{-1})}{(1-e^{-ip_i}x)(1-e^{ip_l}z)(z+e^{-i\mathcal{P}_4}x)}\ , \tag{3.6.28}$$

and the function $c_{jkl}(z)$ is defined as

$$c_{123}(x) = \frac{(\kappa-\kappa^{-1})x}{(x-e^{ip_1})\,(x-e^{ip_2})\,(x-e^{ip_3})\,(\kappa-2\kappa x\varepsilon_3+x(\kappa x+2))}\Bigg(\frac{e^{i(p_1+p_2)}-2\kappa x+1}{e^{ip_3}(\kappa-\kappa^{-1})}$$
$$+e^{i\mathcal{P}}\left[x+x\left(e^{ip_1}-2\kappa\right)\left(e^{ip_2}-2\kappa\right)-2\kappa\right]+x\left(e^{ip_1}+e^{ip_2}-2\kappa\right)\left(e^{i(p_1+p_2)}-2\kappa x+1\right)\Bigg)\ . \tag{3.6.29}$$

As in the previous cases, the analyticity of the two-magnon interacting equations is satisfied by fixing the leftover freedom with respect to the curve $h_1(x,z)=0$ and $e^{-i\mathcal{P}_4}x+z=0$ that passes through the origin. Since previously we used all the single-variable generating functions to fix the analytic structure of two-magnon interaction from left and right, now we use the undetermined pieces of the three-magnon solution (in our conventions they are $\partial_y\tilde{G}^{(3)}_{ijk}(x,0)$ and $\partial_y\tilde{H}^{(3)}_{jkl}(0,z)$). After this step, all the pieces of the generating functions are fixed by the three-magnon solution and the only thing left to do is to ensure the analyticity of non-interacting equations in which we bring all parts together (3.5.33).

We can assemble the four-magnon solution before imposing the non-interacting analyticity conditions as[19]

$$\begin{aligned}\tilde{G}^{(4)}_{ijkl}(x,y,z) = {}& \frac{A^{(4)}_{ijkl}}{A^{(3)}_{ijk}}\frac{r_1\,\tilde{G}^{(3)}_{ijk}(x,0)+r_2\,\tilde{G}^{(3)}_{ijk}(0,y)+r_3\,\partial_y\tilde{G}^{(3)}_{ijk}(x,0)+r_4\,\partial_x\tilde{G}^{(3)}_{ijk}(0,y)+xyz\,c_{ijk}(x)}{Q_4(x,y,z)(1-e^{ip_l}z)}\\ &+\frac{A^{(4)}_{ijkl}}{A^{(3)}_{jkl}}\frac{r_5\,\tilde{H}^{(3)}_{jkl}(y,0)+r_6\,\tilde{H}^{(3)}_{jkl}(0,z)+r_7\,\partial_z\tilde{H}^{(3)}_{jkl}(y,0)+r_8\,\partial_y\tilde{H}^{(3)}_{jkl}(0,z)+xyz\,c_{jkl}(z)}{Q_4(x,y,z)(1-e^{-ip_i}x)}\\ &+\frac{2xyzA^{(4)}_{ijkl}\left(\kappa-\kappa^{-1}\right)\left(1-e^{ip_l}z-e^{-ip_i}x\right)}{Q_4(x,y,z)(1-e^{ip_l}z)(1-e^{-ip_i}x)}+\frac{C_{ijkl}(x,y,z)}{Q_4(x,y,z)}\ .\end{aligned} \tag{3.6.30}$$

[19] Notice that we do not need to compute the value of the one-variable generating functions $\partial_y\tilde{G}^{(4)}_{ijkl}(x,0,0)$, $\partial_z\tilde{G}^{(4)}_{ijkl}(x,0,0)$, $\partial_x\tilde{G}^{(4)}_{ijkl}(0,0,z)$ and $\partial_y\tilde{G}^{(4)}_{ijkl}(0,0,z)$, as they can be expressed in terms of $\tilde{G}^{(4)}_{ijkl}(x,0,0)$ and $\tilde{G}^{(4)}_{ijkl}(0,0,z)$ using equations (3.4.69) and (3.4.70).

In this expression for the four-magnon generating function, the functions $\tilde{G}_\sigma$ and $\tilde{H}_\sigma$ are the generating functions of the three magnon long-range corrections for the configurations $Q_{12}Q_{21}Q_{12}$ and $Q_{21}Q_{12}Q_{21}$ respectively, related to each other by $\mathbb{Z}_2$ plus parity. Moreover, $c_\sigma(x)$ is given in (3.6.29) and is also a function of only three magnon data. The expression (3.6.30) is naturally divided into four parts according to their poles:

- The part with $(1-e^{ip_l}z)Q_4(x,y,z)$ in the denominator corresponds to the three magnon configuration $Q_{12}Q_{21}Q_{12}$ which captures the asymptotic behavior (3.5.26) (the smearing limit from the right).
- The part with $(1-e^{-ip_i}x)Q_4(x,y,z)$ in the denominator corresponds to the configuration $Q_{21}Q_{12}Q_{21}$ which gives us the asymptotic behavior (3.5.58) (the smearing limit from the left).
- The part with $(1-e^{-ip_i}x)(1-e^{ip_l}z)Q_4(x,y,z)$ has a very simple numerator given directly with factorized scattering coefficients. The numerator of this part is precisely such that upon taking the limits $z \to 1$ or $x \to 1$ it combines with the $Q_{12}Q_{21}Q_{12}$ or $Q_{21}Q_{12}Q_{21}$ parts respectively.
- Lastly, the part with only $Q_4(x,y,z)$ disappears upon taking either the $z \to 1$ or $x \to 1$ limits, but is nonetheless needed to satisfy the four magnon eigenvalue equations. This part differs from the ones above as it is given in terms of the three magnon pieces but evaluated on specific curves (3.4.42), (3.6.15), and (3.6.21). The coefficient $C_{ijkl}(x,y,z)$ is given in Appendix B in [2] where we also spell out the evaluation procedure.

Lastly, the factors r_i refer to the rational functions which are a combination of simple polynomial factors computed throughout this section,

$$r_1 = \frac{\left(Q_4(x,y,z) + e^{i\mathcal{P}_4}y^2z + xy^2\right)\left(2\kappa^{-1} - \varepsilon_3 + x + x^{-1}\right)}{x + z + x^{-1} + z^{-1} + 2\kappa^{-1} - \varepsilon_4}\,, \tag{3.6.31}$$

$$r_2 = \frac{\left(Q_4(x,y,z) + e^{-i\mathcal{P}_4}x^2z + x^2yz\right)\left(2\kappa - \varepsilon_3 + y + y^{-1}\right)}{z + z^{-1} + yz^{-1} + zy^{-1} + 2\kappa - \varepsilon_4}\,, \tag{3.6.32}$$

$$r_5 = \frac{e^{i\mathcal{P}_4}xy\left(Q_4(x,y,z) + xz^2 + xyz^2\right)\left(2\kappa - \varepsilon_3 + y + y^{-1}\right)}{(x^2 + e^{i\mathcal{P}_4}y)(e^{i\mathcal{P}_4}y + 1) - e^{i\mathcal{P}_4}xy(\varepsilon_4 - 2\kappa)}\,, \tag{3.6.33}$$

$$r_6 = \frac{\left(Q_4(x,y,z) + e^{i\mathcal{P}_4}y^2z + xy^2\right)\left(2\kappa^{-1} - \varepsilon_3 + z + z^{-1}\right)}{x + z + x^{-1} + z^{-1} + 2\kappa^{-1} - \varepsilon_4}\,, \tag{3.6.34}$$

$$r_3 = -xyz(1 + e^{-i\mathcal{P}_4}x)\,, \qquad r_4 = -xyz(1 + e^{i\mathcal{P}_4}y)\,, \tag{3.6.35}$$

$$r_7 = -xyz(1+e^{-i\mathcal{P}_4}y) \ , \qquad\qquad r_8 = -xyz(1+e^{i\mathcal{P}_4}z) \ . \tag{3.6.36}$$

Then we can expand the generating function given above and obtain the solution of the four-magnon position-dependent corrections. After imposing the analyticity condition as described in Appendix B in [2] we extract the position-dependent corrections $\tilde{D}^{n,m,r}$ up to $n+m+r=8$ and check that they satisfy the eigenvalue equations given in Section 3.4 independently. Although the connection between the four-magnon solution and the three-magnon solution is rather implicit we are able to determine each four-magnon position-dependent correction from the three-magnon solution and define the common function that gives all position-dependent corrections,

$$D_\sigma^{n,m,r} = (\kappa-\kappa^{-1})A_\sigma f(\vec{p}_\sigma;n,m,r,\kappa) = \oint_B \frac{dxdydz}{(2\pi i)^3}\frac{G_\sigma^{(4)}(x,y,z)}{x^{n+1}y^{m+1}z^{r+1}} \ . \tag{3.6.37}$$

This final form of the solution still possesses the permutational symmetry highlighted at the end of Section 3.3.2 and to point this out further we use the Yang operator formalism in the following section before completing our analysis on the four-magnon solution for open infinite states.

3.7 Yang Operator Formalism

To reveal the structure of the special solutions that we present in Section 3.3.2 and Section 3.6, we use the Yang operator formalism [145]. If a quantum many-body system of N particles has N linearly independent local conserved charges, the CBA provides a universal form for the wave function. This form decomposes into plane wave contributions modulated by scattering coefficients. Implicitly, this structure precludes any intrinsically three-body events and diffraction. In this case, the Yang operator formalism is used to reveal the consequences of the large number of conserved charges, for a detailed review see [60].

We consider a quantum many-body problem that admits N conserved charges for N-bodies. For a kinematic domain characterized by the positions of the magnons $l_1 < \cdots < l_N$, the solution of the Schrödinger equation reads

$$\Psi(l_1,\cdots,l_N) = \sum_{\sigma\in\mathcal{S}_N}\mathcal{A}_\sigma(p_1,\cdots,p_N)e^{i\vec{p}_\sigma\cdot\vec{l}} \,, \tag{3.7.1}$$

such that the coefficients are labeled by the permutation indices. We can generalize this wave function to any kinematic domain by specifying the order of the magnons using $\tau\in\mathcal{S}_N$. This means that, with respect to the initial set of coordinates, the following wave function is the solution of the stationary Schrödinger equations for $l_{\tau(1)} < \cdots < l_{\tau(N)}$,

$$\Psi(l_1, \cdots, l_N|\tau) = \sum_{\sigma \in \mathcal{S}_N} \mathcal{A}_{\tau|\sigma}(p_1, \cdots, p_N) e^{i\vec{p}_\sigma \cdot \vec{l}_\tau} \; . \tag{3.7.2}$$

In other words, we identify the N magnons with their coordinates and permute them by changing the form of the incoming plane wave

$$e^{ip_1 l_1 + \cdots + p_N l_N} \longrightarrow e^{ip_1 l_{\tau(1)} + \cdots + p_N l_{\tau(N)}} \; . \tag{3.7.3}$$

We encode the scattering coefficients of the wave function for a fixed permutation of momenta, σ, within any kinematic domain labeled by τ into a column vector formed by the coefficients accompanying the plane wave contributions,

$$\Phi(\sigma) = \{\mathcal{A}_{\tau|\sigma}, \quad \forall \tau \in \mathcal{S}_N\} \; . \tag{3.7.4}$$

We can further combine these columns into an $N! \times N!$ matrix such that the rows and columns of this matrix would implicitly encode the permutational symmetry structure of the model. To make this structure more explicit, the *Yang operator* is defined as the map that relates two vectors in different permutations of momenta

$$\Phi(\alpha_j \sigma) = Y_j(\alpha_j)\Phi(\sigma) \; , \tag{3.7.5}$$

for any transposition $\alpha_j \in \mathcal{S}_N$ and any permutation $\sigma \in \mathcal{S}_N$. For an integrable system that admits a non-diffracting solution to the Schrödinger equation, the coefficients of the wave function satisfy the following relations

$$\mathcal{A}_{\tau|\alpha_j\sigma} = A(p_{\tau(j)}, p_{\tau(j+1)})\mathcal{A}_{\tau|\sigma} \; , \tag{3.7.6}$$

$$\mathcal{A}_{\alpha_j\tau|\alpha_j\sigma} = B(p_{\tau(j)}, p_{\tau(j+1)})\mathcal{A}_{\tau|\sigma} \; . \tag{3.7.7}$$

Here, $\alpha_j \in \mathcal{S}_N$ are the transpositions which exchange the jth element with $(j+1)$th. In this case, the Yang operators include the *reflection coefficient*s on the diagonal and the *transmission coefficient*s on the off-diagonal,

$$Y_j(\alpha_j) = A(p_{\tau(j)}, p_{\tau(j+1)})\mathbf{1} + B(p_{\tau(j)}, p_{\tau(j+1)})\pi(\alpha_j) \; , \tag{3.7.8}$$

where $\mathbf{1}$ is the identity matrix for an $N!$-dimensional vector space, and the $\pi(\alpha_j)$ is an $N!$-dimensional faithful representation of the transposition α_j. Note that once we specify the representation of the symmetric group and compute the Yang operator for the transpositions for $(j, j+1)$, we can generate all other permutations by applying the Yang operators successively. Furthermore, they obey the YBE,

$$Y_j(p_2, p_3)Y_{j+1}(p_1, p_3)Y_j(p_1, p_2) = Y_{j+1}(p_1, p_2)Y_j(p_1, p_3)Y_{j+1}(p_2, p_3) \; . \tag{3.7.9}$$

We conclude by highlighting that the Yang operators are a powerful tool for quantifying the degree of permutational symmetry in a model. In the general form of the wave function (3.7.2), the plane wave contributions are the only components that remain symmetric under the transformation $\vec{p}_\sigma \cdot \vec{l} \leftrightarrow \vec{p} \cdot \vec{l}_{\sigma^{-1}}$. Therefore, when comparing scattering coefficients across different regimes, we express them in a plane wave basis and use the Yang operators to capture the effects of permuting momenta and positions. We investigate whether the Yang operators, given as $Y_j(p,q)$, admit a consistent definition for any j and for any pair of momenta (p,q). Additionally, we examine potential relationships among the diagonal and off-diagonal entries of the operator. In the same spirit, to analyze our long-range solution, we define a Yang operator for our solution which is more involved than this one.

The Yang operators of our model. We start by computing the Yang operator for the wave function of two magnons, as given in (3.2.11). Recall that the two-magnon problem is solved by CBA and has a wave function of the form (3.7.1). Therefore, applying the Yang operator formalism is straightforward. We identify the magnons by their positions, considering the excitation Q_{12} located at l_1 and the excitation Q_{21} located at l_2. This implies that the kinematic domain $l_1 < l_2$ corresponds to the wave function associated with the state $|\Psi(p_1,p_2)\rangle_{11}$, while the kinematic domain $l_2 < l_1$ corresponds to the wave function associated with the state $|\Psi(p_1,p_2)\rangle_{22}$. We can express both wave functions together as

$$\begin{pmatrix} \langle l_1, l_2|\Psi(p_1,p_2)\rangle_{11} \\ \langle l_2, l_1|\Psi(p_1,p_2)\rangle_{22} \end{pmatrix} = \begin{pmatrix} 1 & S_\kappa(p_1,p_2) \\ S_{1/\kappa}(p_1,p_2) & 1 \end{pmatrix} \begin{pmatrix} \exp(ip_1 l_1 + ip_2 l_2) \\ \exp(ip_2 l_1 + ip_1 l_2) \end{pmatrix} . \tag{3.7.10}$$

Here, the vectors of coefficients are given by the first and the second columns of the 2×2 matrix on the right-hand side of the equation,

$$\Phi(12) = \begin{pmatrix} 1 \\ S_{1/\kappa}(p_1,p_2) \end{pmatrix} , \qquad \Phi(21) = \begin{pmatrix} S_\kappa(p_1,p_2) \\ 1 \end{pmatrix} . \tag{3.7.11}$$

The definition (3.7.5) of the Yang operator implies that

$$\Phi(21) = Y_1(p_1,p_2)\Phi(12) , \qquad \Phi(12) = Y_1(p_2,p_1)\Phi(21) . \tag{3.7.12}$$

Therefore, the resulting Yang operator takes the form

$$Y_j(p_1,p_2) = \begin{pmatrix} S_\kappa(p_1,p_2) & 0 \\ 0 & S_{1/\kappa}(p_2,p_1) \end{pmatrix} , \tag{3.7.13}$$

and $Y_1(p_1,p_2)^{-1} = Y_1(p_2,p_1)$. As anticipated, the transmission coefficients vanish, indicating that the model permits only the reflection of magnons.

Let us consider now the case of an arbitrary number of magnons. If the magnon associated to the position l_j is Q_{12}, then $Y_j(p_1, p_2)$ has the above form. The Yang operator for the excitations $(j+1, j+2)$ follows a similar behavior, with κ replaced by $1/\kappa$. This substitution arises because the Hamiltonian's action on sites $(j+1, j+2)$ mirrors its action on $(j, j+1)$ under the transformation $\kappa \to 1/\kappa$. Consequently, the Yang operator is expected to take the following form

$$Y_{j+1}(p_1, p_2) = \begin{pmatrix} S_{1/\kappa}(p_1, p_2) & 0 \\ 0 & S_\kappa(p_2, p_1) \end{pmatrix} . \tag{3.7.14}$$

Then, the YBE for the Yang operators, (3.7.9), is not satisfied, as it suffers from the same mismatch as (3.2.32)

$$Y_{j+1}(p_1, p_2) Y_j(p_1, p_3) Y_{j+1}(p_2, p_3) \neq Y_j(p_2, p_3) Y_{j+1}(p_1, p_3) Y_j(p_1, p_2) . \tag{3.7.15}$$

Instead of directly generalizing the Yang operators to many-body solutions we explicitly define the new form of the Yang operators for the long-range ansatz solution of the three-magnon problem.

The Yang operators of the long-range solution. As discussed at the end of the previous section, directly generalizing the Yang operators to an arbitrary number of excitations is not feasible. This limitation is expected, as the constraints imposed by the color contraction rules significantly reduce the dimensionality of the column vectors $\Phi(\sigma)$. For the three-magnon problem, these vectors reduce from being six-dimensional (for all $\tau \in S_3$) to just two-dimensional, as only two kinematic domains are allowed for each configuration, $Q_{ij}Q_{ji}Q_{ij}$, which arises from exchanging the first and last magnons,

$$l_1 < l_2 < l_3 \qquad \text{and} \qquad l_3 < l_2 < l_1 . \tag{3.7.16}$$

Moreover, the kinematic domains for the configurations $Q_{12}Q_{21}Q_{12}$ and $Q_{21}Q_{12}Q_{21}$ are separated because they include different numbers of Q_{12} and Q_{21}.

When we explicitly derive the Yang operators for the long-range ansatz (3.3.2), we realize that Yang operators need to incorporate the additional position dependence on the coefficients in addition to the change of dimensions of $\Phi(\sigma)$,

$$\mathcal{A}_{\tau|\sigma}(p_1, p_2, p_3; l_2 - l_1, l_3 - l_2) = A_\sigma(p_1, p_2, p_3) + D_\sigma^{n_\tau, m_\tau}(p_1, p_2, p_3) , \tag{3.7.17}$$

where $n_\tau = l_{\tau(2)} - l_{\tau(1)} - 1$ and $m_\tau = l_{\tau(3)} - l_{\tau(2)} - 1$.

To construct the Yang operator, we first write the plane wave basis for the case of three magnons as

$$\mathbf{v} = \big(\exp(ip_1 l_1 + ip_2 l_2 + ip_3 l_3) \;\; \cdots \;\; \exp(ip_3 l_1 + ip_2 l_2 + ip_1 l_3)\big)^t . \tag{3.7.18}$$

This is the set of plane waves that define a basis of a vector space in which we can define a representation of $\mathcal{S}_3$. This would be the natural choice for defining the three-magnon $\Phi(\tau)$ vectors with respect to CBA solution. Here, we take this as a starting point and later on observe that it can be altered. Then, the matrix that contains the coefficients of the wave function is given as

$$\begin{pmatrix} \langle l_1, l_2, l_3 | \Psi(p_1, p_2, p_3) \rangle_{12} \\ \langle l_3, l_2, l_1 | \Psi(p_1, p_2, p_3) \rangle_{12} \end{pmatrix} = \begin{pmatrix} \Phi(123) & \cdots & \Phi(321) \end{pmatrix} \mathbf{v} \,, \tag{3.7.19}$$

where

$$\Phi(\sigma) = \begin{pmatrix} A_\sigma(\kappa) + D^{n,m}_\sigma(\kappa) \\ A_{\sigma^r}(\kappa) + D^{m,n}_{\sigma^r}(\kappa) \end{pmatrix} \,. \tag{3.7.20}$$

Here σ^r is the permutation σ read backwards. From these expressions, the definition (3.7.5) of the Yang operator gives us

$$Y^{n,m}_j(p_{\tau(j)}, p_{\tau(j+1)}, p_k) = \begin{pmatrix} \frac{A_\sigma(\kappa) + D^{n,m}_\sigma(\kappa)}{A_{\alpha_j \sigma(\kappa)} + D^{n,m}_{\alpha_j \sigma}(\kappa)} & 0 \\ 0 & \frac{A_{\sigma^r}(\kappa) + D^{m,n}_{\sigma^r}(\kappa)}{A_{\alpha_{j+1}\sigma^r(\kappa)} + D^{m,n}_{\alpha_{j+1}\sigma^r}(\kappa)} \end{pmatrix} , \tag{3.7.21}$$

where k is the third index, which labels the momentum parameter for $k \neq \tau(j)$ and $k \neq \tau(j+1)$. Additionally, we can define the $\mathbb{Z}_2$ conjugate Yang operator by using the vector, by looking at the $\mathbb{Z}_2$ conjugate configurations,

$$\begin{pmatrix} \langle l_1, l_2, l_3 | \Psi(p_1, p_2, p_3) \rangle_{21} \\ \langle l_3, l_2, l_1 | \Psi(p_1, p_2, p_3) \rangle_{21} \end{pmatrix} = \begin{pmatrix} \tilde{\Phi}(123) & \cdots & \tilde{\Phi}(321) \end{pmatrix} \mathbf{v} \,, \tag{3.7.22}$$

where

$$\tilde{\Phi}(\sigma) = \begin{pmatrix} A_\sigma(1/\kappa) + D^{n,m}_\sigma(1/\kappa) \\ A_{\sigma^r}(1/\kappa) + D^{m,n}_{\sigma^r}(1/\kappa) \end{pmatrix} \,. \tag{3.7.23}$$

Note that the above form of the Yang operators comes only from the initial form of the long-range Bethe ansatz and it does not know anything about our special solution yet, therefore at this stage we cannot conclude about the fate of permutational symmetry. We can address this issue only after we insert the special solution. When we input the S_κ solution presented in Section 3.3.2 by substituting the solutions (3.3.91)-(3.3.96), it reduces to

$$Y^{n,m}_j(p_1, p_2, p_3) = \begin{pmatrix} S_\kappa(p_1, p_2) \frac{1 + f(p_2, p_1, p_3; n, m; \kappa)}{1 + f(p_1, p_2, p_3; n, m; \kappa)} & 0 \\ 0 & S_\kappa(p_2, p_1) \frac{1 + f(p_3, p_1, p_2; m, n; \kappa)}{1 + f(p_3, p_2, p_1; m, n; \kappa)} \end{pmatrix} \,. \tag{3.7.24}$$

Note that if we used the other special solution for the $S_{1/\kappa}$ or the $S_{\kappa=1}$ solutions presented in [1] with the corresponding f function the form of the Yang operator would still be the same.

Additionally, as in the two-magnon solution (3.7.13), we do not have transmission coefficients, which is expected. Secondly, we observe that the factors that appear on the diagonals have completely opposite order for both momenta and position variables, which is also consistent with both our two-magnon solution and the Yang operators that were presented in beginning of Section 3.7. Crucially, the form of the factors ensures that

$$Y_j^{n,m}(p_1, p_2, p_3)Y_j^{n,m}(p_2, p_1, p_3) = \mathbf{1} \ , \tag{3.7.25}$$

which is how unitarity appears at the level of Yang operators. Finally, we point out that since f is a known function given in (3.3.97), the form of the Yang operators admits a common description for any j and any permutation of the labels. We believe that, by changing the plane-wave basis to a modified version like $\Big(1 + \tilde{f}(p_{\sigma(1)}, p_{\sigma(2)}, p_{\sigma(3)}; n, m; \kappa)\Big)$ $e^{ip_{\sigma(1)}l_1 + ip_{\sigma(2)}l_2 + ip_{\sigma(3)}l_3}$,[20] we may derive a Yang operator satisfying the YBE solely in terms of the scattering coefficients, S_κ. The physical relevance of this basis change, however, requires further investigation.

An infinite tower of modified Yang-Baxter equations. At this point, it is easy to check that the following identity holds for any $n, m \geq 0$

$$\begin{aligned} &Y_j^{n,m}(p_2, p_3, p_1)Y_{j+1}^{n,m}(p_1, p_3, p_2)Y_j^{n,m}(p_1, p_2, p_3) \\ &\qquad\qquad = Y_{j+1}^{n,m}(p_1, p_2, p_3)Y_j^{n,m}(p_1, p_3, p_2)Y_{j+1}^{n,m}(p_2, p_3, p_1) \ , \end{aligned} \tag{3.7.26}$$

which can be identified as an infinite tower of modified YBEs. Although each factor of Yang operator takes all three momenta as input, the order in which the momentum variables enter specifies the particular 'scattering process' that takes place. It is crucial to highlight that the modified YBEs are not factorized only in terms of two-magnon scattering coefficients which means that we are learning extra information about the exchange of momenta in the level of three magnons.[21] The tower of modified YBEs is a direct consequence of the special solutions of the long-range ansatz, given in Section 3.3.2. The fact that there is a common description of the Yang operators for permutations with any two indices is a highly non-trivial feature of this model which was revealed by special solutions. This was revealed by establishing the relations between the solution of the second class of equations in Section 3.3 and further developed by

[20]Note that we do not yet know the explicit coordinate transformation which would define $\tilde{f}$. It should be related to f which is given in (3.3.97) but at the same time it should be symmetric under the transformation $\vec{p}_\sigma \cdot \vec{l} \leftrightarrow \vec{p} \cdot \vec{l}_{\sigma^{-1}}$.

[21]This reminds the authors of the coassociator defined in (3.7.37), and we would like to explore this point of view further in the future.

choosing symmetric solutions to the minimum separation equations in Section 3.3.2. In Figure 3.6 we present the tower of modified YBEs together with the inconsistency of the naive three-magnon CBA.

The Yang operators for the four-magnon long-range solution. Similarly, we would have expected to have kinematic domains $\vec{l_\tau} = (l_{\tau(1)}, l_{\tau(2)}, l_{\tau(3)}, l_{\tau(4)})$ for each $\tau \in \mathcal{S}_4$ for the four-magnon problem, but the color contractions only allow for $\tau \in \mathcal{S}_2 \times \mathcal{S}_2$. Specifically, only the following four kinematic domains are allowed

$$l_1 < l_2 < l_3 < l_4\ , \quad l_1 < l_4 < l_3 < l_2\ , \quad l_3 < l_2 < l_1 < l_4\ , \quad l_3 < l_4 < l_1 < l_2\ . \tag{3.7.27}$$

The second difference is the presence of position-dependent corrections. In the presence of these corrections, the permutation labels for momentum and position variables take the following roles

$$\mathcal{A}_{\tau|\sigma}(\vec{p};\vec{l}) = A_\sigma(\vec{p}) + D_\sigma^{n_\tau,m_\tau,r_\tau}(\vec{p})\ , \tag{3.7.28}$$

where $n_\tau = l_{\tau(2)} - l_{\tau(1)} - 1$, $m_\tau = l_{\tau(3)} - l_{\tau(2)} - 1$ and $r_\tau = l_{\tau(4)} - l_{\tau(3)} - 1$. Therefore, the column vector $\Phi(\sigma)$ takes the form,

$$\Phi^{n,m,r}(\sigma_0) = \begin{bmatrix} \mathcal{A}_{1234|\sigma_0} \\ \mathcal{A}_{1432|\sigma_1} \\ \mathcal{A}_{3214|\sigma_2} \\ \mathcal{A}_{3412|\sigma_3} \end{bmatrix} = \begin{bmatrix} A_{\sigma_0}(\vec{p}) + D_{\sigma_0}^{n,m,r}(\vec{p}) \\ A_{\sigma_1}(\vec{p}) + D_{\sigma_1}^{r+m+n+2,-2-r,-2-m}(\vec{p}) \\ A_{\sigma_2}(\vec{p}) + D_{\sigma_2}^{-2-m,-2-n,r+m+n+2}(\vec{p}) \\ A_{\sigma_3}(\vec{p}) + D_{\sigma_3}^{r,-4-r-m-n,n}(\vec{p}) \end{bmatrix}\ , \tag{3.7.29}$$

such that for the given permutation $\sigma_0 = (ijkl)$ the rest of the labels are defined as

$$\sigma_1 = (ilkj)\ , \quad \sigma_2 = (kjil)\ , \quad \sigma_3 = (klij)\ , \tag{3.7.30}$$

related to the kinematic domains given in (3.7.27). The Yang operator Y_1, which is associated to the transposition $\alpha_1 = (12)$ and relates the vector $\Phi((1234))$ to the vector $\Phi((2134))$ as

$$\Phi^{n,m,r}((2134)) = Y_1^{n,m,r}(\vec{p})\Phi^{n,m,r}((1234))\ , \tag{3.7.31}$$

can be computed for the solution discussed in the previous section by substituting the explicit expressions of the column vectors Φ for the long-range Bethe ansatz and using (3.6.37),

$$\begin{bmatrix} S_\kappa(p_1,p_2)\,(1+(\kappa-\kappa^{-1})f(\vec{p}_{2134},n,m,r,\kappa)) \\ S_\kappa(p_1,p_2)S_\kappa(p_1,p_3)S_\kappa(p_1,p_4)S_\kappa(p_3,p_4)\,(1+(\kappa-\kappa^{-1})f(\vec{p}_{2431},n_{\tau_1},m_{\tau_1},r_{\tau_1},\kappa)) \\ S_\kappa(p_1,p_3)S_\kappa(p_2,p_3)\,(1+(\kappa-\kappa^{-1})f(\vec{p}_{3124},n_{\tau_2},m_{\tau_2},r_{\tau_2},\kappa)) \\ S_\kappa(p_1,p_2)S_\kappa(p_1,p_3)S_\kappa(p_2,p_3)S_\kappa(p_1,p_4)S_\kappa(p_2,p_4)\,(1+(\kappa-\kappa^{-1})f(\vec{p}_{3421},n_{\tau_3},m_{\tau_3},r_{\tau_3},\kappa)) \end{bmatrix}$$

$$= Y_1^{n,m,r}(\vec{p}) \begin{bmatrix} (1+(\kappa-\kappa^{-1})f(\vec{p},n,m,r,\kappa)) \\ S_\kappa(p_2,p_3)S_\kappa(p_2,p_4)S_\kappa(p_3,p_4)\,(1+(\kappa-\kappa^{-1})f(\vec{p}_{1432},n_{\tau_1},m_{\tau_1},r_{\tau_1},\kappa)) \\ S_\kappa(p_1,p_2)S_\kappa(p_1,p_3)S_\kappa(p_2,p_3)\,(1+(\kappa-\kappa^{-1})f(\vec{p}_{3214},n_{\tau_2},m_{\tau_2},r_{\tau_2},\kappa)) \\ S_\kappa(p_1,p_3)S_\kappa(p_2,p_3)S_\kappa(p_1,p_4)S_\kappa(p_2,p_4)\,(1+(\kappa-\kappa^{-1})f(\vec{p}_{3412},n_{\tau_3},m_{\tau_3},r_{\tau_3},\kappa)) \end{bmatrix} \tag{3.7.32}$$

where the momentum and position variables with no labels refer to identity permutation (1234) and the permutation labels on the position variables, τ_i refer to the different kinematic domains listed in the same order in (3.7.29). In this case the Yang operator is given as

$$\begin{aligned} Y_1^{n,m,r}(\vec{p}) = S_\kappa(p_1,p_2)\cdot\mathrm{diag}\Bigg(& \frac{1+(\kappa-\kappa^{-1})f(\vec{p}_{2134},\vec{l})}{1+(\kappa-\kappa^{-1})f(\vec{p},\vec{l})}, \\ & \frac{S_\kappa(p_1,p_3)S_\kappa(p_1,p_4)}{S_\kappa(p_2,p_3)S_\kappa(p_2,p_4)}\frac{1+(\kappa-\kappa^{-1})f(\vec{p}_{2431},\vec{l}_{\tau_1})}{1+(\kappa-\kappa^{-1})f(\vec{p}_{1432}),\vec{l}_{\tau_1}))}, \\ & \frac{1}{S_\kappa(p_1,p_2)^2}\frac{1+(\kappa-\kappa^{-1})f(\vec{p}_{3124},\vec{l}_{\tau_2})}{1+(\kappa-\kappa^{-1})f(\vec{p}_{3214}),\vec{l}_{\tau_2}))}, \frac{1+(\kappa-\kappa^{-1})f(\vec{p}_{3421},\vec{l}_{\tau_3})}{1+(\kappa-\kappa^{-1})f(\vec{p}_{3412}),\vec{l}_{\tau_3}))}\Bigg) . \end{aligned} \tag{3.7.33}$$

Note that apart from an overall factor of $S_\kappa(p_1,p_2)$ the Yang operator includes additional factors of scattering coefficients which are related to the relative position of the permutation indices that are being permuted. In the case of three magnons as given in (3.7.24) we only had S_κ and S_κ^{-1}, however in the case of four-magnon these factors are more subtle. We can repeat this computation for all possible permutations and we conclude that the Yang operator that relates the permutation σ to the permutation $\alpha_j\sigma$ has to have the form.

$$Y_j^{n,m,r}(\vec{p}_{\sigma_0}) = \mathrm{diag}\left(\frac{A_{\alpha_j\sigma_0}}{A_{\sigma_0}}\frac{1+(\kappa-\kappa^{-1})f(\vec{p}_{\alpha_j\sigma_0},\vec{l})}{1+(\kappa-\kappa^{-1})f(\vec{p}_{\sigma_0},\vec{l})}, \frac{A_{\alpha_j\sigma_1}}{A_{\sigma_1}}\frac{1+(\kappa-\kappa^{-1})f(\vec{p}_{\alpha_j\sigma_1},\vec{l_{\tau_1}})}{1+(\kappa-\kappa^{-1})f(\vec{p}_{\sigma_1},\vec{l_{\tau_1}})}, \cdots\right) , \tag{3.7.34}$$

such that starting from $\sigma_0 = (ijkl)$ the rest of the permutations read as (3.7.30). The transposition α_n is defined as nth and $(n+1)$th integers that are given inside index $\sigma_0 = (ijkl)$. Then it acts on any permutation by exchanging the positions of those two integers.[22] It is straightforward to check that this Yang operator fulfills

$$Y_j^{n,m,r}(\vec{p}_{\alpha_j})Y_j^{n,m,r}(\vec{p}) = \mathbf{1} , \tag{3.7.35}$$

[22]In the example (3.7.33), $\sigma_0 = (1234)$ and Yang operator $Y_1(\vec{p})$ has the index 1. Therefore, the corresponding transposition is $\alpha_1 = (12)$. Then the Yang operator acts on $\Phi(\sigma_0)$ and exchanges the permutation indices 1 with 2 in each row. This is achieved by having the diagonal factors given in (3.7.33).

and the modified[23] YBE reads,

$$Y_j^{n,m,r}(\vec{p}_{\alpha_j\alpha_{j+1}})Y_{j+1}^{n,m,r}(\vec{p}_{\alpha_j})Y_j^{n,m,r}(\vec{p}) = Y_{j+1}^{n,m,r}(\vec{p}_{\alpha_{j+1}\alpha_j})Y_j^{n,m,r}(\vec{p}_{\alpha_{j+1}})Y_{j+1}^{n,m,r}(\vec{p}) \ . \quad (3.7.36)$$

Indeed, this modified form of the Yang–Baxter equation holds for all choices of n, m, and r, thereby giving rise to an infinite tower of modified Yang–Baxter equations, analogous to the case of the three-magnon solution. The Yang operators corresponding to the special three-magnon solution are given in (3.7.24), and they satisfy the associated three-magnon modified Yang–Baxter equations as presented in (3.7.26). Furthermore, since the explicit relation between the three- and four-magnon solutions is established in Section 3.6, the Yang operators for the four-magnon problem are completely determined by the special three-magnon solution.

In light of Sections 3.5 and 3.6, we observe that once the relative position of the magnon located at either end of the spin chain is fixed, the remaining three magnons exhibit behavior identical to that of a purely three-magnon state. This correspondence is explicitly visible in the final form of the generating function given in (3.6.30). Since we do not have control over the large-separation behavior, as emphasized at the beginning of this section, this observation is meaningful either when one of the relative distances is fixed, or when an average is taken over all possible relative configurations, as carried out in Section 3.5. Consequently, the Yang operators for the four-magnon problem are directly related to those of the three-magnon problem.

In [1], we interpreted the form of the Yang operators (3.7.24) heuristically as a combination of scattering coefficients and coassociators. Drawing inspiration from the elliptic quantum groups which admit R-matrices that satisfy DYBE, coassociators govern the co-associativity of the co-product,

$$\varphi_{ijk} : (v_i \tilde{\otimes} v_j)\tilde{\otimes} v_k \to v_i \tilde{\otimes}(v_j \tilde{\otimes} v_k) \ . \quad (3.7.37)$$

We believe that our solution at the level of a CBA-like solution exhibits this behavior. To demonstrate the analogy, we think of a scattering operator that acts as

$$S_{12}(p,\lambda)((p_1 \otimes p_2)\otimes p_3) = S_\kappa(p_1,p_2)((p_2 \otimes p_1)\otimes p_3) \ , \quad (3.7.38)$$

the modified YBE should take the following form,

$$\varphi_{321}\ S_{23}(p,\lambda)\ \varphi_{231}^{-1}\ S_{13}(p,\lambda)\ \varphi_{213}\ S_{12}(p,\lambda) = S_{12}(p,\lambda)\ \varphi_{312}\ S_{13}(p,\lambda)\ \varphi_{132}^{-1}\ S_{23}(p,\lambda)\ \varphi_{123} \ , \quad (3.7.39)$$

[23]Here, the Yang–Baxter equation involving only the scattering coefficients S_κ is modified by the presence of position-dependent coefficients in two ways: first, by the introduction of κ dependence, and second, by position dependence. When we take $\kappa \to 1$ or $n,m,r \to 0$ the modified YBE reduces to YBE with only S_κs.

acting on a configuration $((p_1 \otimes p_2) \otimes p_3)$ from left to right. With respect to this analogy, the form of the four-magnon Yang operator given in (3.7.34) should include the contributions of scattering coefficients and four-site coassociator φ_{ijkl} which is a combination of $\varphi_{ijk} \otimes \mathbf{1}$ or $\mathbf{1} \otimes \varphi_{jkl}$. It would be very interesting to make this interpretation concrete and have a definition of scattering operators (equivalently R-matrix) and coassociators in our context.

Finally, the existence of a Yang operator for the four-magnon problem demonstrates that contrary to the naive expectation that color contractions would break permutational symmetry, such symmetry remains present in our solution. This tower of modified YBEs is implicitly related to the one obtained in the three-magnon problem because the generating function is fully determined by the three-magnon solutions and analyticity condition over them as given in (3.6.30).

3.8 Periodic Boundary Conditions

In this section, we introduce periodic boundary conditions into the spin chain model. The spectrum of these finite-length spin chains corresponds to the single-trace operators of the interpolating theory. From the gauge theory perspective, it is known that operators with generalized traces—introduced in [81]—belong to either the untwisted or twisted sectors, which correspond to the $\mathbb{Z}_2$-even and $\mathbb{Z}_2$-odd states of the spin chain, respectively. We define the single-trace operators of the interpolating theory by relating them to their counterparts in $\mathcal{N}=4$ SYM. Using the orbifold projection dictionary for the scalar fields provided in (3.1.1), along with the projection matrix γ defined in (2.1.39), the twisted and untwisted operators map to the single-trace operators of $\mathcal{N}=4$ SYM as follows:

$$\mathrm{Tr}\left(Z \cdots Z X Z \cdots Z X\right) \to \mathrm{Tr}\left(\phi \cdots \phi Q \phi \cdots \phi Q\right) \ , \tag{3.8.1}$$

$$\mathrm{Tr}\left(\gamma Z \cdots Z X Z \cdots Z X\right) \to \mathrm{Tr}\left(\gamma \phi \cdots \phi Q \phi \cdots \phi Q\right) \ . \tag{3.8.2}$$

Furthermore, a generalized single-trace operator can be decomposed into a sum of two distinct traces, depending on how the representations of the gauge group factors $SU(N)_1 \times SU(N)_2$ are contracted. In particular, the overall trace can be expressed as:

$$\mathrm{Tr}\left(\phi \cdots \phi Q \phi \cdots \phi Q\right) = \mathrm{tr}_1\left(\phi_1 \cdots \phi_1 Q_{12} \phi_2 \cdots \phi_2 Q_{21}\right) + \mathrm{tr}_2\left(\phi_2 \cdots \phi_2 Q_{21} \phi_1 \cdots \phi_1 Q_{12}\right) \ . \tag{3.8.3}$$

This operator belongs to the untwisted sector, where tr_i denotes the trace over the $SU(N)_i$ gauge group. Similarly,

$$\mathrm{Tr}\left(\gamma\phi\cdots\phi Q\phi\cdots\phi Q\right)=\mathrm{tr}_1\left(\phi_1\cdots\phi_1 Q_{12}\phi_2\cdots\phi_2 Q_{21}\right)-\mathrm{tr}_2\left(\phi_2\cdots\phi_2 Q_{21}\phi_1\cdots\phi_1 Q_{12}\right)\ , \tag{3.8.4}$$

is an operator from the twisted sector and equivalently it corresponds to a $\mathbb{Z}_2$-odd operator.

To compute the eigenvalues of these states in the spin chain picture, first, we add the periodic boundary conditions to the Hamiltonian (3.1.18),

$$\mathcal{H}=\sum_{i=1}^{L}\mathcal{H}_{i,i+1}\ , \qquad \mathcal{H}_{L,L+1}=\mathcal{H}_{L,1}\ . \tag{3.8.5}$$

Due to the color contraction rules that govern the states, the Hilbert space is restricted to spin chains containing an even number of Q_{12} and Q_{21} excitations. In the following subsections, we present solutions for the eigenstates of the Hamiltonian (3.8.5) in the two-magnon case—previously studied in [81]—and in the four-magnon case, which we examined in earlier sections. To implement periodic boundary conditions, we consider finite spin chain states of the form:

$$\begin{aligned}\left(Q_{12}(l_1)Q_{21}(l_2)\right)_{11}&=\left(\phi_1\cdots\phi_1 Q_{12}\phi_2\cdots\phi_2 Q_{21}\phi_1\cdots\phi_1\right)_{11}\ ,\\ \left(Q_{21}(l_1)Q_{12}(l_2)\right)_{22}&=\left(\phi_2\cdots\phi_2 Q_{21}\phi_1\cdots\phi_1 Q_{12}\phi_2\cdots\phi_2\right)_{22}\ ,\end{aligned} \tag{3.8.6}$$

for $1\leq l_1<l_2\leq L$ such that by using parenthesis $\left(\cdots\right)_{ii}$ we distinguish between the closed finite states and the open infinite states, denoted by $|\cdots\rangle_{ii}$ and keep track of the corresponding trace tr_i by using the overall color labels. Similarly, for the four magnons, we have the states in position space,

$$\left(Q_{12}(l_1)Q_{21}(l_2)Q_{12}(l_3)Q_{21}(l_4)\right)_{11}\ ,\quad \text{and}\quad \left(Q_{21}(l_1)Q_{12}(l_2)Q_{21}(l_3)Q_{12}(l_4)\right)_{22}\ , \tag{3.8.7}$$

for $1\leq l_1<l_2<l_3<l_4\leq L$. In addition to the finite length, the periodic boundary conditions imply

$$\left(Q_{ij}(l_1)Q_{ji}(l_2)\right)_{ii}\equiv\left(Q_{ji}(l_2)Q_{ij}(l_1+L)\right)_{jj}\ , \tag{3.8.8}$$

$$\left(Q_{ij}(l_1)Q_{ji}(l_2)Q_{ij}(l_3)Q_{ji}(l_4)\right)_{ii}\equiv\left(Q_{ji}(l_2)Q_{ij}(l_3)Q_{ji}(l_4)Q_{ij}(l_1+L)\right)_{jj}\ , \tag{3.8.9}$$

for $i,j\in\{1,2\}$, which holds both for twisted and untwisted states. Note that the periodicity condition transforms a state with overall color structure $\left(\cdots\right)_{11}$ into $\left(\cdots\right)_{22}$, and vice versa. Moreover, when the beginning and end of a closed finite-position state do not match in terms of ϕ and Q fields, the action of the Hamiltonian (3.8.5) induces a transformation of the overall color structure. For example:

$$\mathcal{H}_{L1}(Q_{12}\cdots Q_{21}\cdots\phi_1)_{11} = \kappa^{-1}(Q_{12}\cdots Q_{21}\cdots\phi_1)_{11} - (\phi_2\cdots Q_{21}\cdots Q_{12})_{22}\ , \quad (3.8.10)$$

where $\mathcal{H}_{L1}$ is the Hamiltonian density (3.1.19) acting on the last and the first elements of the state. As a result, the momentum eigenstates must incorporate both color structures. Since the states are given in terms of closed chains, we can sum over states with distinct color indices—an operation that is not possible for open infinite states. The momentum eigenstate for a length L state with $2M$ magnons is defined as

$$\begin{aligned} |\Psi(\vec{p})\rangle_{L,\pm} = & \sum_{l_1<\cdots<l_{2M}} \psi_{11}(\vec{p},\vec{l})(Q_{12}(l_1)\cdots Q_{21}(l_{2M}))_{11} \\ & + T_\pm(\vec{p},\kappa)\sum_{l_1<\cdots<l_{2M}} \psi_{22}(\vec{p},\vec{l})(Q_{21}(l_1)\cdots Q_{12}(l_{2M}))_{22}\ , \end{aligned} \quad (3.8.11)$$

such that $T_\pm(\vec{p},\kappa)$ is the relative normalization factor between the $\mathbb{Z}_2$ conjugate wave functions ψ_{11} and ψ_{22} which depends on $2M$ momentum variables and κ and it proves to be essential to the solution. This factor may vary depending on if the state is untwisted $|\Psi(\vec{p})\rangle_{L,+}$ or twisted $|\Psi(\vec{p})\rangle_{L,-}$. These distinct states act as follows under the action of the $\mathbb{Z}_2$ under a particular normalization,

$$\mathbb{Z}_2\,|\Psi(\vec{p})\rangle_{L,\pm} = \pm\,|\Psi(\vec{p})\rangle_{L,\pm}\ . \quad (3.8.12)$$

For the two-magnon case, the wave function is expressed in the CBA form, incorporating the scattering coefficients given in equations (3.2.14) and (3.2.15). The Bethe equations are then solved to determine the two momenta, and thus the spectrum. In contrast, for the four-magnon case, we adopt a different approach due to the more involved form of the wave function. Similarly to the wave functions of open infinite states (3.4.4), we start with a long-range Bethe ansatz,

$$\psi_{ii}(n,m,r,s) = \sum_{\sigma\in\mathcal{S}_4}(A_\sigma + D_\sigma^{n,m,r,s})\,e^{i\vec{p}_\sigma\cdot\vec{l}}\,, \quad (3.8.13)$$

such that $n = l_2 - l_1 - 1$, $m = l_3 - l_2 - 1$, $r = l_4 - l_3 - 1$ and the distance between the first and the last magnon is denoted by an additional positive integer variable, $s = l_1 + L - l_4 - 1$. Also in (3.8.13), we omit the momentum variables for simplicity and change the usual notation of the wave function in terms of $l_i \in \{0, 1, \cdots, L-1\}$ to distances between magnons to make the connection between the distinct position-dependent corrections more apparent. Note that this way we also omit the difference between the configurations $\{l_1, l_2, l_3, l_4\}$ and $\{l_1+a, l_2+a, l_3+a, l_4+a\}$ for $a \in \mathbb{Z}$ as this distinction disappears under the vanishing of total momentum condition $\mathcal{P}_4 = 0$. In contrast to the open infinite long-range Bethe ansatz given in (3.4.4), the position-dependent corrections for the closed spin chains are finitely many, and they are enumerated by four integers instead of three. However, this additional variable is fixed in terms of the other three variables and total length,

$$s = L - 4 - n - m - r \, . \tag{3.8.14}$$

Here, we analyze the position-dependent corrections for closed spin chains separately from those of the open infinite chains, whose special solutions were presented in Section 3.4.2 and Section 3.6. Despite their differences, we adopt the same strategy for closed and open boundary conditions: deriving the position-dependent corrections while ensuring that the solution respects the permutation symmetry of the wave function. Along the way, we highlight the connections we observe between the eigenvalue problems of closed finite and open infinite spin chains.

Although the analytic form of the position-dependent corrections obtained after imposing periodicity differs significantly from the open infinite case (3.4.76), it retains key structural features—such as the overall $(\kappa - \kappa^{-1})A_\sigma$ factor and the partial factorization property (3.4.51). Notably, as the length of the spin chain increases, the similarities between the closed finite and open infinite position-dependent corrections become more pronounced. This observation suggests a deeper interplay between the open infinite and closed finite solutions, which we aim to further elucidate through the development of an appropriate rapidity parametrization. Establishing such a parametrization is expected to clarify the role of boundary conditions in models governed by a long-range Bethe ansatz.

A direct connection between the open infinite and closed finite solutions has not yet been established within the framework of the long-range Bethe ansatz. Nevertheless, the shared structural features of their position-dependent corrections suggest that a deeper relationship remains to be uncovered. At the level of position-dependent corrections we expect to have a relation between the open-infinite and closed-finite coefficients as

$$\tilde{D}^{n,m,r,s} \propto c_1 \tilde{D}^{n,m,r} + c_2 \tilde{D}^{m,r,n} + c_3 \tilde{D}^{r,n,m} + \cdots \tag{3.8.15}$$

such that c_i are coefficients in terms of momenta and κ. Once this map is understood, with an appropriate truncation procedure, the generating function of the closed finite chain, currently a polynomial in four complex variables, should be related to the open infinite generating function via the transformation,

$$t^{L-4} G\left(\frac{x}{t}, \frac{y}{t}, \frac{z}{t}\right) \longrightarrow G(x, y, z, t) \, , \tag{3.8.16}$$

such that

$$G_\sigma(x,y,z,t) = \sum_{\substack{n,m,r=0 \\ n+m+r<L-4}}^{L-4} D_\sigma^{n,m,r,L-4-n-m-r} x^n y^m z^r t^{L-4-n-m-r} \,. \tag{3.8.17}$$

However, truncating the sum over relative distances alone does not yield a meaningful solution for (un)twisted boundary conditions without introducing a suitable boundary term, the precise form of which remains to be discovered.

In the following subsections we consider the eigenvalue problem of the two- and four-magnons separately and present our results. We solve the four-magnon problem for short lengths, $L = 4, 5, 6$ and obtain the corresponding position-dependent corrections.

3.8.1 Finite Length Two-Magnon Solution

In this section, we impose periodic boundary conditions on the two-magnon problem. The CBA solution was originally studied in [81]; here, we combine the two distinct CBA solutions corresponding to the two possible orderings of the magnons, as given in (3.2.10), since the periodic boundary conditions mix these two states (3.8.10). To fully account for this mixing, we include a relative normalization factor, as the overall normalization of the wave functions depends on the parameter κ. We then derive the Bethe equations from the periodicity condition, which also explicitly depends on κ. After solving the Bethe equations, we compare the resulting eigenvalues and eigenstates with brute-force diagonalization of the spin chain Hamiltonian for $L = 4, 5, 6$, and find complete agreement.

To impose periodic boundary conditions, we consider the momentum state for a generic two-magnon spin chain,

$$|\Psi(p_1,p_2)\rangle_{L,\pm} = \big(\psi(p_1,p_2)\big)_{11} + T_\pm(p_1,p_2,\kappa)\big(\psi(p_1,p_2)\big)_{22} \,. \tag{3.8.18}$$

In this case, the periodic boundary conditions on wave functions imply,

$$\psi_{11}(p_1,p_2;l_2,l_1+L) = T_\pm(p_1,p_2,\kappa)\psi_{22}(p_1,p_2;l_1,l_2) \,, \tag{3.8.19}$$

which leads to the following Bethe equations,

$$e^{-ip_1L} = T_\pm(p_1,p_2,\kappa)S_{1/\kappa}(p_1,p_2) \,, \tag{3.8.20}$$

$$S_\kappa(p_1,p_2) = T_\pm(p_1,p_2,\kappa)e^{ip_2L} \,. \tag{3.8.21}$$

Due to the color structure of the spin chain states, the scattering coefficients in the Bethe equations exhibit distinct dependencies on the κ factor. This difference distinguishes (3.8.20) and (3.8.21) from the Bethe equations of the Heisenberg XXZ model, which is characterized by an anisotropy parameter $(\kappa + \kappa^{-1})/2$ while sharing the same dispersion relation as the present model. The κ-structure of the scattering coefficients implies that the Bethe equations determine the momentum variables along with a non-trivial relative normalization factor ($T \neq 1$), while still satisfying the vanishing total momentum condition,

$$p_1 + p_2 = 2\pi m \; . \tag{3.8.22}$$

As we want both momenta p_1 and p_2 to be in the first Brillouin zone $p \in (-\pi, \pi]$, we set $m = 0$ from now on and focus on the case $p = p_1 = -p_2$. We observe that for $L > 2$ and $E_2 \neq 0$, we can obtain the solution of the momentum variables analytically for any length L. However, the $E_2 = 0$ cases require special attention, since for $L = 2$ it corresponds to a Q-vacuum state (a bound state derived from the ϕ-vacuum), and for $L > 2$ we obtain a descendant of the vacuum state. To validate our results, we compare the spectrum of the two-magnon states with numerical diagonalization of the Hamiltonian (3.1.19) for short closed spin chains ($L = 4, 5, 6$), finding perfect agreement up to an overall normalization factor.

Solving the two-magnon Bethe equations. For the spin chains with length $L > 2$, the Bethe equations (3.8.20) and (3.8.21), together with the total momentum condition (3.8.22), provide the following solution for the relative normalization factor,

$$T_{\pm}(p, \kappa) \equiv T_{\pm}(p, -p, \kappa) = \pm \frac{\kappa - e^{ip}}{1 - \kappa e^{ip}} \tag{3.8.23}$$

which obeys the property $T(p, \kappa) = \left(T(p, \kappa^{-1})\right)^{-1}$ and, for the untwisted states, the remaining Bethe equation takes the following form,

$$e^{-ipL} = e^{-ip} \tag{3.8.24}$$

and this equation is solved for

$$p = \frac{2n\pi}{L - 1} \; , \tag{3.8.25}$$

whereas for the twisted states the remaining Bethe equation takes the form,

$$e^{-ipL} = e^{-ip + i\pi} \; , \tag{3.8.26}$$

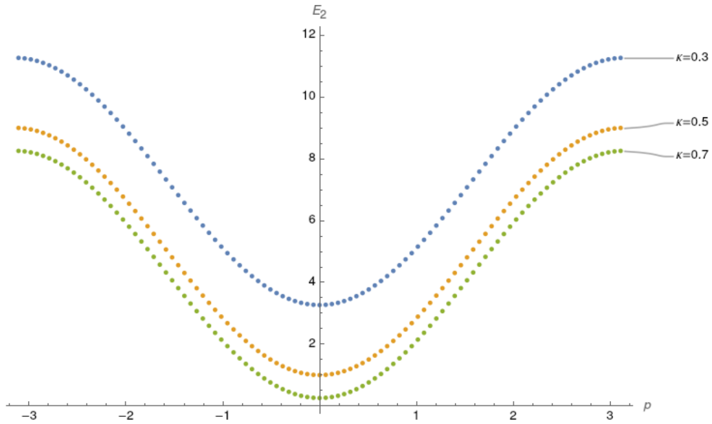

Figure 3.7: *For length* $L = 100$*, the spectrum of the untwisted states for* $\kappa = 0.3, 0.5, 0.7$ *where* E_2 *denotes the energy eigenvalues.*

and it is solved for

$$p = \frac{(2n+1)\pi}{L-1}\,, \tag{3.8.27}$$

for $n \in \mathbb{Z}$ with $\frac{L-1}{2} > n > 0$ since the states $|\Psi(p,-p)\rangle_{L,\pm}$ and $|\Psi(-p,p)\rangle_{L,\pm}$ are the same up to a proportionality factor. Note that the solution $p = 0$ and $p = \pi$ make the wave function vanish, therefore we do not consider them as valid solutions.

At this point, we should perform a counting of states to check if we are finding the complete spectrum. On the one hand, if we ignore for a moment the color contractions, the counting of states is the same as for the two copies of the XXZ spin chain, which is $\lfloor \frac{L}{2} \rfloor$ for the case of two excitations and zero total momentum for each copy. Taking into account the color contractions, we naively would guess that we have $2\lfloor \frac{L}{2} \rfloor$ states. However, for even L we have the state with total momentum $p_1 + p_2 = 0$ created from $(\phi_1^{\frac{L-2}{2}} Q_{12} \phi_2^{\frac{L-2}{2}} Q_{21})_{11}$, which maps into itself under $\mathbb{Z}_2$. This implies that we have to subtract one state from the naive counting for even values of L. Taking this into account, we have $L-1$ states both for even and odd values of L. On the other hand, for even values of L both (3.8.25) and (3.8.27) have $\frac{L-2}{2}$ solutions. In contrast, for odd values of L the equation (3.8.25) has $\frac{L-3}{2}$ and the equation (3.8.27) has $\frac{L-1}{2}$. Thus, in total, we have $L-2$ solutions both for even and odd values of L. This means that we are missing exactly one solution for every value of L for untwisted and twisted states. Apart from these two states, the distribution of eigenvalues for each of these eigenstates for $L = 100$ is given in Figure 3.7.

Vacuum solution and descendants. Notice that, among the momenta (3.8.25) and (3.8.27), we are missing the state that corresponds to the $Q-$vacuum of the model for $L = 2$. This means that the missing solution is a descendant of the $Q-$vacuum (or the $Q-$vacuum itself for $L = 2$). Therefore, we first use the vanishing of the total momentum, $p_1 = -p_2$ and plug this relation into the total energy to find the solution of the momentum variables,

$$E_2(p, -p) = 2\kappa + 2\kappa^{-1} - 2e^{ip} - 2e^{-ip} = 0 \; . \tag{3.8.28}$$

This equation has two solutions,

$$p = \pm i \log(\kappa) \; , \tag{3.8.29}$$

which correspond to a bound state of the two magnons, as it gives

$$S_{1/\kappa}(i \log(\kappa), -i \log(\kappa)) = 0 \; . \tag{3.8.30}$$

In this case, the previous form of the relative normalization coming from the Bethe equations is not valid, therefore we directly use the periodicity relation (3.8.19) to define the relative normalization such that fixing $e^{ip} = \kappa$ gives

$$T(p, \kappa) = \frac{\psi_{11}(p, -p, 2, L+1)}{\psi_{22}(p, -p, 1, 2)} = \frac{1}{\kappa^L - \kappa^{L-2}}(1 - e^{ip}/\kappa) \; . \tag{3.8.31}$$

If we consider this zero as a divergence of $\psi_{22}(p, -p, 1, 2)$, we can extract the following two solutions, which correspond to the $\mathbb{Z}_2$ even and $\mathbb{Z}_2$ odd states

$$|\Psi(-i\log(\kappa)\,, i\log(\kappa)\rangle_{L=2,+} = \big(Q_{12}(1)Q_{21}(2)\big)_{11} + \big(Q_{21}(1)Q_{12}(2)\big)_{22} \; , \tag{3.8.32}$$

and

$$|\Psi(-i\log(\kappa)\,, i\log(\kappa)\rangle_{L=2,-} = \big(Q_{12}(1)Q_{21}(2)\big)_{11} - \big(Q_{21}(1)Q_{12}(2)\big)_{22} \; . \tag{3.8.33}$$

The twisted $L = 2$ state, as given above, does not correspond to a non-trivial single-trace operator because the trace over the two components cancels out. Specifically, $\mathrm{tr}_1(Q_{12}Q_{21}) - \mathrm{tr}_2(Q_{21}Q_{12}) = 0$. For $L = 2$, it is trivial to check that indeed the action of the Hamiltonian on these two states gives zero eigenvalue. Furthermore, the single-trace operator which corresponds to the $\mathbb{Z}_2$ odd state does not exist because under the tracing the two distinct states cancel each other for $L > 2$. An example of a less trivial check is the $L = 4$ solution. For the untwisted sector, it is given as

$$|\Psi(-p, p)\rangle_{4,+} = \kappa^2\big(Q_{12}(0)Q_{21}(1)\big)_{11} + \kappa^2\big(Q_{12}(1)Q_{21}(2)\big)_{11} + \kappa^2\big(Q_{12}(2)Q_{21}(3)\big)_{11}$$

$$+\kappa\big(Q_{12}(0)Q_{21}(2)\big)_{11}+\kappa\big(Q_{12}(1)Q_{21}(3)\big)_{11}+\big(Q_{12}(0)Q_{21}(3)\big)_{11}$$
$$+\big(Q_{21}(0)Q_{12}(1)\big)_{22}+\big(Q_{21}(1)Q_{12}(2)\big)_{22}+\big(Q_{21}(2)Q_{12}(3)\big)_{22}$$
$$+\kappa\big(Q_{21}(0)Q_{12}(2)\big)_{22}+\kappa\big(Q_{21}(1)Q_{12}(3)\big)_{22}+\kappa^2\big(Q_{21}(0)Q_{12}(3)\big)_{22}\,. \tag{3.8.34}$$

This solution for the zero-energy eigenstate, along with its $L = 5, 6$ analogs, agrees with the numerical diagonalization of the Hamiltonian (3.8.5). Therefore, the momentum $p = i\log(\kappa)$, together with the momenta (3.8.25) and (3.8.27), give us the full spectrum for $M = 2$.

3.8.2 Finite Length Four-Magnon Solution

We now turn to the momentum state for a generic four-magnon spin chain with long-range Bethe ansatz, and impose periodic boundary conditions,

$$|\Psi(p_1,p_2,p_3,p_4)\rangle_{L,\pm}=\big(\Psi(p_1,p_2,p_3,p_4)\big)_{11}+T_\pm(p,\kappa)\big(\Psi(p_1,p_2,p_3,p_4)\big)_{22}\,. \tag{3.8.35}$$

In this case, the periodic boundary conditions imply,

$$\psi_{11}(n,m,r,s)=T_\pm(p,\kappa)\psi_{22}(m,r,s,n)\,, \tag{3.8.36}$$

such that the wave functions are defined in (3.8.13) and the relative normalization factor initially is a function of the four momenta and κ. Due to the contributions from the position-dependent corrections, only omitting plane wave corrections and obtaining Bethe-like equations do not capture the solution of the periodic boundary conditions. The underlying reason is that the position-dependent corrections imply a subtle modification of the plane wave basis, as we discussed using the Yang operators in Section 3.7. Consequently, simply omitting the plane wave factors without altering the position-dependent corrections and reducing the periodicity relations to Bethe-like equations does not yield a solution. We plan to report on a more systematic approach for solving the periodic boundary conditions once the appropriate coordinate transformations and the rapidity structure of the model are fully understood.

Now, we focus on the periodicity conditions at the level of wave functions. By using the general property of the relative normalization factor, $T(p,\kappa) = \big(T(p,\kappa^{-1})\big)^{-1}$ in addition to (3.8.36), we conclude that the model is 2L periodic both in untwisted and twisted sectors,

$$\psi_{ii}(n,m,r,s)=\psi_{ii}(r,s,n,m)\,, \tag{3.8.37}$$

for $i \in \{1,2\}$, which will play an important role in our solution, since it gives a relation between the wave functions with the same color indices. To impose the periodic boundary conditions, we follow an experimental route and discover how to solve the eigenvalue problem for the long-range Bethe ansatz while keeping the permutationally symmetric form of the solution. We focus on short chains ($L = 4, 5, 6$) and we compute the action of the Hamiltonian on the momentum states, $(\mathcal{H} - E_4) |\Psi(p_1, p_2, p_3, p_4)\rangle_L$. Since the action of the Hamiltonian mixes the $\mathbb{Z}_2$ conjugate states as demonstrated in (3.8.10), we distinguish between the eigenvalue equations coming from $(\mathcal{H} - E_4) |\Psi(p_1, p_2, p_3, p_4)\rangle_L$ which involve both of the $\mathbb{Z}_2$ conjugate contributions and those which do not, by referring to the former as *boundary eigenvalue equations* and to the latter as *bulk eigenvalue equations*. We observe that, by combining the bulk eigenvalue equations with the eigenvalue equations for open infinite states as presented in Section 3.4 we are able to determine the position-dependent corrections analytically as a function of momenta and κ for each distinct separation of magnons.[24] To make use of the eigenvalue equations coming from the open infinite case we transform those position-dependent corrections of the open infinite states to closed ones by

$$\tilde{D}_{\sigma}^{n,m,r} \to \tilde{D}_{\sigma}^{n,m,r,L-4-n-m-r} \,. \tag{3.8.38}$$

Then, by solving the combined set of bulk equations and the open-infinite equations for short separation using the procedure we demonstrated in Section 3.4.2, we obtain a solution for the position-dependent corrections. Then, we compute the relative normalization factor from one of the boundary eigenvalue equations and impose all periodicity relations as given in (3.8.37) to ensure that all boundary eigenvalue equations are solved. Imposing these relations for all wave functions, we numerically solve for momentum variables for fixed values of κ and obtain eigenstates of the closed Hamiltonian (3.8.5). To improve the numerical accuracy of our solution we fix one of the wave functions (for example $\psi_{ii}(0,0,0,L-4)$) to have only constant position-dependent corrections which are very similar to having a CBA type wave function. This improves the numerical accuracy of the solution significantly. Finally, we check our solution against brute-force diagonalization of the Hamiltonian for $L = 5, 6$. Up to an overall normalization factor, we obtain agreement.

$\boldsymbol{L = 4.}$ As in the case of zero-energy two-magnon states given in Section 3.8.1, the four-magnon states for $L = 4$ correspond to the Q-vacuum of the model. Unlike the rest of the four-magnon states with finite length, this state does not include non-trivial

[24]The fact that we can fully fix the form of position-dependent corrections once we impose boundary conditions without leftover freedom was a claim of [1] and here we confirm that this is the case.

position-dependent corrections since four magnons can only be next to each other.[25] Therefore, we obtain the solution by using the periodicity relation (3.8.36), and choose the relative normalization to be defined as,

$$T_{\pm}(p,\kappa) = \pm\frac{\psi(0,0,0,1)_{11}}{\psi(0,0,0,1)_{22}} \; . \tag{3.8.39}$$

The relative normalization factor given for the descendants of the vacuum in the two-magnon problem, (3.8.31) also has the same description. Here, the wave function in the numerator is coming from the state $(l_1,l_2,l_3,l_4) = (1,2,3,4)$ whereas the wave function in the denominator is coming from $(l_1,l_2,l_3,l_4) = (0,1,2,3)$. Nevertheless, under the vanishing total momentum, these are the same wave functions up to $\kappa \to \kappa^{-1}$. In addition to the vanishing total momentum condition, we impose the vanishing of the total energy (3.4.2)

$$E_4(p_1,p_2,p_3,-p_1-p_2-p_3) = 0 \; . \tag{3.8.40}$$

Moreover, the $L=4$ state corresponds to a bound state solution from the perspective of the ϕ vacuum. Therefore, we select two distinct scattering coefficients and solve for the momentum configurations that cause them to vanish:

$$S_{\kappa}(p_1,p_2) = 0 \; , \qquad\qquad S_{1/\kappa}(p_2,p_3) = 0 \; . \tag{3.8.41}$$

Note that these choices are not unique, but the other solutions are related to each other by permutation of momentum indices. Under these conditions, we obtain the eigenvectors,

$$|\Psi(p_1,p_2,p_3,p_4)\rangle_{L=4,\pm} = \mathcal{N}(\kappa)\Big[(Q_{12}Q_{21}Q_{12}Q_{21})_{11} \pm (Q_{21}Q_{12}Q_{21}Q_{12})_{22}\Big] \; , \tag{3.8.42}$$

for the momentum variables,

$$p_1 = -i\log\left(\frac{3\kappa}{\kappa^2+2}\right) \; , \quad p_2 = i\log\left(\frac{\kappa(1+2\kappa^2)}{\kappa^2+2}\right) \; , \quad p_3 = i\log\left(\frac{3\kappa}{2\kappa^2+1}\right) \; . \tag{3.8.43}$$

and the overall normalization,

$$\mathcal{N}(\kappa) = -\frac{2\,(\kappa^2+2)\,(4\kappa^4+9\kappa^2+5)}{9\kappa^4} \; . \tag{3.8.44}$$

As in the two-magnon case, the $\mathbb{Z}_2$-odd state vanishes when we map the spin chain states to the single-trace operators. In the following sections, we continue our search for the eigenstates in the long-range Bethe ansatz formalism and omit the overall factors of the normalization, as they are not relevant to our discussion.

[25] In principle, this state contains the position-dependent corrections denoted as $D^{0,0,0}$ but they do not play any crucial role and they can be absorbed into the definition of scattering coefficients.

$\boldsymbol{L=5.}$ The momentum states for the $L=5$ spin chains take the form,

$$|\Psi(p_1,p_2,p_3,p_4)\rangle_{L=5,\pm} = (\Psi(p_1,p_2,p_3,p_4))_{11} + T_\pm(p_1,p_2,p_3,p_4,\kappa)(\Psi(p_1,p_2,p_3,p_4))_{22} \; . \tag{3.8.45}$$

As there are five distinct position states for each color index, we can write

$$(\Psi(p_1,p_2,p_3,p_4))_{11} = \sum_{\substack{n,m,r=0\\ m+n+r\ \leq 1}}^{1} \psi_{11}(n,m,r,1-n-m-r)(\phi(i))_{11} \; . \tag{3.8.46}$$

Here, we use the short-hand notation, $(\phi(j))_{11}$ to refer to the length five position state which is characterized by the ϕ_i state in the jth position, for example, $(\phi(2))_{11} = (Q_{12}\phi_2 Q_{21}Q_{12}Q_{21})_{11}$. The eigenvalue problem for each of these position-space states takes a distinct form, which we label by α_i and $\tilde{\alpha}_i$

$$(\mathcal{H}-E_4)\,|\Psi(p_1,p_2,p_3,p_4)\rangle_{L=5} = \sum_{i=1}^{5}\alpha_i(\phi(i))_{11} + \sum_{i=1}^{5}\tilde{\alpha}_i(\phi(i))_{22} \; . \tag{3.8.47}$$

Here, the distinct eigenvalue expressions correspond to permuted versions of the four-magnon interacting equation. This can be seen by taking the open infinite four-magnon interacting equation (3.4.52) and applying the transformation (3.8.38). After this transformation, the resulting expressions can be rewritten in terms of the wave functions of the $L=5$ closed-chain states,

$$\alpha^c = \left(2\kappa^{-1}-E_4\right)\psi_{11}(0,0,0,1) - \psi_{11}(1,0,0,0) - \psi_{11}(0,0,1,0) \; . \tag{3.8.48}$$

Then, by applying the periodicity condition given in (3.8.36), we reproduce all the eigenvalue equations that arise in (3.8.47). As a consequence of the $\mathbb{Z}_2$ symmetry, the eigenvalue equations transform to their conjugates $\alpha_i \leftrightarrow \tilde{\alpha}_i$. Explicitly, these expressions are given by

$$\alpha_1 = \left(2\kappa^{-1}-E_4\right)\psi_{11}(0,0,0,1) - \psi_{11}(1,0,0,0) - T_\pm(p,\kappa)\psi_{22}(0,0,0,1) = 0 \; , \tag{3.8.49}$$
$$\alpha_2 = (2\kappa-E_4)\,\psi_{11}(1,0,0,0) - \psi_{11}(0,0,0,1) - \psi_{11}(0,1,0,0) = 0 \; , \tag{3.8.50}$$
$$\alpha_3 = \left(2\kappa^{-1}-E_4\right)\psi_{11}(0,1,0,0) - \psi_{11}(1,0,0,0) - \psi_{11}(0,0,1,0) = 0 \; , \tag{3.8.51}$$
$$\alpha_4 = (2\kappa-E_4)\,\psi_{11}(0,0,1,0) - \psi_{11}(0,1,0,0) - \psi_{11}(0,0,0,1) = 0 \; , \tag{3.8.52}$$
$$\alpha_5 = \left(2\kappa^{-1}-E_4\right)\psi_{11}(0,0,0,1) - \psi_{11}(0,0,0,1) - T_\pm(p,\kappa)\psi_{22}(0,0,0,1) = 0 \; . \tag{3.8.53}$$

As an intermediate step, we check whether taking the four distinct wave functions $\psi_{11}(n,m,r,s)$ as unknowns and solving the bulk equations $\{\alpha_2,\alpha_3,\alpha_4\}$ is sufficient to obtain the correct solution. For the $E_4=0$ state we obtain

$$\left(\frac{\psi_{11}(1,0,0,0)}{\psi_{11}(0,0,0,1)},\frac{\psi_{11}(0,1,0,0)}{\psi_{11}(0,0,0,1)},\frac{\psi_{11}(0,0,1,0)}{\psi_{11}(0,0,0,1)}\right) = \left(\kappa^{-1},1,\kappa^{-1}\right) \; , \tag{3.8.54}$$

which agrees with the result obtained from brute-force diagonalization. Since in this check we only solve for the bulk equations, this provides a nontrivial check of our method. The same approach produces the correct result for $E_4 = 2\kappa + 2\kappa^{-1}$ as well.

Remarkably, if we also include the four-magnon interacting equation from the open infinite case, as given in (3.8.48), we find that the tentative solution obtained in (3.8.54) ensures the vanishing of the open infinite expression as well. This observation suggests a deeper connection between the open infinite case and the closed periodic boundary conditions, which we will uncover step by step in the following sections.

Then, by imposing the factorization of the scattering coefficients, (3.4.50) and 2L periodicity relation (3.8.37) we bring all the bulk eigenvalue equations $(\alpha_2, \alpha_3, \alpha_4, \tilde{\alpha}_2, \tilde{\alpha}_3, \tilde{\alpha}_4)$ into a similar form to the special four-magnon interacting equation (3.4.52), for example[26]

$$\begin{aligned}\alpha_2 = \sum_{ijkl\in\mathcal{S}_4} e^{i(2p_j+2p_k+4p_l)}\Bigg(&\frac{e^{-ip_j-ip_k}\left(\kappa^{-1}-\kappa\right)\left(e^{ip_j}-e^{ip_k}\right)\left(1+e^{ip_j+ip_k}\right)^2}{a(p_j,p_k,\kappa)} A_{ijkl} \\ &+ \left(2\kappa - E_4 - e^{-ip_i}a(p_i,p_l,\kappa^{-1})\right) e^{ip_k} D^{1,0,0,0}_{ijkl} - e^{-ip_j+ip_k} D^{0,1,0,0}_{ijkl} \\ &- e^{ip_i+p_k-i\mathcal{P}_4} D^{0,0,0,1}_{ijkl} + e^{-i(p_j+p_k)} a(p_k,p_j,\kappa^{-1}) D^{0,0,1,0}_{ijkl} \Bigg)\,, \end{aligned} \tag{3.8.55}$$

such that scattering coefficients are always accompanied by a factor $\kappa - \kappa^{-1}$. This ensures that the position-dependent corrections vanish at the orbifold point. We also observe that the factor $\left(e^{ip_j}-e^{ip_k}\right)\left(1+e^{ip_j+ip_k}\right)/a(p_j,p_k,\kappa)$ is reminiscent of a solution of position-dependent corrections which satisfies partial factorization (3.4.51). Additionally, we can always solve the linear equations for each permutation label σ separately and obtain a solution of the position-dependent corrections with a common description for each permutation. The analytical solution of these position-dependent corrections is given in the Mathematica file attached to our paper [2] since the expressions are highly complicated and do not offer additional insight beyond the features described here.

Next, we obtain the solution of the relative normalization factor from the boundary eigenvalue equation α_1 given in (3.8.49),

$$T_\pm(p,\kappa) = \frac{\left(2\kappa^{-1}-E_4\right)\psi_{11}(0,0,0,1) - \psi_{11}(1,0,0,0)}{\psi_{22}(0,0,0,1)}\,. \tag{3.8.56}$$

[26]Note that to obtain this particular form of the four-magnon interacting equations α_i we need to use the 2L periodicity equations (3.8.37) and replace the wave functions with their permuted versions if necessary.

While we obtain a different solution from the boundary eigenvalue equation α_5, given in (3.8.53), both results reduce to the same expression under the 2L periodicity conditions. The distinction between the relative normalization factor for the $\mathbb{Z}_2$ even and odd states comes into play when we fix the eigenvalue to specific values.[27] Therefore, by imposing

$$\psi_{11}(0,1,0,0) = \psi_{11}(0,0,0,1) \ , \qquad \psi_{11}(1,0,0,0) = \psi_{11}(0,0,1,0) \ , \tag{3.8.57}$$

together with vanishing total momentum and total energy we can solve for the momentum variables and obtain the spectrum of the model. However, with (3.8.57), we could only match the result of the brute-force diagonalization to 2 digits.[28] To improve the accuracy, we leave one of the equations $\{\alpha^c, \alpha_2, \alpha_3, \alpha_4\}$ out. This leaves us with an undetermined position-dependent correction which we choose to be $D_\sigma^{0,0,0,1}$ without loss of generality. Then we assume that for any permutation σ the undetermined position-dependent correction $D_\sigma^{0,0,0,1}$ is a constant and we solve the periodicity relations, total energy and total momentum conditions to fix the four momenta and $D_\sigma^{0,0,0,1}$. We include an additional relation between the wave functions,

$$\frac{\psi_{11}(1,0,0,0)}{\psi_{11}(0,0,0,1)} = \kappa^{-1} \ , \tag{3.8.60}$$

which is coming from the observation (3.8.54). This way, we obtain the solution of the momentum variables which matches the brute-force diagonalization to 7 digits. Additionally, this solution requires the $D_\sigma^{0,0,0,1}$ to be $0.0852016 - 0.103424i$ which effectively sets the wave function $\psi_{11}(0,0,0,1)$ to be a CBA-like solution shifted by a constant scattering coefficient. The results for two distinct values of κ and both twisted and untwisted states of $L = 5$, normalized such that $\psi_{11}(0,0,0,1) = 1$, are given in Table 3.3. The solution of the momentum variables for $E_4 = 0$ and $\kappa = 0.7$ is given as

$$\{p_1 = 0.327198 - 2.38999i \ , \ \ p_2 = -3.05876 + 0.639858i \ , \ \ p_3 = 1.90333 + 1.128i\} \ , \tag{3.8.61}$$

[27] In the case of $L = 5$, zero energy ($E_4 = 0$) gives the $\mathbb{Z}_2$ even state and $E_4 = 2\kappa + 2\kappa^{-1}$ gives the $\mathbb{Z}_2$ odd state.

[28] Note that we compute the relative error by

$$\text{Relative Error} = \left| \frac{x_{\text{numerical}} - x_{\text{analytical}}}{x_{\text{analytical}}} \right| \ , \tag{3.8.58}$$

then one can compute the number of significant digits as

$$\text{Correct Digits} \approx -\log_{10}\left(\text{Relative Error}\right) \ . \tag{3.8.59}$$

E_4	κ	$\psi_{11}(0,0,0,1)$	$\psi_{11}(1,0,0,0)$	$\psi_{11}(0,1,0,0)$	$\psi_{11}(0,0,1,0)$	$T\psi_{22}(0,0,0,1)$
0	0.7	1.	1.42857	1.	1.42857	1.
0	0.4	1.	2.5	1.	2.5	1.
$2\kappa+2\kappa^{-1}$	0.7	1.	-0.7	1.	-0.7	1.
$2\kappa+2\kappa^{-1}$	0.4	1.	-0.4	1.	-0.4	1.

Table 3.3: *Numerical Solution for the periodicity relations between the position states.*

while for $E_4 = 2\kappa + 2\kappa^{-1}$, it is given as,

$$\{p_1 = -1.36434\, i\ , p_2 = 3.14159\ - 0.176988i, p_3 = 1.35999i\}\ , \tag{3.8.62}$$

in this case, we obtain the relative normalization factor from $T\psi_{22}(2,3,4,5)$, while the rest of the wave functions can be calculated by using $\mathbb{Z}_2$ conjugation. The exact result coming from the brute-force diagonalization for the $E_4 = 0$ untwisted state is

$$\begin{aligned}|\Psi(p_1,p_2,p_3,p_4)\rangle_{L=5,+} = &\big(\phi(1)\big)_{11} + \kappa^{-1}\big(\phi(2)\big)_{11} + \big(\phi(3)\big)_{11} + \kappa^{-1}\big(\phi(4)\big)_{11} + \big(\phi(5)\big)_{11}\\ &+ \kappa^{-1}\big(\phi(1)\big)_{22} + \big(\phi(2)\big)_{22} + \kappa^{-1}\big(\phi(3)\big)_{22} + \big(\phi(4)\big)_{22} + \kappa^{-1}\big(\phi(5)\big)_{22}\ ,\end{aligned} \tag{3.8.63}$$

and for $\kappa = 0.7$, $\kappa^{-1} \approx 1.42857$ which is the result we obtain from the numerical solution. Similarly, the eigenstate for the eigenvalue $E_4 = 2\kappa + 2\kappa^{-1}$ is the twisted state of $L = 5$ and it is given as

$$\begin{aligned}|\Psi(p_1,p_2,p_3,p_4)\rangle_{L=5,-} = &\big(\phi(1)\big)_{11} - \kappa\big(\phi(2)\big)_{11} + \big(\phi(3)\big)_{11} - \kappa\big(\phi(4)\big)_{11} + \big(\phi(5)\big)_{11}\\ &- \kappa\big(\phi(1)\big)_{22} + \big(\phi(2)\big)_{22} - \kappa\big(\phi(3)\big)_{22} + \big(\phi(4)\big)_{22} - \kappa\big(\phi(5)\big)_{22}\ .\end{aligned} \tag{3.8.64}$$

These two states are the only states that correspond to single-trace operators for $L = 5$, and we obtain them using the long-range Bethe ansatz and this computation can be performed for any $0 < \kappa < 1$. However, solving the periodic boundary conditions within this framework is methodologically demanding and not readily tractable. A key source of this complexity is the necessity of working with momentum variables instead of rapidities, which leads to highly intricate wave function expressions. Nevertheless, this solution shows that the long-range Bethe ansatz is compatible with the periodic boundary conditions and it gives the spectrum of the Hamiltonian. We perform the same method for $L = 6$ to gain more insight into the problem.

***L* = 6.** We compute the eigenvectors of the $L = 6$ closed spin chains by applying the method we outlined for $L = 5$. The momentum states for the $L = 6$ spin chains take the form as expected,

$$|\Psi(p_1,p_2,p_3,p_4)\rangle_{L=6,\pm} = \big(\Psi(p_1,p_2,p_3,p_4)\big)_{11} + T_\pm(p_1,p_2,p_3,p_4,\kappa)\big(\Psi(p_1,p_2,p_3,p_4)\big)_{22} \tag{3.8.65}$$

such that there are fifteen distinct position states for each color index, denoted as

$$\big(\Psi(p_1,p_2,p_3,p_4)\big)_{11} = \sum_{n,m,r=0}^{2} \psi_{11}(\vec{p},n,m,r,2-n-m-r)\big(\phi(i)\phi(j)\big)_{11} \,. \tag{3.8.66}$$

The eigenvalue problem brings variations of four-magnon interacting equations (3.4.52),

$$(\mathcal{H}-E_4)\,|\Psi(p_1,p_2,p_3,p_4)\rangle_{L=6} = \sum_{i=1}^{15} \alpha_{ij}\big(\phi(i)\phi(j)\big)_{11} + \sum_{i=1}^{15} \tilde{\alpha}_{ij}\big(\phi(i)\phi(j)\big)_{22} \,. \tag{3.8.67}$$

As in the $L=5$ case, we use the short-hand notation, $\big(\phi(i)\phi(j)\big)_{11}$ to refer to the length-six position state which is characterized by the ϕ_i state in the ith and jth positions. Depending on the configuration of the ϕ fields, the eigenvalue equations are a variation of the four-magnon interaction (above symbolically we denoted all with α_{ij}), the three-magnon interaction or the two two-magnon interacting equations. We refer to the states that have different types of fields at the beginning and the end of the spin chain state as *boundary eigenvalue equations*, and these are

$$\{\alpha_{12},\alpha_{56},\beta_{13},\beta_{46},\beta_{15},\beta_{26},\gamma_{14},\gamma_{36}\}\,, \tag{3.8.68}$$

while the *bulk eigenvalue equations* are listed as

$$\{\alpha_{16},\alpha_{23},\alpha_{34},\alpha_{45},\beta_{24},\beta_{35},\gamma_{25}\}\,. \tag{3.8.69}$$

In addition to these equations, we also use the eigenvalue equations coming from the open infinite states which we transform under the map (3.8.38) which are listed as

$$\{\alpha^c,\beta^c_l(1),\beta^c_r(1),\gamma^c_{rl}(1)\}\,. \tag{3.8.70}$$

First, we observe that two of the distinct eigenvalue equations match,

$$\alpha_{16} = \alpha^c\,, \tag{3.8.71}$$

which supports the expectation that, as we increase the length of the periodic chain, the closed finite and open infinite problems look more and more alike, and the special solution given in Section 3.4.2 becomes more relevant. Then, we combine the bulk eigenvalue equations with the open infinite eigenvalue equations and bring all of them to a form similar to (3.8.55), which means that the scattering coefficients for each permutation are accompanied by a factor of $\kappa - \kappa^{-1}$ and $\omega(p_{\sigma(2)}, p_{\sigma(3)})$ as defined in (3.4.53). To achieve this form we used the 2L periodicity relations (3.8.37) when it is necessary. This way, we obtain as many equations as the number of distinct position-dependent corrections,

$$\{\alpha_{16} = \alpha^c, \alpha_{23}, \alpha_{34}, \alpha_{45}, \beta_{24}, \beta_{35}, \gamma_{25}, \beta^c_l(1), \beta^c_r(1), \gamma^c_{rl}(1)\} \; . \tag{3.8.72}$$

First, to check that this set of equations is indeed compatible with the brute-force diagonalization, we solve the linear set of equations generated by these equations by taking the wave functions as unknowns. Then, for $E_4 = 0$, normalised such that $\psi_{11}(0,0,0,2) = 1$, we obtain,

$$\begin{aligned}&\{\psi_{11}(0,0,1,1), \psi_{11}(0,0,2,0), \psi_{11}(0,1,0,1), \psi_{11}(0,1,1,0), \psi_{11}(0,2,0,0), \psi_{11}(1,0,0,1),\\ &\psi_{11}(1,0,1,0), \psi_{11}(1,1,0,0), \psi_{11}(2,0,0,0), \psi_{11}(0,0,0,2), \psi_{11}(0,0,1,1), \psi_{11}(0,1,0,1),\\ &\qquad\qquad \psi_{11}(1,0,0,1)\} = \left\{\frac{1}{\kappa}, \frac{1}{\kappa^2}, 1, \frac{1}{\kappa}, 1, \frac{1}{\kappa}, \frac{1}{\kappa^2}, \frac{1}{\kappa}, \frac{1}{\kappa^2}, 1, \frac{1}{\kappa}, 1, \frac{1}{\kappa}\right\} \; .\end{aligned} \tag{3.8.73}$$

This perfectly agrees with the brute-force diagonalization. We solve for the distinct position-dependent corrections as a function of momenta and κ.[29] Therefore, we obtain the analytic description of the position-dependent corrections and they exhibit the same properties as the special function and the $L = 5$ solution. Finally, we impose the 2L periodicity conditions,

$$\psi_{11}(0,0,0,2) = \psi_{11}(0,2,0,0) \; , \qquad \psi_{11}(0,0,2,0) = \psi_{11}(2,0,0,0) \; , \tag{3.8.74}$$

$$\psi_{11}(1,1,0,0) = \psi_{11}(0,0,1,1) \; , \qquad \psi_{11}(0,1,1,0) = \psi_{11}(1,0,0,1) \; . \tag{3.8.75}$$

Together with the $E_4 = 0$ condition and the vanishing total momentum condition, we obtain the solution

$$\{p_1 = -0.0218877i, p_2 = 0.501353i \; , p_3 = -0.501353i \; , p_4 = 0.0218877i \; \} \tag{3.8.76}$$

which correctly matches the brute-force diagonalization with a relative error of 0.05. The same can be done for the twisted state with $E_4 = 2\kappa + \frac{2}{\kappa}$. We think it is possible to

[29] In order to reduce the complexity of the analytic part of the computation, we transform the position-dependent corrections to scaled position-dependent corrections as given in (3.4.12) and also impose the partial factorization (3.4.51) from the beginning. Note that due to the extra factors of $\omega(p_{\sigma(2)}, p_{\sigma(3)})$ we deduce that the partial factorization is manifest in the solution even if we do not impose it by hand. However, imposing it from the beginning of the analytical computation simplifies the expressions drastically and both the scaling of the position-dependent corrections and the partial factorization condition prove to be computationally useful for closed finite spin chains.

improve the numerics further by following the same technique as $L = 5$ and choosing to prioritize what we learn from (3.8.73). However, we postpone this to future work and hope to gain a deeper understanding of the parameter space before attempting to solve this problem analytically. For now, we take this as a proof of concept for long-range Bethe ansatz and move on to discover the connection between the solutions of various numbers of excitations.

Chapter 4

Conformal Field Theory at Finite Temperature

In this chapter, we study conformal field theories placed on a d-dimensional cylinder. As explained via the Matsubara formalism in Section 2.3.1, such backgrounds naturally correspond to CFTs at finite temperature. From the perspective of the conformal bootstrap where a CFT is defined non-perturbatively by its CFT data (2.2.26), this setting is considered to answer a natural and intriguing question: how does the CFT data depend on the underlying d-dimensional geometry? More specifically, can one formulate and solve bootstrap consistency conditions for CFTs defined on manifolds other than flat d-dimensional space-time? Another motivation, closely related to the main theme of this thesis, is to generalize the bootstrap techniques developed for CFTs on flat space which rely heavily on the highly restrictive nature of conformal symmetry to systems with reduced symmetry.

The CFT on $S^1_\beta \times \mathbb{R}^{d-1}$ has several novel features compared to the flat space case and we then proceed to develop an analytic bootstrap framework. We focus on the analytic structure of thermal correlators and derive the associated dispersion relation, which forms the basis of the analytic bootstrap approach. We further uncover a remarkable connection between this dispersion relation and the momentum space OPE. We subsequently apply this formalism to holographic setups, highlighting several striking ways in which holographic theories deviate from their non-holographic counterparts. There, we discuss the implications of the presence of a black brane or a black hole in the dual gravitational EFT. Finally, we turn to the three-dimensional Ising model, where we formulate a numerical bootstrap framework and explore the interplay between numerical and analytic bootstrap approaches. This chapter is primarily based on the work [3, 4].

4.1 Turning on the Temperature

When a CFT is placed on $S^1_\beta \times \mathbb{R}^{d-1}$, a scale is introduced through the circumference of the thermal circle, β, and a substantial part of the conformal symmetry (as given in (2.2.16)) is explicitly broken. While an $SO(d-1)$ rotational symmetry in the non-compact directions and the discrete symmetry $\tau \to -\tau$ along the thermal circle remain intact, dilatations and special conformal transformations are no longer preserved. As a consequence, CFT operators other than the identity may acquire nontrivial one-point functions.[1]

According to the spectral decomposition given in (2.3.6), these new one-point functions can in principle be determined by the zero temperature data by using the thermal density matrix $\rho = e^{-\beta H}$,

$$\langle \mathcal{O}_1(x_1)\rangle_\beta = \frac{\sum_\alpha \langle \varepsilon_\alpha | e^{-\beta\varepsilon_\alpha} \mathcal{O}_1(x_1) | \varepsilon_\alpha\rangle}{\sum_\alpha \langle \varepsilon_\alpha | e^{-\beta\varepsilon_\alpha} | \varepsilon_\alpha\rangle} \; . \tag{4.1.1}$$

However, in practice it is extremely hard to know the entire spectrum and determine the one-point functions from the weighted sum over the three point-functions. Therefore, we remain agnostic to these relations and consider the thermal one-point functions as an addition to the CFT-data that needs to be determined.

Since these one-point functions are still constrained by the residual symmetries of the CFT on the cylinder, translation invariance along both the compact and non-compact directions implies that they cannot depend on spacetime coordinates. In particular,

$$\langle P^\mu \mathcal{O}^{\mu_1\cdots\mu_J}(\tau, x)\rangle_\beta = \partial^\mu \langle \mathcal{O}^{\mu_1\cdots\mu_J}(0,0)\rangle_\beta = 0 \; . \tag{4.1.2}$$

Moreover, invariance under $SO(d-1) \oplus \mathbb{Z}_2 \simeq O(d-1)$ implies that only symmetric traceless operators with even spin J can acquire non-trivial one-point functions. Consequently, we are left with

$$\langle \mathcal{O}^{\mu_1\cdots\mu_J}(\tau, x)\rangle_\beta = \frac{b_\mathcal{O}}{\beta^{\Delta_\mathcal{O}}} \left(e^{\mu_1} \cdots e^{\mu_J} - \text{traces}\right) \; , \tag{4.1.3}$$

where $\Delta_\mathcal{O}$ is the scaling dimension of the operator $\mathcal{O}$, e^μ denotes the unit vector along the compact direction, and $b_\mathcal{O}$ is a constant.

Combining this result with the OPE (2.2.23) of two identical scalar operators, we obtain

$$\langle \phi(\vec{x})\phi(0)\rangle_\beta = \sum_{\mathcal{O}\in\phi\times\phi} \frac{f_{\phi\phi\mathcal{O}}}{c_\mathcal{O}} |\vec{x}|^{\Delta_\mathcal{O} - 2\Delta_\phi - J} x_{\mu_1} \cdots x_{\mu_J} \langle \mathcal{O}^{\mu_1\cdots\mu_J}\rangle_\beta \; , \tag{4.1.4}$$

[1] At zero temperature, only the identity operator acquires a non-trivial one-point function whose contribution can be seen in (2.2.24).

$$= \sum_{\mathcal{O}\in\phi\times\phi} \frac{a_{\mathcal{O}}}{\beta^{\Delta_{\mathcal{O}}}} |\vec{x}|^{\Delta_{\mathcal{O}}-2\Delta_\phi} C_J^{(\nu)}\left(\frac{\tau}{|\vec{x}|}\right) , \tag{4.1.5}$$

where we have defined

$$a_{\mathcal{O}} = \frac{f_{\phi\phi\mathcal{O}}\, b_{\mathcal{O}}}{c_{\mathcal{O}}} , \tag{4.1.6}$$

and $C_J^{(\nu)}$ are Gegenbauer polynomials with $\nu = \frac{d-2}{2}$. Crucially, on the d-dimensional cylinder the OPE converges only for $|\vec{x}| < \beta$. This restriction follows from the ultraviolet divergence of correlation functions when the two operators coincide, together with the periodicity of thermal correlators along the compact direction,

$$\langle \phi(\tau, r)\phi(0)\rangle_\beta = \langle \phi(\tau + \beta, r)\phi(0)\rangle_\beta , \tag{4.1.7}$$

which is known as the KMS relation as it was given in (2.3.9). Here we have defined $|\vec{x}|^2 - \tau^2 = r^2$ and used the $SO(d-1)$ symmetry to express the correlator solely in terms of τ and r. In addition, thermal correlators obey a reflection property along the compact direction,

$$\langle \phi(\tau, r)\phi(0)\rangle_\beta = \langle \phi(-\tau, r)\phi(0)\rangle_\beta , \tag{4.1.8}$$

which holds independently of whether the CFT is parity invariant under $\vec{x} \to -\vec{x}$. Combining the invariance under reflection with the KMS condition leads to a fundamental set of sum rules for CFTs at finite temperature [146, 147]. In particular, these two properties imply

$$\langle \phi\big(\tfrac{\beta}{2} + \tau, r\big)\, \phi(0)\rangle_\beta = \langle \phi\big(\tfrac{\beta}{2} - \tau, r\big)\, \phi(0)\rangle_\beta . \tag{4.1.9}$$

This relation shows that, at the KMS-invariant point $\tau = \frac{\beta}{2}$, all odd derivatives of the correlator with respect to τ must vanish. More precisely,

$$\frac{\partial^{2l+1}}{\partial\tau^{2l+1}} \frac{\partial^n}{\partial r^n} \langle \phi(\tau, r)\phi(0)\rangle_\beta \bigg|_{\tau=\frac{\beta}{2},\, r=0} = 0 , \qquad \text{for all } l, n \in \mathbb{N} . \tag{4.1.10}$$

These conditions can be interpreted as an infinite system of linear equations for the thermal one-point functions, obtained by inserting the zero-temperature CFT data (2.2.26). These sum rules were first derived in [146] and subsequently applied in [147–149] to extract OPE coefficients in various contexts. In Section 4.4, we will study these relations in detail and further develop them, as they constitute one of the two main approaches used in this thesis to determine OPE coefficients at finite temperature.

Note that the two-point function in (4.1.5) simplifies dramatically in the limit $r = 0$,

$$\langle \phi(\tau)\phi(0)\rangle_\beta = \frac{1}{\tau^{2\Delta_\phi}} \sum_{\Delta} a_\Delta \left(\frac{\tau}{\beta}\right)^{\Delta} , \qquad a_\Delta = \sum_{\mathcal{O}:\, \Delta_{\mathcal{O}}=\Delta} a_{\mathcal{O}}\, C_J^{(\nu)}(1) . \tag{4.1.11}$$

However, in this limit the dependence on the spin quantum numbers is lost. When several operators share the same scaling dimension but carry different spins, the coefficient a_Δ becomes degenerate. This situation frequently arises in perturbative regimes or in highly symmetric models.

By contrast, in strongly interacting theories, where little or no degeneracy is typically present, the $r = 0$ limit is often sufficient to extract a substantial amount of finite-temperature data.

4.1.1 Hamiltonian Formalism

Up to now, we have introduced the thermal correlators without committing to a particular quantization. Following the approach introduced in Section 2.2.2, we mainly consider quantization on $\mathbb{R}^{d-1}$ slices and interpret the S^1 factor as the Euclidean time direction. This point of view is valid for $|x| < \beta$ and leads to the operator product expansion representation given in (4.1.5).

Within this framework, one can define the Hamiltonian and momentum operators by analyzing the broken Ward identities associated with dilatations and boosts [150]. Since treating a compact direction as time explicitly breaks dilatation and boost symmetries, the resulting action of the dilatation operator becomes equivalent to time translations. In particular, the Hamiltonian is given by

$$\mathbf{H} = -\frac{1}{\beta}\mathbf{D} - E_0 \ , \tag{4.1.12}$$

where E_0 denotes a non-trivial Casimir energy. Starting from this interpretation, one can derive the operatorial expressions for the Hamiltonian and momentum operators,

$$H = -\int_{\mathbb{R}^{d-1}} d^{d-1}x \left(T^{00}(\vec{x}) + \frac{d-1}{d}\frac{b_T}{\beta^d} \right) \ , \qquad P^i = i\int_{\mathbb{R}^{d-1}} d^{d-1}x \, T^{0i}(\vec{x}) \ , \tag{4.1.13}$$

where $\vec{x} = (\tau, x^1, \ldots, x^{d-1})$, and the thermal expectation value of the energy density is given by

$$\langle T^{00} \rangle_\beta = \frac{d-1}{d}\frac{b_T}{\beta^d} \ . \tag{4.1.14}$$

Additionally, the Hamiltonian can be interpreted as the Hamiltonian of the $(d-1)$ dimensional interacting QFT [146, 151]. From this perspective the thermal mass of the CFT at finite temperature,

$$\langle \phi(\tau, r)\phi(0,0) \rangle_\beta = \langle \phi(0)^2 \rangle_\beta + O(e^{-m_{\text{th}} r}) \tag{4.1.15}$$

is directly related to the mass gap of the $(d-1)$-dimensional theory by using the operators defined in (4.1.13),

$$\langle\phi(\tau,r)\phi(0,0)\rangle_\beta = \langle 0|\phi(0)e^{i\tau H - rP^1}\phi(0)|0\rangle \ , \tag{4.1.16}$$

where we used the $(d-1)$-dimensional rotational symmetry and $|0\rangle = |0\rangle_{\mathbb{R}^{d-1}}$ is the ground state in the radial quantization. Combining this expression with the definition (4.1.15), we conclude that the thermal mass is given by the lowest eigenvalue of the momentum operator.

This primary perspective can be related to a secondary point of view coming from the radial quantization of the flat space given in (2.2.20), by compactifying the time direction $\mathbb{R}$ and obtaining $S^1\times S^{d-1}$ then taking the radius of the $(d-1)$ dimensional sphere to infinity [146]. However, it is very hard to perform computations in this setting, therefore we omit discussing this setup until Section 4.3.5.

Another alternative description is obtained by quantizing the theory on $S^1\times\mathbb{R}^{d-2}$ slices and taking $\mathbb{R}$ as the time direction. This third point of view is closely connected to the second one. In this picture, the states live on $(d-1)$-dimensional slices, with one direction compactified. In the Kaluza–Klein (KK) compactification formalism, the momentum generator in the S^1 direction, P_{KK}, becomes a global $U(1)$ symmetry with a discrete spectrum. One can then define the momentum and Hamiltonian operators as

$$H_{KK} = \int_0^\beta d\tau \int_{\mathbb{R}^{d-2}} d^{d-2}x \left(-T^{11}(\vec{x}) - \frac{b_T}{d}\frac{1}{\beta^d}\right) \tag{4.1.17}$$

$$P_{KK} = \int_0^\beta d\tau \int_{\mathbb{R}^{d-2}} d^{d-2}x \left(-iT^{10}(\vec{x})\right) \ . \tag{4.1.18}$$

We can easily compare these operators to those given in (4.1.13). Moreover, since these charges are conserved, they can be used to define the correlator at any point on the d-dimensional cylinder. This is precisely why they provide an alternative formulation of thermal correlation functions away from the OPE convergence regime.

Explicitly, for any $\vec{x} = (\tau, x^1, \cdots, x^d)$, we may use the $SO(d-1)$ rotational invariance to restrict to $\vec{x}' = (\tau, x^1, 0, \cdots, 0)$ and describe the correlator

$$\langle\phi(\vec{x}'), \phi(0)\rangle_\beta = \langle 0|\phi(0)e^{-H_{KK}x^1 + i\tau P_{KK}}\phi(0)|0\rangle \tag{4.1.19}$$

such that $|0\rangle = |0\rangle_{S^1\times\mathbb{R}^{d-2}}$ is the ground state. Similar to the expression given in (4.1.16), H_{KK} is Hermitian and bounded from below, and its appearance leads to an exponential suppression at large distances which is quantified by thermal mass (4.1.15).

We will return to the KK formulation of thermal correlators when analyzing the analytic structure of the thermal correlator across the entire d-dimensional cylinder. Before discussing the different bootstrap frameworks in detail, it is important to introduce two toy models that can be solved exactly. These models will therefore serve as testing grounds for the various bootstrap approaches.

4.1.2 Interlude on Generalized Free Fields

The simplest theory we can put on a d-dimensional cylinder is the generalized free scalar theory. This theory features a fundamental scalar field ϕ of scaling dimension Δ_ϕ, satisfying the equation of motion

$$\Box^{\frac{d}{2}-\Delta_\phi}\,\phi = 0. \tag{4.1.20}$$

The theory is non-local unless $\Delta_\phi = d/2-1$, which corresponds to the standard free scalar field theory. The OPE expansion of two fundamental fields can be schematically represented as follows

$$\phi \times \phi = \mathbb{1} + [\phi\phi]_{n,J}\ , \tag{4.1.21}$$

where $[\phi\phi]_{n,J}$ denotes the double-twist operators, of the form $\phi\Box^n\partial_{\mu_1}\cdots\partial_{\mu_J}\phi$, with conformal dimension $\Delta = 2\Delta_\phi + 2n + J$.

This theory is one of the few exactly solvable models at finite temperature and it is well studied for any spacetime dimension [146, 152] thanks to the possibility to employ the method of images. Since it is non-interacting, the thermal two-point function is given by the method of images over the free propagator:

$$g_{\text{GFF}}(\tau, x) = \langle\phi(\tau, x)\phi(0,0)\rangle_\beta = \sum_{m=-\infty}^{\infty} \frac{1}{[(\tau+m)^2 + x^2]^{\Delta_\phi}}\ . \tag{4.1.22}$$

When restricted to zero spatial coordinates this infinite sum can be recognized as a linear combination of Hurwitz ζ-functions[2],

$$g_{\text{GFF}}(\tau) = \sum_{m=-\infty}^{\infty} \frac{1}{|\tau+m|^{2\Delta_\phi}} = \zeta_H(2\Delta_\phi, \tau) + \zeta_H(2\Delta_\phi, 1-\tau)\ . \tag{4.1.24}$$

[2]The Hurwitz ζ-function is defined as

$$\zeta_H(s,a) = \sum_{n=0}^{\infty} \frac{1}{(n+a)^s}\ . \tag{4.1.23}$$

More concretly, let us consider the GFF theory with $\Delta_\phi = 1$,

$$\langle \phi(\tau)\phi(0)\rangle_\beta = \frac{\pi^2}{\beta^2}\csc^2\left(\frac{\pi\tau}{\beta}\right) \ . \tag{4.1.25}$$

This two-point function is particularly interesting since it also corresponds to the two-point functions of a four-dimensional fundamental free scalar $\varphi_{\rm 4d}$

$$\langle \phi(\tau)\phi(0)\rangle_\beta = \lim_{r\to 0}\langle \varphi_{\rm 4d}(\tau, r)\varphi_{\rm 4d}(0,0)\rangle_\beta \ . \tag{4.1.26}$$

The two-point function (4.1.25) also corresponds to the restriction to $r = 0$ of the energy-energy two-point function $\langle \epsilon(\tau, r)\epsilon(0,0)\rangle_\beta$ in the critical two-dimensional Ising model

$$\langle \phi(\tau)\phi(0)\rangle_\beta = \lim_{r\to 0}\langle \epsilon(\tau, r)\epsilon(0,0)\rangle_\beta \ . \tag{4.1.27}$$

Another special case is given by the GFF with $\Delta_\phi = 2$. In this scenario, the two-point function reduces to

$$\langle \phi(\tau)\phi(0)\rangle_\beta = \frac{\pi^4}{3\beta^4}\left(2 + \cos\left(\frac{2\pi\tau}{\beta}\right)\right)\csc^4\left(\frac{\pi}{\beta}\tau\right) \ . \tag{4.1.28}$$

Similarly to the previous example, this case can also be interpreted as the restriction of the two-point function of a six-dimensional fundamental free scalar $\varphi_{\rm 6d}$,

$$\begin{aligned}\langle \varphi_{\rm 6d}(\tau, r)\varphi_{\rm 6d}(0)\rangle_\beta = \frac{\pi}{4\beta^2 r^3}\Bigg[\beta\coth\left(\frac{\pi(r - i\tau)}{\beta}\right) + \beta\coth\left(\frac{\pi(r + i\tau)}{\beta}\right) + \\ \pi r\ \mathrm{csch}^2\left(\frac{\pi(r - i\tau)}{\beta}\right) + \pi r\ \mathrm{csch}^2\left(\frac{\pi(r + i\tau)}{\beta}\right)\Bigg] \ .\end{aligned} \tag{4.1.29}$$

These particular examples and GFF theories in general represent an optimal playground to test the equation (4.1.9) and its various different formulations since the OPE coefficients a_Δ can be easily extracted from the exact solution (4.1.22). It will be also the base of the analytic bootstrap framework we will develop in Section 4.2.

4.1.3 Interlude on $2d$ CFTs on Cylinder

It is particularly instructive to test our finite temperature bootstrap methods in the case of Virasoro primaries in two spacetime dimensions. In two dimensions, the two-point functions of identical Virasoro primaries can be computed exactly as a consequence of the conformal map between the plane and the cylinder because the conformal symmetry remains unbroken. For this reason, two-dimensional CFTs provide an ideal setting to test our finite-temperature bootstrap methods and verify their consistency.

Moreover, since the conformal map is anomalous, the only non-vanishing thermal one-point functions arise from operators in the Virasoro vacuum module, which are sensitive to conformal anomalies. In particular, for a primary operator of conformal weights $(h, \bar{h})$, we have

$$\langle\phi(\tau, r)\phi(0,0)\rangle_\beta = \left(\frac{\pi}{\beta}\right)^{h+\bar{h}} \csc^h\left(\frac{\pi}{\beta}(\tau + ir)\right) \csc^{\bar{h}}\left(\frac{\pi}{\beta}(\tau - ir)\right) . \tag{4.1.30}$$

We then simplify the setup by considering the case of a scalar primary such that $h = \bar{h} = \Delta_\phi/2$. The operators that contribute to the OPE of this correlator are such that $\Delta \geq J$, with $\Delta \in 2\mathbb{N}$ and $J \in 2\mathbb{N}$. In the following, for simplicity, we focus on the cases in which $\Delta_\phi = 1$.

It is useful to notice that the thermal blocks defined in general dimension in (4.1.5) are not well-defined for $d = 2$. This is due to the fact that the OPE coefficients contain a factor $\Gamma(\nu)$, which is diverging when $\nu = 0$, i.e., $d = 2$. On the other hand, the blocks contain the Gegenbauer polynomial $C_J^{(0)}(\eta)$ which is zero and compensates the infinity of the OPE coefficient. Therefore, it is convenient to redefine the blocks and OPE coefficients such that

$$\tilde{f}_{\Delta,J}(\tau, r) = \lim_{\nu\to 0} \frac{J!}{(\nu)_J}(\tau + ir)^{\frac{\Delta}{2}-\Delta_\phi}(\tau - ir)^{\frac{\Delta}{2}-\Delta_\phi} C_J^{(\nu)}\left(\frac{\tau}{\sqrt{\tau^2 + r^2}}\right) , \tag{4.1.31}$$

and

$$a_{\mathcal{O}} = \frac{f_{\phi\phi\mathcal{O}} b_{\mathcal{O}}}{2^J c_{\mathcal{O}}} . \tag{4.1.32}$$

By using this OPE we can extract the OPE coefficients from the thermal correlator given in (4.1.30). For example, for $\Delta_\phi = 1$, we obtain the OPE coefficients,

$$a_J = -2^{J+1}\mathrm{Li}_J(-1) . \tag{4.1.33}$$

Equipped with the basic understanding of the finite temperature correlators and two essential examples of such theories we move on to develop an analytic bootstrap framework to compute one-point functions that arise with temperature.

4.2 Analytic Structure and Setting up the Analytic Bootstrap

In this section, we establish an analytic bootstrap framework for CFTs at finite temperature. Throughout, we focus on the two-point function of identical scalar operators and exploit the analytic structure of this correlator. To investigate the analyticity properties of the thermal correlator, we begin by denoting the finite-temperature two-point function of identical scalars as

$$g(\tau, x) = \langle \phi(\tau, x)\phi(0,0)\rangle_\beta \ , \tag{4.2.1}$$

where we use the shorthand notation $x = |\vec{x}|$ for the spatial dependence. An important part of this work focuses on the study of these correlators at zero spatial coordinates as given in (4.1.11), in which case we write

$$g(\tau) = g(\tau, 0) \ . \tag{4.2.2}$$

When the spatial dependence is preserved, it is convenient to use the variables

$$z = \tau + ix \, , \qquad \bar{z} = \tau - ix \, . \tag{4.2.3}$$

For compactness, we often write $g(z,\bar{z}) = g(\tau, x)$ similar to the parametrization used for the zero temperature four-point function given in (2.2.27) and the parameters in (2.2.33). In the same spirit, another useful change of variables is given by

$$r^2 = z\bar{z} \ , \qquad w^2 = \frac{z}{\bar{z}} \ . \tag{4.2.4}$$

Both sets of variables are frequent in the literature and reminiscent of four-point functions at zero temperature. In the $z, \bar{z}$ parametrization, OPE given in (4.1.5) can be written as

$$g(z,\bar{z}) = \sum_{\mathcal{O}} a_{\mathcal{O}} \, f_{\Delta,J}(z,\bar{z}) \, , \tag{4.2.5}$$

where the regime of convergence is $\sqrt{z\bar{z}} = \sqrt{\tau^2 + \vec{x}^2} < \beta$. The thermal blocks $f_{\Delta,J}(z,\bar{z})$ which are explicitly given in (4.1.5) are the leading contribution of the conformal blocks at zero temperature (2.2.32) under the heavy-heavy-light-light limit. This limit is obtained by taking two out of four external scalar operators to have large scaling dimensions compared to the other two and it is related to the Eigenstate Thermalization Hypothesis (ETH) introduced in [153]. Later on we discuss this point of view in more detail in the context of holography in Section 4.3.

For the rest of this section, we set $\beta = 1$ without loss of generality. Then we can rewrite the periodicity condition as stated in (4.1.9) in terms of the complex coordinates (4.2.3),

$$g(z,\bar{z}) = g(1-\bar{z}, 1-z) \, . \tag{4.2.6}$$

Each side of this equation can be expanded into thermal blocks following (4.2.5). In the following, we call the left-hand side the *s-channel* and the right-hand side *t-channel*, by analogy to crossing symmetry at zero temperature as depicted in (2.2.34). The strength of the KMS relation is that it holds outside of the OPE regime, and using it to reconstruct full correlators is the main goal of the thermal bootstrap program.

Note also that as a result of the reflection positivity and the hermiticity, the correlator at finite temperature is *real*, which results in the relations

$$g(z,\bar{z}) = g(\bar{z},z) \quad \longleftrightarrow \quad g(r,w) = g(r,w^{-1})\,, \tag{4.2.7}$$

and that *discrete symmetry* imposes

$$g(z,\bar{z}) = g(-z,-\bar{z}) \quad \longleftrightarrow \quad g(r,w) = g(r,-w)\,. \tag{4.2.8}$$

Beyond the basic properties of the thermal correlator listed above, there exists a set of bootstrap axioms that will serve as our guiding principles. In deriving the dispersion relations, we will assume throughout that these consistency conditions are satisfied. After obtaining the dispersion relations for the cases $r = 0$ and $r \neq 0$, we will return to these assumptions and explicitly verify their validity. An important question is whether these conditions are also satisfied by holographic correlators; this issue will be addressed in Section 4.3.

Consistency conditions. In order to reconstruct the full correlator including the out of OPE regime we can use the following conditions:

1. *KMS condition.* A fundamental property of thermal two-point functions is the KMS condition (4.2.6).

2. *Analytic structure.* The analytic structure of thermal two-point functions must match the ones described in Section 4.2.1 and 4.2.2 and illustrated in Figure 4.1 and Figure 4.2. In particular, the arc terms must have vanishing discontinuity.

3. *Consistency with the OPE.* The thermal two-point function must be consistent with the operator product expansion as given in (4.1.5). The dispersion relation is expected to reproduce the correct OPE spectrum up to low-spin operators, which would then be encoded in g_{arcs}. Additionally, g_{arcs} can include low spin corrections to the OPE coefficients of all operators.

4. *Regge boundedness.* In the variables (r, w), the thermal two-point function is expected to be *polynomially* bounded in the Regge limit

$$g(r,w) \leq w^{J_0} \quad \text{as} \quad w \to \infty\,, \quad r \text{ fixed.} \tag{4.2.9}$$

Here, J_0 is expected to be the low spin cutoff for the arc contributions.

5. *Clustering at large distances.* At large spatial separation, the two-point function must satisfy the clustering condition which was introduced in (4.1.15),

$$g(z,\bar{z}) \xrightarrow{x\to\infty} \langle\phi\rangle_\beta^2. \tag{4.2.10}$$

In general, for theories without an enhanced symmetry structure,[3] the expected behavior is an exponential decay as given in (4.1.15),

$$g(z,\bar{z}) \xrightarrow{(z,\bar{z})\to(i\infty,-i\infty)} \langle\phi\rangle_\beta^2 + O(e^{im_{\text{th}}(z-\bar{z})}), \tag{4.2.11}$$

where $m_{\text{th}} \propto 1/\beta$ is the thermal mass.

With these conditions in place, we are ready to formulate the analytical bootstrap framework.

4.2.1 Case $r = 0$

In this section, we derive a novel dispersion relation for thermal correlators at zero spatial separation and discuss how these correlators can be reconstructed using an expansion in generalized free field correlators. We show that the zero spatial distance limit, $r = 0$, introduces several interesting features. In this limit, the correlator $g(\tau)$ depends solely on the Euclidean time coordinate, rendering the problem effectively one-dimensional.

In this case, the OPE (4.1.11) is convergent everywhere on the thermal circle for $\tau \in \mathbb{R}$. Upon analytic continuation in τ, this property is no longer manifest; however, we demonstrate that the convergence persists in the analytically continued correlator.

Analytic structure in the complex τ-plane. When we consider $g(\tau)$ as a function of the complex variable $\tau \in \mathbb{C}$, the analytic structure is strongly constrained by the KMS condition: the function has simple poles on the real axis located at[4]

$$\tau = n\beta\ , \quad n \in \mathbb{Z}\ . \tag{4.2.12}$$

[3] A simple counterexample is the $4d$ free scalar theory, where the correlator between fundamental scalars decays as a power law: $g(\tau, x) \sim 1/x$.

[4] Note that there are other ways to fix the analytic structure as we analytically continue to complex τ. A compelling way would be considering the light-cone singularities that are present when $r \neq 0$ and choosing the cuts to extend in both directions. This would leave us with a strip of analyticity. We can see that this is equivalent to our case by taking $r = \epsilon$ very small and computing the dispersion relation in this case and then take $\epsilon \to 0$.

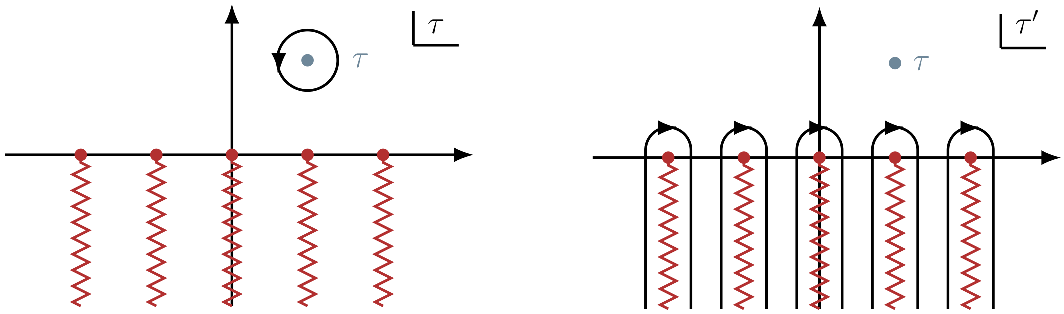

Figure 4.1: Left panel: *Analytic structure in the complex τ-plane of the thermal two-point function at zero spatial separation, $g(\tau)$.* ***Right panel:*** *The contours considered to compute the correlation function in τ via a dispersion relation.*

Branch cuts might additionally be present. To determine this, we focus on the region $|\tau| < \beta$, where we can expand the two-point function using the OPE (4.1.11). As mentioned in Section 4.1, this system is effectively one-dimensional and the OPE is not sensitive to the spin of the operators. The branching points in (4.2.12) would depend on the conformal dimensions of the operators present in the OPE. Because of periodicity ($\tau \sim \tau + n\beta$) and time reversal ($\tau \sim -\tau$), such branch cuts cannot be placed in arbitrary directions but are forced to lie along the imaginary time direction, as shown in Fig. 4.1. It should also be noticed that if such branch cuts exist, they must extend all the way to infinity.

Dispersion relation. Knowledge of the analytic structure in the complex τ-plane allows us to write an explicit formula for $g(\tau)$ in terms of the discontinuity along the branch cuts. To do this, we compute the correlation function around a point τ by using the Cauchy integral formula

$$g(\tau) = \frac{1}{2\pi i} \oint_{\mathcal{C}} \mathrm{d}\tau' \, \frac{g(\tau')}{\tau' - \tau} \ . \tag{4.2.13}$$

The next step is to deform the contour $\mathcal{C}$. We must consider two contributions: the first comes from the infinite set of discontinuities along the cuts, while the second one arises from the arcs at $|\tau| \to \infty$. We denote the latter as $g_{\mathrm{arcs}}(\tau)$, and the two-point function becomes

$$g(\tau) = g_{\mathrm{dr}}(\tau) + g_{\mathrm{arcs}}(\tau) \ , \tag{4.2.14}$$

with

$$g_{\mathrm{dr}}(\tau) = \sum_{m=-\infty}^{\infty} \int_{-i\infty}^{0} \frac{\mathrm{d}\tau'}{2\pi i} \frac{\mathrm{Disc}\, g(\tau')}{\tau' + m - \tau} \ . \tag{4.2.15}$$

Here the sum runs over all the locations of the poles, automatically encoding the KMS condition. Note that (4.2.15) is independent of d, the number of spacetime dimensions.

Arc contributions. In the following, we discuss the arc contributions in the dispersion relation (4.2.15), and show that they correspond at most to a constant.

The starting point is to notice that $g_{\rm dr}(\tau)$ captures the whole analytic structure of the full correlator $g(\tau)$, which implies that $g_{\rm arcs}(\tau)$ has to be an entire function. Similarly, $g_{\rm dr}(\tau)$ is periodic by construction and thus

$$g_{\rm arcs}(\tau) = g_{\rm arcs}(1-\tau)\,. \tag{4.2.16}$$

We now have to discuss the boundedness of the function $g_{\rm arcs}(\tau)$. On the real axis, the absence of finite poles and the periodicity ensure that the function is bounded. Hence, we only need to focus on the behavior in the upper complex τ-plane; the lower counterpart would be analogous.

Boundedness conditions. First of all, we prove that the function $g(\tau)$ is bounded as $|\tau|\to\infty$. This can be shown by adapting one of the arguments in [146]. We can quantize the thermal theory by identifying spatial slices $\mathbb{R}^{d-2}\times S^1_\beta$ on the thermal geometry $\mathbb{R}^{d-1}\times S^1_\beta$, where the quantum states are defined; the time variable is represented by the missing spatial direction. This point of view was introduced in (4.1.17) and (4.1.18). The circle compactification is now interpreted as a Kaluza–Klein compactification. The two-point function can be rewritten as

$$g(\tau) = \langle\phi(\tau)\phi(0)\rangle_\beta = \langle\Psi|e^{i\tau \boldsymbol{P}_{\rm KK}}|\Psi\rangle\ , \tag{4.2.17}$$

where $|\Psi\rangle = \phi(0)|0\rangle_{\mathbb{R}^{d-2}\times S^1_\beta}$. The complex time evolution operator can be rewritten in terms of two operators V and U defined as

$$V = e^{-\operatorname{Im}(\tau)\boldsymbol{P}_{\rm KK}}\ ,\quad U = e^{i\operatorname{Re}(\tau)\boldsymbol{P}_{\rm KK}}\ ,\quad e^{i\tau\boldsymbol{P}_{\rm KK}} = V^{\frac12}UV^{\frac12}\ . \tag{4.2.18}$$

Observe that V is a positive Hermitian operator while U is a unitary operator. By Cauchy–Schwarz inequality we have

$$|g(\tau)|^2 \leq \langle\Psi|V^{\frac12}V^{\frac12}|\Psi\rangle\langle\Psi|V^{\frac12}U^\dagger UV^{\frac12}|\Psi\rangle = \langle\Psi|V|\Psi\rangle^2\ . \tag{4.2.19}$$

Therefore we have

$$|g(\tau)| \leq |g(i\operatorname{Im}(\tau))|\ . \tag{4.2.20}$$

This equation shows that the problem of bounding the function $g(\tau)$ throughout the upper half of the complex τ-plane can be reduced to bounding it along the imaginary axis, that is, to bounding the real-time correlator. The real-time correlator is free of poles at finite real time and is bounded at infinity by the clustering decomposition of the correlator in the limit $|t| \to \infty$.

Using a similar argument, but employing the spectral decomposition (2.3.7) as discussed in Section 2.3.1, one can show that the correlator is bounded in the complex τ-plane by its values on the real axis [154],

$$|g(\tau)| \;\geq\; |g(\tau + i\eta)|\,, \qquad \tau, \eta \in \mathbb{R}\,, \tag{4.2.21}$$

which will also be useful in the holographic setup in Section 4.3.

Given the absence of finite poles on the imaginary axis, we conclude that $g(\tau)$ is bounded by a constant on the imaginary axis and then on the entire upper complex τ-plane. Secondly, we need to discuss the boundedness of the function $g_{\rm dr}(\tau)$ in the upper complex τ-plane. By construction, this function is *polynomially* bounded. Hence, we conclude that $g_{\rm arcs}(\tau)$ is at least polynomially bounded, but for the purposes of our discussion it is enough to say

$$|g_{\rm arcs}(\tau)| < Ce^{|\tau|}\;, \qquad |\tau| \to \infty\,, \tag{4.2.22}$$

for any constant real number C, which is a weaker assumption than the polynomial bound.

We conclude that the function $g_{\rm arcs}(\tau)$ is entire, periodic on the real axis, and surely exponentially bounded as in (4.2.22). As shown in [3], these conditions lead to the conclusion

$$g_{\rm arcs}(\tau) = \kappa\;, \qquad \kappa \in \mathbb{R}\;. \tag{4.2.23}$$

A formula for $\boldsymbol{g(\tau)}$. We can now combine the insights we collected throughout this section to derive a formula for $g(\tau)$ that is manifestly KMS invariant. Our strategy is to insert the OPE (4.1.11) in the dispersion relation (4.2.15) and to commute the discontinuity with the sum. Following the same arguments we used to understand the arc contributions (4.2.23), this procedure misses at most a constant which can be reabsorbed in κ. We then compute the discontinuity of single thermal blocks and find

$$\text{Disc}_{\text{Im}(\tau)<0}\, \tau^{\Delta-2\Delta_\phi} = \tau^{\Delta-2\Delta_\phi} e^{\frac{3}{2}\pi i(\Delta-2\Delta_\phi)} \left[1 - e^{-2\pi i(\Delta-2\Delta_\phi)}\right]\;, \tag{4.2.24}$$

where the overall phase reflects the fact that we are parametrizing a contour surrounding the lower imaginary axis. From this formula, one can immediately conclude that all $\Delta - 2\Delta_\phi = 2n$ for $n \in \mathbb{Z}$ contributions vanish. If we only focus on the $\left[1 - e^{-2\pi i(\Delta-2\Delta_\phi)}\right]$ factor in (4.2.24), it looks like the odd integers $\Delta - 2\Delta_\phi = 2n+1$ also do not contribute.

However, we should keep in mind that for odd integers the integral in (4.2.15) diverges and when we carefully regularize the vanishing of the discontinuity with the divergence of the integral we conclude that they contribute as derivatives of delta functions.

Resumming the discontinuities for each operator that makes a non-vanishing contribution to the dispersion relation, we obtain an alternative expansion for the correlator:

$$g(\tau) = \sum_{\Delta} a_{\Delta} \Big[\zeta_H(2\Delta_\phi - \Delta, \tau) + \zeta_H(2\Delta_\phi - \Delta, 1-\tau) \Big] + \kappa \ , \tag{4.2.25}$$

where in each term we find a kernel written in terms of Hurwitz ζ-functions multiplied by the OPE coefficients a_Δ that encode the dynamical information. The dependence on β can be reintroduced by dimensional analysis, in that case it is also straightforward to check that the limit $\beta \to \infty$ gives the correct zero-temperature correlator. A similar equation appeared before in [155], where it was employed in the study of holographic correlators through a different setup: in our work, this formula is derived by inverting operators via dispersion relation.

In the rest of this section, we discuss the implications of (4.2.25). This expression is powerful, as KMS invariance is built in term by term, as opposed to the thermal block expansion (4.1.11). Furthermore, we note that (4.2.25) can be suggestively interpreted as an infinite sum over two-point functions of fundamental scalars in GFF, which is given in (4.1.24).

More explicitly, we conclude that *thermal two-point functions at zero spatial separation admit an expansion in terms of GFF correlators*, with coefficients given by the thermal OPE data.[5] At zero temperature, a similar structure was proposed for one-dimensional systems initially in [156] and later on in [157], in which solutions to the crossing equation are expressed in terms of *extremal solutions* — minimal solutions that individually satisfy crossing. In the same spirit, (4.2.25) implies that GFF correlators form a basis for thermal two-point functions.

This formulation can be made immediately useful in perturbative settings or in cases where the spectrum is protected by additional symmetries (for instance free or supersymmetric theories). The kernel $g_{\mathrm{GFF}}(\tau, \Delta)$ vanishes identically when $\Delta - 2\Delta_\phi \in 2\mathbb{Z}^{>0}$, leading to considerable simplifications in favorable circumstances. For example, for GFFs as described in Section 4.1.2, the double-twist operators $[\phi\phi]_{n,J}$ do not contribute in a generalized free field theory, and the correlator $g(\tau)$ is fully reconstructed

[5] Note that correlators produced with the dispersion relation can escape this statement if they are not consistent with the boundedness condition discussed in this section. The arc contributions are non-trivial in this case which will be the case for holographic setups.

by the term corresponding to the identity operator. In a general interacting theory, the double-twist operators acquire anomalous dimensions, and in principle their contribution needs to be considered. Nonetheless, a classical result from analytic conformal bootstrap [39, 158–160] gives

$$\Delta = 2\Delta_\phi + 2n + J + \gamma \ , \qquad \gamma \sim O\left(\frac{1}{J}\right) \quad \text{as } J \to \infty \ . \tag{4.2.26}$$

This means that in the large spin limit, the OPE spectrum approaches that of a generalized free field. Therefore the double-twist operators do not contribute to the discontinuity, since

$$\mathrm{Disc}_{\mathrm{Im}(\tau)<0}\, \tau^{\Delta - 2\Delta_\phi} \propto \frac{1}{J} \ . \tag{4.2.27}$$

Clearly, this conclusion is correct only if a_Δ does not grow as J in the large spin limit. This behavior is theory dependent. The simplest setting in which one can explicitly illustrate the dispersion relation (4.2.15) and see the generalized free field (GFF) approximation at work in the $r = 0$ limit is the GFF theory itself.

GFF in τ-plane. We first test (4.2.25). Odd-spin double-twist operators do not contribute to the discontinuity due to parity symmetry; using the identity

$$\zeta_H(-2n, \tau) + \zeta_H(-2n, 1-\tau) = 0 \ , \qquad \forall\, n \in \mathbb{Z}^{>0} \ , \tag{4.2.28}$$

we conclude that even-spin double-twist operators do not contribute as well, since GFF is non-interacting and anomalous dimensions do not arise. We conclude that the identity operator is the only operator contributing to the discontinuity. The formula (4.2.25) becomes

$$g(\tau) = \zeta_H(2\Delta_\phi, \tau) + \zeta_H(2\Delta_\phi, 1-\tau) \ , \tag{4.2.29}$$

matching the known result from (4.1.22). A remarkable general observation about the $r = 0$ limit is that, due to the simplified structure of the OPE in (4.1.11), the entire spectrum of a non-trivial interacting theory collapses into a collection of double-twist families, mirroring the structure found in GFF theory.

The $2d$ $\Delta_\phi = 1$ in complex τ-plane. As the second example we consider the $2d$ Virasoro correlator. Here, we would like to use (4.2.25) to compute the correlator in the complex τ-plane. All the operators in the OPE, being the operators in the vacuum module, have dimensions $\Delta = 2 + \mathbb{N}$, and since odd-spin operators do not contribute, all the dimensions corresponding to non-zero one-point functions are associated with

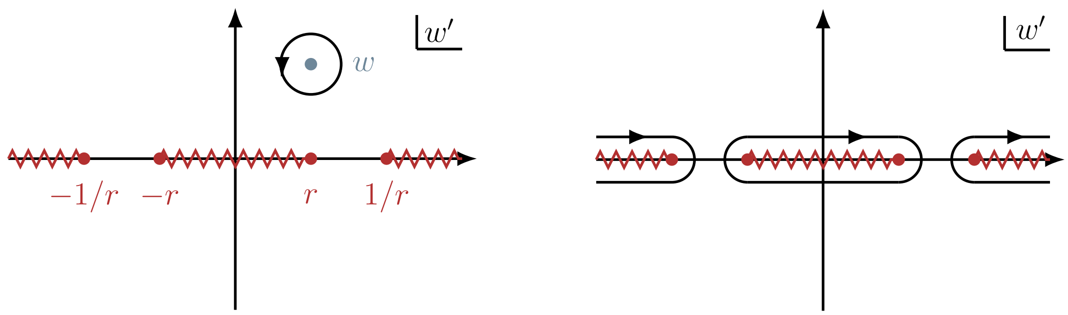

***Figure 4.2: Left panel**: Analytic structure of a thermal correlator in the complex w-plane. **Right panel**: Contours used in the derivation of the dispersion relation.*

even conformal dimensions. As a consequence of (4.2.28), we find that only the identity operator contributes to the correlator. This leads straightforwardly to

$$g(\tau) = \zeta_H(2,\tau) + \zeta_H(2,1-\tau) + \kappa = \pi^2 \csc^2(\pi\tau) + \kappa \,, \tag{4.2.30}$$

which perfectly matches the exact result in (4.1.30) with $\kappa = 0$. Later on we will detailly consider the $O(N)$ model as an example in Section 4.2.4. And consider the Fourier transform of the KMS invariant thermal blocks given in (4.2.25) in Section 4.2.3, but for now we move on to the general case of $r \neq 0$.

4.2.2 Case $r \neq 0$

We now extend our analysis of the previous section to the case in which the spatial distance between the two external operators is kept non-vanishing. We first review the derivation of the dispersion relation presented in [152] and discuss the arc contributions. We then lay out our strategy for reconstructing correlators, using the OPE and a set of consistency conditions. This is applied through two different methods: the first one is numerical and relies on the form of the large-spin expansion for OPE coefficients. The second one is analytical, where correlators are obtained through promoting the dispersion relation of [152] to a version that is KMS invariant by construction.

For non-zero spatial coordinates, a dispersion relation was already derived in [152]; we review here the derivation from the analytic structure and the formula.

Analytic structure in the w-plane. The procedure to compute the dispersion relation is similar to the one described above for the case of the τ-plane, but using the analytic structure in the complex w-plane. It was argued in [146] that the corresponding analytic structure is the one depicted in Fig. 4.2. This particular structure can be extracted from the thermal conformal blocks which are explicitly given in (4.1.5). However, to argue that there are no singularities apart from the poles and the cuts that may appear on the real w axis depending on the spectrum of the theory we need the KK formalism presented in Section 4.1.1 to extend this to the entire complex w-plane. Here, we review the argument. Firstly, the convergence of the s-channel OPE is enough to ensure analyticity in the annulus

$$r < |w| < \frac{1}{r} \ , \tag{4.2.31}$$

this region is also highlighted in the Right Panel of Figure 4.4. To ensure analyticity in a larger region we consider the KK picture (4.1.19) in a similar but more general way than (4.2.20) and rewrite the thermal correlator as

$$\begin{aligned} g(z,\bar{z}) &= \langle\Psi|e^{-H_{KK}x^1+i\tau P_{KK}}|\Psi\rangle \\ &= \langle\Psi|e^{\frac{i}{2}(H_{KK}+P_{KK})z-\frac{i}{2}(H_{KK}-P_{KK})\bar{z}}|\Psi\rangle \end{aligned} \tag{4.2.32}$$

Here, both operators H_{KK} and P_{KK} are hermitian. By using the following definitions we can separate the correlator into a combination of a unitary and hermitian operator respectively,

$$U = e^{\frac{i}{2}(H_{KK}+P_{KK})Re(z)-\frac{i}{2}(H_{KK}-P_{KK})Re(\bar{z})} \tag{4.2.33}$$

$$V = e^{-\frac{1}{2}(H_{KK}+P_{KK})Im(z)+\frac{1}{2}(H_{KK}-P_{KK})Im(\bar{z})} \ . \tag{4.2.34}$$

Then we can bound the correlator by using Cauchy-Schwarz inequality,

$$\begin{aligned} |\langle\Psi|V^{1/2}UV^{1/2}|\Psi\rangle| &\leq \langle\Psi|V^{1/2}V^{1/2}|\Psi\rangle^{1/2}\langle\Psi|V^{1/2}U^{\dagger}UV^{1/2}|\Psi\rangle^{1/2} \\ &= \langle\Psi|V|\Psi\rangle \ . \end{aligned} \tag{4.2.35}$$

To argue that the correlator is indeed bounded and there are no additional poles on the w-plane we need the operators $H_{KK} \pm P_{KK}$ to be bounded from below. Although this is the case in flat space, the positivity of these operators for any discrete eigenvalue of P_{KK} is not obvious. In [146], the authors claim that for sufficiently large quantized momentum, the spectrum of H_{KK} approaches the flat space one, thus the assumption of the operator $H_{KK} \pm P_{KK}$ being positive for all momenta is physically reasonable. We also use this assumption to ensure boundedness of the correlator and fix the analytic structure of the correlator on w-plane to the one given in Figure 4.2.

Dispersion relation. As always, the starting point is to consider the two-point function at a generic point w and make use of Cauchy's formula to rewrite it as a contour integration:

$$g(r,w) = \oint_{\mathcal{C}} \frac{\mathrm{d}w'}{2\pi i}\frac{g(r,w')}{w'-w} \ . \tag{4.2.36}$$

We can then deform the contour to go around the cuts: this turns into an integral over the discontinuity of $g(r,w)$, and dropping the arcs we obtain[6]

$$g_{\rm dr}(r,w) = \int_0^r \frac{{\rm d}w'}{2\pi i}\, \frac{w^2(1-w'^4)}{w'(w'-w)(w'+w)(1-w^2w'^2)}\, {\rm Disc}\, g(r,w')\ . \tag{4.2.37}$$

The full correlator is then in principle given by[7]

$$g(r,w) = g_{\rm dr}(r,w) + g_{\rm arcs}(r,w)\,, \tag{4.2.38}$$

where $g_{\rm arcs}(r,w)$ comes from the contribution of the integral in the limit $|w| \to \infty$.

Inserting OPE. After deriving the dispersion relation as above to attempt to compute the correlator we insert the t-channel of the OPE (4.2.5) in the dispersion relation (4.2.37) and commute the discontinuity with the sum:

$$\text{Disc}_{\text{Re}(\bar z)>0}\, g(z,\bar z) = \sum_{\mathcal{O}} a_{\mathcal{O}}\, \text{Disc}_{\text{Re}(\bar z)>0}\, f_{\Delta,J}(1-z,1-\bar z)\,. \tag{4.2.39}$$

Similarly to what we already discussed in Section 4.2.1, the blocks do not contribute when $\Delta - 2\Delta_\phi \in 2\mathbb{Z}^{>0}$, and in favorable settings the correlator can be reconstructed from a finite number of contributions. This happens because the thermal blocks behave schematically near $\bar z = 1$ as

$$f_{\Delta,J}(1-z,1-\bar z) \sim \sum_{k=1}^{\Delta_\phi-(\Delta-J)/2} \frac{1}{(1-\bar z)^k} + \text{regular}\,, \tag{4.2.40}$$

while the discontinuity vanishes for integer powers (the regular terms):

$$\text{Disc}_{\text{Re}(\bar z)>0}(1-\bar z)^\alpha = 0\ , \quad \alpha \in \mathbb{Z}^{>0}\ . \tag{4.2.41}$$

For the blocks that survive the discontinuity, the following identity holds both when $\alpha \in \mathbb{Z}^{<0}$ or when α is not an integer:

$$\text{Disc}_{\text{Re}(\bar z)>0}(1-\bar z)^\alpha = 2i\sin(\alpha\pi)\,(\bar z-1)^\alpha\,\Theta(\text{Re}(\bar z)-1)\ , \quad \alpha \notin \mathbb{Z}^{>0}\,. \tag{4.2.42}$$

[6] The precise derivation involves making use of the reality and parity conditions given in (4.2.7) and (4.2.8) to combine the contours into one expression. The steps are in one-to-one agreement with the derivation provided in [161, 162] for the defect case, which shares the same analytic structure, apart from the fact that parity has to be imposed. Note that, in Eq. (5.5) of [152], there is an additional term with a residue. We do not keep track of this term here, as its main purpose is to reconstruct the identity contribution.

[7] It should be emphasized at this point that the dispersion relation (4.2.37) is fully equivalent to the Lorentzian inversion formula of [146] (see Section 5.2 of [152] for details). The fact that it relates the discontinuity of the correlator to itself simply provides a shortcut to calculating the OPE coefficients individually.

OPE and out-of-OPE contributions. At zero temperature, the procedure described above typically already reproduces the correlator up to the arc contributions. An additional obstacle is introduced at finite temperature, which stems from the fact that the OPE is not convergent everywhere. Compared to the complex τ-plane case, the prescription to exchange the discontinuity operation with the OPE expansion requires additional consideration. This can be seen directly from (4.2.37), since the integral runs over $w \in (0, r)$, with $r = \sqrt{x^2 + \tau^2}$, and the OPE only converges for $r < 1$. One can indeed verify that the function $g_{\mathrm{dr}}(r, w)$ is in this case *not KMS invariant*. This discrepancy can be understood by employing the Lorentzian inversion formula of [146], which returns a function $a(\Delta, J)$, whose poles correspond to the OPE coefficients of our correlator of interest. As already identified in [146],[8] we need to distinguish two types of contributions:

- ⋆ *OPE contributions.* This type of contribution schematically appears in the inversion formula through integrals of the following form:

$$\int_1^\infty \frac{\mathrm{d}\bar{z}}{\bar{z}} \bar{z}^{\Delta_\phi - \bar{h} - m} \, \mathrm{Disc}(1 - \bar{z})^c \sim J^{-c-1} + \dots \ , \tag{4.2.43}$$

  where $\bar{h} = (\Delta + J)/2$ and $m \in \mathbb{Z}^{\geq 0}$. This highlights the fact that contributions from the OPE region to the coefficients are *polynomially* suppressed in the spin J;

- ⋆ *Out-of-OPE contributions.* This type of contribution is schematically represented instead as integrals of the form

$$\int_2^\infty \frac{\mathrm{d}\bar{z}}{\bar{z}} \bar{z}^{\Delta_\phi - \bar{h} - m} f(\bar{z}) \sim 2^{-J} + \dots \ . \tag{4.2.44}$$

  In this case, we learn instead that the out-of-OPE region encodes terms that are *exponentially* suppressed in the spin J. These terms are missing from the Lorentzian inversion formula, and similarly they are not captured by the dispersion relation (4.2.37).

This analysis suggests that the thermal correlator $g(z, \bar{z})$ can be split into two parts, each associated to one type of contribution:

$$g(z, \bar{z}) = g_{\mathrm{OPE}}(z, \bar{z}) + g_{\text{out-of-OPE}}(z, \bar{z}) \ , \tag{4.2.45}$$

where $g_{\mathrm{OPE}}(\tau, x)$ can be identified with the dispersion relation and its arc completion.

[8] See Section 6 for additional detail.

Consistency conditions. We now discuss the consistency conditions that can be imposed on the correlator in order to reconstruct the function $g_{\text{out-of-OPE}}(z, \bar{z})$:

1. *KMS condition.* A fundamental property of thermal two-point functions is the KMS condition (4.2.6);

2. *Analytic structure.* The analytic structure of thermal two-point functions must match the one described above and illustrated in Fig. 4.2. In particular, the arc terms must have vanishing discontinuity;

3. *Consistency with the OPE.* The thermal two-point function must be consistent with the operator product expansion. The dispersion relation is expected to reproduce the correct OPE spectrum up to low-spin operators, which would then be encoded in g_{arcs};

4. *Regge boundedness.* In the variables (r, w), the thermal two-point function is expected to be *polynomially* bounded in the Regge limit
$$w \to \infty\,, \quad r \text{ fixed;} \tag{4.2.46}$$

5. *Clustering at large distances.* At large spatial separation, the two-point function must satisfy the clustering condition
$$g(z, \bar{z}) \xrightarrow{x\to\infty} \langle\phi\rangle_\beta^2. \tag{4.2.47}$$
The precise approach to this asymptotic value depends on the theory. In general, for theories without an extensive symmetry structure,[9] the expected behavior is an exponential decay
$$g(z, \bar{z}) \xrightarrow{x\to\infty} \langle\phi\rangle_\beta^2 + O(e^{-m_{\text{th}}x}), \tag{4.2.48}$$
where $m_{\text{th}} \propto 1/\beta$ is the thermal mass.

A numerical approach. Our first approach to reconstruct $g_{\text{out-of-OPE}}(z, \bar{z})$ is based on the fact that the corrections in spin are organised into a set of *exponential corrections* to the large-spin expansion of the OPE coefficients:[10]
$$a_{\mathcal{O}} = a_{\mathcal{O}}^{(\text{dr})}\left(1 + \sum_{n=1}^{\infty} \frac{c_n}{n^J}\right)\,. \tag{4.2.49}$$

[9] A simple counterexample is the $4d$ free scalar theory, where the correlator between fundamental scalars decays as a power law: $g(\tau, x) \sim 1/x$.

[10] Strictly speaking, (4.2.49) is reliable for the spin of the operator being large enough. This is discussed in further detail in this section when we discuss arc contributions. For the sake of the discussion, we ignore the arc contributions here.

where $c_1 = 1$ and the blue term is the contribution to $a_{\mathcal{O}}$ given by the dispersion relation applied to the t-channel expansion, and contained in $g_{\text{OPE}}(z, \bar{z})$. $a_{\mathcal{O}}^{(\text{dr})}$ has at most a polynomial dependence on J. The red terms instead are part of $g_{\text{out-of-OPE}}(z, \bar{z})$ and they encode the exponential dependence on J. Intriguingly enough this expansion is reminiscent of expansion of one-point functions in terms of polylogarithms [163, 164]. Each exponential correction in the spin comes with an unknown coefficient c_n to be fixed.

These coefficients can be fixed numerically by requiring that the candidate correlator satisfies KMS invariance

$$g_{\text{cand}}(z, \bar{z}) \stackrel{!}{=} g_{\text{cand}}(1-z, 1-\bar{z}) \ . \tag{4.2.50}$$

In practice, this procedure requires truncating the sum over exponential corrections to a finite order n_{max}. One can then solve for a finite number of coefficients c_n numerically and verify the stability and convergence of the procedure by varying n_{max}.

In the free theory we know that the only operator contained in the arcs is the identity operator: its one-point function is simply the normalization of the scalar field ϕ and we can decide to unit-normalize its zero-temperature two-point functions so that $a_{\mathbb{1}} = 1$. Even after adding this contribution by hand, the function is not KMS invariant. According to the discussion above, the ansatz for the correlator is

$$g(z, \bar{z}) = g_{\text{dr}}(z, \bar{z}) + \frac{1}{z\bar{z}} + \sum_{n=1}^{\infty} c_n g_{\text{comp.}}^{(n)}(z, \bar{z}) \ , \tag{4.2.51}$$

where the first term is simply the outcome of the dispersion relation, the second term the identity operator contribution, which in this case is the only term in the arcs, and the last term should be the contribution to the thermal OPE coefficients coming from the region out of the OPE regime. The Ansatz for this contribution is given by

$$a_{\mathcal{O}} = a_{\mathcal{O}}^{(\text{dr})} \left(1 + \sum_{n=0}^{\infty} \frac{c_n}{n^J} \right) \ . \tag{4.2.52}$$

In the free scalar case, the only operators in the OPE are the higher-spin currents $[\phi\phi]_{0,J}$: the compensation at any order in n, i.e., in $1/n^J$, can be computed directly by summing over all the operators. As a result we have

$$g_{\text{comp.}}^{(n)} = \frac{n^2 \left(n^2 + z\bar{z}\right)}{\left(n^2 - z^2\right)\left(n^2 - \bar{z}^2\right)} \ . \tag{4.2.53}$$

In order to impose KMS, we need to truncate the Ansatz 4.2.51 to some n_{max} and numerically find the coefficients c_n by expanding the correlator both around $z, \bar{z} \sim 0$ and

Table 4.1: *Results for the first coefficients c_k for the corrections in spin for the case $\Delta_\phi = 1$, obtained from the KMS condition.*

$n_{\max}$	2	3	4	5	10	Exact results
c_2	0.614	0.486	0.501	0.500	0.500	$1/2 = 0.5$
c_3	-	0.384	0.172	0.232	0.222	$2/9 = 0.222\ldots$
c_4	-	-	0.323	0.017	0.125	$1/8 = 0.125$

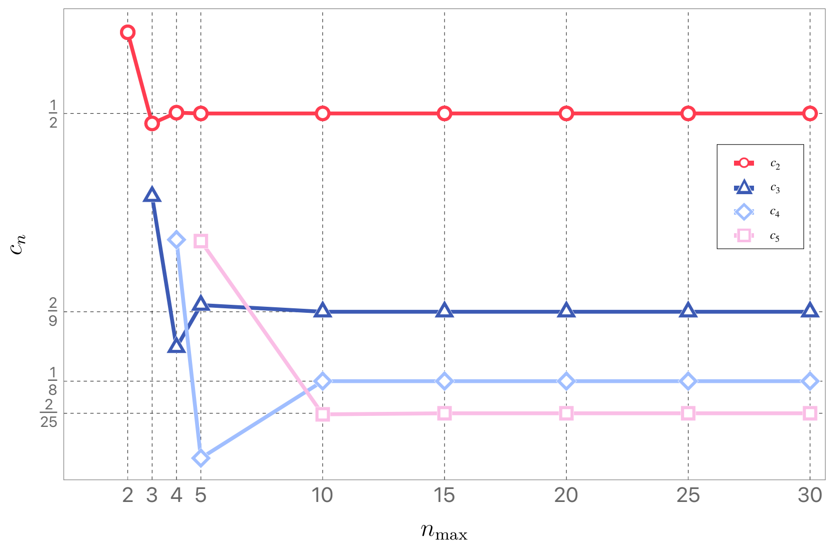

Figure 4.3: *Coefficients of the first five corrections of Eq. (4.2.51) as a function of n_{max}. Notice that when n_{max} increases, the corrections stabilize rather quickly to the values that correctly re-establish KMS invariance of the corrected correlator.*

$z, \bar{z} \sim 1$. The value of $n_{\max}$ can be then modified to verify the stability of the solutions explicitly. In this specific case, by considering $n_{\max}$ large enough it is possible to notice that all the coefficients are rational (as expected from the analytic solution) and the exact value can be determined with the function `Rationalize` in MATHEMATICA.

For the sake of clarity we show in Table 4.1 and Fig. 4.3 the evolution of the solutions for the first coefficients imposing KMS while varying the number of corrections $n_{\max}$. We observe a very fast convergence, in particular for the first corrections. The reader can already notice a clear pattern, which is confirmed also from higher coefficients. In particular,

$$c_n = \frac{2}{n^2} \; . \tag{4.2.54}$$

In fact, this fixes the OPE coefficients to be $a_{[\phi\phi]_{0,J}} = 2\zeta(2+J)$, in perfect agreement

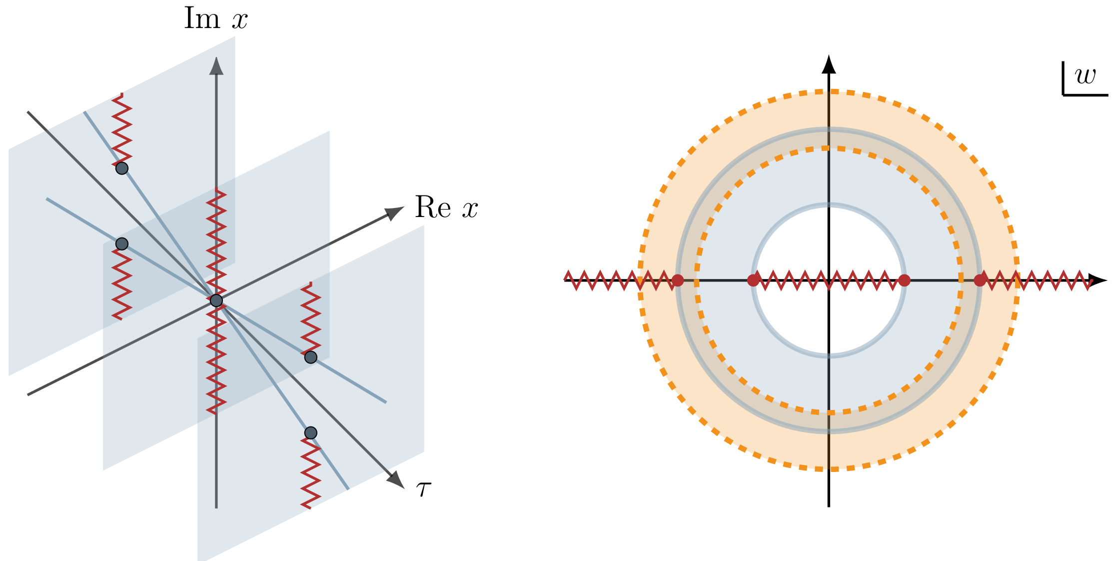

***Figure 4.4: Left panel**: Illustration of the analytic structure of the thermal two-point function in the complex x-plane, following [165]. The different planes represent integer shifts in τ. The lines crossing the end points of the cuts show the lightcone $\tau^2 = (ix)^2$.* ***Right panel**: The blue-shaded annulus (with the solid contours) represents the region of convergence of the OPE in the s-channel in the w-plane, as shown in [146]. The orange-shaded annulus (with the dashed contours) schematically depicts how the region of convergence of the OPE shifts with one image. This illustrates how (4.2.56) captures the full correlator by starting with one OPE region (in this case the t-channel) and summing over its images.*

with the exact results. The same analysis can be carried out for the $O(N)$ model in $4-\epsilon$ dimensions as well. However, for theories with much more complicated spectra, such computations quickly become intractable, necessitating a more powerful approach.

The generalized method of images. The numerical method discussed above is conceptually straightforward, but it can become technically challenging when many operators contribute to the dispersion relation. For this reason, it is useful to explore an alternative approach and impose KMS invariance *explicitly*, starting directly from the output of the dispersion relation. To motivate this, let us recall the dispersion relation in the complex τ-plane (4.2.15). In that case, each operator in the OPE contributes via a KMS-invariant function, constructed by summing over all its thermal images. Figure 4.4 shows that this is also the case in the complex x-plane.

One might wonder whether a similar construction can be generalized to the case of non-zero spatial distance. The key observation is that any non-periodic function $f(\tau)$ can be used to build a function $\widetilde{f}(\tau)$ periodic by construction

$$\widetilde{f}(\tau) = \sum_{m=-\infty}^{\infty} f(\tau - m) \ , \tag{4.2.55}$$

and, conversely, any periodic function admits such a decomposition through Poisson resummation. This suggests a natural Ansatz for the correlator: since $g_{\mathrm{dr}}(\tau, x)$ is not KMS-invariant, periodicity can be reinstated by construction as follows[11]

$$g(z, \bar{z}) = \frac{1}{2} \sum_{m=-\infty}^{\infty} g_{\mathrm{dr}}(z - m, \bar{z} - m) + g_{\mathrm{arcs}}(z, \bar{z}) \ . \tag{4.2.56}$$

We refer to (4.2.56) as the *generalized method of images*. This conjecture can be seen to satisfy most of the consistency requirements listed in Section 4.2:

1. *KMS condition.* This condition is automatically satisfied by construction in (4.2.56), as the sum over images ensures periodicity;

2. *Analytic structure.* This requirement is also satisfied, since each image is built out of the dispersion relation, which by definition implements the correct analytic behavior;

3. *Consistency with the OPE.* In equation (4.2.44), we showed that the image terms contribute only $1/n^J$ corrections to the thermal OPE coefficients, and thus (4.2.56) is consistent with the OPE structure by construction. In the right panel of Figure 4.4 we show the OPE contribution (blue shaded region) and the same contribution shifted by one unit of β (orange shaded region), which therefore is an out of OPE contribution in the sense of (4.2.45). The figure provides a pictorial demonstration of the mechanism underlying the generalized method of images;

4. *Regge boundedness.* This assumption plays a crucial role in the dispersion relation. In fact one has that for the term $m = 0$ in the Regge limit the result of the dispersion relation is polynomially bounded. If $m \neq 0$, this is less trivial to conclude since under $z \to z - m$ and $\bar{z} \to \bar{z} - m$ we have

$$r \to \tilde{r} = \sqrt{r^2 - mz - m\bar{z} + m^2} \ , \tag{4.2.57}$$

[11]The factor $1/2$ comes from the fact that by summing in $m \in \mathbb{Z}$ we are over-counting the images, since when we computed the dispersion relation we already used the symmetry $w \to -w$.

and therefore for $w \to \infty$ and r fixed for $m \neq 0$ we have $\tilde{r} \to \infty$ in the images. Nonetheless the images of the dispersion relation can be defined by considering (4.2.37) and making the change of variable $z \to z - m$ and $\bar{z} \to \bar{z} - m$. One can notice that if the integral is polynomially bounded for $m = 0$ this is also the case for $m \neq 0$. Therefore every $g^{(\mathcal{O})}(z - m, \bar{z} - m)$ is bounded and thus we expect the full sum over the generalized images to converge;

5. *Clustering at large distances.* This condition is *not* automatically built into (4.2.56), and must be checked on a case-by-case basis. If the sum over images does not reproduce the correct large-distance behavior, the term g_{arcs} must compensate for it.

One may now insert the OPE inside (4.2.56) to produce a formula in the gist of (4.2.25). We then obtain the following convenient expression:

$$g(z, \bar{z}) = \frac{1}{2} \sum_{\mathcal{O}} a_{\mathcal{O}} \sum_{m=-\infty}^{\infty} f_{\Delta,J}(z + m, \bar{z} + m) + g_{\text{arcs}}(z, \bar{z}) \,, \tag{4.2.58}$$

i.e., the correlator can be reconstructed by summing the thermal blocks over images.

Arc contributions. In the case of the complex τ-plane, we were able to show that the arc terms are given at most by a constant. When spatial separation is non-zero, we need to distinguish between the arcs of the dispersion relation, i.e. the function g_{arcs} in (4.2.38) , and the arcs after generalized images defined in (4.2.56). In this Section we bound the piece with arc contributions. Here we should expect operators of low spin $J < J^*$ to appear in $g_{\text{arcs}}(\tau, x)$:

$$\begin{aligned} g_{\text{arcs}}(\tau, x) &= \sum_{\Delta} \sum_{J<J_\star} a_{\mathcal{O}}^{(\text{arcs})} \left(x^2 + \tau^2\right)^{\frac{\Delta}{2} - \Delta_\phi} C_J^{(\nu)} \left(\frac{\tau}{\sqrt{x^2 + \tau^2}}\right) \\ &= \sum_{J<J_\star} F_J(\tau, x)\, C_J^{(\nu)} \left(\frac{\tau}{\sqrt{x^2 + \tau^2}}\right) \,, \end{aligned} \tag{4.2.59}$$

where J^* is an assumption in practical cases. If the generalized method of images suggested in this section produces the correct clustering decomposition behavior at large distances, then we must have

$$\lim_{x\to\infty} g_{\text{arcs}}(\tau, x) = 0 \quad \Rightarrow \quad \lim_{x\to\infty} F_J(\tau, x) = 0 \,, \tag{4.2.60}$$

as given in [152]. However the only function $F_J(\tau, x)$ satisfying this property with g_{arcs} being KMS invariant is $F_J(\tau, x) = 0$. To see this, use $\tau \to \tau + m$ and the limit $m \to \infty$

Table 4.2: *Thermal OPE coefficients in the* 4d *free scalar theory extracted by expanding the exact correlator, using the dispersion relation (DR), which is shown to match the result of the Lorentzian inversion formula (LIF), and generalized method of images (GMI). Only even-spin operators contribute.*

$\mathcal{O}$	$a_{\mathcal{O}}^{(\text{exact})} = a_{\mathcal{O}}^{(\text{GMI})}$	$a_{\mathcal{O}}^{(\text{DR})}$
$\mathbb{1}$	1	0
$[\phi\phi]_{0,J}$	$2\zeta(2+J)$	2

while considering (4.2.60). Clearly, this argument fails in cases where the generalized images do not exhibit the correct behavior as $x \to \infty$. The contribution from g_{arcs} is therefore theory-dependent and must be analyzed on a case-by-case basis.

The argument presented above supports the uniqueness of the function g_{arcs} within the given framework. Specifically, for any candidate function that satisfies the axioms of the thermal bootstrap — most notably, the correct clustering decomposition of the correlator — the reasoning can be repeated to confirm that no additional contributions are required. While this does not amount to a full uniqueness theorem for the thermal bootstrap in the sense of [150, 152], as it relies on prior knowledge of the correlator's discontinuity, it does imply that the generalized method of images may omit, at most, a uniquely determined and well-characterized function. As such, the correlator remains unambiguous within this approach.

After discussing the main intricate details of the generalized method of images, we can now apply it to the simplest examples in order to gain intuition about the construction and demonstrate the power of this approach.

GFF in $r \neq 0$ case. For simplicity, we focus on the $4d$ free scalar theory, with $\Delta_\phi = 1$. We first perform the sum over the images to obtain

$$\frac{1}{2}\sum_{m=-\infty}^{\infty} g_{\text{dr}}(z-m, \bar{z}-m) = -\frac{\pi}{(z-\bar{z})}\left[\cot(\pi z) - \cot(\pi\bar{z})\right] . \tag{4.2.61}$$

This expression already encodes the correct clustering behaviour at infinite distance, hence we conclude that the sum over images already solves the thermal bootstrap problem without any arc correction.

One may ask whether the usual method of images, Eq. (4.1.22), coincides with the generalized method of images, Eq. (4.2.61): the two methods can be shown to be equivalent, since in the case of GFF, the dispersion relation can be reshaped into the sum over the images of the free propagator, by using the relation

$$\sum_{m=-\infty}^{\infty} \frac{1}{(z-m+n)^{\Delta_\phi}(\bar{z}-m+n)^{\Delta_\phi}} = \sum_{m=-\infty}^{\infty} \frac{1}{(z-m)^{\Delta_\phi}(\bar{z}-m)^{\Delta_\phi}} \ , \tag{4.2.62}$$

for any integer n, by a simple change of summation variable.

Virasoro primaries with $\Delta_\phi = 1$ in $r \neq 0$ case. In two spacetime dimensions, operators with twist zero, i.e., $\Delta = J$, contribute to the discontinuity in the dispersion relation (4.2.37). The contribution of each single block is

$$g_{\text{dr}}^{(J)}(z,\bar{z}) = 2^{1-J} a_J \frac{(1+z\bar{z})(1-z\bar{z})^J}{z\bar{z}\,(1-z^2)\,(1-\bar{z}^2)} \ . \tag{4.2.63}$$

In order to sum over all these contributions, we need the thermal OPE coefficients a_J given in (4.1.33). In this case, we have access to the exact result and in particular[12]

$$a_J = -2^{J+1}\text{Li}_J(-1) \ . \tag{4.2.64}$$

Summing over all the contributions, we conclude that

$$g_{\text{dr}}(z,\bar{z}) = \frac{2\pi\,(1-z^2\bar{z}^2)}{z\bar{z}\,(1-z^2)\,(1-\bar{z}^2)} \csc(\pi z\bar{z}) \ . \tag{4.2.65}$$

This expression can be expanded in blocks as usual, from which we find that $a_{\mathbb{1}} = 0$ while all the other OPE coefficients organize in the following sequence:

$$a_{\Delta,J} = -4\,\text{Li}_{\frac{\Delta-J}{2}}(-1) \ , \tag{4.2.66}$$

which can be verified to be the correct large-spin behavior of all the OPE coefficients that can be extracted from (4.1.30).

In order to reproduce (4.1.30), our prescription would be to sum over all the images of the output of the dispersion relation. Here for simplicity we limit ourselves to two limits ($z = \bar{z}$ and $z = -\bar{z}$) and show that they correspond to the expectation (4.1.30).

The first case corresponds to the limit in which the two operators are placed on the same thermal circle, i.e., at zero spatial separation. It is easy to show that only the sum of images over the identity block gives a non-zero result, we get

$$g(z,z) = \pi^2 \csc^2(\pi z) \ , \tag{4.2.67}$$

[12]Notice that all twists appear in the thermal block expansion of (4.1.30) for $\Delta_\phi = 1$. Using our dispersion relation, we only need one family ($\Delta = J$) to reconstruct them all.

Table 4.3: *Thermal OPE coefficients in the 2d Virasoro primary ($\Delta_\phi = 1$) two-point function extracted by expanding the exact correlator, using the dispersion relation (DR), and generalized method of images (GMI). Only even-spin operators in the vacuum module contribute.*

$\mathcal{O}$	$a_{\mathcal{O}}^{(\text{exact})} = a_{\mathcal{O}}^{(\text{GMI})}$	$a_{\mathcal{O}}^{(\text{DR})}$
$\mathbb{1}$	1	0
$\mathcal{O}_{\Delta,J}$	$4\ \text{Li}_{\frac{\Delta-J}{2}}(-1)\text{Li}_{\frac{\Delta+J}{2}}(-1)$	$-4\ \text{Li}_{\frac{\Delta-J}{2}}(-1)$

which matches (4.2.30).

The other limit is $z = -\bar{z} = ix$, which corresponds to the case in which the time distance is zero but the spatial distance is finite. In this case, we have

$$\begin{aligned} g(ix, -ix) &= \sum_{m=-\infty}^{\infty} g_{\text{dr}}(m + ix, m - ix) \\ &= \frac{1}{2} \sum_{m=-\infty}^{\infty} \left(\frac{1}{x^2 + (m-1)^2} + \frac{1}{x^2 + (m+1)^2} \right) \\ &\quad - \sum_{\Delta \geq 2} 2^\Delta \text{Li}_\Delta(-1) \sum_{m=-\infty}^{\infty} \left(\frac{(m-1)^\Delta}{x^2 + (m-1)^2} + \frac{(m+1)^\Delta}{x^2 + (m+1)^2} \right) , \end{aligned} \tag{4.2.68}$$

where we already neglected terms which are zero after analytic continuation. We find

$$g(ix, -ix) = \pi^2 \text{csch}^2(\pi x) , \tag{4.2.69}$$

which matches (4.1.30) when $h = \bar{h} = 1/2$ and $\bar{z} \to -z = -ix$.

4.2.3 Momentum Space

A complementary approach to implementing the generalized method of images for the dispersion relation in position space is to transition to a momentum-space description. In this context, it is natural to ask whether an analogue of the operator product expansion exists in momentum space.[13] It turns out that the notion of the OPE in momentum space is closely tied to the dispersion relation in position space.

[13]Related questions for zero-temperature four-point functions are discussed in [166–168].

OPE in momentum space. The main obstacle to translating the OPE expansion into momentum space is that the OPE converges only within a finite region determined by the size of the thermal circle, specifically $\tau^2 + x^2 < \beta^2$. As a result, the Fourier transform does not commute with the OPE. Nevertheless, the concept of OPE can still be applied in the regime of large momenta, which corresponds to small distances. In fact, a well-defined OPE has been shown to exist in momentum space in the limit $\omega \to \infty$, with $\xi = |\vec{k}|/\omega$ held fixed [169].

Only in this limit can one claim that the two-point function in momentum space is approximated by its OPE

$$g(\omega, k) = \langle \phi(\omega, k)\phi(-\omega, -k)\rangle_\beta \overset{\omega\to\infty}{\sim} \sum_{\mathcal{O}} a_{\mathcal{O}} \tilde{f}_{\Delta,J}(\omega_n, k) \ , \tag{4.2.70}$$

where $\tilde{f}_{\Delta,J}$ represents the Fourier transform of the thermal OPE block. The blocks have been determined in [165]:

$$\tilde{f}_{\Delta,J}(\omega_n, k) = \sum_{j=0}^{J/2} c^{(\nu)}_{J,j} \frac{2^{\beta_-}\pi^{\frac{d}{2}}\Gamma(\beta_+)}{\Gamma(\alpha)} \frac{{}_2F_1\left(\beta_-, 1-\beta_-; 1-\beta_+; \frac{k+i\omega_n}{2k}\right)}{k^{\beta_-}(k+i\omega_n)^{\beta_+}} + O(e^{-k}) \ , \tag{4.2.71}$$

where we denote $k = |\vec{k}|$ and $\omega_n = 2\pi n$ are the Matsubara modes. We also define

$$\tilde{j} = \frac{J}{2} - j, \quad \tilde{\Delta} = \frac{\Delta}{2} - \Delta_\phi \ , \quad \alpha = \tilde{j} - \tilde{\Delta} \ , \quad \beta_\pm = \frac{d}{2} + \tilde{\Delta} \pm \tilde{j} \ , \tag{4.2.72}$$

and

$$c^{(\nu)}_{J,j} = (-1)^j \frac{\Gamma(J-j+\nu)}{\Gamma(\nu)\, j!\,(J-2j)!} 2^{J-2j} \ . \tag{4.2.73}$$

Notice that all the blocks corresponding to the operators $[\phi\phi]_{n,J}$ with dimensions $\Delta = 2\Delta_\phi + 2n + J$ do not appear in the momentum space OPE, and these are the operators which also do not contribute to the dispersion relation as given in (4.2.41).

In general, up to exponentially suppressed corrections at small momenta, the momentum space correlator can be transformed back to position space by performing an inverse Fourier transform in flat space, followed by a Poisson resummation to lift the result to the thermal manifold:

$$g_{\text{pert}}(\tau, x) = \sum_{m=-\infty}^{\infty} \frac{1}{(2\pi)^d} \int_{\mathbb{R}^d} \mathrm{d}\omega\, \mathrm{d}^{d-1}\vec{k}\ g(\omega, \vec{k})\ e^{i(\tau+m)\omega + i\vec{k}\cdot\vec{x}} \ . \tag{4.2.74}$$

This final expression for the two-point function closely resembles the generalized method of images introduced in (4.2.56). For the GFF and Virasoro primaries considered in 4.2.2, we compute the corresponding momentum-space thermal blocks and compare them to the dispersion relation results computed previously.

GFF in momentum space. We compute the contributions of the momentum space conformal blocks to the momentum space correlator by using (4.2.70). Out of all the operators that are contributing to the OPE (4.1.21), only the identity operator has a non-zero contribution in momentum space:

$$\tilde{f}_{0,0}(\omega_n, \vec{k}) = \frac{4\pi^2}{(k^2 + \omega_n^2)} \ . \tag{4.2.75}$$

In particular, exponential corrections e^{-k} are not present, since the theory is free. As a check, we transform the $4d$ momentum-space correlator back to position space, expecting to recover the exact known result. To do so we perform the four-dimensional inverse Fourier transformation on flat space $\mathbb{R}^4$, followed by a Poisson resummation to recover the result on $S^1_\beta \times \mathbb{R}^3$. The result is

$$g(\tau, x) = \frac{\pi}{2x} \left[\coth(\pi(x + i\tau)) + \coth(\pi(x - i\tau))\right] \ , \tag{4.2.76}$$

which coincides with (4.2.61) when translated into $z, \bar{z}$ coordinates.

Virasoro primary with $\mathbf{\Delta_\phi = 1}$ in momentum space. In momentum space, the only non-trivial contributions come from the identity operator and the operators obeying the condition $\Delta = J$. In this case, the Fourier thermal blocks read

$$\tilde{f}_{0,0}(\omega_n, k) = -\frac{1}{2}\pi \left[\log\left(k^2 + \omega_n^2\right) + 2\gamma_E - 2\log 2\right] \ , \tag{4.2.77}$$

$$\tilde{f}_{\Delta,\Delta}(\omega_n, k) = 2^{\Delta-1}\pi\Gamma(\Delta)\frac{1}{(k + i\omega_n)^\Delta} \ . \tag{4.2.78}$$

Summing over all these contributions by inserting the correct OPE coefficients only gives us the momentum space OPE contributions:

$$\tilde{g}_{\text{OPE}}(\omega_n, k) = -2\tilde{f}_{0,0}(\omega_n, k) - 2\sum_{\Delta=2}^{\infty} \text{Li}_{-1}(\Delta)\tilde{f}_{\Delta,\Delta}(\omega_n, k) \ . \tag{4.2.79}$$

We can perform the sum over all twist-zero operators above. The sum over these operators diverges, nonetheless it is possible to perform the Borel transformations and Laplace transform back the result: this procedure results in a regularization of the sum over the twist zero operators.

We conclude that the momentum space OPE contribution of the two-point function is given by

$$\tilde{g}_{\text{OPE}}(\omega_n, k) = \pi \left[\log\left(k^2 + \omega_n^2\right) + 2\gamma_E - 2\log 2 + 1\right]$$

$$- \frac{i(k+2\pi i n)}{4}\psi^{(1)}\left(\frac{1-n}{2}+\frac{ik}{4\pi}\right) - \frac{i(-k+2\pi i n)}{4}\psi^{(1)}\left(\frac{1-n}{2}-\frac{ik}{4\pi}\right) . \quad (4.2.80)$$

On the other hand, the Fourier transform of the full thermal two-point function given in (4.1.30) is

$$\tilde{g}(\omega_n, k) = -\pi\left[\psi^{(0)}\left(\frac{1+n}{2}-\frac{ik}{4\pi}\right)+\psi^{(0)}\left(\frac{1+n}{2}+\frac{ik}{4\pi}\right)\right] , \quad (4.2.81)$$

which also appears in [170]. While (4.2.80) does not capture the non-perturbative corrections at small k, those are captured by the Fourier transform of the generalized method of images in (4.2.81). In contrast, the momentum-space thermal blocks clearly miss these contributions, as expected.

In the theories that admit a perturbative expansion in terms of a small parameter (coupling constant, dimensional regularization parameter ε etc.), we find perfect agreement between the Fourier transform of the momentum-space OPE and the result obtained from the dispersion relation. This agreement holds not only at the level of the full correlator, but also block by block. This is not surprising, given that the momentum-space correlator can itself be expressed in terms of the discontinuity of the position space correlator (see equation (4.5) in [165]).

The distinctive feature of perturbative correlators is the fact that terms of the form e^{-k} cannot appear: any such contribution would originate from diagrams that behave as exponentials of momenta, which would violate locality in quantum field theory. As a consequence, there are non-analytic corrections to the OPE in momentum space, explaining the exact match between the momentum-space OPE and the full correlator reconstructed via the generalized method of images.

When the correlator is considered at the non-perturbative level, corrections of the type e^{-k} may appear either throughf resummations of diagrams or as renormalon/instanton corrections. These contributions do not allow us to have a full control over the momentum space OPE of the correlator, as shown explicitly above for correlators in two dimensions.

Nonetheless, we emphasize that the exact knowledge of the correlator provided by the generalized method of images offers a constructive way to compute the exponential corrections to the OPE blocks. As previously noted, the method of images applied to the inversion of each block $g_{\text{dr}}^{(\mathcal{O})}(r,w)$ can be interpreted as a KMS-symmetric inversion of the contribution from the operator $\mathcal{O}$. In perturbation theory, this quantity coincides — upon Fourier transformation — with the momentum-space OPE block associated with

$\mathcal{O}$. This observation naturally suggests a non-perturbative extension: we propose that the Fourier transform of (4.2.56), applied to a single block, defines the momentum-space OPE block associated with the operator $\mathcal{O}$ beyond perturbation theory. Explicitly, this leads to the following non-perturbative definition of the momentum-space OPE block:

$$\tilde{f}_{\Delta,J}(\omega_n,\vec{k}) = \int_0^1 \mathrm{d}\tau\, e^{i\omega_n\tau} \int_{\mathbb{R}^{d-1}} \mathrm{d}^{d-1}\vec{x}\, e^{i\vec{k}\cdot\vec{x}} \left(\frac{1}{2}\sum_{m=-\infty}^{\infty} g_{\mathrm{dr}}^{(\mathcal{O})}(\tau-m,x) + g_{\mathrm{arcs}}^{(\mathcal{O})}(\tau,x)\right)\,, \tag{4.2.82}$$

where $g_{\mathrm{arcs}}^{(\mathcal{O})}(\tau,x)$ is the contribution of g_{arcs} of the operator $\mathcal{O}$ ($J_{\mathcal{O}} < J_\star$), $\omega_n = 2\pi n$, and where $\tilde{f}_{\Delta,J}$ is not defined as the Fourier transform of the thermal block in the original OPE, but matches it in perturbative theories.

Momentum space and the $\boldsymbol{\tau}$-plane. In (4.2.25), we showed that thermal two-point functions at zero spatial separation can be decomposed into generalized free field correlators. In this way, the correlator admits a block decomposition where each block is individually KMS invariant. This structure is particularly convenient, as it allows us to perform a discrete Fourier transform of each block separately.

Consider the block associated with an operator of conformal dimension Δ

$$g^{(\Delta)}(\tau) = a_\Delta\Big[\zeta_H(2\Delta_\phi-\Delta,\tau)+\zeta_H(2\Delta_\phi-\Delta,1-\tau)\Big]\,. \tag{4.2.83}$$

The discrete Fourier transform of this function yields

$$\tilde{g}_n^{(\Delta)} = a_\Delta\,\frac{\pi\,\sec\left[\frac{\pi(2\Delta_\phi-\Delta)}{2}\right]}{\Gamma(2\Delta_\phi-\Delta)}\,|\omega_n|^{2\Delta_\phi-\Delta-1}\,. \tag{4.2.84}$$

Summing over all contributions, we obtain an expression for the generic Fourier mode

$$\tilde{g}_n = \sum_\Delta \tilde{g}_n^{(\Delta)} = \pi\sum_\Delta a_\Delta\,\frac{\sec\left[\frac{\pi(2\Delta_\phi-\Delta)}{2}\right]}{\Gamma(2\Delta_\phi-\Delta)}\,|\omega_n|^{2\Delta_\phi-\Delta-1}\,. \tag{4.2.85}$$

This equation is the exact analog of (4.2.82) in the case where the correlator is evaluated at zero spatial separation. Indeed, the Fourier coefficients computed here correspond precisely to the spatial-momentum ($\vec{k}$) integral of the momentum-space OPE blocks defined in (4.2.82). This procedure showcases the power of (4.2.25) and its equivalent form (4.2.82), as it allows for the straightforward computation of observables — such as the low-frequency contribution to thermal correlators — that were previously difficult to access.

Interestingly, if we perform the Fourier transform along the shifted imaginary τ direction, corresponding to real time, the Fourier transform is not discrete. Concretely we perform the Fourier transform in t, where $\tau = 1/2 + it$ (see Eq. (4.2) of [171]). In this case, the result for a block associated with conformal dimension Δ corresponds to the two-sided Wightman correlator, given by:

$$\tilde{g}^{(\Delta)}(\omega) = \frac{\pi\, a_\Delta}{\Gamma(2\Delta_\phi - \Delta)} \left[\coth\left(\frac{|\omega|}{2}\right) + \frac{\omega}{|\omega|}\right] |\omega|^{2\Delta_\phi - \Delta - 1} e^{-\frac{\omega}{2}} \,. \tag{4.2.86}$$

This expression differs from the thermal (Matsubara) case due to the absence of periodicity in imaginary time. From this form we can extract the imaginary part of the retarded Green function in frequency space for each operator contributing to the thermal two-point function. It would be interesting to understand the connection of this formula with the quasi-normal modes in holographic theories, as discussed in [171]. Note that in the limit $|\omega| \to \infty$, (4.2.86) reproduces the known OPE limit [169, 171]

$$\tilde{g}^{(\Delta)}(\omega) \sim a_\Delta e^{-\frac{\omega}{2}} |\omega|^{2\Delta_\phi - \Delta - 1} \,. \tag{4.2.87}$$

It would be interesting to extend this formula for the two-point functions at non-zero spatial separation to obtain the Fourier transform $\tilde{g}(\omega, k)$.

4.2.4 Application: $O(N)$ Model

In this section, we begin with a brief introduction to the $O(N)$ model, which plays a central role in the study of critical phenomena and has been realized experimentally in a variety of physical systems. A more comprehensive review can be found in [117, 172–174]. We then apply the dispersion relation techniques developed in the previous sections to the $O(N)$ model, both in the ϵ-expansion and in the large-N expansion.

In their seminal work, Wilson and Fisher [175] investigated three-dimensional critical phenomena by studying the scalar $\lambda\phi^4$ field theory defined in $d = 4 - \epsilon$ dimensions. Remarkably, for $\epsilon \ll 1$, the renormalization-group flow of this theory can be analyzed perturbatively using Feynman-diagram techniques, leading to the existence of a nontrivial fixed point known as the Wilson–Fisher fixed point [176–178]. The critical exponents computed within the ϵ-expansion and subsequently extrapolated to three dimensions exhibit very good agreement with experimental results.[14]

[14] See [179] for a comprehensive treatment of applications and experimental realizations of $O(N)$ models. While experimental studies have primarily focused on leading critical exponents, such as $\eta = 2\Delta_\phi - (d-2)$ and $\nu = \frac{1}{d - \Delta_{\phi^2}}$, more systematic determinations of larger sets of conformal data have been carried out both in $4 - \epsilon$ dimensions [98, 180–183] and in the large-N expansion [184, 185].

The generalization of the $\lambda\phi^4$ theory to a vector model with global $O(N)$ symmetry has also proven to be highly fruitful. Owing to universality, such theories are realized in a wide range of phenomenological settings. Beyond statistical spin models, the $N = 1$ Ising case—which we study in detail in Section 4.4—describes second-order phase transitions in uniaxial antiferromagnets, liquid–gas transitions in atomic and simple molecular fluids at the critical point of the phase diagram, and phase transitions in binary fluid mixtures.

The $N = 2$ theory captures the λ-line in helium, as well as phase transitions in XY ferromagnets and in the statistical XY model, while the $N = 3$ theory describes isotropic magnets and the statistical Heisenberg model. Beyond these finite-N cases, one may also study the $O(N)$ model in the large-N expansion. In this limit, the singlet sector has been proposed to admit a dual description in terms of a higher-spin Vasiliev theory [186, 187].

In what follows, we first focus on the Landau–Ginzburg realization and the ϵ-expansion, and subsequently turn to the large-N expansion.

The $O(N)$ model can be defined starting from the Ginzburg–Landau action

$$\mathcal{A} = \int \mathrm{d}^d x \left[\frac{1}{2}(\partial_\mu \phi_i)^2 + \frac{\lambda}{4!}(\phi_i\phi_i)^2 \right] \ , \tag{4.2.88}$$

where $i = 1, \ldots, N$, and the upper critical dimension is $d = 4$. In practice, this means that one possible definition of the O(N) fixed point is as the infrared fixed point of the Lagrangian in (4.2.88) for dimensions in the range $2 < d < 4$. In $d = 4$, the only fixed point is the free theory, corresponding to $\lambda = 0$, whereas in $d = 4-\varepsilon$ the Wilson–Fisher fixed point appears at [188]

$$\frac{\lambda}{4\pi^2} = \frac{3}{N+8}\epsilon + O(\epsilon^2) \ . \tag{4.2.89}$$

For $d < 4$, the interaction term in the Lagrangian (4.2.88) is a relevant operator and triggers an RG flow away from the free theory. For $\epsilon \ll 1$, the theory can be studied perturbatively. However, far from $d = 4$ (that is, for $\epsilon \sim 1$), the theory becomes strongly coupled, and in general it is very difficult to predict either zero-temperature or finite-temperature observables in the physical dimension $d = 3$.[15] In the following, we focus on the ϵ-expansion and defer the study of strongly coupled three-dimensional theories to Section 4.4.

[15] For $N = 1, 2, 3$, numerical bootstrap results are available in [148, 189].

A major simplification arises in the limit $N \to \infty$, where the action (4.2.88) becomes

$$\mathcal{A} = \int \mathrm{d}^3 x \left[\frac{1}{2}(\partial_\mu \phi_i)^2 + \frac{1}{2}\sigma(\phi_i\phi_i) - \frac{\sigma^2}{4\lambda} \right] \ , \tag{4.2.90}$$

with σ the Hubbard–Stratonovich field. The critical point is located at $\lambda \to \infty$, so the last term is suppressed at large N. This theory is free and massive, with $\langle\sigma\rangle_\beta$ playing the role of an effective mass. To compute the effective thermal mass we consider the path integral formalism [185, 190, 191], the partition function after integrating out the ϕ field takes the following form,

$$Z[\sigma] = \int \mathcal{D}\sigma e^{-\frac{N}{2}\log\det\left(-\partial^2+\sigma\right)} \tag{4.2.91}$$

$$\mathcal{F}(\sigma) = \frac{1}{2}V(\mathbb{R}^2)\sum_{n=-\infty}^{\infty}\int \frac{d^2p}{(2\pi)^2}\log\left(\left(\frac{2\pi n}{\beta}\right)^2 + p^2 + \sigma\right) \tag{4.2.92}$$

where $\mathcal{F}(\sigma) = -\frac{1}{\beta}\log Z[\sigma]$, then we compute

$$\frac{d\mathcal{F}(\sigma)}{d\sigma} = -\frac{V_2}{4\pi}\log\left(2\sinh\frac{\beta\sqrt{\sigma}}{2}\right) \tag{4.2.93}$$

by extremizing $\mathcal{F}$ we can find the one-point function of σ at the critical point given as

$$\langle\sigma\rangle_\beta = m_{\text{th}}^2 = \beta^{-2}\left[2\log\left(\frac{1+\sqrt{5}}{2}\right)\right]^2 + O\left(N^{-1}\right) \ . \tag{4.2.94}$$

and conclude that

$$\mathcal{F}_{3d \text{ large N}} = -V_2\beta^{-2}\frac{4}{5}\frac{\zeta(3)}{2\pi} = \frac{4}{5}\mathcal{F}_{\text{free}} \ . \tag{4.2.95}$$

Both the $O(N)$ model in the ϵ-expansion and in the large-N expansion contain towers of double-twist operators,

$$[\phi\phi]n, J = \phi\Box^n\partial\mu_1\cdots\partial_{\mu_J}\phi \ , \qquad \Delta = 2\Delta_\phi + 2n + J + \gamma, \tag{4.2.96}$$

whose anomalous dimensions γ receive corrections at order ϵ or $1/N$. In addition, in the large-N expansion, the presence of the Hubbard–Stratonovich field leads to a tower of scalar operators,

$$\sigma^m; , \qquad \Delta = 2m + O\left(\frac{1}{N}\right) \ . \tag{4.2.97}$$

By using the spectra of these two realizations of the $O(N)$ model as input, we compute thermal two-point functions via dispersion relations.

Dispersion relation applied to ε-expansion. Here, we bootstrap the two-point function $\langle\phi\phi\rangle_\beta$ at first order in the parameter ε. This operator does not receive an anomalous contribution at this order and the scaling dimension corresponds to the free point

$$\Delta_\phi = 1 - \frac{\varepsilon}{2} + O(\varepsilon^2) \ . \tag{4.2.98}$$

One can perform an ε-counting of the two and three-point functions to convince ourselves that the only operators relevant at first order are the identity $\mathbb{1}$, the higher-spin currents $[\phi\phi]_{0,J}$ and the operator $[\phi\phi]_{1,J}$.[16] The latter classically corresponds to $\phi\partial^J\Box\phi$: at the free point, i.e., the $d=4$, equation of motion makes them zero vectors in the Hilbert space of the theory. Nonetheless the equations of motion for the O(N) model give $\phi\partial^J\Box\phi \sim \lambda\phi\partial^J\phi^3 \sim \varepsilon\phi\partial^J\phi^3$, recalling that the critical value of the quartic coupling is proportional to ε. Because of equations of motion, operators of the type $[\phi\phi]_{n,J}$ for $n>1$ will only appear at higher order in ε.

The last ingredient that we need to consider is the anomalous dimension. Due to the fact that OPE coefficients for $[\phi\phi]_{1,J}$ start at order $O(\varepsilon)$, we only need to consider the corrections to the operators of $[\phi\phi]_{0,J}$. In fact, only the operator ϕ^2 (corresponding to $[\phi\phi]_{0,0}$) receives an anomalous contribution at this order, meaning that most of the terms in (4.2.25) and (4.2.56) will simply vanish [172, 173].

Note that it is also possible to calculate the correlator directly through Feynman diagrams. We performed this analysis in Appendix B of [3] to compare with our bootstrap result.

The complex τ-plane in ϵ-expansion. We first test (4.2.25). Due to the ε-counting above, the two-point function in complex τ-plane consists of only two contributions:

$$g(\tau) = g^{(\mathbb{1})}(\tau) + g^{(\phi^2)}(\tau) \ . \tag{4.2.99}$$

The identity contribution is simple and is again given by

$$g^{(\mathbb{1})}(\tau) = \zeta_H\left(2-\varepsilon,\tau\right) + \zeta_H\left(2-\varepsilon,1-\tau\right) \ . \tag{4.2.100}$$

The contribution of ϕ^2 is new and corresponds to

$$g^{(\phi^2)}(\tau) = \zeta_H\left(-\gamma_{\phi^2},\tau\right) + \zeta_H\left(-\gamma_{\phi^2},1-\tau\right) = -a_2^{(0)}\gamma_{\phi^2}\log\left[\frac{\csc(\pi\tau)}{2}\right] + O(\varepsilon^2) \ , \tag{4.2.101}$$

where $a_2^{(0)}$ corresponds to the coefficient a_2, i.e., a_Δ with $\Delta=2$, in the $4d$ free theory, while γ_{ϕ^2} refers to the anomalous dimension of the operator ϕ^2 at first order in ε, which

[16] See for instance Section 2.1 of [192] for a detailed counting.

is known to be [117, 172]

$$\gamma_{\phi^2} = \varepsilon \frac{N+2}{N+8} \,. \tag{4.2.102}$$

The correlator obtained differs from the free correlator in $d = 4 - \varepsilon$ as

$$g(\tau) - g_{\rm free}(\tau) = -a_2^{(0)} \gamma_{\phi^2} \log \left[\frac{\csc(\pi\tau)}{2} \right] + O(\varepsilon^2) \,. \tag{4.2.103}$$

This matches exactly the diagrammatic computation presented in Appendix D in [3] up to a constant which should be considered as arcs.

Non-zero spatial separation in ϵ-expansion. Equation (4.2.61) already presents the contribution of the identity block to $g_{\rm dr}$ for any value of Δ_ϕ and any spacetime dimension. Separating the first order in ε, we have

$$g_{\rm dr}^{(\mathbb{1})} = \frac{(z\bar{z}+1)}{(z^2-1)\,(\bar{z}^2-1)} \log \left[\frac{(z-1)(\bar{z}-1)}{z\bar{z}} \right] + \frac{1}{(z+1)\,(\bar{z}+1)} \left[\tanh^{-1}(z) + \tanh^{-1}(\bar{z}) \right] \,. \tag{4.2.104}$$

The only new contributions come from ϕ^2. The calculation of the discontinuity is straightforward:

$$\text{Disc}[\phi^2] = i\pi\, \gamma_{\phi^2}\, z\bar{z}\, \Theta(\text{Re}(\bar{z}) - 1) \,. \tag{4.2.105}$$

The integration against the kernel is again non-trivial but can be performed, as in the free case, switching to (w, r) coordinates and expanding order by order in r, from which we can guess the full closed form. The result is

$$g_{\rm dr}^{(\phi^2)} = \frac{1}{2} a_{\phi^2}^{(0)} \gamma_{\phi^2} \left[\log(1-z^2) + \log(1-\bar{z}^2) \right] \,, \tag{4.2.106}$$

where $a_{\phi^2}^{(0)}$ is the thermal OPE coefficient at order $O(\varepsilon^0)$. We can expand these results in thermal blocks, and obtain the OPE coefficients given in Table 4.4.

Let us further observe that by solving the KMS condition (4.2.6), one also finds that

$$a_{\phi^2}^{(0)} = \frac{2\varepsilon}{\varepsilon - \gamma_{\phi^2}} \,. \tag{4.2.107}$$

This equation is, however, not consistent with the previous findings: $a_{\phi^2}^{(0)}$ is a free theory quantity that should not depend on γ_{ϕ^2}. We interpret this result as a consequence of the fact that contributions to ϕ^2 appear in the arcs, and therefore it has to be treated separately.

Table 4.4: *Thermal OPE coefficients in the OPE between the two fundamental scalars in the free theory computed by expanding the exact correlators in blocks, using the dispersion relation (DR), generalized method of images (GMI), which matches the results of the Lorentzian inversion formula (LIF) by computing the discontinuity in the OPE. In the latter cases the only contribution to the discontinuity is given by the identity contribution. It is taken for granted that $J \in 2\mathbb{N}$: odd spin operators have zero one-point functions. The operator ϕ^2 is not included but it is discussed in the main text.*

$\mathcal{O}$	$a_{\mathcal{O}}^{(\text{exact})} = a_{\mathcal{O}}^{(\text{GMI})}$	$a_{\mathcal{O}}^{(\text{DR})}$
$\mathbb{1}$	1	0
$[\phi\phi]_{0,J>2}$	$-2\zeta'(2+J) - \frac{1}{J} a_{\phi^2}^{(0)} \gamma_{\phi^2} \zeta(J)$	$-\frac{1}{J} a_{\phi^2}^{(0)} \gamma_{\phi^2}$
$[\phi\phi]_{1,J}$	$\frac{1}{J+2} \zeta(2+J) a_{\phi^2}^{(0)} \gamma_{\phi^2}$	$\frac{1}{J+2} a_{\phi^2}^{(0)} \gamma_{\phi^2}$

The generalized method of images in ϵ-expansion. We can now perform the sum over images of the dispersion relation as prescribed in (4.2.56). We are only interested in $g(\tau) - g_{\text{free}}(\tau)$ since the free part can be exactly solved in $4-\varepsilon$ dimensions. We perform the sum:

$$\frac{1}{2} \sum_{m=-\infty}^{\infty} g_{\text{dr}}^{(\phi^2)}(z-m, \bar{z}-m) = \frac{a_{\phi^2}^{(0)}}{4} \gamma_{\phi^2} \sum_{m=-\infty}^{\infty} \left[\log(1-(z-m)^2) + \log(1-(\bar{z}-m)^2)\right] \ , \tag{4.2.108}$$

which is strictly speaking divergent on the real axis. It can however be obtained as a result of an analytic continuation. By using the fact that

$$\log(1+(x-m)) = -\left.\frac{\partial}{\partial s} \frac{1}{(1+x-m)^s}\right|_{s\to 0} \ , \tag{4.2.109}$$

we find that the following sum can be regularized via (Hurwitz) ζ-function regularization, and the real part reads

$$\sum_{m=-\infty}^{\infty} \log(1+(x-m)) = -\log\left[\frac{\csc(\pi x)}{2}\right] \ . \tag{4.2.110}$$

Using this result, it is easy to show that the sum (4.2.108) gives the exact same correlator which perfectly agrees with the Feynman-diagram computation in [3], apart from a constant

$$g(z,\bar{z}) - g_{\text{free}}(z,\bar{z}) = \frac{1}{2} \sum_{m=-\infty}^{\infty} g_{\text{dr}}^{(\phi^2)}(z-m, \bar{z}-m) = -\frac{1}{2} a_{\phi^2}^{(0)} \gamma_{\phi^2} \log\left[\frac{\csc(\pi z)\csc(\pi \bar{z})}{4}\right] \ . \tag{4.2.111}$$

This constant can be understood as the contribution of the arc coming from the block of ϕ^2 and cannot be constrained by KMS, as it corresponds to a constant term.

The momentum space interpretation in ϵ-expansion. Similarly to the dispersion relation, at the order $O(\varepsilon^0)$ only the identity operator has a non-vanishing contribution. At the order $O(\varepsilon)$, it was computed in [165] that both the identity and the ϕ^2 operators contribute:

$$\tilde{f}_{0,0}(\omega_n, k) = 4^{\Delta_\phi}\pi^{2-\frac{\varepsilon}{2}}\left(\frac{1}{\Gamma\left(\Delta_\phi\right)}\right)\frac{1}{(k^2+\omega_n^2)^{\Delta_\phi}} \ , \tag{4.2.112}$$

$$\tilde{f}_{2+\gamma_{\phi^2},0}(\omega_n, k) = 4^{2\Delta_\phi+\gamma_{\phi^2}}\pi^{2-\frac{\varepsilon}{2}}\left(\frac{\Gamma\left(2\Delta_\phi+\gamma_{\phi^2}\right)}{\Gamma\left(-\frac{1}{2}\gamma_{\phi^2}\right)}\right)\frac{1}{(k^2+\omega_n^2)^{2\Delta_\phi+\gamma_{\phi^2}}} \ . \tag{4.2.113}$$

Therefore the inverse Fourier transform back to position space gives the contribution

$$\begin{aligned} f_{0,0}(\tau, x) =& \frac{\pi}{2x}\left[\coth(\pi(x+i\tau))+\coth(\pi(x-i\tau))\right] \\ &+\frac{\varepsilon}{4}\sum_{m=-\infty}^{\infty}\frac{\log\left[(\tau-m)^2+x^2\right]+\gamma_E-2-\log\pi}{(\tau-m)^2+x^2}+O(\varepsilon^2) \ , \end{aligned} \tag{4.2.114}$$

while the ϕ^2 operator contributes as follows

$$f_{2+\gamma_{\phi^2},0}(\tau, x) = \frac{\gamma_{\phi^2}}{4}\sum_{m=-\infty}^{\infty}\Big(\log\left[(\tau-m)^2+r^2\right]-2\log 2+2\gamma_E\Big)+O(\varepsilon^2) \ . \tag{4.2.115}$$

We perform the Poisson resummation by using the ζ-function regularization and we match the result coming from the perturbative computation and generalized method of images as given in (4.2.56).

Dispersion relation applied to large N. We now study the large N limit of the O(N) model at finite temperature. The relevant operators in the OPE between two fundamental scalars are the double-twist $[\phi\phi]_{n,\ell}$ and the σ^m operators given in (4.2.96) and (4.2.97),[17] where the spectrum in $d=3$ is given by

$$\Delta_\phi = \frac{1}{2}+O\left(\frac{1}{N}\right) \ , \qquad \Delta_\sigma = 2+O\left(\frac{1}{N}\right) \ . \tag{4.2.116}$$

Moreover, any anomalous dimension of composite operators is suppressed in $1/N$. In the following, we will make use of the golden ratio $\varphi = \frac{1+\sqrt{5}}{2}$.

[17] Due to the equations of motion, we have $\partial^2\phi_i \sim \sigma\phi_i$. As a consequence, degeneracies in the conformal dimension may arise between additional operators and those in the families $[\phi\phi]_{n,\ell}$ and σ^m. For instance, certain operators in the family $[\phi_i\sigma\phi_i]_{0,\ell}$ can be degenerate with operators in the family $[\phi\phi]_{n,\ell}$.

The complex τ-plane in large N. The first step is to understand how the two-point function can be reconstructed in the complex τ-plane. We aim to apply (4.2.25) to the spectrum indicated above. It is useful to recall the identity

$$\zeta_H(2\Delta_\phi - \Delta, \tau) + \zeta_H(2\Delta_\phi - \Delta, 1-\tau) = \sum_{n=-\infty}^{\infty} |\tau + n|^{\Delta - 2\Delta_\phi} \ , \tag{4.2.117}$$

from which we can compute first the sum over operators, and then the sum over images (i.e., over n in the equation above). This strategy turns out to be particularly convenient in our case.

Let us consider the operators σ^m, which are the only ones contributing to the discontinuity. We obtain

$$g(\tau) - \kappa = \sum_{n=-\infty}^{\infty} \sum_{m=0}^{\infty} a_{\sigma^m} |\tau + n|^{2m-1} = \sum_{n=-\infty}^{\infty} \frac{\cosh(m_{\text{th}}|\tau + n|)}{|\tau + n|} \ , \tag{4.2.118}$$

where the thermal coefficients are given by $a_{\sigma^m} = m_{\text{th}}^{2m}/\Gamma(2m+1)$ [146] and the thermal mass is $m_{\text{th}} = \log \varphi^2$ [193]. Notice that in the computation above we identified $\sigma^0 = \mathbb{1}$.

Having computed the sum over operators, we now consider the sum over images. This sum is clearly divergent and needs to be regularized. To do so, we split the hyperbolic cosine into exponentials, perform the sum, and then analytically continue in the exponential variable, rendering the sum convergent. Following this procedure, one can verify that the final result is

$$g(\tau) = \mathrm{B}_{1/\varphi^2}(\tau, 0) + \mathrm{B}_{1/\varphi^2}(1-\tau, 0) \ , \tag{4.2.119}$$

where the incomplete Euler B-function appears. This result is a reformulation of the result presented in [146, 147]. Notice that the equation (4.2.119) should be considered only in the strip $0 < \mathrm{Re}(\tau) < 1$, since this assumption was needed to perform the sum in (4.2.118).

Non-zero spatial coordinates in large N. We now consider the case of non-zero spatial coordinates. To do so, we start from the thermal blocks corresponding to the operators σ^m and compute the outcome of the dispersion relation when inverting a single operator. This gives

$$g_{\text{dr}}^{(\sigma^m)}(z, \bar{z}) = \frac{m_{\text{th}}^{2m}}{\Gamma(2m+1)} \left\{ \frac{1}{[(1-z)(1-\bar{z})]^{\frac{1}{2}-m}} + \frac{1}{[(1+z)(1+\bar{z})]^{\frac{1}{2}-m}} \right\} \ . \tag{4.2.120}$$

The contribution above can be resummed together with the identity contribution. This results in

$$g_{\rm dr}(z,\bar z)=\frac{1}{\sqrt{(1-z)(1-\bar z)}}\coth\left(m_{\rm th}\sqrt{(1-z)(1-\bar z)}\right)\\ +\frac{1}{\sqrt{(1+z)(1+\bar z)}}\coth\left(m_{\rm th}\sqrt{(1+z)(1+\bar z)}\right)\ . \quad (4.2.121)$$

The expansion of the coefficients above gives the large spin contribution to the operators in the OPE. In order to complete the result we need to consider the sum over generalized images.

The generalized method of images and momentum space in large N. Applying the generalized method of images to the result of (4.2.121) requires regularization, as already observed in the case of the O(N) model in the ε-expansion. The regularization appears to be more subtle in the present case. To verify the correctness of the result, it is more efficient to compute the Fourier transform of the images of the individual blocks, and to show that they reproduce the correct massive propagator, with mass given by $m_{\rm th}$.

For a single term corresponding to the family σ^m, we have

$$g^{(\sigma^m)}(z,\bar z)=\frac{m_{\rm th}^{2m}}{2\Gamma(2m+1)}\sum_{n=-\infty}^{\infty}\left[\frac{1}{((1-z-n)(1-\bar z-n))^{\frac{1}{2}-m}}\right.\\ \left.+\frac{1}{((1+z-n)(1+\bar z-n))^{\frac{1}{2}-m}}\right]\ . \quad (4.2.122)$$

This corresponds to the standard method of images for a generalized free field of dimension $\Delta_\phi=1/2-m$. Retaining the appropriate prefactors, the Fourier transform of this expression is

$$\tilde g^{(\sigma^m)}(\omega_n,k)=4\pi(-1)^{m+1}\frac{m_{\rm th}^{2m}}{(k^2+\omega_n^2)^{m+1}}\ . \quad (4.2.123)$$

This coincides with the corresponding block computed using the momentum-space OPE.

In fact, the Fourier transform of the thermal blocks is non-vanishing only for the identity operator and the operators σ^m, whose scaling dimensions are given by $\Delta_{\sigma^m}=2m$. As expected those operators are the same ones contributing to the discontinuity. The corresponding Fourier blocks are [165]

$$\tilde{f}_{\mathbb{1}}(\omega_n, k) = \frac{4\pi}{k^2 + \omega_n^2} \ , \quad \tilde{f}_{\sigma^m}(\omega_n, k) = \frac{4\pi \cos(\pi m)\, \Gamma(2m+1)}{(k^2 + \omega_n^2)^{m+1}} \ . \tag{4.2.124}$$

It is now possible to resum all blocks explicitly, and the final result reads

$$\tilde{g}(k, \omega) = \frac{4\pi}{k^2 + \omega^2 + m_{\text{th}}^2} \ . \tag{4.2.125}$$

This is manifestly the correct propagator, consistent with the Lagrangian in (4.2.90), since $\langle \sigma \rangle_\beta = m_{\text{th}}^2$. Performing the inverse Fourier transform to position space yields

$$\frac{1}{(2\pi)^3} \int_0^\infty \mathrm{d}k\, k^2 \int_0^\pi \mathrm{d}\theta\, \sin\theta\, e^{-ikr\cos\theta}\, \tilde{g}(\omega_n, k) = \frac{e^{-m_{\text{th}} r}}{r} \ . \tag{4.2.126}$$

The full thermal two-point function in position space is therefore given by

$$g(\tau, x) = \sum_{m=-\infty}^{\infty} \frac{e^{-m_{\text{th}}\sqrt{(\tau - m)^2 + x^2}}}{\sqrt{(\tau - m)^2 + x^2}} \ , \tag{4.2.127}$$

which matches the exact result obtained in [146]. As expected, because the $\mathrm{O}(N)$ model at large N is a quasi-free theory, the momentum-space OPE is sufficient to reconstruct the full thermal correlator. The dispersion relation reproduces precisely the same result.

Since the clustering condition is satisfied, note that we also have $g_{\text{arcs}} = 0$, i.e., the problem is fully solved by the generalized method of images. Let us take this example as an opportunity to emphasize that the function g_{arcs}, defined in (4.2.56), is not necessarily equal to the missing low-spin contribution in the dispersion relation before applying the method of images. Indeed, as we have shown here, $g_{\text{arcs}} = 0$. However, in this case the arc contribution appearing in (4.2.37) is non-zero, as explicitly demonstrated in [146, 194]: it contains contributions from scalar operators of the form σ^m.

4.3 Analytic Bootstrap on Holographic CFTs

In this section, we analyze generic holographic setups in the spirit of [195], using dispersion relations as a tool to access bulk physics from CFT data. By inputting the spectrum and OPE coefficients of multi–stress tensor operators, we determine the OPE coefficients of the associated double-twist operators.

An important conceptual result of this analysis is a novel interpretation of KMS-invariant blocks as Witten diagrams in the dual AdS spacetime, providing a direct geometric realization of thermal crossing symmetry. Our main focus will be on black brane backgrounds, where translational invariance allows for a particularly transparent implementation of the dispersion relations. Nevertheless, we briefly discuss how the framework extends to black hole backgrounds at the end of the section. The results presented here are based on [4].

4.3.1 Introduction to the Holographic Setup

The AdS/CFT correspondence provides a powerful framework for understanding large-N, strongly coupled gauge theories and quantum gravity [31, 32, 55]. At its core, the correspondence relates a string theory defined on a spacetime of the form

$$X = \mathrm{AdS}_{d+1} \times M_1^{9-d} \tag{4.3.1}$$

to a CFT living in d dimensions on a manifold M_2, which is identified with the conformal boundary of X. Consistency of the string background requires the internal manifold M_1 to be compact. In the semiclassical limit, this duality is encoded in the equality between the CFT partition function and the bulk string theory partition function, which in the supergravity approximation reduces to

$$Z_{\mathrm{CFT}}(M_2) = \exp(-I_S(X)) \ , \tag{4.3.2}$$

where $I_S(X)$ denotes the on-shell bulk action evaluated on X. The best-understood and most concrete realization of this correspondence for $d = 4$, arises when we take $M_1 = S^5$. In this case, the duality can be stated as

$$\boxed{\mathcal{N} = 4 \text{ SYM with gauge group } SU(N) \text{ and coupling } g_{\mathrm{YM}}}$$

$$\Updownarrow$$

$$\boxed{\text{Type IIB string theory with string length } l_s = \sqrt{\alpha'} \text{ and coupling } g_s}$$

with the string theory propagating on $\mathrm{AdS}_5 \times S^5$, where both factors have a common radius of curvature ℓ, and with N units of the self-dual five-form flux $F_{(5)}$ threading the S^5. In this setting, the dynamical parameters of the two theories are related by

$$g_{\mathrm{YM}}^2 = 2\pi g_s \,, \qquad 2g_{\mathrm{YM}}^2 N = \frac{\ell^4}{\alpha'^2} \,, \tag{4.3.3}$$

so that the large-N, strong 't Hooft coupling limit of the gauge theory corresponds to the classical supergravity regime in the bulk. In practice, it is incredibly hard to perform any checks for this strongest form of AdS/CFT. In fact, all known checks of AdS/CFT are done in some perturbative regime. Concretely, we can state the correspondence in two distinct perturbative ways. For $\lambda = g_{YM}^2 N$[18]:

- Strong form, $N \to \infty$, λ fixed corresponds to classical string theory with $g_s \to 0$, α'/ℓ^2 fixed.
- Weak form, N , $\lambda \to \infty$ corresponds to classical supergravity with $g_s \to 0$ and $\frac{\alpha'}{\ell^2} \to 0$.

Here, we focus on the strong form of the AdS/CFT correspondence. One of its most remarkable features is that it is believed to hold beyond the realm of exact supersymmetry and conformal invariance [55]. A particularly striking manifestation of this robustness arises when the AdS bulk contains a black brane or black hole geometry. In such cases, the dual boundary CFT is driven into a thermal state.

In the presence of black branes, which constitute the primary focus of this section, the boundary geometry takes the form $S^1 \times \mathbb{R}^{d-1}$, corresponding to a CFT at finite temperature on flat space. By contrast, when the bulk geometry contains a black hole, which will be discussed in Section 4.3.5, the boundary geometry becomes $S^1 \times S^{d-1}$, describing a thermal CFT on the sphere.

To set up the analytical bootstrap framework appropriate for black brane and black hole backgrounds, we consider a generic large-N conformal field theory in the sense of [195]. In that work, the authors develop a bottom-up derivation of (sub-)AdS bulk locality starting from general CFT consistency conditions such as unitarity, the operator product expansion, and crossing symmetry, together with a small set of spectral assumptions, rather than relying on an explicit string-theoretic construction.

The central conjecture of [195] is that bulk locality emerges provided the CFT admits a parametrically large parameter N, which controls the hierarchy between the AdS radius

[18] For a ccomprehensive review see [196].

and the string scale, and exhibits a large gap in the spectrum separating a finite set of light single-trace operators from the higher-spin sector, beginning above spin two. Under these assumptions, the leading $1/N^2$ corrections to CFT correlators are shown to be exhaustively captured by local interactions in an effective AdS field theory.

This bottom-up effective field theory perspective on AdS/CFT was subsequently developed in a series of works [197–199], and reached its modern formulation in [200]. There, an additional criterion was identified: the Mellin amplitudes associated with CFT correlation functions must be polynomially bounded. Together, these conditions provide a precise CFT characterization of holographic theories with local bulk duals and form the conceptual foundation for the analytical bootstrap approach adopted in this work.

The connection between AdS/CFT at zero temperature and at finite temperature can be understood through the ETH, as introduced in Section 4.3.1. More concretely, consider a scalar four-point function involving two heavy and two light operators, which can be interpreted as describing a light probe propagating in a background created by a heavy state. In this sense, the heavy operators ϕ_H prepare a highly excited state that effectively behaves as a thermal ensemble,

$$g_{\beta/R}(\tau, x) \sim \langle\, \mathcal{O}_H(\infty)\phi(z,\bar{z})\phi(1)\mathcal{O}_H(0)\,\rangle\,, \tag{4.3.4}$$

where the dimension of the heavy operator Δ_H is taken to be large and $z, \bar{z}$ are flat four-point cross-ratios. $g_{\beta/R}$ refers to the finite-temperature finite-volume correlators which arise in black hole backgrounds. We discuss them more detailly in Section 4.3.5. In the limit where the scaling dimension of the heavy operator satisfies $\Delta_H \sim N$, and at leading order in the expansion in Δ_H/N, the four-point function reduces to the thermal two-point function of the light operators ϕ_L. Thus, the heavy–light correlator provides direct access to finite-temperature physics within a pure-state CFT framework, establishing a bridge between zero-temperature CFT data and thermal correlation functions [201].

The holographic realization of this correspondence has been extensively studied in [201–209]. However, the case in which the dimension of the light scalar operator Δ_ϕ is an integer turns out to be more subtle and technically challenging, and only limited data are currently available [204, 207]. Having analytic expressions for thermal two-point functions may thus prove useful, as they can be directly compared with heavy–heavy–light–light correlator data. This provides an additional motivation to further investigate the thermal two-point function at non-zero spatial separation, where the degeneracy in spin is lifted. In this regime, one could also identify which contributions are perturbative and which are non-perturbative in the large-spin expansion, potentially allowing new predictions for these correlation functions.

In light of the discussion above, we specialize our study to the case of holographic two-point functions in the presence of a black brane background in asymptotic AdS_{d+1} spacetime. We will consider a simplified problem where the gravity dual is given by a free massive scalar field Φ in the bulk, assuming that other matter fields decouple and Φ does not self-interact. This amounts to studying the (Euclidean) action

$$S = \int \mathrm{d}^{d+1}y \sqrt{g}\, (\mathcal{L}_\Phi + \mathcal{L}_{\text{grav}}) + S_{\text{bdry}}\,, \tag{4.3.5}$$

with

$$\mathcal{L}_\Phi = \frac{1}{2} g^{MN} \partial_M \Phi \partial_N \Phi + \frac{1}{2} m^2 \Phi^2\,, \qquad \mathcal{L}_{\text{grav}} = R + \Lambda + \dots\,, \tag{4.3.6}$$

where the ellipses denotes possible higher-derivative curvature corrections and S_{bdry} denotes the Gibbons–Hawking boundary term. Here $y^{M=0,1,\dots,d} = \{z, \tau, \vec{x}\}$. The bulk field ϕ is dual to the scalar operator in the boundary theory. The holographic dictionary relates the mass of the scalar field in AdS to the conformal dimension of the scalar field on the boundary $\phi(\tau, \vec{x})$ through

$$m^2 = \Delta_\phi(\Delta_\phi - d)\,. \tag{4.3.7}$$

Here we set the AdS radius ℓ to unity. The rotationally invariant and stationary metric in Euclidean signature corresponding to a black brane in AdS can be written as

$$\mathrm{d}s^2 = \frac{1}{z^2}\left(\frac{\mathrm{d}z^2}{h(z)} + f(z)\,\mathrm{d}\tau^2 + \mathrm{d}x^2\right)\,. \tag{4.3.8}$$

The asymptotic AdS boundary conditions further constrain the form of the functions $f(z)$ and $h(z)$, in particular

$$f(z) = 1 - f_0 z^d + \dots\ , \qquad h(z) = 1 - h_0 z^d + \dots\ . \tag{4.3.9}$$

The ellipsis are related to higher-derivative curvature corrections and are discussed in Section 4.3.4. In [210] it was shown that conformal invariance on the boundary necessarily imposes $f_0 = h_0$. Restricting (4.3.9) to f_0 corresponds to the case of the AdS-Schwarzschild black brane, for which the horizon z_{h} is related to f_0 and to the inverse temperature of the black brane via

$$f_0 = \frac{1}{z_{\text{h}}^d} = \left(\frac{4\pi}{d\beta}\right)^d\,. \tag{4.3.10}$$

The two-point functions in the boundary theory can be computed by solving the equations of motion for the scalar propagator $\Phi(z,\tau,x)$ in the AdS black brane background, namely,

$$\left(\Box - m^2\right)\Phi(z,\tau,x) = 0\,, \tag{4.3.11}$$

and taking the limit

$$g(\tau,x) = \lim_{z\to 0}\frac{\Phi(z,\tau,x)}{z^{\Delta_\phi}}\,. \tag{4.3.12}$$

Solving this equation analytically in the presence of a black hole background is challenging. We refer to [209, 211, 212] and references therein for further discussions and results. In the following we discuss the spectrum of the OPE $\phi\times\phi$ in the black brane background, as it plays an essential role in our bootstrap method.

Black brane spectrum from gravity. At leading order in $1/C_T$ (with C_T the central charge of the CFT), the gravity action (4.3.5) is effectively classical. This means that quantum gravity effects are absent and the only fields appearing in the bulk are bound states of two scalar fields and multi-particle states of gravitons. On the dual CFT side, the former correspond to the sector of operators appearing in a (generalized) free scalar OPE – namely operators with conformal dimensions $\Delta = 2\Delta_\phi + 2n + J$, corresponding to double-twist (or *double-trace*) operators; the latter to multi-stress tensor operators in the CFT at finite temperature. The expected spectrum appearing in the OPE can therefore be summarized as:

$$\begin{aligned}
&\mathbb{1}: && \Delta = 0,\;\; J = 0\,,\\
&[\phi\phi]_{n,J}: && \Delta_{n,J} = 2\Delta_\phi + 2n + J\,,\\
&[T^n]: && \Delta_n = dn, \quad J_n = 0,2,\ldots,dn/2 \qquad (n\geq 1)\,.
\end{aligned} \tag{4.3.13}$$

As observed in [210], from the bulk perspective the equation of motion (4.3.11) admits a perturbative solution at small values of z, τ, and x by incorporating the structure of the OPE (4.1.5), and in particular the spectrum given in (4.3.13). This procedure is valid only when there is no mixing between double-trace operators and multi–stress tensor operators, which occurs when the scaling dimension Δ_ϕ is non-integer.

To construct the bulk-to-boundary propagator in the black hole background, one must solve the bulk field equation in that geometry. Since obtaining exact analytic solutions in a general black hole background is not feasible, we instead determine the boundary two-point function perturbatively in a short-distance expansion, namely through the OPE. In the limit where the boundary operator insertions approach one another, the corresponding two-point function is expected to be sensitive only to the bulk geometry in the near-boundary region. Consequently, order by order in the expansion, the result depends solely on the near-boundary form of the bulk metric. This expectation is borne out explicitly for the contributions associated with the T^n operators.

This method was applied to obtain the following multi-stress tensor OPE coefficients in four dimensions, assuming no higher-order curvature corrections, i.e., $f_k = h_k = 0$ except $k = 0$:

$$a_{4,2} = \frac{\tilde{f}_0 \Delta_\phi}{120}\,, \tag{4.3.14}$$

$$a_{8,4} = \frac{\tilde{f}_0^2 \Delta_\phi \left(7\Delta_\phi^2 + 6\Delta_\phi + 4\right)}{201600(\Delta_\phi - 2)}\,, \tag{4.3.15}$$

$$a_{8,2} = \frac{\tilde{f}_0^2 \Delta_\phi \left(7\Delta_\phi^3 - 23\Delta_\phi^2 + 22\Delta_\phi + 12\right)}{201600(\Delta_\phi - 3)(\Delta_\phi - 2)}\,, \tag{4.3.16}$$

$$a_{8,0} = \frac{\tilde{f}_0^2 \Delta_\phi \left(7\Delta_\phi^4 - 45\Delta_\phi^3 + 100\Delta_\phi^2 - 80\Delta_\phi + 48\right)}{201600(\Delta_\phi - 4)(\Delta_\phi - 3)(\Delta_\phi - 2)}\,, \tag{4.3.17}$$

$$\vdots$$

where the coefficients are labeled by the conformal dimension and the spin of the operator contributing to the OPE as $a_{\Delta,J}$. We have also defined $\tilde{f}_0 = \beta^d f_0$. These coefficients do not admit a known closed form in terms of the scaling dimensions and spins of the multi-stress tensor operators. The OPE coefficients associated with double-trace operators remain elusive, as one needs to impose additional boundary conditions on the bulk propagator $\Phi(z, \tau, x)$. These results are consistent with the ETH as described above [213]. See for instance [204] for bootstrap results on such correlation functions. In this setup, higher-curvature corrections correspond to $1/\lambda$ corrections. They alter the form of the OPE coefficients but do not induce anomalous dimensions for any operators of the spectrum (4.3.13). Quantum corrections come into play at the order $1/N^2$, with $C_T \sim N^2$ [214, 215].

Note that the OPE coefficients in (4.3.14)-(4.3.17) have poles at specific integer values of Δ_ϕ. This crucial point requires us to read the OPE and (4.2.25) carefully in order to derive the associated correlators. In the following we show how to reconstruct the holographic correlators and how to handle these poles.

We now focus on two-point functions of identical scalars at zero spatial separation and with a spectrum consisting only of operators with integer conformal dimensions. If all conformal dimensions are integer and the corresponding OPE coefficients are finite, then the correlator $g(\tau)$ is analytic except for the Matsubara poles, i.e., poles that are located at $\tau = \beta k$, $k \in \mathbb{Z}$, as illustrated in Figure 4.5. On the other hand, if the OPE coefficients have poles at specific values of Δ_ϕ, then (4.2.25) generates

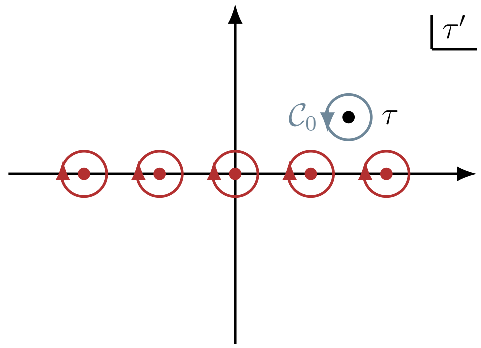

Figure 4.5: *Analytic structure of two-point functions at finite temperature and infinite volume in the complex τ-plane for integer spectrum, for the case in which the OPE coefficients do not contain poles. In this case the correlator contains poles at the locations βk, $k \in \mathbb{Z}$, along the real axis which corresponds to Euclidean time. The corresponding correlator is then given by the sum over the residues. In the holographic case this corresponds to the dominant terms in the OPE.*

derivatives of Hurwitz ζ functions with respect to the first argument. In this case the analytic structure consists of the branch cuts already discussed in [3]. Previously in this section, we showed that both cases are relevant and can be treated separately in the holographic case.

4.3.2 Two-point Functions for Integer Δ_ϕ in 4d

We now study correlators in the black brane background for the case $d = 4$. According to the AdS/CFT dictionary, the parameters of the 4d CFT (the coupling constant $\lambda = g^2_{\mathrm{YM}}N$ and the rank of the gauge group N) are mapped to the parameters of the 5d gravity dual via relations given in (4.3.3). Additionally, Newton's constant behaves as $G_N \sim 1/N^2$. Keeping this map and the OPE data derived from the gravity side in mind, we now turn to the finite temperature CFT perspective. Our approach consists in applying the formula in (4.2.25), using the spectrum specified in (4.3.13). Two distinct cases arise:

- ⋆ **Non-integer external dimension Δ_ϕ:** In this case the expansion in (4.2.25) contains an infinite tower of contributions, corresponding to all multi-stress tensor operators. Since we do not have analytic control over all the (thermal) OPE coefficients of these operators, exact results are not available. Nevertheless, one can approximate their contributions by using the asymptotic values at large dimensions, as first shown in [149, 216]. In Appendix C of [4] we show how to reproduce these results with the methods developed in this thesis;

- ⋆ **Integer external dimension Δ_ϕ:** In this case the expansion in (4.2.25) still contains an infinite number of contributions, but they can be organized into two sets: one finite sum containing the lowest-lying multi-stress tensor operators that satisfy $\Delta < 2\Delta_\phi$ and do not contain poles, and one infinite sum coming from the regularization of the poles. We show in the following that the first term can be evaluated exactly, while the second one can be approximated using the OPE coefficients of the asymptotic model. Doing so introduces spurious poles associated to the bouncing singularities that must be removed by adding arc contributions.

In what follows we focus exclusively on the second case and show how to obtain the correlators. When Δ_ϕ is an integer, solving the equation of motion in (4.3.11) analytically becomes a harder task due to the mixing between double-trace and multi-stress tensor operators. Moreover, as mentioned above, some of the multi-stress tensor OPE coefficients develop poles at integer values of Δ_ϕ. For instance, all the operators of dimension $\Delta = 8$ given in (4.3.15)–(4.3.17) diverge at $\Delta_\phi = 2$. Similarly, $a_{8,2}$ and $a_{8,0}$ diverge for $\Delta_\phi = 3$, while $a_{8,0}$ diverges for $\Delta_\phi = 4$. A similar pattern is observed for higher operators. We identify two possibilities:

- ⋆ The coefficient a_Δ in (4.2.25) is not divergent for the chosen Δ_ϕ. This is the case for a finite number of multi-stress operators satisfying $\Delta < 2\Delta_\phi$. In the OPE, these operators are not degenerate in Δ with any double-trace operator, and the OPE contribution reads

$$a_\Delta \frac{\tau^{\Delta - 2\Delta_\phi}}{\beta^\Delta}\,. \tag{4.3.18}$$

  The dispersion relation converts it into the following contribution to the correlator:

$$\sum_{\Delta < 2\Delta_\phi} a_\Delta \, g_{\text{GFF}}\left(\Delta_\phi - \frac{\Delta}{2}, \tau\right)\,, \tag{4.3.19}$$

  as discussed in Section 4.3.1.

⋆ The coefficient a_Δ *diverges*[19] for the chosen Δ_ϕ, with a pole structure

$$a_\Delta \sim \frac{1}{\Delta_\phi - n}\,, \quad n \in \mathbb{N}\,. \tag{4.3.20}$$

This is the case for an *infinite* number of multi-stress operators of dimension $\Delta \geq 2\Delta_\phi$. In the OPE, these operators are degenerate in Δ with a number of double-trace operators, and the OPE contribution needs to be regularized. It can be shown that this reads:[20]

$$-2\frac{\mathrm{Res}_{\Delta_\phi}\, a_\Delta}{\beta^\Delta}\tau^{\Delta-2\Delta_\phi}\log\left(\frac{\tau}{\beta}\right)\,, \tag{4.3.21}$$

where the residue of a_Δ is taken for the external dimension $\Delta_\phi \to n$. Due to the logarithm, these OPE contributions produce a cut in the complex τ-plane, and consequently a finite contribution to the expansion in GFF correlators. This can be easily determined by employing the following regularization of the generic GFF block:

$$\frac{1}{\Delta_\phi - n}\, g_{\mathrm{GFF}}\left(\Delta_\phi - \frac{\Delta}{2}, \tau\right) \to \frac{1}{\Delta_\phi + \varepsilon - n} g_{\mathrm{GFF}}\left(\Delta_\phi + \varepsilon - \frac{\Delta}{2}, \tau\right)\,. \tag{4.3.22}$$

If we define

$$g^{(1,0)}_{\mathrm{GFF}}\left(\Delta, \tau\right) = \frac{1}{\beta^{2\Delta}}\frac{\partial}{\partial s}\left[\zeta_H\left(s, \frac{\tau}{\beta}\right) + \zeta_H\left(s, 1-\frac{\tau}{\beta}\right)\right]_{s=2\Delta}\,, \tag{4.3.23}$$

then the finite contribution is given by

$$-2\frac{\mathrm{Res}_{\Delta_\phi}\, a_\Delta}{\beta^\Delta}\, g^{(1,0)}_{\mathrm{GFF}}\left(\Delta_\phi - \frac{\Delta}{2}, \tau\right)\,. \tag{4.3.24}$$

Note that even if this scenario escapes the analytic structure of Figure 4.5, its contribution consists nonetheless in (derivatives of) GFF blocks. Such expressions have already been observed in perturbative setups, see for instance [3] for the case of the $\mathrm{O}(N)$ model in the ε-expansion.

In summary, the thermal two-point function of two scalars can be expressed as

$$g(\tau) = \sum_{\Delta<2\Delta_\phi}\frac{a_\Delta}{\beta^\Delta}g_{\mathrm{GFF}}\left(\Delta_\phi - \frac{\Delta}{2}, \tau\right) - 2\sum_{\Delta\geq 2\Delta_\phi}\frac{\mathrm{Res}_{\Delta_\phi}\, a_\Delta}{\beta^\Delta}g^{(1,0)}_{\mathrm{GFF}}\left(\Delta_\phi - \frac{\Delta}{2}, \tau\right) + g_{\mathrm{arcs}}(\tau)\,. \tag{4.3.25}$$

[19]It is worth noting that a similar situation can arise in extremal three-point functions at zero temperature [217]. In this case the logarithms can be reinterpreted as arising from mixing between single- and higher-trace operators [218]. It would be interesting to understand if a similar mechanism exists at finite temperature. We thank Nikolay Bobev for bringing this to our attention.

[20]We thank Simon Caron-Huot for pointing out to us.

In the following, we split the three contributions into a *principal* part, a *regularized* part, and an *arc* part:

$$g(\tau) = g_{\text{pr}}(\tau) + g_{\text{reg}}(\tau) + g_{\text{arcs}}(\tau)\,. \tag{4.3.26}$$

We now focus on applying the dynamical data extracted from the holographic computation to the kinematic result (4.3.25), extracting the principal, the regularized, and the arc contributions.

Principal contributions. As pointed out above, the principal contribution coming from the non-singular $a_{[T^n]}$ contributions does not require any regularization. It can be computed by considering

$$g_{\text{pr}}(\tau) = g_{\text{GFF}}(\Delta_\phi, \tau) + \sum_{n=1}^{\lfloor(\Delta_\phi-1)/2\rfloor} \frac{a_{[T^n]}}{\beta^{4n}} g_{\text{GFF}}(\Delta_\phi - 2n, \tau)\,, \tag{4.3.27}$$

where the GFF correlator is defined as in (4.1.24) and with

$$a_{[T^n]} = \sum_{J=0}^{2n} C_J^{(1)}(1)\, a_{4n,J} = \sum_{J=0}^{2n} (J+1)\, a_{4n,J}\,, \tag{4.3.28}$$

with the coefficients $a_{4n,J}$ given in (4.3.14)–(4.3.17) and more generally in [210].

For completeness we write down the principal contributions to the correlators corresponding to $\Delta_\phi = 1, 2, \dots, 5$ as a function of a_T and $a_{[T^2]}$:

$$\Delta_\phi = 1: \qquad g_{\text{pr}}(\tau) = \frac{\pi^2}{\beta^2}\csc^2\left(\frac{\pi\tau}{\beta}\right)\,, \tag{4.3.29}$$

$$\Delta_\phi = 2: \qquad g_{\text{pr}}(\tau) = \frac{\pi^4}{3\,\beta^4}\csc^4\left(\frac{\pi\tau}{\beta}\right)\left[\cos\left(\frac{2\pi\tau}{\beta}\right) + 2\right]\,, \tag{4.3.30}$$

$$\begin{aligned}\Delta_\phi = 3: \qquad g_{\text{pr}}(\tau) = {}& \frac{\pi^6}{60\,\beta^6}\csc^6\left(\frac{\pi\tau}{\beta}\right)\left[\cos\left(\frac{4\pi\tau}{\beta}\right) + 26\cos\left(\frac{2\pi\tau}{\beta}\right) + 33\right] \\ & + a_T \frac{\pi^2}{\beta^6}\csc^2\left(\frac{\pi\tau}{\beta}\right)\,,\end{aligned} \tag{4.3.31}$$

$$\begin{aligned}\Delta_\phi = 4: \qquad g_{\text{pr}}(\tau) = {}& \frac{\pi^8}{2520\,\beta^8}\csc^8\left(\frac{\pi\tau}{\beta}\right)\left[\cos\left(\frac{6\pi\tau}{\beta}\right) + 120\cos\left(\frac{4\pi\tau}{\beta}\right)\right. \\ & \left. + 1191\cos\left(\frac{2\pi\tau}{\beta}\right) + 1208\right]\end{aligned}$$

$$+\, a_T \frac{\pi^4}{3\,\beta^8}\csc^4\left(\frac{\pi\tau}{\beta}\right)\left[\cos\left(\frac{2\pi\tau}{\beta}\right)+2\right], \tag{4.3.32}$$

$$\begin{aligned}\Delta_\phi = 5: \qquad g_{\rm pr}(\tau) = &\frac{\pi^{10}}{181440\,\beta^{10}}\csc^{10}\left(\frac{\pi\tau}{\beta}\right)\left[\cos\left(\frac{8\pi\tau}{\beta}\right)+502\cos\left(\frac{6\pi\tau}{\beta}\right)\right.\\ &\left.+14608\cos\left(\frac{4\pi\tau}{\beta}\right)+88234\cos\left(\frac{2\pi\tau}{\beta}\right)+78095\right]\\ &+ a_T\frac{\pi^6}{60\,\beta^{10}}\csc^6\left(\frac{\pi\tau}{\beta}\right)\left[\cos\left(\frac{4\pi\tau}{\beta}\right)+26\cos\left(\frac{2\pi\tau}{\beta}\right)+33\right]\\ &+ a_{[T^2]}\frac{\pi^2}{\beta^{10}}\csc^2\left(\frac{\pi\tau}{\beta}\right). \end{aligned} \tag{4.3.33}$$

We explicitly see the implications of (4.3.27): For $\Delta_\phi \geq 3$, the multi-stress tensor operators start contributing with additional GFF blocks. The values of a_T and $a_{[T^2]}$ can be read from (4.3.14)–(4.3.17) with (4.3.28), yielding

$$a_T = \frac{\pi^4\Delta_\phi}{40}, \quad a_{[T^2]} = {a_T}^2\frac{63\Delta_\phi^4 - 413\Delta_\phi^3 + 672\Delta_\phi^2 - 88\Delta_\phi + 144}{126\Delta_\phi(\Delta_\phi-4)(\Delta_\phi-3)(\Delta_\phi-2)}, \tag{4.3.34}$$

from which we obtain explicit results in (4.3.29)–(4.3.33). In principle one can produce the principal part of the correlators for arbitrarily high Δ_ϕ, provided that sufficiently many multi-stress tensor OPE coefficients are known. Note that the limit $\Delta_\phi \to \infty$ in (4.3.27) trivially reproduces the geodesic approximation [219] by excluding all the regularized contributions.[21]

It can be argued from the OPE point of view that the principal contributions, being associated with the lightest operators in the OPE, constitute the *dominant* component of the holographic correlator around $\tau \sim 0$ and $\tau \sim \beta$. This can be tested numerically, as we show at the end of this section. Hence, the principal contribution can be considered a good approximation of the full holographic two-point function. Note however that this term is clearly not complete as it does not capture the log contributions in the OPE nor the correct asymptotic OPE expansion at large frequency.

Regularized contributions. We now come to the analysis of the regularized contributions, encoding the dynamical information of an infinite number of multi-stress tensors:

$$g_{\rm reg}(\tau) = -2\sum_{\Delta\geq 2\Delta_\phi}\frac{\mathrm{Res}_{\Delta_\phi}\, a_\Delta}{\beta^\Delta} g^{(1,0)}_{\rm GFF}\left(\Delta_\phi - \frac{\Delta}{2}, \tau\right). \tag{4.3.35}$$

[21] It is easy to see that the other contributions in (4.3.25) drop in this limit.

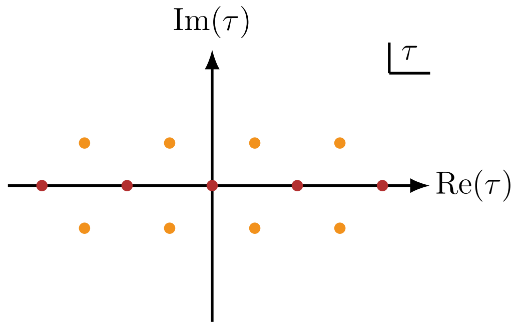

Figure 4.6: *The regularized part of the correlator, $g_{reg}(\tau)$, has additional poles in the complex τ-plane called bouncing singularities. The analytic structure of the regularized part therefore consists of KMS poles (colored red) and bouncing singularities (colored orange). The latter are removed from the full correlator by adding the arc contributions.*

An exact computation can only be performed with the knowledge of an infinite number of coefficients $\mathrm{Res}_{\Delta_\phi}\, a_\Delta$. In principle, we can compute as many OPE coefficients as we desire from the wave equation as in [210]. However, the analytic form (or the closed form) of the multi-stress OPE coefficients for any scaling dimension is currently unknown, to the best of our knowledge.

It is nevertheless possible to produce an *approximated* resummation[22], which reveals the presence of new poles in the strip $0 < \tau < \beta$ in the complex τ-plane and they are depicted in Figure 4.6. These poles correspond precisely to the so-called *bouncing singularities* in AdS [154, 220], which were first identified through the geodesic approximation. Such singularities are unphysical for the Euclidean correlator, in the sense that a generic two-point function should only exhibit the Matsubara poles, as discussed in Section 4.3.1. The presence of the bouncing singularities implies that the contribution from the arcs is no longer constant:[23] Instead, they must cancel the poles, as explicitly shown for the asymptotic model in [149, 221] and reviewed in Appendix C in [4].

Since the bouncing singularities are produced by the resummation of an infinite number of multi-stress tensor contributions, we can substitute the coefficients with their

[22]To refine this approximation, one may replace the OPE coefficients of operators with low scaling dimensions by their exact values as computed in [210], rather than using their large–scaling-dimension approximations. A systematic analysis of this improvement is left for future work.

[23]Note that the appearance of this pole violates the analytic structure of the correlator and thus escapes the theorem presented in [3] to show that the arc terms are constant.

asymptotic behaviour in $\Delta = 4n$, as derived in [221]:

$$a_{4n} = \frac{\pi}{20}(-4)^n n^{2\Delta_\phi - 3} \left(\frac{4^{2\Delta_\phi}\Delta_\phi^2(\Delta_\phi - 1)}{\Gamma\left(2\Delta_\phi + \frac{3}{2}\right)} \right) \csc(\pi\Delta_\phi)\,, \tag{4.3.36}$$

leading to the residue

$$-2\text{Res}_{\Delta_\phi}\, a_{4n} = \frac{1}{40}(-4)^{\Delta_\phi+n+1} n^{2\Delta_\phi - 3} \left(\frac{4^{\Delta_\phi}\Delta_\phi^2(\Delta_\phi - 1)}{\Gamma\left(2\Delta_\phi + \frac{3}{2}\right)} \right) . \tag{4.3.37}$$

We write explicitly the regularized contributions for the correlators with $\Delta_\phi < 4$. The expressions for $\Delta_\phi \geq 4$ are easily obtainable, but we omit them for the sake of clarity:

$$\Delta_\phi = 1: \quad g_{\text{reg}}(\tau) = 0\,, \tag{4.3.38}$$

$$\Delta_\phi = 2: \quad g_{\text{reg}}(\tau) = \sum_{m=-\infty}^{\infty} k_2 \log|m\beta + \tau| \frac{(m\beta+\tau)^4\left(2(m\beta+\tau)^4 + \beta^4\right)}{\beta^4\left(4(m\beta+\tau)^4+\beta^4\right)^2}\,, \tag{4.3.39}$$

$$\begin{aligned}\Delta_\phi = 3: \quad g_{\text{reg}}(\tau) = \sum_{m=-\infty}^{\infty} k_3 \log|\beta m + \tau| \Bigg[&\frac{27(\beta m+\tau)^6}{\beta^3\left(4(\beta m+\tau)^4+\beta^4\right)^4} \\ &+ \frac{16\left(32(\beta m+\tau)^8 + 31(\beta m+\tau)^4\beta^4 + 11\beta^8\right)(\beta m+\tau)^{10}}{\beta^3\left(4(\beta m+\tau)^4+\beta^4\right)^4}\Bigg]\,,\end{aligned} \tag{4.3.40}$$

where

$$k_2 = -\frac{524288}{4725\sqrt{\pi}}\,, \quad k_3 = -\frac{33554432}{75075\sqrt{\pi}}\,. \tag{4.3.41}$$

Note that the correlator corresponding to $\Delta_\phi = 1$ reproduces the free scalar two-point function as expected. In this framework, this can be seen as a consequence of the absence of poles at $\Delta_\phi = 1$ in the OPE coefficients. The expressions for $\Delta_\phi = 2, 3$ exhibit instead new poles $\tau_c = \pm\frac{\beta}{2} \pm i\frac{\beta}{2}$, previously identified in the literature as encoding the bouncing singularities [221]. Their position depends only on the number of spacetime dimensions and not on the conformal dimension of the external operators. Around τ_c we have:

$$g_{\text{reg}}(\tau) \sim \frac{1}{(\tau - \tau_c)^{2\Delta_\phi - 2}} + \text{subleading poles}\,, \tag{4.3.42}$$

The degree of divergence agrees with the prediction of [221], while the number of subleading poles depends explicitly on the value of Δ_ϕ. Moreover, we observe that the (regularized) sum for $\Delta_\phi = 2$, displayed in (4.3.39), exhibits a linear growth along the real-time direction (i.e., for $t = i\tau \to \infty$). This behaviour is inconsistent with the clustering decomposition of the correlator, as expressed in (4.2.48). The discrepancy can be traced back to the approximation used for the OPE coefficients in (4.3.36).

One might attempt to restore the correct large-t behaviour by introducing an additional arc contribution. However, such a term would, by construction, have vanishing discontinuity in the complex plane (except at $|\tau| \to \infty$) and must also satisfy KMS invariance. It is straightforward to verify that no function with these properties exists. Consequently, the only viable resolution is to modify the discontinuity of the two-point function itself. Equivalently, this requires correcting the asymptotic coefficients appearing in (4.3.36) so as to recover the correct late-time behavior.[24]

A detailed analysis of these corrections lies beyond the scope of the present work. Nevertheless, recent progress in this direction has been made in [222, 223], suggesting that a systematic computation of such corrections is a promising avenue for future investigation.

Arc contributions. Arcs are not captured by the dispersion relation and thus by the expansion in GFF correlators. Their contribution can be fixed by imposing the full correlator to satisfy the analytic structure and then invoking the uniqueness of the correlator, as explained in Section 4.3.1. Indeed, it was proven in Appendix A of [3] that if the two-point function satisfies all the analytic structure expected by the thermal correlator, then the correlator is fixed up to a real constant; the clustering property then fixes this constant. The problem of computing the arcs is therefore well-posed.

In the analysis of the regularized contributions, we highlighted how the infinite tower of multi-stress tensor operators generates an extra set of poles in the complex τ-plane. As shown in [216] and reviewed in Appendix C in [4] for the case of half-integer Δ_ϕ, it is natural to take as a candidate for the arcs the sum over images of the bouncing singularity pole. This appears to be the only possibility to restore the correct analytic properties of the two-point function.

The regularized contribution behaves as follows in the neighbourhood of the bouncing singularity pole $\tau_c = \frac{\beta}{2}(1+i)$:

$$g_{\text{reg}}(\tau) \sim -\sum_{\ell=1}^{2\Delta_\phi-2} \frac{\alpha^{(\ell)}_{\Delta_\phi}}{\beta^{2\Delta_\phi-\ell}} \frac{1}{(\tau-\tau_c)^\ell} + \text{regular}\,, \tag{4.3.43}$$

[24] For example, including a subleading $1/n$ correction in (4.3.36) appears to be sufficient to restore the correct large-t asymptotics.

while similar poles also appear in $\overline{\tau}_c$ with complex conjugate coefficients, $\overline{\alpha}^{(\ell)}_{\Delta_\phi}$, as well as in all the images of the strip $0 < \tau < \beta$. Here the $\alpha^{(\ell)}_{\Delta_\phi}$ are constants determined by the regularized contribution discussed before. Therefore, in order to cancel the poles we need to consider[25]

$$h(\tau) \sim \sum_{\ell=1}^{2\Delta_\phi-2} \sum_{m=-\infty}^{\infty} \frac{\alpha^{(\ell)}_{\Delta_\phi}}{\beta^{2\Delta_\phi-\ell}} \frac{1}{|\tau + m - \tau_c|^\ell} + (\tau_c \to \overline{\tau}_c \ , \ \alpha^{(\ell)}_{\Delta_\phi} \to \overline{\alpha}^{(\ell)}_{\Delta_\phi}) \, . \tag{4.3.44}$$

We recognize in this expression the definition of the GFF correlators, however shifted by τ_c. We thus have

$$h(\tau) = \frac{1}{\beta^{2\Delta_\phi}} \sum_{\ell=1}^{2\Delta_\phi-2} \alpha^{(\ell)}_{\Delta_\phi} \, g_{\mathrm{GFF}} \left(\frac{\ell}{2}, \tau - \tau_c \right) + (\tau_c \to \overline{\tau}_c \ , \ \alpha^{(\ell)}_{\Delta_\phi} \to \overline{\alpha}^{(\ell)}_{\Delta_\phi}) \, . \tag{4.3.45}$$

Note that, because of the shift $\tau \to \tau_c$, we need to express these GFF correlators in terms of Hurwitz ζ functions, valid in the strip $\mathrm{Re}(\tau) \in (0, \beta)$, with more attention. In particular we consider the arc contributions to be given by the manifestly parity-invariant combination of the expression (4.3.45)

$$g_{\mathrm{arcs}}(\tau) = h(\tau) + h(-\tau) \, , \tag{4.3.46}$$

where the purpose of the second term is to take into account all the poles in $\tau \in (-\beta, \beta)$ and images thereof.

This method provides closed forms for the arc contributions for arbitrary Δ_ϕ. In particular, the only relevant quantities to determine the arcs are the coefficients $\alpha^{(\ell)}_{\Delta_\phi}$. We give here the coefficients relevant for $\Delta_\phi < 4$:

$$\alpha_2^{(1)} = -\frac{2048\,(1+i)}{4725\sqrt{\pi}} \left(-1 + 3\log\tau_c\right) \ , \qquad \alpha_2^{(2)} = \frac{2048\, i}{4725\sqrt{\pi}} \log\tau_c \, , \tag{4.3.47}$$

$$\begin{aligned} \alpha_3^{(1)} &= \frac{8192\,(1-i)}{3003\sqrt{\pi}} \left(-3 + 5\log\tau_c\right) \ , \qquad & \alpha_3^{(2)} &= \frac{8192}{75075\sqrt{\pi}} \left(-27 + 61\log\tau_c\right) \ , \\ \alpha_3^{(3)} &= \frac{8192\,(1+i)}{25025\sqrt{\pi}} \left(-1 + 4\log\tau_c\right) \ , \qquad & \alpha_3^{(4)} &= -\frac{8192\, i}{25025\sqrt{\pi}} \log\tau_c \ . \end{aligned} \tag{4.3.48}$$

To conclude this discussion, we observe that the leading pole depends only on the asymptotic value of the OPE coefficients $a_{[T^n]}$. In other words, we expect this contribution in the arcs to remain the same even if the regularized contributions are modified to account for the exact coefficients. We reserve to future work a systematic analysis of how corrections of the OPE coefficients affect the subleading poles.

[25]It is worth highlighting that the absolute value holds on the real axis only, while the outcome of the resummation is analytically continued to the whole complex τ-plane.

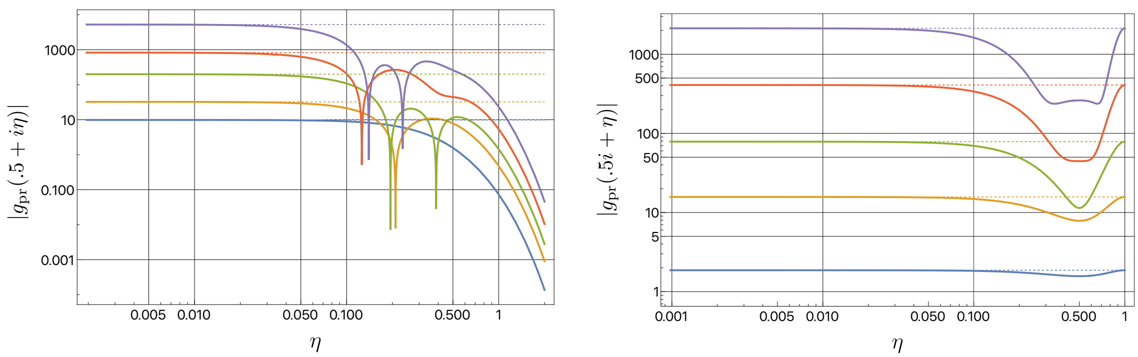

Figure 4.7: *Analysis of the boundedness conditions* (4.2.20)*–*(4.2.21) *for the principal contributions and* $1 \leq \Delta_\phi \leq 5$*.* ***Left:*** *Absolute value of* $g_{pr}(\tau)$ *evaluated along the line* $\tau = 1/2 + i\eta$*. They are consistently bounded by their values on the real axis.* ***Right:*** *Absolute value of* $g_{pr}(\tau)$ *for the same range of* Δ_ϕ*, evaluated along the line* $\tau = \eta + i/2$*. They are consistently bounded by their values on the imaginary axis. Both panels use log–log scaling with* $\beta = 1$ *without loss of generality. Note that these terms obey the KMS condition by construction as we vary the real part of* τ *and this generates bumps in the log-log scale.*

The results above are expected to represent an approximation for the holographic correlators at finite temperature. Since the OPE consistency, the KMS condition, and the required analytic properties are built-in by construction, the only non-trivial bootstrap check is the boundedness condition in (4.2.21) and (4.2.20). Figure 4.7 shows the behavior of the principal contribution for different Δ_ϕ along the imaginary axis for $\mathrm{Re}(\tau) = 1/2$ and along the real axis for $\mathrm{Im}(\tau) = 1/2$. In both cases, the boundedness is surprisingly satisfied for all values of $\mathrm{Im}(\tau)$and $\mathrm{Re}(\tau)$ respectively, in spite of ignoring the regularized and arc contributions. Figure 4.8 shows the behavior of the full correlator for $\Delta_\phi = 3$. It reveals that the approximated result does not satisfy the boundedness condition (4.2.20), which can again be interpreted as an effect of the asymptotic approximation of the OPE coefficients.[26]

Furthermore, we argue that the sum rules derived in [147] and successfully applied in [148, 149, 216] are automatically satisfied by the holographic correlators studied in this section. As a result, the OPE coefficients of the multi-stress tensor operators remain input data of the problem. The argument is the following. Consider, as an example in which the sum rules are predictive, a strongly-coupled theory such as the $3d$ Ising model. In this case, one is allowed to expand the correlator in terms of GFF blocks, as we do in this thesis; however, they would immediately encounter spurious

[26]This violation was already observed in [149] for non-integer Δ_ϕ.

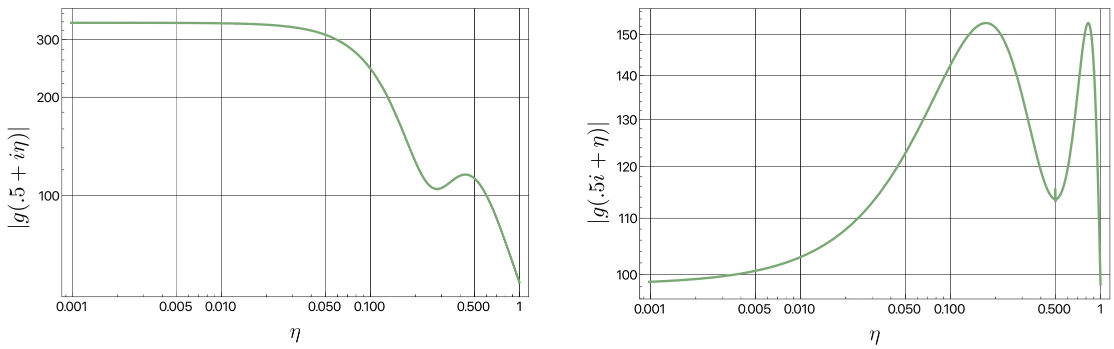

Figure 4.8: *Analysis of the boundedness conditions (4.2.20)–(4.2.21) for the approximated correlator with $\Delta_\phi = 3$.* ***Left:*** *Absolute value of $g(\tau)$ evaluated along the line $\tau = 1/2 + i\eta$. The correlator is consistently bounded by its values on the real axis.* ***Right:*** *Absolute value of $g(\tau)$ evaluated along the line $\tau = \eta + i/2$. The correlator is not bounded by its values on the imaginary axis. We associate this inconsistency with the fact that we use the asymptotic value of the OPE coefficients instead of their exact values. Both panels use log–log scaling with $\beta = 1$ without loss of generality.*

contributions associated with the classical, i.e., without anomalous dimensions, double-twist operators. These operators are excluded from the OPE spectrum, which is an input of the problem. Eliminating these unphysical terms requires tuning the thermal OPE coefficients to specific values – this is an alternative way of explaining the logic underlying [148]: in fact, these specific values constitute the solutions of the sum rules for the given spectrum. An even clearer illustration arises in the O(N) model at large N: the GFF expansion naturally generates a contribution from the operator ϕ^2 with dimension $\Delta_{\phi^2} = 1$, which is absent from the correct spectrum and must instead be replaced by the Hubbard–Stratonovich field σ with $\Delta_\sigma = 2$. Only a precise combination of thermal OPE coefficients – or, equivalently, a specific value of the thermal mass m_{th} – cancels the ϕ^2 contribution, enabling one to solve for the correct thermal OPE data (either analytically or numerically).

In contrast, for the holographic correlators studied in this work, the situation is different. The GFF expansion, even when modified to cure the poles in the OPE coefficients of the multi-stress tensor operators, already reproduces all the physical operators in the theory. There is therefore no spurious term to cancel and no fine tuning occurs. This leads to the conclusion that in this case the sum rules are an indeterminate problem. In fact, it is easy to see that there is not a unique solution: While there exist specific values of the coefficients $a_{[T^n]}$ corresponding to the holographic setup, setting $a_{[T^n]} = 0$ still yields a consistent (pure GFF) solution, for example. Hence it is a difficult task

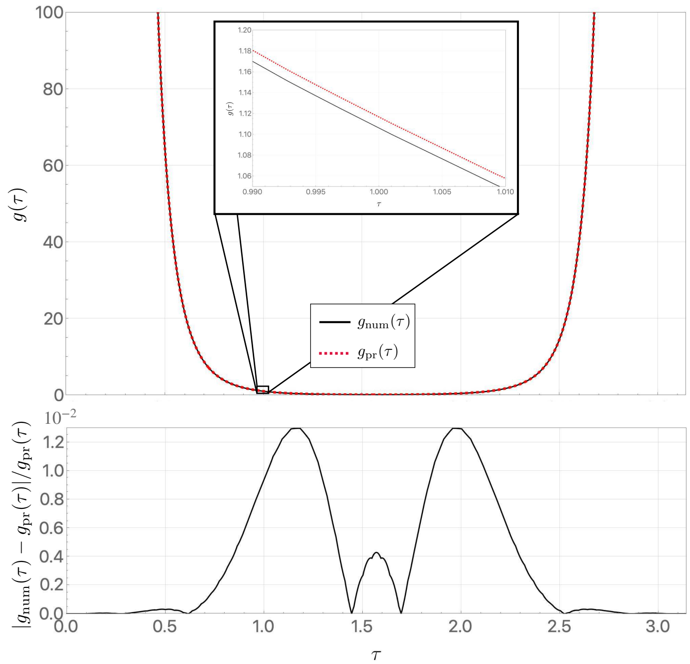

Figure 4.9: *Comparison between the bootstrapped principal part of the two-point function for $\Delta_\phi = 3$, $g_{pr}(\tau)$, and the boundary limit of the numerical solution of the AdS_5 wave equation, $g_{num}(\tau)$. The plot below displays the relative discrepancy between $g_{pr}(\tau)$ and $g_{num}(\tau)$ for $\beta = \pi$. The discrepancy is always below 1.3% for $\tau \in (0, \beta)$.*

to further constrain the thermal OPE coefficients within the present framework. However, we noted that the asymptotic expression for $a_{[T^n]}$ does not produce a consistent correlator for $\Delta_\phi = 2, 3$, as it is either not bounded for large $t = i\tau$ or by its value on the imaginary axis. Additional constraints might emerge by considering correlators at non-zero spatial separation or by including $1/N^2$ corrections beyond the classical large N limit.

Numerical checks for $\boldsymbol{\Delta_\phi = 3}$. Since all bootstrap conditions are satisfied and the solution is expected to be unique [3], given the input, the correlators bootstrapped in (4.3.29)–(4.3.33) should approximately coincide with the solution of the bulk wave equation (4.3.11) in AdS in the appropriate limit. While the latter is difficult to solve analytically in position space (see, e.g., [155, 210, 224] for some analytical results), it can be addressed numerically. In this section, we solve the scalar wave equation in AdS for a bulk field dual to a boundary operator of dimension $\Delta_\phi = 3$. Since the first correlator to involve the stress tensor coefficient in the principal contribution corresponds to $\Delta_\phi = 3$, we focus on this specific example. Further details on this

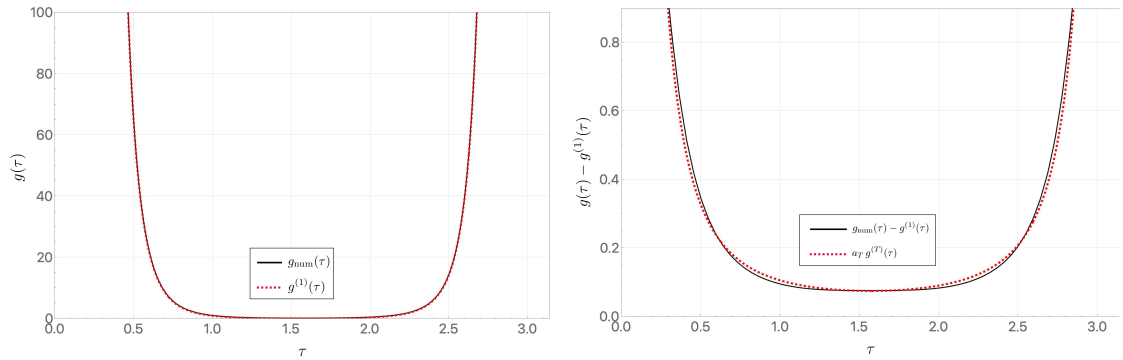

Figure 4.10: ***Left:*** *Comparison between the numerical two-point function $g_{num}(\tau)$ for $\Delta_\phi = 3$ and the identity block $g^{(\mathbb{1})}(\tau)$.* ***Right:*** *Comparison between $g_{num}(\tau)$ after subtraction of the identity block and the stress tensor block $a_T g^{(T)}(\tau)$.*

computation are provided in Appendix D in [4].

Figure 4.9 shows that the principal contribution to the two-point function from our bootstrap construction and the numerical bulk solution differ by at most $\sim 1.3\%$. As argued in Appendix C in [4], this small discrepancy can be attributed to numerical accuracy. We expect that a better numerical estimation of the two-point function could in principle also show the (subleading) regularized and arc contributions presented in Section 4.3.2. For $\Delta_\phi = 3$, the principal contribution is composed of only two blocks: the identity and the stress tensor blocks, as can be seen from (4.3.31). In Figure 4.10 we compare the numerical two-point function with the identity block (left panel), and with the stress tensor block after subtracting the identity contribution (right panel). The apparent agreement supports the fact that the principal contributions (4.3.29)–(4.3.33) represent the dominating component of the holographic correlators.

In Appendix C in [4] we also considered the case of $\Delta_\phi = 1$ as a testing playground, since the prediction for the associated correlator is exact.

4.3.3 Bulk Interpretation through Witten Diagrams

We now discuss an interpretation of our bootstrap results in terms of Witten diagrams. In particular, we show a one-to-one correspondence between our expansion in GFF correlators (regularized to their derivatives, in the case of higher multi-stress tensors contributions) and an expansion of the action around the thermal AdS background for the case of the AdS-Schwarzschild black brane.

Perturbative expansion around thermal AdS. Inspired by the form of our correlators, we perform an expansion of the action around thermal AdS. We define the expansion parameter

$$\varepsilon = \frac{\ell}{\beta}\,, \tag{4.3.49}$$

with ℓ the AdS radius, which we keep explicit to allow dimensional analysis. For small ε, the black brane metric can be expanded in powers of ε^d around the thermal AdS metric as follows:[27]

$$g_{MN} = g_{\mathrm{AdS}\,MN} + \varepsilon^d h^{(d)}_{MN} + \varepsilon^{2d} h^{(2d)}_{MN} + \dots\,, \tag{4.3.50}$$

$$g^{MN} = g^{MN}_{\mathrm{AdS}} + \varepsilon^d h^{(d)\,MN} + \varepsilon^{2d}\left(h^{(d)\,M}{}_P h^{(d)\,PN} - h^{(2d)\,MN}\right) + \dots\,. \tag{4.3.51}$$

Under this expansion the action (4.3.5) takes the form

$$S = S_{\mathrm{thAdS}} + \varepsilon^d \delta S^{(d)} + \varepsilon^{2d}\delta S^{(2d)} + \dots\,, \tag{4.3.52}$$

with the thermal AdS action given by

$$S_{\mathrm{thAdS}} = \frac{1}{2}\int_\beta \mathrm{d}^{d+1}y\,\sqrt{g_{\mathrm{AdS}}}\left(g^{MN}_{\mathrm{AdS}}\partial_M\phi\partial_N\phi + m^2\phi^2\right)\,. \tag{4.3.53}$$

Here we defined the shorthand notation

$$\int_\beta \mathrm{d}^{d+1}y \;= \int_0^\infty \mathrm{d}z \int_0^\beta \mathrm{d}\tau \int \mathrm{d}^{d-1}x\,. \tag{4.3.54}$$

Notice that in order to use the thermal AdS propagators we have changed the integration boundaries of z to $[0,\infty)$ instead of $[0, z_{\mathrm{h}}]$. This manipulation leaves a residual *non-perturbative* term which we consider later. From the action (4.3.53) we can determine the scalar propagators in the thermal background:

$$\text{Bulk-to-boundary:}\qquad K_\Delta(z_1,\tau_{12},x_{12}) = \sum_{m=-\infty}^{\infty} K^{(\mathrm{AdS})}_\Delta(z_1,\tau_{12}+m\beta,x_{12})\,, \tag{4.3.55}$$

$$\text{Bulk-to-bulk:}\qquad G_\Delta(z_{12},\tau_{12},x_{12}) = \sum_{m=-\infty}^{\infty} G^{(\mathrm{AdS})}_\Delta(z_{12},\tau_{12}+m\beta,x_{12})\,, \tag{4.3.56}$$

which are given in terms of zero-temperature propagators given as

$$K^{(\mathrm{AdS})}_\Delta(z_1,\tau_{12},x_{12}) = \mathcal{C}_\Delta\left(\frac{z_1}{z_1^2+\tau_{12}^2+x_{12}^2}\right)^\Delta\,, \tag{4.3.57}$$

[27] Note that $h^{(d)}$ is traceless.

$$
G_{\Delta}^{(\mathrm{AdS})}(z_{12},\tau_{12},x_{12}) = 2^{\Delta}\tilde{\mathcal{C}}_{\Delta}\xi_{12}^{\Delta}\,{}_2F_1\left(\frac{\Delta}{2},\frac{\Delta+1}{2};\Delta+1-\frac{d}{2};\xi_{12}^2\right)\,, \tag{4.3.58}
$$

Further details about the expansion of the metric at small ε are provided in Appendix E in [4], for simplicity here we present the main ingredients and resulting expressions. The corrections to the action then take the general form

$$
\begin{aligned}
\delta S^{(d)} &= -\frac{1}{2}\int_{\beta} \mathrm{d}^{d+1}y\,\sqrt{g_{\mathrm{AdS}}}\,h^{(d)\,MN}\partial_M\phi\partial_N\phi\,, && (4.3.59)\\
\delta S^{(2d)} &= \frac{1}{2}\int_{\beta} \mathrm{d}^{d+1}y\,\sqrt{g_{\mathrm{AdS}}}\left[\left(\frac{1}{2}h^{(2d)}-\frac{1}{4}h^{(d)}_{MN}h^{(d)\,MN}\right)\left(g^{MN}_{\mathrm{AdS}}\partial_M\phi\partial_N\phi+m^2\phi^2\right)\right.\\
&\quad \left.+\left(h^{(d)\,M}{}_{P}h^{(d)\,PN}-h^{(2d)\,MN}\right)\partial_M\phi\partial_N\phi\right]\,, && (4.3.60)\\
&\ \vdots
\end{aligned}
$$

We can therefore express the boundary thermal correlator perturbatively in ε as

$$
g(\tau,x) = g_{\mathrm{thAdS}}(\tau,x)+\varepsilon^d g_T(\tau,x)+\varepsilon^{2d}g_{[T^2]}(\tau,x)+\ldots\,, \tag{4.3.61}
$$

where the choice of notation $g_{[T^n]}$ will soon be justified. Under this expansion the boundary correlator can be represented conveniently using Witten diagrams. The insertion rules associated with this action can be gathered as follows:

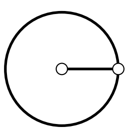
$$
= \ K_{\Delta}(z_1,\tau_{12},x_{12})\,, \tag{4.3.62}
$$

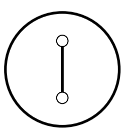
$$
= \ G_{\Delta}(z_{12},\tau_{12},x_{12})\,, \tag{4.3.63}
$$

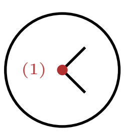

$$
= \ -\frac{1}{2}\int_{\beta}\mathrm{d}^{d+1}y\,\sqrt{g_{\mathrm{AdS}}}\,h^{(d)\,MN}\,\partial_{1M}\partial_{2N}\,, \tag{4.3.64}
$$

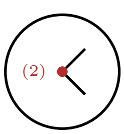

$$
\begin{aligned}
= \ &\frac{1}{2}\int_{\beta}\mathrm{d}^{d+1}y\,\sqrt{g_{\mathrm{AdS}}}\left[\left(\frac{1}{2}h^{(2d)}-\frac{1}{4}h^{(d)}_{MN}h^{(d)\,MN}\right)\left(g^{MN}_{\mathrm{AdS}}\partial_{1M}\partial_{2N}+m^2\right)\right.\\
&\left.+\left(h^{(d)\,M}{}_{P}h^{(d)\,PN}-h^{(2d)\,MN}\right)\partial_{1M}\partial_{2N}\right]\,,
\end{aligned} \tag{4.3.65}
$$

$\vdots$

The explicit expressions for $h^{(d)}$ and $h^{(2d)}$ are given in Appendix E in [4]. Since the action consists only of ϕ^2 vertices, the correlator takes the form

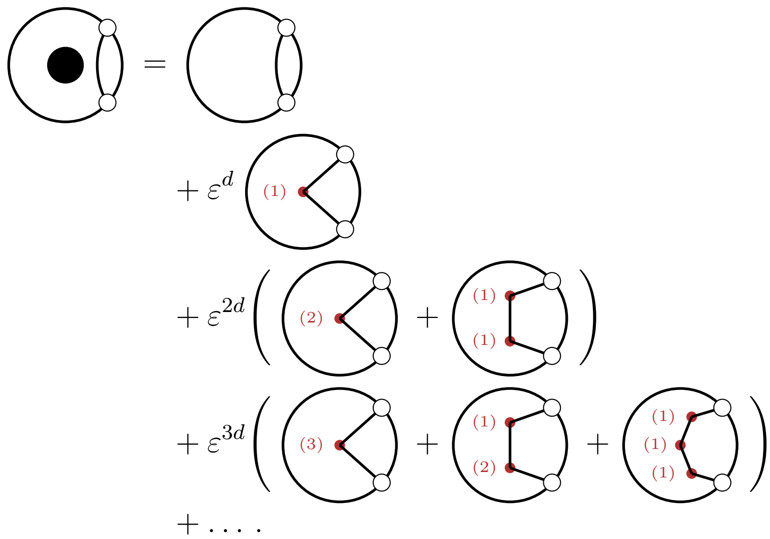

(4.3.66)

The first diagram of each line is a contact diagram, for which the graviton mode is indicated by the number in parenthesis. The other (exchange) diagrams involve bulk-to-bulk propagators and follow from multiplicative terms in the expansion of e^{-S}. Note that no loops are allowed in this expansion.

In Appendix E in [4] we perform an explicit computation of the diagrams up to order ε^{2d}. We observe that the resulting expression matches with the bootstrap result for the principal and regularized terms. We expect that this connection holds for any order in ε^{d} as a consequence of the following observations:

1. Each diagram can be reduced to a *single* sum of images. This can be shown by using the standard trick of shifting the τ-integrals and the sums. Generally, any Witten diagram has a number of sums of images given by[28]

$$\text{number of sums} = \text{number of propagators} - \text{number of vertices}\,, \tag{4.3.67}$$

which is always 1 in this case, as follows from the fact that only ϕ^2 vertices exist;

2. For each order, one can analyze which are the operators that contribute to the zero mode by reading the power of β and assuming that the correlator follows the principles of CFT at finite temperature. It is straightforward to see that, here, the zero mode is given exactly by the multi-stress-tensor contributions, since they

[28]Incidentally, this is also true for Feynman diagrams.

are the only universal operators to have dimension $\Delta = nd$ independently of Δ_ϕ. This means in turn that the zero mode of each order n is given by a sum of the thermal blocks associated to the operators $[T^n]$.

Therefore we conclude that, in this expansion, the n-th order has to be given exactly by

$$g_{[T^n]}(\tau, x) = \sum_{J=0}^{nd/2} a^{(T)}_{nd,J} \sum_{m=-\infty}^{\infty} f_{nd,J}(\tau + m\beta, x)\,, \tag{4.3.68}$$

where $f_{nd,J}(\tau + m\beta, x)$ are the thermal blocks defined through (4.1.5) and $a^{(T)}_{nd,J}$ are multi-stress tensor OPE coefficients. This expression matches the generalized sum of images discussed in [3]. If we set the spatial separation to zero, we recover

$$g_{[T^n]}(\tau) = \frac{a_{[T^n]}}{\beta^{2\Delta_\phi}} \left[\zeta_H\left(2\Delta_\phi - nd, \frac{\tau}{\beta}\right) + \zeta_H\left(2\Delta_\phi - nd, 1 - \frac{\tau}{\beta}\right)\right]\,, \tag{4.3.69}$$

in perfect agreement with our bootstrap framework up to the arc contributions.[29] Hints at this structure were already – directly or indirectly – observed in [149, 210, 224]. It is important to note that this expansion is not *per se* an expansion of the correlator at small temperature; instead it corresponds to an expansion in the graviton field. In fact, each term in (4.3.61) admits its own expansion in powers of β due to the sum of images.

To better understand this statement, let us view the computation from another perspective, namely as an expansion around thermal AdS interpreted as a high-frequency expansion. The effective parameter in the correlators is in fact $\omega z_{\rm h}$, which is here taken to be large, similarly to Section 5.4 of [155]. Perturbatively at large frequencies, one therefore expects to recover the OPE in momentum space [165, 169]. Double-trace operators do not appear in this OPE, in agreement with (4.2.25), and this matches the fact that multi-stress tensor operators are zero modes in the expansion around thermal AdS. This can also be seen by considering the frequency space form of (4.2.25), as discussed in [3]. While the framework of this section provides a holographic interpretation for the expansion in GFF correlators (4.2.25), note that the arc contributions are not captured by this high-frequency expansion. From the connection between the momentum space OPE and the GFF expansion of the correlators, these contributions can be understood as the piece of the correlator that governs the late-time dynamics [225, 226].[30]

[29] The regularized part is also included in this expression after suitably expanding the divergent coefficient multiplying a vanishing GFF block.

[30] We thank Tom Hartman for useful discussions on this point.

Non-perturbative effects and arcs. It is well known that the OPE in momentum space needs to be corrected with non-perturbative contributions, which become relevant at low frequencies while being exponentially suppressed at high frequencies [165, 169]. Since the connection between the momentum space OPE and the dispersion relation is pointed out in [3], here we focus on the relation between the arc contributions and the non-perturbative corrections at small frequencies.

Since the expansion in thermal AdS discussed above admits the interpretation of a high-frequency expansion, we expect these contributions to correspond to non-perturbative effects in that setup. Indeed during the calculation we made the crucial approximation of extending the integration region from z_{h} to ∞ in the Witten diagrams. If z_{h} is large but finite, this approximation is justified because the corrections are exponentially suppressed. More precisely, consider the full action

$$\begin{aligned} S &= \int_0^{z_{\mathrm{h}}} \mathrm{d}z \int_0^\beta \mathrm{d}\tau \int \mathrm{d}^{d-1}x \, \mathcal{L} \\ &= \int_0^\infty \mathrm{d}z \int_0^\beta \mathrm{d}\tau \int \mathrm{d}^{d-1}x \, \left(\mathcal{L}_{\mathrm{thAdS}} + \ldots\right) - \int_{z_{\mathrm{h}}}^\infty \mathrm{d}z \int_0^\beta \mathrm{d}\tau \int \mathrm{d}^{d-1}x \, \mathcal{L} \,. \end{aligned} \tag{4.3.70}$$

The first term corresponds to our calculation, while the second term is difficult to evaluate exactly and encodes the non-perturbative effects at high frequencies. It is possible however to give an estimation of its contribution. The simplest way is to observe that

$$\int \mathcal{D}[\phi] \exp\left(-\int_{z_{\mathrm{h}}}^\infty \mathrm{d}z \int_0^\beta \mathrm{d}\tau \int \mathrm{d}^{d-1}x \, \mathcal{L}\right) \sim e^{-(F_{\mathrm{thAdS}} - F)} \sim e^{-\mathcal{S}} \sim \mathcal{O}\big(e^{-\varepsilon^{d-1}}\big) \,, \tag{4.3.71}$$

where here $\mathcal{S}$ is the entropy of the black brane. This estimation highlights the fact that this contribution is non-perturbative in ε. In other words, the expansion around thermal AdS that reproduces the GFF expansion (4.2.25) does not (perturbatively) take into account horizon effects.

A yet more accurate estimation of the non-perturbative contributions can be obtained by considering

$$\int_{z_{\mathrm{h}}}^\infty \mathrm{d}z \int_0^\beta \mathrm{d}\tau \int \mathrm{d}^{d-1}x \, \mathcal{L} \,, \tag{4.3.72}$$

expanded near the horizon, i.e., at $z \sim z_{\mathrm{h}}$. It is straightforward to estimate the leading order contribution. At this order, the equation of motion reduces to

$$\psi'_{\omega,k}(z) + \frac{\ell^2}{4 z_{\mathrm{h}}} \left(\frac{m^2 \ell^2}{z_{\mathrm{h}}^2} + k^2 + \omega^2\right) \psi_{\omega,k}(z) = 0 \,, \tag{4.3.73}$$

where we have defined

$$\Phi(z,\tau,x) = T\sum_n \int \frac{\mathrm{d}^{d-1}k}{(2\pi)^{d-1}} e^{\omega_n\tau+ikx}\psi_{\omega,k}(z)\,, \quad \omega_n = \frac{2\pi n}{\beta}\,. \tag{4.3.74}$$

The solution of (4.3.73) is

$$\psi_{\omega,k}(z) = \psi_c \exp\left[-\frac{z\ell^2}{4z_{\mathrm{h}}}\left(\frac{m^2\ell^2}{z_{\mathrm{h}}^2} + k^2 + \omega^2\right)\right]\,, \tag{4.3.75}$$

with ψ_c a constant fixed by boundary conditions. The contribution of the bulk-to-boundary propagator given above to the thermal two-point function of the boundary CFT is therefore

$$g_{\mathrm{n.p.}}(k,\omega) \sim e^{-(k^2+\omega^2)}\,. \tag{4.3.76}$$

As a consequence, $g_{\mathrm{n.p.}}$ precisely captures the non-perturbative terms in momentum space as expected from the arguments above. Since the perturbative expansion in ε matches the GFF expansion in (4.2.25), we identify

$$g_{\mathrm{n.p.}}(\tau,x) \;=\; g_{\mathrm{arcs}}(\tau,x)\,. \tag{4.3.77}$$

This gives a novel interpretation of $g_{\mathrm{arcs}}(\tau,x)$ as encoding horizon effects, which are not captured by the GFF expansion.

Since in this work we have been interested in the zero spatial separation limit, an interesting direction, currently under investigation, is the extension of the present analysis to non-zero spatial separation, $x \neq 0$, as proposed in [3]. In this case, we expect $g_{\mathrm{arcs}}(x,\tau)$ to encode extra dynamical information, like the thermal mass of the theory for instance. This expectation can in principle be tested by employing exact momentum-space formulae [209, 211, 212] and/or by developing a more precise version of the near-horizon expansion, which we have only sketched here. We hope to report our results in future work.

4.3.4 Higher-Curvature Corrections

We now conclude our study of the black brane background by considering higher-order curvature corrections. Such extensions may correspond to different types of gravitational theories [227–230] as well as stringy corrections with $\alpha' \sim 1/\sqrt{\lambda}$ as a parameter. In order to preserve conformal symmetry, they can only modify the functions $f(z)$ and $h(z)$ presented in (4.3.9). We parameterize them as an expansion around the black brane metric,

$$f(z) = 1 - f_0 z^4 - f_4 z^8 - f_8 z^{12} - \ldots\,, \tag{4.3.78}$$

$$h(z) = 1 - h_0 z^4 - h_4 z^8 - h_8 z^{12} - \dots\,, \tag{4.3.79}$$

with $f_0 = h_0$ needed as before for consistency with conformal symmetry. There is no such constraint, however, on f_4, h_4, and higher-order terms. It is also important to note that, from the perspective of the thermal CFT, those corrections do not induce anomalous dimensions. Thus only the thermal OPE coefficients are expected to be modified.

In order to obtain the principal contributions to the correlators with modified thermal OPE coefficients, it is sufficient to consider (4.3.29)–(4.3.33) and insert the corrected multi-stress tensor OPE coefficients [210], namely,

$$a_T = \frac{\pi^4 \Delta_\phi}{40}\,, \tag{4.3.80}$$

$$\begin{aligned} a_{[T^2]} = {a_T}^2 &\frac{63\Delta_\phi^4 - 413\Delta_\phi^3 + 672\Delta_\phi^2 - 88\Delta_\phi + 144}{126\Delta_\phi(\Delta_\phi-4)(\Delta_\phi-3)(\Delta_\phi-2)} \\ &- \frac{\Delta_\phi(\Delta_\phi+1)(4\Delta_\phi(5-2\Delta_\phi)\tilde{f}_4 + (\Delta_\phi(\Delta_\phi-4)+24)\tilde{h}_4)}{5040(\Delta_\phi-4)(\Delta_\phi-3)(\Delta_\phi-2)}\,, \end{aligned} \tag{4.3.81}$$

where we set $f_0 = \pi^4/\beta^4$ and defined the dimensionless quantities $\tilde{f}_4 = f_4\beta^8$ and $\tilde{h}_4 = h_4\beta^8$. Note that the first affected coefficients are those of the $[T^2]$ sector, specifically $a_{8,2}$ and $a_{8,0}$, while $a_{8,4}$ belongs to the universal lowest-twist family that depends only on $\tilde{f}_0$. Since a_T depends solely on $\tilde{f}_0$, the correlators for $\Delta_\phi \leq 4$ are identical across all backgrounds. The correlator with $\Delta_\phi = 5$ is the first to contain higher terms ($\tilde{f}_4$ and $\tilde{h}_4$). Correlators with higher Δ_ϕ involve higher and higher corrections $\tilde{f}_k$ and $\tilde{h}_k$; they can be derived systematically following the same procedure. Corrections to the regularized contributions (and consequently, to the arc contributions) can be derived following a similar strategy, even though (as already highlighted before) a full prediction requires the knowledge of an infinite number of OPE coefficients.

4.3.5 Black Hole Background

We now apply the analytic bootstrap framework to holographic thermal correlators in spherically symmetric black hole backgrounds. We first extend the analysis of the analytic properties of thermal two-point functions to the case of correlators at finite temperature and finite volume, namely on the geometry $S^1_\beta \times S^{d-1}_R$, which has seen interesting developments in recent years from a finite temperature point of view [222, 231–237]. We show that the two-point function in the zero spatial separation limit admits an expansion in finite volume GFF correlators, which is the analogue of (4.2.25).

This decomposition is valid for theories whose spectrum contains only operators of integer conformal dimension. We specialize this formula to the study of holographic correlators and obtain analytic results for the principal contribution in the case $d = 4$.

Thermal two-point functions in BH background. We study two-point functions of identical scalar operators at finite temperature and finite volume. More precisely, we consider correlators on the geometry $S^1_\beta \times S^{d-1}_R$. We denote by R the radius of the $(d-1)$-dimensional sphere. As in the infinite volume case it is convenient to define

$$g_{\beta/R}(\tau, x) = \langle\, \phi(0,0)\, \phi(\tau, x)\,\rangle_{\beta/R} \equiv \langle\, \phi(0,0)\, \phi(\tau, x)\,\rangle_{S^1_\beta \times S^{d-1}_R} . \tag{4.3.82}$$

We focus on the limit in which the two operators have zero spatial separation and denote the correlator by $g_{\beta/R}(\tau) \equiv g_{\beta/R}(\tau, 0)$.

In this section we discuss the adaptation of the bootstrap axioms of Section 4.3.1 to the finite volume case.

OPE. The OPE remains valid on the geometry $S^1_\beta \times S^{d-1}_R$ but converges only when $\tau^2 + x^2 < \min(\beta^2, 4\pi^2 R^2)$. In the limit $x = 0$, the two-point function admits the following expansion in thermal blocks:

$$g_{\beta/R}(\tau) = \frac{1}{\beta^{2\Delta_\phi}} \sum_\Delta a_\Delta(\beta/R) \left[\frac{1}{2}\left(\frac{\beta}{R}\right) \operatorname{csch}\left(\frac{\tau}{2R}\right)\right]^{2\Delta_\phi - \Delta} , \tag{4.3.83}$$

with

$$a_\Delta(\beta/R) = \sum_{\mathcal{O}:\, \Delta_\mathcal{O} = \Delta} f_{\phi\phi\mathcal{O}} b_\mathcal{O}(\beta/R) \left(\frac{J!}{2^J (\nu)_J}\right) C_J^{(\nu)}(1) . \tag{4.3.84}$$

The decomposition is justified by the fact that (4.1.3) generalizes as follows [146]:

$$\langle\, \mathcal{O}^{\mu_1 \dots \mu_J}\,\rangle_{\beta/R} = \frac{b(\beta/R)}{\beta^\Delta} \left(e^{\mu_1} \dots e^{\mu_J} - \text{traces}\right) . \tag{4.3.85}$$

Starting from this expression, it is possible to express the OPE similarly to the infinite volume case. Then, using finite volume variables leads to the expansion (4.3.83).

KMS condition. The two-point function of identical scalars satisfies the KMS condition which, associated with time reversal symmetry, reads [238, 239]

$$g_{\beta/R}(\tau) = g_{\beta/R}(\beta - \tau) . \tag{4.3.86}$$

At finite volume there is an additional periodicity coming from the sphere geometry S^{d-1}_R. In this work we focus on correlators at zero-spatial coordinates and thus leave the implication of this condition for future studies.

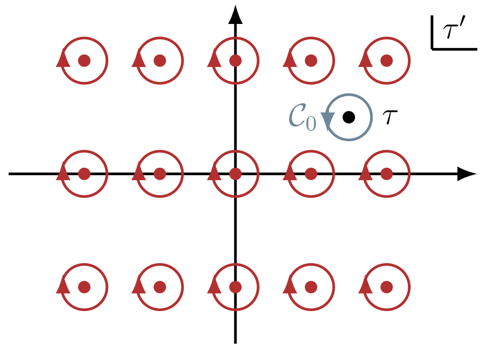

Figure 4.11: *Analytic structure at finite temperature and finite volume for integer spectrum, when the OPE coefficients do not contain poles. Due to the periodicity, poles are now located at every $m\beta$, $m \in \mathbb{Z}$, in the real direction and every $2\pi nR$, $n \in \mathbb{Z}$, in the imaginary direction. The principal part of the correlator is given by the sum of residues of these poles.*

Analytic structure and GFF expansion. In [3] the authors discuss the analytic structure of finite temperature correlators at infinite volume. Here we extend the conclusions to include the case in which the geometry is $S^1_\beta \times S^{d-1}_R$. We focus on the case in which the spectrum consists only of operators of integer dimensions, i.e., we restrict here our analysis to the principal contribution of the correlators, in the sense defined in Section 4.3.2. In the following we describe the associated analytic structure in the complex τ-plane and its consequences.

The restriction to integer conformal dimensions (and no pole in the OPE coefficients) implies that only poles are allowed in the τ-plane. Because of the compact space, the poles are replicated not only along the real τ-axis but also along the imaginary τ-axis, together with their Matsubara images. This can be seen by noticing that the zero-temperature finite volume two-point function is given by

$$\langle \phi(\tau)\phi(0)\rangle_{\mathbb{R}\times S^{d-1}_R} = \left[\frac{1}{2R}\operatorname{csch}\left(\frac{\tau}{2R}\right)\right]^{2\Delta_\phi}\,, \tag{4.3.87}$$

which has poles on the imaginary τ-axis corresponding to UV images located at $i\tau = 2\pi Rk$, $k \in \mathbb{Z}$. Equivalently, this follows from the observation that

$$\mathrm{d}s^2_{\mathbb{R}^d} = \mathrm{d}r^2 + r^2\,\mathrm{d}s^2_{S^{d-1}_R} = \frac{e^{2\tau/R}}{R^2}\left(\mathrm{d}\tau^2 + R^2\mathrm{d}s^2_{S^{d-1}_R}\right) = \frac{e^{2\tau/R}}{R^2}\,\mathrm{d}s^2_{\mathbb{R}\times S^{d-1}_R}\,. \tag{4.3.88}$$

We conclude that the analytic structure of the principal part of thermal correlators at finite volume for integer Δ_ϕ is the one presented in Figure 4.11.

It is now straightforward to apply Cauchy's integral formula to rewrite the correlator as

$$g_{\beta/R}(\tau) = \oint_{\mathcal{C}_0} \frac{\mathrm{d}\tau'}{2\pi i} \frac{g_{\beta/R}(\tau')}{\tau' - \tau}\,, \tag{4.3.89}$$

which can then be expressed as a sum over residues:

$$g_{\beta/R}(\tau) = -\sum_{m=-\infty}^{\infty} \sum_{n=-\infty}^{\infty} \operatorname*{Res}_{\tau'=0} \left[\frac{g_{\beta/R}(\tau')}{\tau' - \tau + m\beta + 2\pi i n R}\right] + g_{\text{arcs}}(\tau)\,. \tag{4.3.90}$$

The next step is to substitute the OPE into this expression, which yields

$$\begin{aligned} g_{\beta/R}(\tau) = &-\frac{1}{\beta^{2\Delta_\phi}} \sum_{\Delta} a_\Delta(\beta/R) \left(\frac{\beta}{2R}\right)^{2\Delta_\phi - \Delta} \sum_{m=-\infty}^{\infty} \sum_{n=-\infty}^{\infty} \operatorname*{Res}_{\tau'=0} \left[\frac{\sinh^{2\Delta_\phi-\Delta}\left(\frac{\tau'}{2R}\right)}{\tau' - \tau + m\beta + 2\pi i n R}\right] \\ &+ g_{\text{arcs}}(\tau)\,. \end{aligned} \tag{4.3.91}$$

The residues reduce to propagators in the complex τ-plane, shifted along both the real and imaginary directions. Moreover, they give a non-zero contribution only for $\Delta \leq 2\Delta_\phi - 1$. After performing the sum over images, we identify each block accompanying an OPE coefficient with a GFF correlator, producing the decomposition

$$g_{\text{pr}}(\tau) = \sum_{\Delta} \frac{a_\Delta}{\beta^\Delta} g_{\text{GFF}}\left(\Delta_\phi - \frac{\Delta}{2}, \tau\right) + g_{\text{arcs}}(\tau)\,, \tag{4.3.92}$$

where the GFF blocks are defined as

$$g_{\text{GFF},\beta/R}(\Delta, \tau) = \frac{1}{\beta^{2\Delta}\Gamma(2\Delta)} \sum_{\ell=1}^{\Delta} \left(\frac{\beta^2}{R^2}\right)^{\Delta-\ell} c(\Delta,\ell) \left[\psi^{(2\ell-1)}_{e^{-\beta/R}}\left(\frac{\tau}{\beta}\right) + \psi^{(2\ell-1)}_{e^{-\beta/R}}\left(1 - \frac{\tau}{\beta}\right)\right]\,, \tag{4.3.93}$$

where $\psi_q^{(n)}(z)$ is the n-th derivative of the q-Polygamma function defined as

$$\psi_q^{(n)}(z) = \frac{\partial^n \psi_q(z)}{\partial z^n}\,, \qquad \psi_q(z) = \frac{\partial}{\partial z} \log \Gamma_q(z)\,, \tag{4.3.94}$$

with $\Gamma_q(z)$ the q-Gamma function.[31] The derivation of the thermal finite volume GFF correlators and their basic properties can be found in Appendix A in [4]. As a consistency check, in Appendix B in [4], we show that the two-point function of lightest scalars in the large N limit of the $3d$ $\mathrm{O}(N)$ model satisfies the expansion in (4.3.92).

The black hole correlators are expected to additionally consist of regularized and arc contributions, as discussed in Section 4.3.2 for the black brane. We reserve the study of these contributions to future work, however we note that there is no apparent obstacle in developing a strategy similar to the one used for the black brane background.

[31]The q-Gamma function can be defined as $\Gamma_q(x) = (1-q)^{1-x} \prod_i \left(1 - q^{i+1}\right)/(1 - q^{i+x})$.

Boundedness conditions. As in the infinite volume case, the correlator is bounded in the complex τ-plane by its value on the real axis,

$$|g(\tau)| \;\geq\; |g(\tau+i\eta)|\,, \qquad \tau,\eta\in\mathbb{R}\,, \tag{4.3.95}$$

and also by its value on the imaginary axis,

$$|g(i\eta)| \;\geq\; |g(\tau+i\eta)|\,, \qquad \tau,\eta\in\mathbb{R}\,. \tag{4.3.96}$$

The proofs are available in the literature for the infinite volume case [3, 154] and can be straightforwardly adapted to the finite volume case.

Clustering condition. At finite volume the clustering condition no longer holds. Additionally the real-time correlators (such as the Wightman correlator) are periodic in $t=i\tau$ and thus the limit $t\to\infty$ is not sufficient to fix the arc contributions. Fixing the arcs is a very interesting problem on its own and we leave this to future work.[32]

Holographic thermal correlators. We consider, as before, a free massive scalar field in the bulk, described by the action (4.3.5), with the difference that the spatial integral is now over the spatial sphere. The black hole background corresponding to a spherical horizon can be written as

$$\mathrm{d}s^2=\left(1+\frac{f(z)}{z^2}\right)\mathrm{d}\tau^2+\frac{\mathrm{d}z^2}{z^4\big(1+h(z)/z^2\big)}+\frac{\mathrm{d}\Omega_{d-1}^2}{z^2}\,, \tag{4.3.97}$$

where $\mathrm{d}\Omega_{d-1}^2$ is the metric on the $(d-1)$-dimensional sphere. The asymptotic AdS boundary conditions again constrain the functions $f(z)$ and $h(z)$ as

$$f(z)=1-f_0z^d+\ldots\,, \qquad h(z)=1-h_0z^d+\ldots\,. \tag{4.3.98}$$

In [210] it was shown that conformal invariance on the boundary requires $f_0=h_0$ as in the black brane case.

Black hole spectrum. The operator spectrum in the black hole background differs slightly from the black brane case presented in (4.3.13). In addition to the multi-stress tensor operators $[T^n]$, operators of the schematic form $\partial^\ell T^n$ must also be included, where the derivatives are arranged such that they produce conformal primaries. A list of the lightest such operators can be found in Table 6 of [210]. Starting at $\Delta=10$,

[32] For the sake of clarity, note that the arcs are unique up to a constant with respect to the position of the operator. This constant is however a function of the dimensionless radius β/R.

additional operators of this type appear in the spectrum of the black hole background with respect to the black brane.

For the low-lying spectrum, i.e., $\Delta \leq 8$, the OPE coefficients coincide with the black brane ones given in (4.3.14)–(4.3.17) when expressed in terms of f_0. However, to make contact with the finite temperature and volume CFT, in the black hole background the dimensionless quantity $\tilde{f}_0$ should be replaced by

$$\tilde{f}_0 = \frac{1}{4}\left(-\frac{\beta^4}{R^4} - 2\pi^2\frac{\beta^2}{R^2} \pm 2\pi^3\sqrt{\pi^2 - 2\frac{\beta^2}{R^2}} + 2\pi^4\right) , \tag{4.3.99}$$

which we obtain by resolving the black hole singularity, i.e.,

$$\frac{R}{\beta} = \frac{1}{4\pi}\frac{\mathrm{d}(f(z)/z^2)}{\mathrm{d}z}\bigg|_{z=z_{\mathrm{H}}} , \tag{4.3.100}$$

and ensuring that $\tilde{f}_0$ reduces to the black brane expression given in (4.3.10) as we take $R \to \infty$. In Equation (4.3.99) the two signs correspond to the two possible solutions, associated to a *small* black hole $(-)$ and a *large* black hole $(+)$. Although in the following we are agnostic about the choice of solution, we mention that the small black hole is known to be unstable thermodynamically while the large one is stable [55, 240, 241].

It should be noticed that, while in the black brane case $\tilde{f}_0$ (and thus the one-point functions of multi-stress tensor operators) is a constant, in the black hole case $\tilde{f}_0$ becomes a *function* of the dimensionless ratio β/R. Consequently, the thermal one-point functions of the multi-stress tensor operators also depend non-trivially on β/R.

In the following we apply the analytic bootstrap framework (of which Equation (4.3.92) is the keystone) to holographic setups in the strong-coupling regime in order to derive the principal contribution to two-point functions of scalar operators. As already mentioned, additional operators of the schematic form $\partial^\ell T^n$ with conformal dimensions $\Delta = dn + \ell$ also appear. The method of [210] can be extended to compute the associated OPE coefficients.[33]

Two-point functions for integer $\boldsymbol{\Delta_\phi}$ in 4$\boldsymbol{d}$ BH background. As noted in [210] and reviewed above, the OPE coefficients for the multi-stress tensor sector for the black brane and spherical black hole can be computed directly from the equations of motion

[33] See in particular Appendix A therein, in which exact expressions were obtained for the operators up to dimension $\Delta = 10$ (see Equations (5.25)–(5.30)), which consist of two stress tensors and two derivatives.

in AdS. We can therefore immediately expand in GFF blocks, following the same logic as in Section 4.3.2, in order to derive the principal contributions to the associated correlators. We focus again on the integer Δ_ϕ case.[34]

Using the finite-volume GFF correlator given in (4.3.93) we define to streamline the notation the object

$$\mathcal{B}^{(\ell)}_{\beta/R}(\tau) = \psi^{(\ell)}_{e^{-\beta/R}}\left(\frac{\tau}{\beta}\right) + \psi^{(\ell)}_{e^{-\beta/R}}\left(1-\frac{\tau}{\beta}\right) . \tag{4.3.101}$$

We readily obtain the following expressions:

$$\Delta_\phi = 1 : \qquad g_{\text{pr},\beta/R}(\tau) = \frac{1}{\beta^2}\mathcal{B}^{(1)}_{\beta/R}(\tau) , \tag{4.3.102}$$

$$\Delta_\phi = 2 : \qquad g_{\text{pr},\beta/R}(\tau) = \frac{1}{\beta^4}\left[\frac{1}{6}\mathcal{B}^{(3)}_{\beta/R}(\tau) - \frac{1}{6}\left(\frac{\beta}{R}\right)^2\mathcal{B}^{(1)}_{\beta/R}(\tau)\right] , \tag{4.3.103}$$

$$\begin{aligned}\Delta_\phi = 3 : \qquad g_{\text{pr},\beta/R}(\tau) &= \frac{1}{\beta^6}\left[\frac{1}{120}\mathcal{B}^{(5)}_{\beta/R}(\tau) - \frac{1}{24}\left(\frac{\beta}{R}\right)^2\mathcal{B}^{(3)}_{\beta/R}(\tau) + \frac{1}{30}\left(\frac{\beta}{R}\right)^4\mathcal{B}^{(1)}_{\beta/R}(\tau)\right] \\ &\quad + a_T\left(\beta/R\right)\frac{1}{\beta^6}\mathcal{B}^{(1)}_{\beta/R}(\tau) ,\end{aligned} \tag{4.3.104}$$

$$\begin{aligned}\Delta_\phi = 4 : \qquad g_{\text{pr},\beta/R}(\tau) &= \frac{1}{\beta^8}\left[\frac{1}{5040}\mathcal{B}^{(7)}_{\beta/R}(\tau) - \frac{1}{360}\left(\frac{\beta}{R}\right)^2\mathcal{B}^{(5)}_{\beta/R}(\tau) + \frac{7}{720}\left(\frac{\beta}{R}\right)^4\mathcal{B}^{(3)}_{\beta/R}(\tau)\right. \\ &\quad \left. -\frac{1}{140}\left(\frac{\beta}{R}\right)^6\mathcal{B}^{(1)}_{\beta/R}(\tau)\right] + a_T\left(\beta/R\right)\frac{1}{\beta^8}\left[\frac{1}{6}\mathcal{B}^{(3)}_{\beta/R}(\tau)\right. \\ &\quad \left. -\frac{1}{6}\left(\frac{\beta}{R}\right)^2\mathcal{B}^{(1)}_{\beta/R}(\tau)\right] ,\end{aligned} \tag{4.3.105}$$

$$\begin{aligned}\Delta_\phi = 5 : \qquad g_{\text{pr},\beta/R}(\tau) &= \frac{1}{\beta^{10}}\left[\frac{1}{362880}\mathcal{B}^{(9)}_{\beta/R}(\tau) - \frac{1}{12096}\left(\frac{\beta}{R}\right)^2\mathcal{B}^{(7)}_{\beta/R}(\tau)\right. \\ &\quad +\frac{13}{17280}\left(\frac{\beta}{R}\right)^4\mathcal{B}^{(5)}_{\beta/R}(\tau) - \frac{41}{18144}\left(\frac{\beta}{R}\right)^6\mathcal{B}^{(3)}_{\beta/R}(\tau) \\ &\quad \left. +\frac{1}{630}\left(\frac{\beta}{R}\right)^8\mathcal{B}^{(1)}_{\beta/R}(\tau)\right] + a_T\left(\beta/R\right)\frac{1}{\beta^{10}}\left[\frac{1}{120}\mathcal{B}^{(5)}_{\beta/R}(\tau) - \frac{1}{24}\left(\frac{\beta}{R}\right)^2\right. \\ &\quad \left. \mathcal{B}^{(3)}_{\beta/R}(\tau) + \frac{1}{30}\left(\frac{\beta}{R}\right)^4\mathcal{B}^{(1)}_{\beta/R}(\tau)\right] + a_{[T^2]}\left(\beta/R\right)\frac{1}{\beta^{10}}\mathcal{B}^{(1)}_{\beta/R}(\tau)\end{aligned}$$

[34]For the non-integer case it would be interesting to develop a finite-volume approximation similar to the asymptotic model of [216].

$$. \tag{4.3.106}$$

This reproduces the pattern observed for the black brane background in (4.3.29)–(4.3.33). The final closed form of these principal contributions can be found by using (4.3.99) to obtain

$$a_T\left(\beta/R\right) = \frac{\Delta_\phi}{160}\left(-\frac{\beta^4}{R^4} - 2\pi^2\frac{\beta^2}{R^2} \pm 2\pi^3\sqrt{\pi^2 - 2\frac{\beta^2}{R^2}} + 2\pi^4\right), \tag{4.3.107}$$

$$a_{[T^2]}\left(\beta/R\right) = a_T\left(\beta/R\right)^2 \frac{63\Delta_\phi^4 - 413\Delta_\phi^3 + 672\Delta_\phi^2 - 88\Delta_\phi + 144}{126\Delta_\phi(\Delta_\phi-4)(\Delta_\phi-3)(\Delta_\phi-2)}. \tag{4.3.108}$$

The principal contributions of the correlators can be obtained by inserting these values in (4.3.102)–(4.3.106). Results for higher Δ_ϕ can be derived in the same way, provided sufficient knowledge of multi-stress tensor OPE coefficients.

It would be of fundamental importance to compute the regularized and arc contributions for the black hole case as well, similarly to the black brane case in Section 4.3.2. However, the lack of an asymptotic form for the OPE coefficients prevents us from studying the arc contributions, whose starting point is the location of the bouncing singularity in the complex τ-plane. Secondly, although we expect the higher multi-stress tensor contributions to be regularized as in Equation (4.3.35), the formula (4.3.93) prevents an exact computation of the derivative of the GFF block for the time being. Finally, finite volume correlators do not satisfy the clustering property (4.2.48) and, as a result, the arc contributions cannot be completely fixed. Future work will be dedicated to a deeper understanding of correlators in the black hole background.

A non-trivial check is the fact that the two-point function at finite volume should reproduce the one at infinite volume, i.e., the black brane, in the infinite volume limit. Since our thermal two-point functions are made up of a finite sum over GFF correlators it is enough to show that this is the case for the GFF correlator. This is discussed in [4], and indeed the correlators in this section reduce to the ones listed in (4.3.29)– (4.3.33). This limit additionally provides a constraint or a check on the expected regularized and arc contributions.

In the case of the black brane, we successfully compared our approximate analytic solution with the numerical solution of the wave equation. However, for the spherical black hole case, there are additional limitations which we discuss now. First, obtaining an accurate numerical solution is technically more challenging due to the increased complexity of the wave equation. Second, the analytic solutions for the black hole background contain an ambiguity encoded in an arbitrary function $\kappa_{\Delta_\phi}(\beta/R)$. By fixing β

and R, one could in principle tune this function to match the numerical result; however, such a procedure reduces the discrepancy in an (almost) arbitrary way. For this reason, we do not consider the numerical solution of the wave equation as a meaningful consistency check in this case.[35] Note that the fact that the solution is unique up to a constant in the kinematics is already a check of our correlators.

The Witten diagram interpretation discussed in Section 4.3.3 also differs in the black hole case. The expansion proposed in Section 4.3.3 effectively corresponds to a large β expansion, which is less meaningful in the black hole background since solutions exist only for $\beta^2 < \pi^2 R^2/2$.[36] Whether an alternative bulk interpretation of these blocks exists remains an open question, which we plan to revisit in future work.

Finally, as discussed in Section 4.3.4, it is also possible to include higher-curvature corrections in the computation of the correlation functions. As in the black brane case, the operator spectrum remains unchanged; the only difference is that the OPE coefficients of the multi-stress tensor operators now depend on the Wilson coefficients multiplying the higher-curvature terms, or equivalently on the parameters $f_4, h_4, \ldots$. Since the procedure to compute these corrections is identical to that described in Section 4.3.4, and the resulting expressions are not particularly illuminating, we do not report them here.

[35]It would be interesting to develop a more stable and precise way to solve the wave equation numerically.

[36]This can be seen from the fact that the square root in Equation (4.3.99) is real only for these values of β/R.

4.4 Sum Rules

A very straightforward way to obtain thermal one-point functions is to solve the sum rules implied by the KMS condition, as given in (4.1.9). While conceptually simple, this approach comes with several challenges. For all but a few special cases, the spectrum of a CFT is infinite, so the sum rules constitute an infinite system of linear equations. In practice, solving them requires either a hard truncation of the spectrum, in the spirit of [242], or the introduction of a cutoff together with an estimate of the contribution from operators above the cutoff. In this work, we adopt the latter approach.

It is also worth noting that the computation of thermal OPE coefficients via sum rules closely parallels the numerical bootstrap at zero temperature. However, unlike the zero-temperature case—where OPE coefficients appearing in four-point functions obey positivity constraints arising from crossing symmetry—the thermal OPE coefficients are not subject to such constraints. As a result, standard semidefinite programming techniques are not directly applicable. Recent progress toward constructing positive-definite quantities in thermal settings was presented in [243].

4.4.1 Derivation of the Sum Rules

To explicitly obtain these sum rules, we begin with (4.1.9) and perform an operator product expansion on both its left- and right-hand sides. The resulting expressions are then further expanded as power series in τ and r. This procedure relies on the definition of the Gegenbauer polynomials,

$$C_J^{(\nu)}\left(\frac{\tau}{\sqrt{\tau^2+r^2}}\right) = \sum_{k=0}^{\lfloor J/2 \rfloor} 2^{J-2k}(-1)^k \frac{\Gamma\left(J-k+\nu\right)}{\Gamma(\nu)\, k!\, (J-2k)!}\left(\frac{\tau}{\sqrt{r^2+\tau^2}}\right)^{J-2k} \, , \tag{4.4.1}$$

together with two successive applications of the binomial theorem. As discussed in (4.1.10), comparison of the two sides of (4.1.9) shows that all terms involving even powers of τ cancel identically. In contrast, the coefficients of odd powers of τ must vanish separately, yielding a set of non-trivial constraints. By enforcing this condition order by order in the variable r, we obtain a family of explicit sum rules for specific combinations of OPE coefficients,

$$\sum_{\mathcal{O}\in\phi\times\phi} \frac{b_{\mathcal{O}} f_{\mathcal{O}\phi\phi}}{c_{\mathcal{O}}}\, F_{\ell,n}(h,J) = 0 \, , \qquad n\in\mathbb{N} \, , \; \ell \in 2\mathbb{N}+1 \, . \tag{4.4.2}$$

Here we have introduced the twist variable

$$h = \Delta - J \, , \tag{4.4.3}$$

and defined the function

$$F_{\ell,n}(h,J) = \frac{1}{2^{h+J}} \binom{\frac{h-2\Delta_\phi}{2}}{n} \binom{h+J-2\Delta_\phi-2n}{\ell} {}_3F_2\left[\left.\begin{matrix} \frac{1-J}{2}, -\frac{J}{2}, \frac{h}{2}-\Delta_\phi+1 \\ \frac{h}{2}-\Delta_\phi-n+1, -J-\nu+1 \end{matrix}\right| 1\right] . \tag{4.4.4}$$

As anticipated, the function $F_{\ell,n}(h,J)$ depends on both the conformal dimension Δ—through the twist h—and the spin J of the exchanged operators, as well as on the two positive integers ℓ and n. This expression arises from setting to zero the $(2\ell+1)$-th derivative with respect to τ and the n-th derivative with respect to r of $f(\tau, r)$, evaluated at $\tau = \beta/2$ and $r = 0$, in accordance with (4.1.10). From this perspective, the sum rules in (4.4.2) can be understood as encoding an expansion of the correlator around its KMS-invariant fixed point.

A straightforward strategy for exploiting the sum rules in (4.4.2) is to truncate the operator product expansion. This approach is reminiscent of the *Gliozzi method* in the conformal bootstrap, originally proposed in [244]. However, there is no guarantee that a naive truncation of the infinite sum over exchanged operators yields reliable results. In order to assess whether the sum rules in (4.4.2)—restricted to the case $n = 0$—admit a consistent truncation, it is necessary to obtain quantitative control over the contribution of heavy operators.

In what follows, we begin by investigating truncations of the operator spectrum and testing this strategy in the context of generalized free field theories and two-dimensional conformal field theories, as reviewed in Sections 4.1.2 and 4.1.3. We then proceed to analyze and approximate the contributions of heavy operators, which will ultimately motivate a more refined method for solving the sum rules.

We start by considering a specific subset of the equations arising from (4.4.2), namely those with $n = 0$. These equations correspond to the one-dimensional case, in which we set the spatial coordinates of the two-point function to zero. In this case, it is possible to reduce the general sum rules (4.4.2) to a simpler form

$$\frac{\Gamma(2\Delta_\phi + \ell)}{\Gamma(2\Delta_\phi)} = \sum_\Delta \frac{a_\Delta}{2^\Delta} \frac{\Gamma(\Delta - 2\Delta_\phi + 1)}{\Gamma(\Delta - 2\Delta_\phi - \ell + 1)} , \tag{4.4.5}$$

where $\ell \in 2\mathbb{N}+1$. The sum above runs over all possible conformal dimensions appearing in the OPE $\phi \times \phi$, and due to this reduction we are no longer sensitive to the spins of the operators. Indeed, when a two-point function of a d-dimensional theory is restricted to vanishing spatial coordinates, the thermal OPE takes the form given in (4.1.11). These equations constitute, in principle, non-trivial constraints on the OPE coefficients and therefore on the one-point functions of operators appearing in the OPE $\phi \times \phi$. In deriving equation (4.4.5), we used the fact that the identity operator $\mathbb{1}$ appears in the OPE.

The conformal dimension of the identity is zero (and so is its spin), and its one-point function and structure constant can be set to $b_{\mathbb{1}} = f_{\phi\phi\mathbb{1}} = 1$. We can then isolate the contribution of the identity on the left-hand side of equation (4.4.5). This information is important for defining a normalization; otherwise, the coefficients a_Δ would only be defined up to an overall rescaling (as is clear from equation (4.4.2)). We now provide an example and discuss interesting consequences of equation (4.4.5), shown in Figure 4.12. Let us also note that equations (4.4.2) and (4.4.5) can be straightforwardly generalized to the case of unequal external operators. The structure of the equations remains the same, but the identity operator is no longer included in the OPE.

Testing on GFF. To solve the sum rules for a GFF theory, we observe that the upper argument of the first binomial in equation (4.4.4) is fixed to zero. Indeed, apart from the identity operator $\mathbb{1}$, the conformal dimensions of the operators $\mathcal{O} \in \phi \times \phi$ are given by $\Delta = 2\Delta_\phi + J$, which implies $h - 2\Delta_\phi = 0$. This in turn implies that all equations with $n \neq 0$ are trivially satisfied. This is expected, since the operators $\mathcal{O} \in \phi \times \phi$ are labeled only by their conformal dimensions. Therefore, it is natural to conclude that setting the spatial coordinates to zero from the outset (which is equivalent to setting $n = 0$) is sufficient to solve for the OPE coefficients. Numerical tests for GFF theories with $\Delta_\phi = 1$ are presented in Figure 4.12.

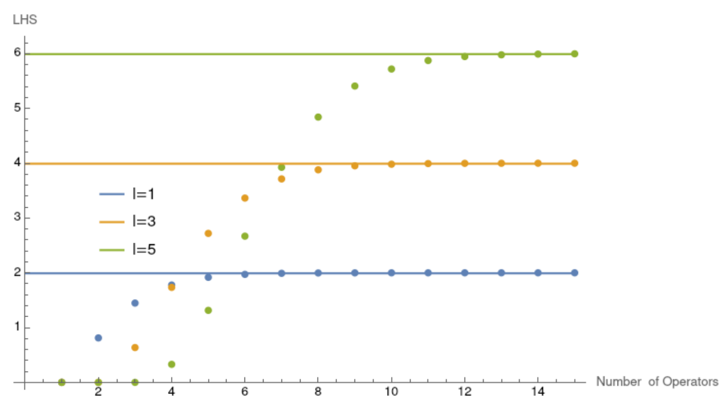

Figure 4.12: Comparison between the left-hand side (solid lines) and the right-hand side (dotted lines) of equation (4.4.5) for different values of ℓ. As ℓ increases, more operators must be included in the sum on the right-hand side for it to converge to the correct value, namely the left-hand side. The figure corresponds to a numerical test for a GFF with $\Delta_\phi = 1$, or equivalently for a four-dimensional free scalar theory. It is convenient to multiply both sides of equation (4.4.5) by a factor $1/\ell!$.

From these simple checks, we immediately learn that although the equations (4.4.5) are satisfied for every odd value of ℓ, larger values of ℓ require summing over an increasing

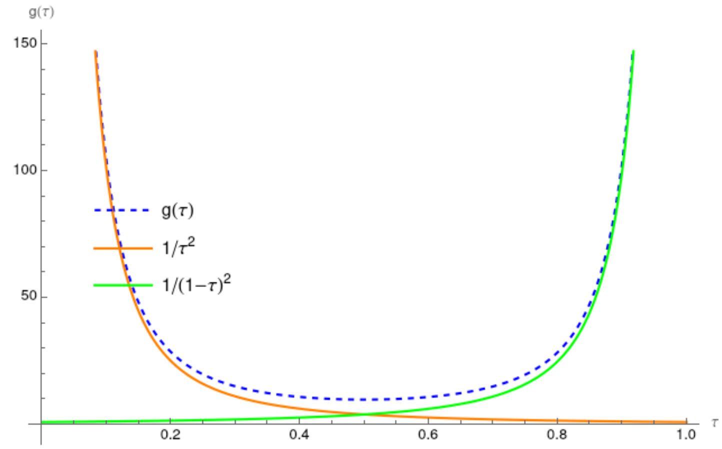

Figure 4.13: *There we plot the GFF correlator with $\Delta_\phi = 1$ and respectively the identity contribution in s-channel and the dual contribution in the t-channel to demonstrate the channel duality.*

number of operators on the right-hand side for the truncated sum to provide a good approximation. This makes the sum rules (4.4.5) extremely difficult to solve via truncation, since extracting more OPE coefficients a_Δ requires including increasingly many operators. We keep this observation in mind and proceed to analyze the contribution of heavy operators.

4.4.2 Estimating the Heavy Operators for $r = 0$

As we set the spatial separation to zero, we reduce the thermal two-point function to an effectively one-dimensional periodic correlation function (4.1.11). In this case, the *channel duality* arising from the periodicity condition becomes very apparent. As can be seen from Figure 4.13, in order to reproduce the identity contribution in the *s-channel*, one must take into account infinitely many operator contributions from the *t-channel*, and vice versa,

$$\frac{1}{\tau^{2\Delta_\phi}} = \sum_{\Delta} \tilde{a}_\Delta (\tau - 1)^{\Delta - 2\Delta_\phi} \; . \tag{4.4.6}$$

Using this relation, we can heuristically derive the asymptotic behavior of the OPE coefficients for large Δ. To this end, we define the *spectral density* $\rho(\Delta)$,

$$\rho(\Delta) = \sum_{\mathcal{O} \in \phi \times \phi} a_{\mathcal{O}} \; \delta(\Delta - \Delta_{\mathcal{O}}) \; , \tag{4.4.7}$$

such that the thermal OPE expansion of the two-point function can be written as

$$g(\tau) = \tau^{-2\Delta_\phi} \sum_{\mathcal{O}\in\phi\times\phi} \frac{a_{\mathcal{O}}}{\beta^{\Delta_{\mathcal{O}}}} \tau^{\Delta_{\mathcal{O}}} = \tau^{-2\Delta_\phi} \int_0^\infty d\Delta\ \rho(\Delta) x^{\Delta}\ , \tag{4.4.8}$$

where $x = \tau/\beta$ is a dimensionless ratio. The thermal OPE does not converge everywhere, but only in the open interval $0 < x < 1$ [146]. This is due to the presence of an infinite number of poles on the real τ axis (see Figure 4.5). From the analytic structure, we can then infer that asymptotically

$$\langle\phi(\tau)\phi(0)\rangle_\beta \overset{\tau\to k\beta}{\sim} (k\beta-\tau)^{-2\Delta_\phi}\ , \tag{4.4.9}$$

for any $k \in \mathbb{Z}$. Hence, by recalling the equation (4.4.8) we can write

$$\int_0^\infty d\Delta\ \rho(\Delta) x^{\Delta} \overset{x\to 1}{\sim} (1-x)^{-2\Delta_\phi}\ . \tag{4.4.10}$$

Now, to match this asymptotic behaviour, we assume that the behavior of $\rho(\Delta)$ in the limit $\Delta \to \infty$ is a power-law behavior

$$\rho(\Delta) \overset{\Delta\to\infty}{\sim} A\Delta^{-\alpha+1}\ . \tag{4.4.11}$$

This ansatz is justified in [147] and a rigorous version of the same OPE asymptotics was derived based on several assumptions on the OPE coefficients. Plugging it in the two-point function (4.4.8) we find

$$g(\tau) \overset{\tau\to\beta}{\sim} A\,\Gamma(2-\alpha)\tau^{-2\Delta_\phi}\left(1-\frac{\tau}{\beta}\right)^{\alpha-2}\ , \tag{4.4.12}$$

from which we can read

$$\alpha = -2\Delta_\phi + 2\ , \qquad A = \frac{1}{\Gamma(2\Delta_\phi)}\ . \tag{4.4.13}$$

Therefore, the behavior of $\rho(\Delta)$ in the limit $\Delta \to \infty$ becomes

$$\rho(\Delta) \overset{\Delta\to\infty}{\sim} \frac{1}{\Gamma(2\Delta_\phi)}\Delta^{2\Delta_\phi-1}\ . \tag{4.4.14}$$

It is important to emphasize that the formula (4.4.14) acquires a correct physical meaning when considered on average,

$$\int_0^\Delta \rho(\widetilde{\Delta})\ d\widetilde{\Delta} \overset{\Delta\to\infty}{\sim} \frac{\Delta^{2\Delta_\phi}}{\Gamma(2\Delta_\phi+1)}\ . \tag{4.4.15}$$

This leading asymptotics is called *Tauberian tail*. And by using this leading asymptotic behaviour we can establish a more refined way of solving the sum-rules which was used in [245] to solve light OPE coefficients for $O(N)$ Model. Later on by employing the insights gained by analytic bootstrap we will refine this approximation.

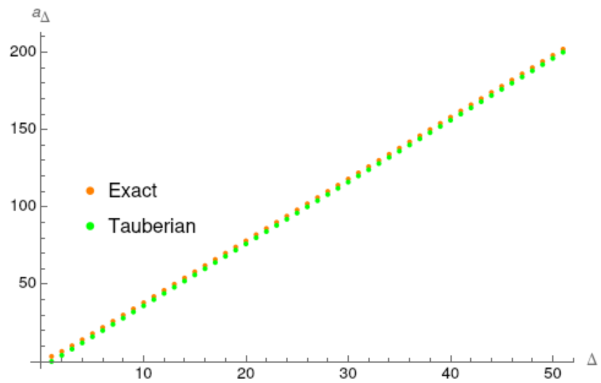

Figure 4.14: *We compare the exact OPE coefficients extracted from the GFF correlator with $\Delta_\phi = 1$ when $r = 0$ and respectively the tauberian approximation of these OPE coefficients with respect to* (4.4.16).

Solving sum rules with Tauberian. Now that we have an estimation of the heavy operator contributions we can set a cut of scale $\Delta_{\max}$ and estimate all operators that are heavier than this value with the *Tauberian tail*. We can define the estimated OPE coefficients as

$$\tilde{a}_\Delta^{\text{Taub}} = \frac{2\Delta^{2\Delta_\phi - 1}}{\Gamma(2\Delta_\phi)} \tag{4.4.16}$$

then the approximated thermal correlator takes the following form,

$$g_{\text{trunc.}}(\tau) = \sum_{\Delta < \Delta_{\max}} \tilde{a}_\Delta \tau^{\Delta - 2\Delta_\phi} + \sum_{\Delta > \Delta_{\max}} \tilde{a}_\Delta^{\text{Taub}} \tau^{\Delta - 2\Delta_\phi} \,. \tag{4.4.17}$$

Similarly we can introduce the same cutoff to the sum rules given in (4.4.5),

$$\frac{\Gamma(2\Delta_\phi + \ell)}{\Gamma(2\Delta_\phi)} = \sum_{0 < \Delta < \Delta_{\max}} \frac{\tilde{a}_\Delta}{2^\Delta} \frac{\Gamma(\Delta - 2\Delta_\phi + 1)}{\Gamma(\Delta - 2\Delta_\phi - \ell + 1)} + \sum_{\Delta > \Delta_{\max}} \frac{\tilde{a}_\Delta^{\text{Taub}}}{2^\Delta} \frac{\Gamma(\Delta - 2\Delta_\phi + 1)}{\Gamma(\Delta - 2\Delta_\phi - \ell + 1)} \,, \tag{4.4.18}$$

By doing so we introduced an error to the sum rules but at the same time reduced the number of unknowns to a finite set $\{\tilde{a}_\Delta\}$ for $\Delta < \Delta_{\max}$. In Figure 4.14 we can see the application to GFF correlator for $\Delta_\phi = 1$.

Improving Tauberian tail by adding corrections. It is clear that the most direct way to improve the estimation of the heavy operators and improve the numerics is to add polynomially suppressed corrections in Δ. To achieve this we refine the Tauberian tail,

$$a_{\widetilde{\Delta}} \overset{\widetilde{\Delta} \gg 1}{\sim} \frac{2\widetilde{\Delta}^{2\Delta_\phi - 1}}{\Gamma(2\Delta_\phi)} \left(1 + \frac{c_1}{\widetilde{\Delta}} + \sum_\ell \frac{c_\ell}{\widetilde{\Delta}^{\alpha_\ell}}\right) \,, \tag{4.4.19}$$

where the coefficients $c_1, \{c_\ell\}$ and the powers $\{\alpha_\ell\}$ are unknown and theory-dependent. Although the leading term already provides a rather good approximation [147], numerical bootstrap procedures require at least the first correction, parametrized by c_1. More refined approximations are required to achieve higher-precision results. We demonstrate that the leading behavior and its corrections can systematically improve the solution for the OPE coefficients. For GFF with $\Delta_\phi = 1$ this is given in Figure 4.14. However, here, in its simplest form we are leaving the coefficients of these corrections c_ℓ completely open and solve them while solving for the light OPE coefficients. A more sophisticated and systematic version of this procedure can be given by looking at the KMS invariant blocks given in (4.2.25).

From dispersion relation to heavy operators. The Hurwitz ζ-function admits a Taylor expansion around $\tau = 0$:

$$\zeta_H(s,\tau) + \zeta_H(s, 1-\tau) = \frac{1}{\tau^s} + \sum_{k=0}^{\infty} \left[1 + (-1)^k\right] \binom{s+k-1}{k} \zeta(k+s)\tau^k \ , \qquad (4.4.20)$$

where $s = 2\Delta_\phi - \Delta$. Observe that we simply recovered the OPE of a GFF correlator with external dimension given by s: the expansion (4.4.20) is given by operators of classical[37] conformal dimension $\widetilde{\Delta} = 2\Delta_\phi + k$. From now on, we will use $\widetilde{\Delta}$ as a variable, instead of k. Moreover, only the terms proportional to even powers of τ contribute, as a consequence of the parity symmetry $\tau \to -\tau$. It makes therefore sense to compare the OPE coefficient $a_{\widetilde{\Delta}}$ and the generic coefficient of (4.4.20) in the limit $\widetilde{\Delta} \to \infty$. We notice that the asymptotic of the two-point function can be approximated by summing over even integer dimensional operators, corresponding classically to the double twist, the associated OPE coefficients can be expanded in terms of the inversion of the light operators. Furthermore, the exponential corrections are completely disentangled and subleading with respect to the polynomial corrections in $1/\Delta$. Therefore, in the following, we will drop them.[38] In the large $\widetilde{\Delta}$ limit we find that the contribution of the operator Δ to the heavy operator of dimensions $\widetilde{\Delta}$ is given by

$$a^{(\Delta)}_{\widetilde{\Delta}} \overset{\widetilde{\Delta} \gg 1}{\sim} a_\Delta \frac{2\widetilde{\Delta}^{2\Delta_\phi - \Delta - 1}}{\Gamma(2\Delta_\phi - \Delta)} \left[1 + \frac{c_1^\Delta}{\widetilde{\Delta}} + \frac{c_2^\Delta}{\widetilde{\Delta}^2} + \dots\right] \ , \qquad (4.4.21)$$

where the correction coefficients are given by

$$c_1^\Delta = \frac{(\Delta + 2\Delta_\phi)(\Delta - 2\Delta_\phi + 1)}{2} \ , \qquad (4.4.22)$$

[37] The anomalous dimensions could be recovered by studying the *pole-shifting* through the inversion formula, as in [146].

[38] They can be easily reintroduced by multiplying each term in the sum by $\zeta(\widetilde{\Delta} - \Delta)$.

$$c_2^{\Delta} = \frac{(\Delta - 2\Delta_\phi + 2)\,(3\Delta^2 + \Delta(12\Delta_\phi + 1) + 2\Delta_\phi(6\Delta_\phi - 1))\,(\Delta - 2\Delta_\phi + 1)}{24} \, . \quad (4.4.23)$$

The asymptotic (4.4.21) should be interpreted as the correction to the Tauberian leading order for the double-twist OPE coefficients (4.4.19) obtained by inverting the operator (or operators, in case of degeneracy) of conformal dimension Δ appearing in the OPE. The main contribution, as expected, comes from the inversion of the identity operator, and it reads

$$a_{\widetilde{\Delta}} \overset{\widetilde{\Delta}\gg 1}{\sim} \frac{2\widetilde{\Delta}^{2\Delta_\phi - 1}}{\Gamma(2\Delta_\phi)} \left[1 - \frac{\Delta_\phi(2\Delta_\phi - 1)}{\widetilde{\Delta}} + \frac{\Delta_\phi(\Delta_\phi - 1)(2\Delta_\phi - 1)(6\Delta_\phi - 1)}{6\,\widetilde{\Delta}^2} + \dots\right] + \dots \, . \quad (4.4.24)$$

Interestingly, the inversion of the identity operator correctly reproduces the Tauberian asymptotic derived in [147]. This section therefore provides a derivation of this asymptotic, under the assumption of analyticity and Regge boundedness of the correlator in the complex τ-plane. From this perspective, it is clear that the result arises from the inversion of operators from the t-channel to the s-channel. In fact, the result of [147] can be effectively interpreted as the inversion of the identity operator. In this work, we generalize that result by promoting it — through the analytic techniques developed here — to the inversion of arbitrary operators, making stronger the idea of the channel duality between light and heavy sectors.

Thanks to the closed form of the thermal two point function in complex τ plane given in (4.2.25) we can improve the tail of the heavy operators further by computing corrections coming from the other light operators in the OPE. If the light operators have conformal dimensions $0 < \Delta_1 < \dots$, the corrections take the following form:

$$\begin{aligned} a_{\widetilde{\Delta}} \overset{\widetilde{\Delta}\gg 1}{\sim} & \, 2\frac{\widetilde{\Delta}^{2\Delta_\phi - 1}}{\Gamma(2\Delta_\phi)} \left(1 + \frac{c_1^0}{\widetilde{\Delta}} + \frac{c_2^0}{\widetilde{\Delta}^2} + \dots\right) \\ & + \sum_{\Delta_i \neq 0} 2a_{\Delta_i} \frac{\widetilde{\Delta}^{2\Delta_\phi - \Delta_i - 1}}{\Gamma(2\Delta_\phi - \Delta_i)} \left(1 + \frac{c_1^{\Delta_i}}{\widetilde{\Delta}} + \frac{c_2^{\Delta_i}}{\widetilde{\Delta}^2} + \dots\right) \, , \end{aligned} \quad (4.4.25)$$

such that for each light operator contribution the coefficients of the order-by-order corrections are defined in (4.4.22) and (4.4.23). This gives us a better understanding of the dominant contributions in terms of the light operators of the theory. This expression can be used to bootstrap thermal OPE coefficient as in [148]: as a proof of concept, in the following section, we make use of Eq. (4.2.25) to compute the two-point function $\langle \epsilon\epsilon \rangle_\beta$ of $3d$ Ising.

It was pointed out in [146] that the inversion of individual operators can only generate operators of the double-twist families $[\phi\phi]_{n,J}$. However in general theories (e.g., in the

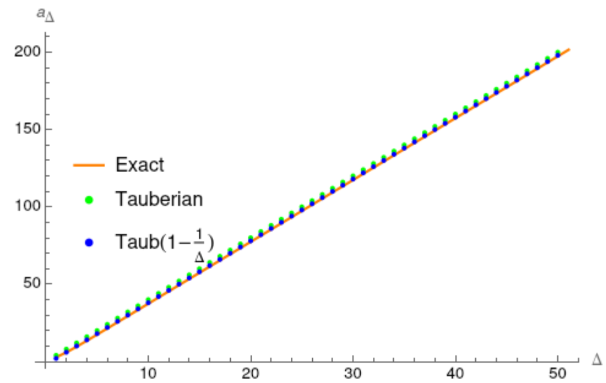

Figure 4.15: *We compare the exact OPE coefficients extracted from the GFF correlator with $\Delta_\phi = 1$ when $r = 0$, the tauberian approximation of these OPE coefficients with respect to (4.4.16) and Tauberian approximation with $\frac{1}{\Delta}$ correction as given in (4.4.22). We observe that the $\frac{1}{\Delta}$ correction gets closer to the exact coefficients.*

$3d$ Ising model) we expect other families of operators to appear, for instance $[\epsilon\epsilon]$ or even multi-twist $[\phi\phi\phi\phi]$. The reason why these other families do not appear in the asymptotics lies in the fact that the sum of operators and the inversion procedure do not commute. In order to see these families one could first resum a family, for instance $[\phi\phi]_{0,J}$, and then invert the result. This procedure is explained in detail in [146] and the formalism presented here can be adapted to this case.

In [149], it was pointed out that certain operators, such as multi-stress tensors, may have alternating sign OPE coefficients, naively rendering the expansion in Eq. (4.4.25) inconsistent. However, by applying the dispersion relation (4.2.25) — for instance, in the case $\Delta_\phi = 3/2$ — by using the OPE coefficients for the multi-stress tensor sector given in this thesis, one recovers the result given in (2.24) of [149]. As discussed in that work, the corresponding solution exhibits unexpected poles in the complex τ-plane.[39] These poles should not appear in physical correlators and indicate that some consistency condition, necessary to derive the dispersion relation, is violated. The authors suggest a procedure to remove by hand these poles, but this has no direct analogue within the dispersion relation (4.2.25) itself. Let us take this opportunity to point out that (4.2.25) requires, as input, the discontinuity of the two-point function. However, not every choice of input is consistent: new, emergent analytic structures – such as the extra poles appearing in (2.24) of [149] – may arise. This imposes nontrivial constraints on the admissible input of the dispersion relation which would be interesting to investigate in future studies.

[39]These unexpected poles are holographically associated with the bouncing singularity [221].

To see how the coefficients of the corrections to the leading behaviour given in (4.4.25) affects the numeric computation, we revisit the GFF $\Delta_\phi = 1$ computation given in Figure 4.14 and refine it by importing the correct c_i as they are given in (4.4.22) and (4.4.23). These new numerics can be seen in Figure 4.15 and as expected after a certain point adding more coeficients does not improve the numerics. In that case the rest of the input should be improved to get a better result. In the following section we will apply this method to 3-dimensional Ising model.

Summing up all tauberian corrections. It is also possible to develop the connection between the Tauberian corrections and the analytic bootstrap framework. We should keep in mind that setting the spatial separation is equivalently a GFF theory approximation to the model. Therefore, by comparing the KMS-invariant blocks with the truncated OPE expansion in complex-τ plane we can also obtain the resummation of the entire Tauberian tail. To demonstrate this, first, we define a single KMS invariant block as

$$g_{\mathrm{GFF}}(\Delta_\phi - \Delta/2, \tau) = \zeta_H\left(2\Delta_\phi - \Delta, 1 - \frac{\tau}{\beta}\right) + \zeta_H\left(2\Delta_\phi - \Delta, \frac{\tau}{\beta}\right) \tag{4.4.26}$$

which is the correlator of a GFF theory with scaling dimension $\Delta_\phi - \Delta/2$ and the thermal correlator in $r = 0$ limit is given by

$$g(\tau) = \sum_{\Delta} \frac{a_\Delta}{\beta^{2\Delta_\phi}} g_{\mathrm{GFF}}(\Delta_\phi - \Delta/2, \tau) + \kappa \,. \tag{4.4.27}$$

Then after subtracting the constant part for simplicity, the KMS invariant blocks admit the expansion given in (4.4.20). We can compare the estimated OPE given in (4.4.17). In this expression the first term corresponds to the contribution of the operator of dimension Δ to the OPE, while the second term corresponds to a family of double-twist operators and represents the contribution of the operator of dimension Δ to the heavy tail. Plugging this into (4.4.17) we obtain,

$$g(\tau) = \sum_{\Delta \le \Delta_{\max}} \frac{1}{\tau^{2\Delta_\phi - \Delta}} + \sum_{\Delta \le \Delta_{\max}} \sum_{n=1}^{\infty} \frac{2\zeta_{2\Delta_\phi - \Delta + 2n} \Gamma(\Delta - 2\Delta_\phi + 1)}{(2n)!\, \Gamma(\Delta - 2\Delta_\phi + 1 - 2n)} \tau^{2n} \tag{4.4.28}$$

Therefore, by comparing (4.4.17) to (4.4.28) and commuting the sums we obtain

$$\tilde{a}_n = \sum_{\Delta \le \Delta_{\max}} a_\Delta \frac{2\zeta_{2\Delta_\phi - \Delta + 2n} \Gamma(\Delta - 2\Delta_\phi + 1)}{(2n)!\, \Gamma(\Delta - 2\Delta_\phi + 1 - 2n)} \,. \tag{4.4.29}$$

This formula can be understood as *resummed* Tauberian and approximates the tail of heavy operators with double-twist operators of dimension $2\Delta_\phi + 2n$. One can expand this formula in large n to see that it gives the leading Tauberian corrections as given in (4.4.25) back. Moreover, $n_{\rm min}$ depends on $\Delta_{\rm max}$; one should ensure that operators do not appear both in the first and in the second terms of truncated sum rules,

$$0 = \sum_{\Delta \le \Delta_{\rm max}} \frac{a_\Delta}{2^\Delta} \binom{\Delta - 2\Delta_\phi}{k} + \sum_{n=n_{\rm min}}^{\infty} \frac{\tilde{a}_n}{2^{2\Delta_\phi + 2n}} \binom{2n}{k}, \qquad \forall k \in 2\mathbb{N} + 1\,. \tag{4.4.30}$$

Quantifying the relation between $n_{\rm min}$ and $\Delta_{\rm max}$. We can make the connection between these two cutoffs precise by defining,

$$n_{\rm min} = \left[\frac{\Delta_{\rm max} - 2\Delta_\phi}{2} \right] + 1 \tag{4.4.31}$$

and recast the *new* sum rules as follows

$$\tilde{a}_n = 0 \qquad \text{for} \qquad n < n_{\rm min}\,. \tag{4.4.32}$$

Here we can immediately see that the number of constraints is not enough to fully fix the exact OPE coefficients a_Δ that we have started with.

4.4.3 $3d$ Ising Semi-Analytic Bootstrap

In Section 4.2, we derived a formula for the thermal two-point function of two scalar operators in the complex τ-plane (see (4.2.25)). Although such a formula completely fixes the kinematics of the correlator, it requires the dynamical information encoded in the OPE coefficients a_Δ as an input. When studying strongly-coupled thermal CFTs, computing these coefficients is usually a formidable challenge, which can be tackled by using a numerical bootstrap approach [148]. In this Section, we combine the formula (4.2.25) and the numerical results of [148] to study correlation functions in the $3d$ Ising model, which is the $O(N)$ Model for $N = 1$ (see the introduction in Section 4.2.4), in particular the correlators $\langle \sigma(\tau)\, \sigma(0) \rangle_\beta$ and $\langle \epsilon(\tau)\, \epsilon(0) \rangle_\beta$ (see Table 4.5 for a short summary of the light operators in this theory).

In applying the formula (4.2.25) to strongly-coupled theories, and in particular to the $3d$ Ising model, we are faced with a problem: since the conformal dimensions appearing in the OPE are non-integers, all of them will contribute to the discontinuity and hence have to be summed over in the formula. Usually only the coefficients for the first light dimensions are explicitly known (see Table 4.5). However, close to $\tau/\beta \sim 0$, the dominant contributions come from the lightest operators, which also dominate the limit $\tau/\beta \sim 1$ thanks to KMS invariance. Therefore, even though in the $3d$ Ising model (and

$\mathcal{O}$	$\mathcal{O}_{\rm GL}$	$\Delta_{\mathcal{O}}$ [100, 103, 246]	$a_{\Delta_{\mathcal{O}}}$ [245] (from $\langle\sigma\sigma\rangle_\beta$)
σ	ϕ	0.518148806(24)	0
ϵ	ϕ^2	1.41262528(29)	0.75(15)
$T_{\mu\nu}$	$T_{\mu\nu}$	3	1.97(7)
ϵ'	ϕ^4	3.82951(61)	0.19(6)
$C'_{\mu\nu\rho\sigma}$	$\phi\,\partial_\mu\partial_\nu\partial_\rho\partial_\sigma\phi$	5.022665(28)	/
$T'_{\mu\nu}$	$\phi\,\partial_\mu\partial_\nu\Box\phi$	5.50915(44)	/

Table 4.5: *Light operators in the* 3d *Ising model, their classical (Ginzburg–Landau) counterparts ($\mathcal{O}_{GL}$), conformal dimensions, and thermal OPE coefficients (when available and considering the $\langle\sigma(\tau)\sigma(0)\rangle_\beta$ correlator).*

other strongly-coupled theories) we cannot perform the full sum over the conformal dimensions appearing in the OPE as prescribed in (4.2.25), it is still meaningful to truncate the sum to the first few light operators. We expect this approximation to hold well close to $\tau/\beta \sim 0$ and $\tau/\beta \sim 1$.

Consistency check for the correlator $\langle\sigma\sigma\rangle_\beta$. In this paragraph, we start by studying the correlator $\langle\,\sigma(\tau)\,\sigma(0)\,\rangle_\beta$. The first light operators appearing in the OPE are, schematically,

$$\sigma\times\sigma\sim \mathbb{1}+\epsilon+T^{\mu\nu}+\epsilon'+\dots\ . \tag{4.4.33}$$

All the operators appearing on the right-hand side of the OPE (4.4.33) contribute to the discontinuity. Their thermal OPE coefficients were bootstrapped in [245] and are listed in Table 4.5, along with their conformal dimensions.

Following the line of thought described above, the correlator can be approximated by truncating the sum in Eq. (4.2.25) and plugging the dynamical data:

$$\langle\sigma(\tau)\,\sigma(0)\rangle_\beta \approx \sum_{\mathcal{O}\in\{\mathbb{1},\,\epsilon,\,T,\,\epsilon'\}}\frac{a_{\Delta_O}}{\beta^{2\Delta_\sigma}}\left[\zeta_H\left(2\Delta_\sigma-\Delta_{\mathcal{O}},\frac{\tau}{\beta}\right)+\zeta_H\left(2\Delta_\sigma-\Delta_{\mathcal{O}},1-\frac{\tau}{\beta}\right)\right]+\frac{\kappa}{\beta^{2\Delta_\sigma}}\,. \tag{4.4.34}$$

As discussed in Section 4.2.1, the only unfixed parameter of the dispersion relation in the complex τ-plane is an additive constant κ. If we were considering all the operators contributing to the discontinuity in the sum above, this constant could be fixed by clustering; however, the truncation of the sum spoils the limit $\tau\to i\infty$. To fix κ we require that the OPE does not contain any constant term: the procedure yields an estimated value $\kappa\approx-55.86\beta^{2\Delta_\sigma}$.

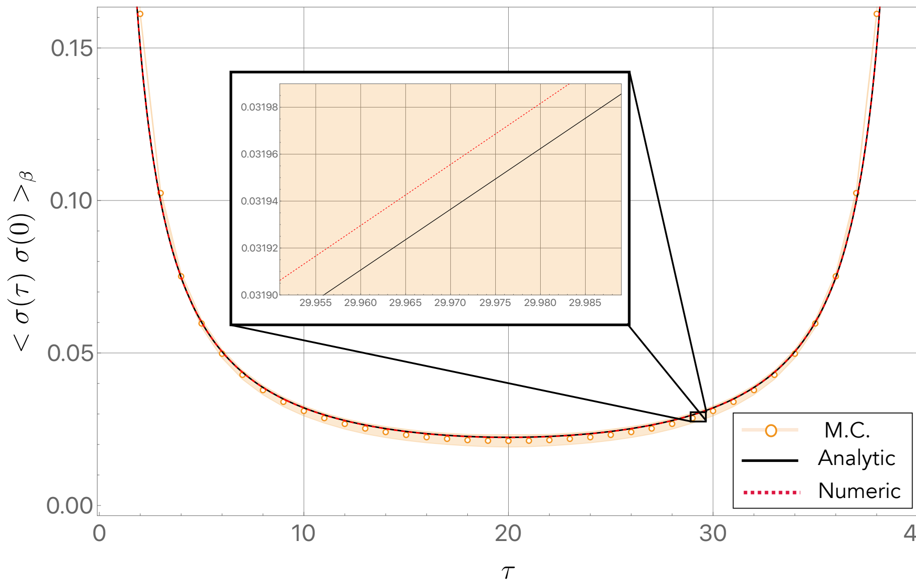

Figure 4.16: *Two point function* $\langle\, \sigma(\tau)\sigma(0)\, \rangle_\beta$ *in the limit in which* $\vec{x} = 0$*. The black continuous line is obtained by using the dispersion relation in the complex* τ*-plane and by inputting the thermal OPE coefficients from [245]. The dashed curve represents directly the OPE result of [148] while the points are the result of a Monte Carlo simulation on a lattice* $500 \times 500 \times 40$ *where the inverse temperature is given by* $\beta = 40$*.*

The result is reported in Fig. 4.16. In the plot, we compare the approximation obtained from the truncated version of Eq. (4.4.34) and the numerical evaluation of [148]. This procedure will clearly decrease the numerical error since the number of Tauberian corrections can be arbitrarily high without adding new unknown coefficient. The relative discrepancy between the two curves is of order 10^{-3}, in agreement with the level of accuracy to which the numerical results in [148] can be trusted. Notably, the largest deviation occurs in the region $\tau \in (1/2, 1)$, which is precisely the region where we expect the corrections to the Tauberian approximation used in [148] to become more significant. The motivation behind the discrepancy lies in the amount of corrections employed in each case to refine the leading Tauberian approximation: in [148], the authors made use of only the first correction appearing in Eq. (4.4.25), of order $1/\widetilde{\Delta}$. Moreover, the coefficient was considered to be an unknown variable. In this work, we instead made use of the formula (4.2.25), which already encodes an infinite amount of corrections, each one with a predetermined coefficient.

For completeness, we also compare our results to Monte Carlo simulations, finding very good agreement. Details on the numerical implementation and simulation parameters are provided in Appendix E in [3]. It is important to note that the two-point function extracted from Monte Carlo simulations is not unit-normalized. As a result, we need to redefine the operator σ in Eq. (4.4.34) so that its zero-temperature two-point function matches the normalization used in the Monte Carlo data. This mismatch amounts to a single overall multiplicative constant, which can be fixed by fitting. We find that this normalization constant is approximately $C_\sigma \approx 0.305$.

Note that one can also adopt the method presented in [148] to implement further corrections in the tail of heavy operators, as shown in Eq. (4.4.24). This is equivalent to comparing the result of [148] with the approximation in (4.4.34), and indeed, this procedure is consistent with the numerical results for thermal OPE coefficients shown in Table 4.5. This confirms the findings of [148]. Interestingly, however, these results do not match the Casimir amplitude computed via Monte Carlo in [247]. It would be worthwhile to investigate this discrepancy in more detail, for instance by comparing additional observables such as the thermal two-point function with higher precision.

New result for the correlator $\langle \epsilon\epsilon \rangle_\beta$. To produce a numerical approximation of the correlator $\langle\, \epsilon(\tau)\epsilon(0)\, \rangle_\beta$ using the methods of [148], we need to address the issue that the external dimension Δ_ϵ is larger than Δ_σ. While $\langle\, \sigma\sigma\, \rangle_\beta$ only required a single correction to the Tauberian leading behaviour, the $\langle\, \epsilon\epsilon\, \rangle_\beta$ correlator requires more corrections to obtain the same level of precision.[40]

The dispersion relation (4.2.25) overcomes this limitation since, as we pointed out in the previous paragraph, it already encodes an infinite number of corrections. We can therefore adopt the same strategy employed for the $\langle\, \sigma\sigma\, \rangle_\beta$ correlator and plug the bootstrap results of [148] in the formula. First we convert the OPE coefficients extracted out of $\langle\, \sigma\sigma\, \rangle_\beta$ (indicated by $a^{\langle\sigma\sigma\rangle}_{\Delta_\mathcal{O}}$) into those relevant for $\langle\, \epsilon\epsilon\, \rangle_\beta$ (indicated by $a^{\langle\epsilon\epsilon\rangle}_{\Delta_\mathcal{O}}$). Specifically, we use the relation

$$a^{\langle\epsilon\epsilon\rangle}_{\Delta_\mathcal{O}} = \left(\frac{f_{\mathcal{O}\epsilon\epsilon}}{f_{\mathcal{O}\sigma\sigma}}\right) a^{\langle\sigma\sigma\rangle}_{\Delta_\mathcal{O}} \ . \tag{4.4.35}$$

This yields the estimates

$$a^{\langle\epsilon\epsilon\rangle}_{\Delta_\epsilon} = 1.09(22) \ , \qquad a^{\langle\epsilon\epsilon\rangle}_{\Delta_T} = 5.37(19) \ . \tag{4.4.36}$$

[40] As argued in [147] and [148], this can be seen heuristically by noticing that the contribution of the heavy tail to the thermal sum rules increases when the external dimension Δ_ϕ increases as well, leading to the conclusion that correlators with higher external dimension require a more precise evaluation of the tail. *A posteriori*, this line of thought is justified by the fully corrected asymptotics (4.4.24) and (4.4.25), where it can be seen that the corrections to the leading order are monotonic functions of Δ_ϕ.

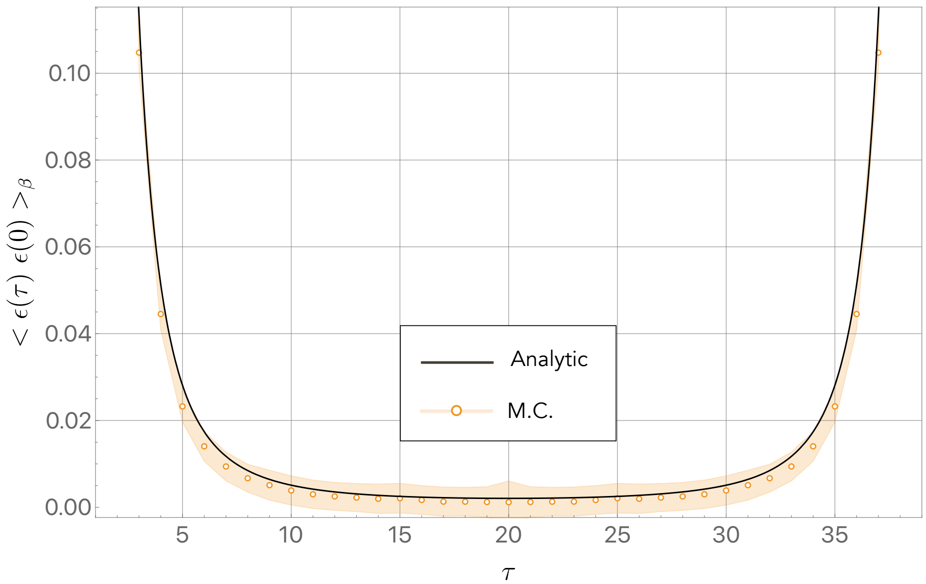

Figure 4.17: *Two-point function $\langle\, \epsilon(\tau)\epsilon(0)\,\rangle_\beta$ computed by inverting the contributions of $\mathbb{1}$, ϵ, and $T_{\mu\nu}$ using the dispersion relation in the complex τ-plane. The result is compared with Monte Carlo simulations on a $500 \times 500 \times 40$ lattice, corresponding to inverse temperature $\beta = 40$.*

Using this information, we approximate the thermal two-point function as

$$\langle\epsilon(\tau)\epsilon(0)\rangle_\beta \approx \sum_{\mathcal{O}\in\{\mathbb{1},\epsilon,T\}} \frac{a_{\Delta_\mathcal{O}}}{\beta^{2\Delta_\epsilon}} \left[\zeta_H\left(2\Delta_\epsilon - \Delta_\mathcal{O}, \frac{\tau}{\beta}\right) + \zeta_H\left(2\Delta_\epsilon - \Delta_\mathcal{O}, 1 - \frac{\tau}{\beta}\right)\right] + \frac{\kappa}{\beta^{2\Delta_\epsilon}}\,. \tag{4.4.37}$$

As before, the dispersion relation is ambiguous up to an additive constant κ. To fix it, we match the result with the OPE-expanded correlator, truncated to the contributions from $\mathbb{1}$, ϵ, and $T_{\mu\nu}$ in the region $\tau/\beta \lesssim 0.05$, where the OPE series is rapidly convergent. One could check that including additional operators (using large Δ asymptotic to estimate their OPE coefficients) does not significantly alter the result. The procedure yields an estimated value $\kappa \approx 1.81$.

In Fig. 4.17, we plot the function (4.4.37) and compare it to the outcome of Monte Carlo simulations, observing again very good agreement. As in the $\langle\,\sigma\sigma\,\rangle_\beta$ case, a multiplicative normalization constant is required. This constant, which amounts to a redefinition of the ϵ operator, is determined by fitting the Monte Carlo data, yielding $C_\epsilon \approx 5.04$.

This concludes our results on the analytic and numeric bootstrap methods that were developed in [3, 4].

Chapter 5

Conclusion

In this thesis, we consider the breaking of two symmetry groups in various QFTs, namely supersymmetry and conformal symmetry. In both cases, we focus on a powerful tool which, in the presence of the respective symmetry, allows us to compute a large number of physical observables. In the case of supersymmetry, this technique is CBA, while in the case of conformal symmetry it is the conformal bootstrap. After breaking the symmetry in a controlled way, by orbifolding and compactifying a flat direction in the respective cases, we develop these techniques further. We then apply them to various examples and gather results. In the following, we consider these two cases separately and outline promising directions for future work.

5.1 Breaking of Supersymmetry

In Chapter 3, we took an important step in the study of spin chains capturing the spectral problem of gauge theories with less than maximal supersymmetry, in particular $\mathcal{N} = 2$ SCFTs. We attacked the up to now unsolved three-magnon and four-magnon problems without which the question of integrability cannot be meaningfully addressed.

Our solutions have additive energy eigenvalues and several novel features, the discussion of which is in order. Firstly, they necessarily have the form of novel long-range wave functions. Secondly, the general solution, as presented in Section 3.3 and in Section 3.4, contains an infinite number of unfixed parameters. This is, at least in part, due to not imposing boundary conditions as three magnon states are non-closable, *i.e.* cannot lead to single trace operators. Nonetheless, for the three-magnon problem, using the symmetries of the problem and our intuition, we can brute force fix all of the position-dependent corrections and get special solutions in Section 3.3.2. A feature of the special solutions is that they can be rendered in odd and even eigenvectors (3.8.3) and (3.8.4) of the combined $\mathbb{Z}_2$ plus parity symmetry, as expected from the orbifold construction. Moreover, for each of these special solutions, the position-dependent corrections to the scattering coefficients modify the position dependence of the wave function as

$$e^{ip_1l_1+ip_2l_2+ip_3l_3} \longrightarrow (1+f(p_1,p_2,p_3;n,m;\kappa))\, e^{ip_1l_1+ip_2l_2+ip_3l_3}\ , \tag{5.1.1}$$

with the modification encoded in the generating function $G_{123}(x,y)$

$$f(p_1,p_2,p_3;n,m,\kappa) = -\oint_\Sigma \frac{dxdy}{4\pi^2}\frac{G_{123}(x,y)}{x^{n+1}y^{m+1}}\ , \tag{5.1.2}$$

the form of which is still quite baroque, but can be explicitly written as in [1]. We believe that this form of the wave function is given by the sum over permutations,

$$\Psi(p_1,p_2,p_3;l_1,l_2,l_3) = \sum_{\sigma\in\mathcal{S}_3} A_\sigma \left(1+f(p_{\sigma(1)},p_{\sigma(2)},p_{\sigma(3)};l_2-l_1,l_3-l_2;\kappa)\right) e^{i\vec{p}_\sigma\cdot\vec{l}}\ , \tag{5.1.3}$$

can be transformed to the case of the usual CBA by a coordinate transformation which remains to be explicitly shown. It is encouraging that the final form of the generating function implies that we can find a solution of the wave function in terms of position-dependent corrections which admit a common description in terms of the function above (5.1.2) for each permutation σ.

For the four-magnon problem, in Section 3.4.2, we begin to fix the coefficients that remained undetermined after solving the eigenvalue equations. The family of solutions is reduced by imposing additional constraints, guided by the symmetries of the problem and following an approach analogous to the three-magnon case. This procedure leads to a special solution characterized by factorized scattering coefficients A_σ, given in equation (3.4.50), and position-dependent corrections $D_\sigma^{n,m,r}$, all proportional to $(\kappa-\kappa^{-1})A_\sigma$ for each permutation $\sigma\in\mathcal{S}_4$. The presence of this factor for all $n,m,r\in\mathbb{Z}\geq 0$ ensures that at the orbifold point ($\kappa=1$) all these position-dependent corrections to the ordinary CBA vanish. The remaining undetermined $D_\sigma^{n,m,r}$'s, after applying these constraints, can be systematically counted and organized, as summarized in Table 3.2.

In Section 3.5, we introduced a physically motivated limiting procedure that relates eigenstates with different magnon numbers. By averaging over all possible positions of one magnon in an $(M+1)$-magnon eigenstate and setting its momentum to zero, we showed that the resulting state reduces to the corresponding M-magnon eigenstate. This procedure, which can be interpreted as smearing a magnon, arises naturally within the standard CBA framework (Subsection 3.5.1) and provides a systematic method for connecting spin chain solutions across successive magnon sectors.

Taken together, these results reveal a coherent underlying structure in the spectrum of eigenstates, with different magnon sectors linked through a well-defined limiting process. This work lays the groundwork for further exploration of long-range CBA and the structure of their eigenstates beyond the sectors considered here.

We make use of this manifest permutation structure of our special long-range solutions, as discussed in Section 3.7, to construct an infinite tower of Yang operators labeled by two integers (or three for the four-magnon case) that parameterize the distances between the three magnons. These Yang operators constructed from the special solutions obey an infinite tower of modified Yang-Baxter equations parameterized by the same two integers. As we take $\kappa \to 1$, the contributions of the position-dependent corrections vanish and the tower of modified YBEs collapses to the single YBE of orbifold point, which is expected from [71].

The long-range correction to the usual Bethe Ansatz captures the fact that the permutation symmetry of the three-magnon states is naively broken because the magnons are bifundamental. For models where the permutation symmetry is present, the solution should always be possible to write in terms of the usual Bethe ansatz. In our case, because of the $\mathbb{Z}_2$ orbifold in tandem with the marginal deformation κ, the permutation group of the three magnons breaks into two subsets, as we discuss in Section 3.3.1 which is summarized in Figure 3.5. The position-dependent corrections of our solution eventually restore the permutation symmetry (5.1.3). This could be a very explicit manifestation of the dynamical nature of the model [82] which deserves further investigation. This must also be related to the fact that even though naively in three of the entries of the YBE we were supposed to have $S_{1/\kappa}$ according to the naive Bethe Ansatz, our long-range solution has S_κ which was achieved by using the analogy between our model and a Felder-like dynamical R-matrix. An attempt to visually capture this is presented in Figure 3.6.

Finally, in Section 3.8, we examined the compatibility of the long-range Bethe ansatz with periodic boundary conditions. We began by solving the two-magnon Bethe equations and then extended the analysis to the four-magnon case. Already in the two-magnon sector, a novel feature emerges: by introducing a relative normalization factor between $\mathbb{Z}_2$-conjugate states, we are able to recover all eigenvectors—both for untwisted and twisted boundary conditions—via a generalized version of the Bethe equations. In contrast, the four-magnon problem does not admit a solution within the standard CBA framework, making it infeasible to directly apply Bethe equations to determine the quantized momenta. To address this challenge, we adopted an alternative strategy: we formulated and solved the periodicity relations at the level of wavefunctions for closed spin chains of finite length ($L = 4, 5, 6$). This construction offers a concrete and practical method for incorporating periodic boundary conditions within the long-range Bethe ansatz framework.

Nevertheless, our current approach is not yet fully scalable to arbitrary chain lengths L, due to the absence of a systematic method for efficiently implementing periodic boundary conditions within this approach. We believe that a key obstacle lies in the necessity of working with momentum variables, rather than rapidities. Identifying an appropriate rapidity parametrization may allow the position-dependent corrections to be reinterpreted as a coordinate transformation. This, in turn, could lead to a derivation of the correct form of the long-range Bethe equations under periodic boundary conditions.

Future Directions. There are many promising future directions one can take. Here we are listing a few:

- As emphasized throughout this work, it would be highly desirable to identify the correct rapidity description of the model by comparing the ϕ-vacuum states studied here to the Q-vacuum states of [82]. We expect that expressing the wave function in terms of rapidities—rather than momenta—will simplify the position-dependent corrections and allow a more efficient treatment of periodic boundary conditions.

- Given our expectation that this spin chain model is elliptic based on a groupoid symmetry, the rapidity variables should likely involve elliptic functions. We intend to explore this further by building on the elliptic parametrization discussed in [82], potentially establishing a connection to an underlying Felder-like R-matrix similar to [139, 140] but for Cyclic SOS (CSOS) models instead of RSOS.

- A suitable rapidity parametrization may also clarify the correct basis transformation from the plane wave basis discussed in Section 3.7, and help refine the structure of the modified Yang–Baxter tower into a single, unified YBE-type equation.

- In parallel, we aim to extend the present results by using the four-magnon solution—expressed in terms of the three-magnon solution—to construct explicit M-magnon eigenstates via the generating function. We believe that the insights from Section 3.5 will make this construction feasible.

- Another important direction is the search for higher conserved charges, following the approach of [248–251]. We are already working on generalizing the boost formalism to Felder-like R-matrices, with the goal of obtaining the higher charges of the model. The restricted Hilbert space, arising from the groupoid structure [252], may simplify this task, particularly if one focuses on permutationally symmetric states.

- It would also be valuable to carry out a detailed numerical analysis of the spectrum of this model, similar to the studies in [253] for spin chains in $\mathcal{N} = 4$ SYM and its $\mathcal{N} = 1$ Leigh–Strassler deformations. In particular, counting spectral degeneracies—as done for small lengths in [254]—could shed light on the integrable versus chaotic behavior of the system.

- An exciting recent development has been the extension of the hexagon formalism [255] to orbifold theories [69, 79]. A promising future direction is to generalize the hexagon approach beyond the orbifold point, and to extend the analysis of [69] to compute three-point functions of operators with four magnon excitations, using the results obtained in this thesis.

- Finally, in light of recent developments on the gauge theory side, we are motivated to revisit the string theory dual. The recent supergravity construction of [68], which resolves the $AdS_5 \times S^5/\mathbb{Z}_2$ orbifold singularity, provides a timely opportunity to study the corresponding two-dimensional worldsheet QFT and explore the string dual of the marginally deformed theory.

5.2 Breaking of Conformality

In chapter 4, we presented our efforts to generalize the conformal bootstrap techniques to finite-temperature setups. The primary bootstrap method we targeted is the dispersion relation derived from first principles that was presented in section 4.1. Additionally, we mixed the results of analytic bootstrap with numerical methods utilizing finite-temperature sum rules and obtained novel results for the $3d$ Ising model.

More detailily, we developed an analytic framework to bootstrap thermal two-point functions based on dispersion relations, the operator product expansion, and the KMS condition. We showed that, in the periodic Euclidean time coordinate and at zero spatial separation, any thermal two-point function can be expanded in terms of generalized free-field correlators. The coefficients of this expansion are given by certain thermal OPE coefficients. This result, explicitly presented in Eq. (4.2.25), follows from expressing the two-point function in terms of its discontinuity in the complex time plane.

We further investigated the dispersion relation at non-zero spatial separation introduced in [152], and its interplay with the OPE and the KMS condition. We found that computing the discontinuity in the OPE regime captures only the leading polynomial behavior at large spin. In contrast, non-polynomial corrections arise from contributions outside the OPE regime, in full agreement with the structure of large-spin perturbation theory described in [146]. Moreover, we observed that the naive result from the dispersion relation within the OPE regime is not KMS invariant. Motivated by the complex τ-plane analysis, we proposed a prescription to restore KMS invariance and simultaneously reconstruct the low-spin contributions. This involves summing over images of the dispersion relation result, leading to what we called the generalized method of images. We demonstrated that this construction satisfies all thermal bootstrap axioms, except clustering, which must be verified on a case-by-case basis. Additionally, we showed that if clustering holds, then the solution is unique — equivalently, arc contributions vanish.

We illustrated the applicability of our method in several examples. In the case of the free scalar theory, the generalized method of images reduces to the standard one, effectively reproducing a sum over propagators. We then studied the $\mathrm{O}(N)$ model in the ε-expansion and found perfect agreement with direct perturbative calculations. Finally, we tested our results in exactly solvable strongly coupled regimes, namely the large N limit of the $\mathrm{O}(N)$ model and in two-dimensional models, reproducing the known results.

From Section 4.3 onward, we analyzed thermal two-point functions of scalar operators with integer scaling dimension Δ_ϕ, both at infinite volume and at finite volume on a sphere. These two settings are holographically dual to AdS black brane and spherical black hole backgrounds, respectively. Our approach is based on expanding thermal correlators at zero spatial separation in terms of GFF correlators,

$$g(\tau) = \sum_{\Delta} \frac{a_\Delta}{\beta^\Delta} g_{\mathrm{GFF}}\left(\Delta_\phi - \frac{\Delta}{2}, \tau\right) + g_{\mathrm{arcs}}(\tau)\,, \tag{5.2.1}$$

a representation that was rigorously established for finite temperature CFTs at infinite volume in this thesis. We further extended its validity to finite volume systems, under the condition that both external and exchanged operator dimensions are integer and focusing on the terms that do not involve poles in the OPE coefficients.

For holographic correlators, the first term in the expansion (5.2.1) splits into two contributions: a *principal contribution*, to which only a finite set of multi-stress tensor operators (associated with $\Delta < 2\Delta_\phi$) contributes directly, and a *regularized part*, encoding an infinite number of multi-stress tensor operators. The regularized term requires to appropriately employ derivatives of the GFF blocks. Similarly to the non-integer Δ_ϕ case, the arcs are non-trivial functions but their contributions can be computed and they also admit an expansion in terms of GFF correlators. These tools allow the derivation of analytical results for any integer value of Δ_ϕ, whose explicit evaluation requires using the asymptotic form of the multi-stress tensor OPE coefficients. To the best of our knowledge, this provides the first approximate expressions for thermal holographic correlators in $d > 2$ as a function of the imaginary time in the case of integer Δ_ϕ. We corroborate these results by solving the scalar wave equation numerically and find convincing agreement for the black brane case, which additionally surprisingly suggests that the principal contributions dominate everywhere. We also provide an AdS interpretation of (5.2.1) as an expansion of the metric in graviton modes around thermal AdS, and we verify this picture through explicit Witten diagram computations up to second order in the expansion parameter. Finally, curvature corrections to the thermal correlators are also included in (5.2.1) as anomalous dimensions are suppressed with respect to N, i.e., only the OPE coefficients a_Δ need to be corrected.

Lastly in Section 4.4, by combining analytic and numerical techniques — in particular the method proposed in [148] — we made substantial progress on the thermal bootstrap program. Using the dispersion relation in the complex time direction, we rederived the Tauberian estimate for the contribution of heavy operators in the OPE, originally obtained through different means in [147]. Furthermore, our method allows the computation of the full tower of corrections to the leading heavy-state contribution, including the coefficient of the first correction used in [148]. As an application, we combined the numerical approach of [148] with our analytic dispersion relation to compute the thermal two-point function $\langle \epsilon\epsilon \rangle_\beta$ in the $3d$ Ising model, finding excellent agreement with Monte Carlo simulations.

The thermal bootstrap program remains rich with open questions, both at the conceptual level and in terms of applications to physically relevant models. We highlight below several promising directions for future work:

- One of the main challenges in thermal bootstrap is the lack of positivity of thermal OPE coefficients, which complicates the derivation of rigorous numerical bounds. While existing studies [146, 148] have circumvented this by developing non-positivity-based methods, it would be highly desirable to find intrinsically positive observables — such as the hydrodynamic moments discussed in [212] — or to reformulate the thermal bootstrap as a semi-definite programming problem.

- This work has focused on conformal field theories at criticality. However, many observables of physical interest arise in theories deformed away from the critical point. Extending the non-perturbative methods developed here to non-conformal theories at finite temperature, or to relevant deformations of CFTs, would open new avenues for understanding finite-temperature dynamics in realistic models. Furthermore the non-perturbative study of QFTs at finite temperature could give further insights on the order or disorder phases at high temperature which are extremely important for the understanding of the thermodynamics of QFTs [256–259].

- In [148], a bootstrap framework was proposed for line defects wrapping the thermal circle. These include, for instance, Polyakov loops in gauge theories, which serve as order parameters for confinement/deconfinement transitions and are closely related to the Kondo effect in low-energy physics [260, 261]. Extending the techniques developed in this thesis to include such line defects would be a significant step forward and would enable the study of setups such as the magnetic line in $\mathrm{O}(N)$ models [192, 262–265] and the supersymmetric Wilson line in $\mathcal{N} = 4$ SYM [266–272] at finite temperature. Many aspects are expected to carry over to correlators of defect operators.

- Most of the equations and results derived in this work concern two-point functions of scalar operators in bosonic theories. It would be highly valuable to generalize this framework to include fermionic operators, enabling the study of theories such as the chiral Gross–Neveu model and the Gross–Neveu–Yukawa model. Recent progress in this direction can be found in [273].

- The results obtained in this work admit several natural extensions. First, it would be interesting to understand how to better approximate the regularized contribution. This boils down to improving the approximation of the asymptotic OPE coefficients, for instance by including $1/n^{\#}$ corrections as in [223] for instance. Second, beyond the kinematic regime $|\vec{x}| = 0$ the OPE contributions become disentangled in spin. Moreover, as noted in [221], the large Δ behavior of the multi-stress tensor sector involves alternating signs that spoil analyticity in Δ. It would be interesting to explore the analyticity in spin J [210, 221], which would imply studying the correlator at non-vanishing spatial separation. Additionally, it might be possible to determine an approximate solution of the wave equation, in analogy with the procedure outlined in this thesis.

⋆ An important check for the non-zero spatial separation correlator would be to compare it with the exact momentum-space correlators computed in [209]. The

τ-plane correlators studied in this thesis correspond to integrating over all momentum modes, which is analytically challenging. Nevertheless, it is worth noting that integrating out the momentum modes reduces the correlator of [209] to the Fourier transform of GFF blocks, as discussed in [3]. The relation between these two exact results should be valuable to understand the IR behaviour of the correlator (such as $\omega \to \infty$) and deserves to be explored more deeply.

- As mentioned in Section 4.3, thermal correlation functions can be viewed as zero-temperature four-point functions where two of the operators are taken to be heavy. For holographic theories, this correspondence was partially verified perturbatively (and at large spin) in [209]. It would be interesting to further investigate this connection in light of the results presented in this thesis. The case in which Δ_ϕ is an integer is intricate from the perspective of four-point functions [204, 207] and the thermal bootstrap may provide useful insights into the structure of these correlators;

- A deeper understanding of the geometry $S^1_\beta \times S^{d-1}_R$ would be valuable, particularly regarding how modifications of the analytic structure might affect Equation (5.2.1). Establishing this would enable the use of the expansion beyond holographic theories, for instance in models such as the $3d$ Ising CFT, in close analogy with the infinite volume analysis of the thermal $3d$ Ising model performed in [3].

- The results presented in this work correspond to the leading term in the $1/N$ expansion. Including quantum effects requires going to next-to-leading order in the same expansion. The main difficulty in this context is that, once CFT operators acquire anomalous dimensions, additional operators – potentially an infinite number – contribute non-trivially to the dispersion relation. Nevertheless, it was shown in [148] that the expansion in (5.2.1) is extremely effective in perturbative setups (in that work, the case of the $\mathrm{O}(N)$ model in the ε-expansion). Furthermore, anomalous dimensions happen to make numerical methods more predictive: in this context we expect to be able to compute unknown OPE coefficients by making use of both analytical and numerical methods in tandem. Incorporating $1/N$ corrections therefore represents one of the key future directions for the thermal analytic and numerical bootstrap.

Bibliography

[1] D. N. Bozkurt, J. M. Nieto García, and E. Pomoni, "Long-range to the Rescue of Yang-Baxter," arXiv:2408.03365 [hep-th].

[2] D. N. Bozkurt, J. M. Nieto García, Z. Kong, and E. Pomoni, "Long-range to the Rescue of Yang-Baxter II," arXiv:2507.08934 [hep-th].

[3] J. Barrat, D. N. Bozkurt, E. Marchetto, A. Miscioscia, and E. Pomoni, "The analytic bootstrap at finite temperature," arXiv:2506.06422 [hep-th].

[4] J. Barrat, D. N. Bozkurt, E. Marchetto, A. Miscioscia, and E. Pomoni, "Analytic thermal bootstrap meets holography," arXiv:2510.20894 [hep-th].

[5] J. C. Maxwell, "A dynamical theory of the electromagnetic field,".

[6] M. Planck, "On the law of distribution of energy in the normal spectrum," *Annalen der Physik* **309** no. 3, (1901) 553–563. Originally published in German as "Ueber das Gesetz der Energieverteilung im Normalspectrum".

[7] A. Einstein, "Zur elektrodynamik bewegter körper," *Annalen der Physik* **322** no. 10, (1905) 891–921. English title: "On the Electrodynamics of Moving Bodies".

[8] A. Einstein, "Die grundlage der allgemeinen relativitätstheorie," *Annalen der Physik* **354** no. 7, (1916) 769–822. English title: "The Foundation of the General Theory of Relativity".

[9] L. de Broglie, *Recherches sur la théorie des quanta*. PhD thesis, University of Paris, 1924. Doctoral thesis. English title: "Research on the Theory of the Quanta".

[10] A. Einstein, "über einen die erzeugung und verwandlung des lichtes betreffenden heuristischen gesichtspunkt," *Annalen der Physik* **322** no. 6, (1905) 132–148. English title: "On a Heuristic Point of View Concerning the Production and Transformation of Light".

[11] W. Heisenberg, "über quantentheoretische umdeutung kinematischer und mechanischer beziehungen," *Zeitschrift für Physik* **33** no. 1, (1925) 879–893. English title: "Quantum-theoretical reinterpretation of kinematic and mechanical relations".

[12] E. Schrödinger, "Quantisierung als eigenwertproblem," *Annalen der Physik* **384** no. 4,

(1926) 361–376. First paper in the series; English title: “Quantization as an Eigenvalue Problem”.

[13] P. A. M. Dirac, “The quantum theory of the electron,” *Proceedings of the Royal Society of London. Series A* **117** no. 778, (1928) 610–624.

[14] S. L. Glashow, “Partial symmetries of weak interactions,” *Nuclear Physics* **22** no. 4, (1961) 579–588.

[15] S. Weinberg, “A model of leptons,” *Physical Review Letters* **19** no. 21, (1967) 1264–1266.

[16] A. Salam, “Weak and electromagnetic interactions,” in *Elementary Particle Theory: Relativistic Groups and Analyticity*, N. Svartholm, ed., pp. 367–377. Almqvist and Wiksell, Stockholm, 1968. Proceedings of the 8th Nobel Symposium, Lerum, Sweden, May 19–25, 1968.

[17] M. B. Green and J. H. Schwarz, “Anomaly cancellation in supersymmetric d=10 gauge theory and superstring theory,” *Physics Letters B* **149** no. 1–3, (1984) 117–122.

[18] E. Witten, “Some properties of o(32) superstrings,” *Physics Letters B* **149** no. 4–5, (1984) 351–356.

[19] E. Witten, “Dimensional reduction of superstring models,” *Physics Letters B* **155** no. 1–2, (1985) 151–155.

[20] E. Noether, “Invariante variationsprobleme,” *Nachrichten von der Gesellschaft der Wissenschaften zu Göttingen, Mathematisch-Physikalische Klasse* **1918** (1918) 235–257. `http://eudml.org/doc/59024`. English title: “Invariant Variation Problems”.

[21] G. Mack, “Partially conserved dilatation current,” *Nuclear Physics B* **5** no. 3, (1968) 499–507. `https://www.sciencedirect.com/science/article/pii/0550321368902320`.

[22] A. M. Polyakov, “Microscopic description of critical phenomena,” *Zhurnal Eksperimental’noi i Teoreticheskoi Fiziki* **55** no. 3, (1968) 1026–1038. [Sov. Phys. JETP 28(3), 533–539 (1969)].

[23] A. M. Polyakov, “Conformal symmetry of critical fluctuations,” *JETP Letters* **12** (1970) 381–383. [Pisma Zh. Eksp. Teor. Fiz. 12, 538 (1970)].

[24] A. A. Migdal, “Correlation functions in the theory of phase transitions: Violation of the scaling laws,” *Zhurnal Eksperimental’noi i Teoreticheskoi Fiziki* **59** (1970) 1015–1031. [Sov. Phys. JETP 32(3), 552–560 (1971)].

[25] E. Witten and D. Olive, “Supersymmetry algebras that include topological charges,” *Physics Letters B* **78** (1978) 97–101.

[26] N. Seiberg, “Electric-magnetic duality in supersymmetric non-abelian gauge theories,” *Nuclear Physics B* **435** (1995) 129–146, `hep-th/9411149`.

[27] V. Pestun, "Localization of gauge theory on a four-sphere and supersymmetric wilson loops," *Communications in Mathematical Physics* **313** (2012) 71–129, 0712.2824.

[28] N. e. a. Beisert, "Review of ads/cft integrability: An overview," *Letters in Mathematical Physics* **99** (2012) 3–32, 1012.3982.

[29] N. Seiberg and E. Witten, "Electric-magnetic duality, monopole condensation, and confinement in $\mathcal{N} = 2$ supersymmetric yang-mills theory," *Nuclear Physics B* **426** (1994) 19–52, hep-th/9407087.

[30] L. F. Alday, D. Gaiotto, and Y. Tachikawa, "Liouville correlation functions from four-dimensional gauge theories," *Letters in Mathematical Physics* **91** (2010) 167–197, 0906.3219.

[31] J. M. Maldacena, "The Large N limit of superconformal field theories and supergravity," *Adv. Theor. Math. Phys.* **2** (1998) 231–252, arXiv:hep-th/9711200.

[32] E. Witten, "Anti-de Sitter space and holography," *Adv. Theor. Math. Phys.* **2** (1998) 253–291, arXiv:hep-th/9802150.

[33] J. I. Kapusta and C. Gale, *Finite-temperature field theory: Principles and applications*. Cambridge Monographs on Mathematical Physics. Cambridge University Press, 2011.

[34] S. Weinberg, *The Quantum Theory of Fields. Vol. 2: Modern Applications*. Cambridge University Press, 1996.

[35] M. E. Peskin and D. V. Schroeder, *An Introduction to quantum field theory*. Addison-Wesley, Reading, USA, 1995.

[36] Y. Nambu, "Axial vector current conservation in weak interactions," *Phys. Rev. Lett.* **4** (1960) 380–382.

[37] J. A. Minahan and K. Zarembo, "The Bethe ansatz for N=4 superYang-Mills," *JHEP* **03** (2003) 013, arXiv:hep-th/0212208.

[38] T. Matsubara, "A new approach to quantum-statistical mechanics," *Progress of Theoretical Physics* **14** no. 4, (1955) 351–378.

[39] D. Simmons-Duffin, "The lightcone bootstrap and the spectrum of the 3d ising cft," *JHEP* **03** (2017) 086, arXiv:1612.08471 [hep-th].

[40] S. Rychkov, *EPFL Lectures on Conformal Field Theory in D>= 3 Dimensions*. SpringerBriefs in Physics. 1, 2016. arXiv:1601.05000 [hep-th].

[41] M. Bertolini, *Supersymmetry*. WORLD SCIENTIFIC, 2025. https://www.worldscientific.com/doi/pdf/10.1142/14026. https://www.worldscientific.com/doi/abs/10.1142/14026.

[42] E. Pomoni, "4D $\mathcal{N} = 2$ SCFTs and spin chains," *J. Phys. A* **53** no. 28, (2020) 283005, arXiv:1912.00870 [hep-th].

[43] L. Eberhardt, "Superconformal symmetry and representations," *J. Phys. A* **54** no. 6, (2021) 063002, arXiv:2006.13280 [hep-th].

[44] N. Seiberg and E. Witten, "Electric - magnetic duality, monopole condensation, and confinement in N=2 supersymmetric Yang-Mills theory," *Nucl. Phys. B* **426** (1994) 19–52, arXiv:hep-th/9407087. [Erratum: Nucl.Phys.B 430, 485–486 (1994)].

[45] N. Seiberg and E. Witten, "Monopoles, duality and chiral symmetry breaking in N=2 supersymmetric QCD," *Nucl. Phys. B* **431** (1994) 484–550, arXiv:hep-th/9408099.

[46] E. Witten, "Supersymmetry and Morse theory," *J. Diff. Geom.* **17** no. 4, (1982) 661–692.

[47] L. Alvarez-Gaume and E. Witten, "Gravitational Anomalies," *Nucl. Phys. B* **234** (1984) 269.

[48] S. R. Coleman and J. Mandula, "All Possible Symmetries of the S Matrix," *Phys. Rev.* **159** (1967) 1251–1256.

[49] S. Weinberg and E. Witten, "Limits on Massless Particles," *Phys. Lett. B* **96** (1980) 59–62.

[50] F. A. Dolan and H. Osborn, "Superconformal symmetry, correlation functions and the operator product expansion," *Nucl. Phys. B* **629** (2002) 3–73, arXiv:hep-th/0112251.

[51] F. A. Dolan and H. Osborn, "On short and semi-short representations for four-dimensional superconformal symmetry," *Annals Phys.* **307** (2003) 41–89, arXiv:hep-th/0209056.

[52] L. Bhardwaj and Y. Tachikawa, "Classification of 4d N=2 gauge theories," *JHEP* **12** (2013) 100, arXiv:1309.5160 [hep-th].

[53] G. Hooft, "A planar diagram theory for strong interactions," *Nuclear Physics B* **72** no. 3, (1974) 461–473. https://www.sciencedirect.com/science/article/pii/0550321374901540.

[54] N. Beisert *et al.*, "Review of AdS/CFT Integrability: An Overview," *Lett. Math. Phys.* **99** (2012) 3–32, arXiv:1012.3982 [hep-th].

[55] E. Witten, "Anti-de Sitter space, thermal phase transition, and confinement in gauge theories," *Adv. Theor. Math. Phys.* **2** (1998) 505–532, arXiv:hep-th/9803131.

[56] C. Copetti, A. Grassi, Z. Komargodski, and L. Tizzano, "Delayed deconfinement and the Hawking-Page transition," *JHEP* **04** (2022) 132, arXiv:2008.04950 [hep-th].

[57] M. de Leeuw, "One-point functions in AdS/dCFT," *J. Phys. A* **53** no. 28, (2020) 283001, arXiv:1908.03444 [hep-th].

[58] M. de Leeuw, A. C. Ipsen, C. Kristjansen, and M. Wilhelm, "Introduction to integrability and one-point functions in n = 4 sym and its defect cousin," 2017.

[59] W. Heisenberg, "Zur Theorie des Ferromagnetismus," *Z. Phys.* **49** no. 9-10, (1928) 619–636.

[60] G. Arutyunov, *Elements of Classical and Quantum Integrable Systems*. UNITEXT for Physics. Springer International Publishing, 2019. https://books.google.de/books?id=o86kDwAAQBAJ.

[61] C. Gómez, M. Ruiz-Altaba, and G. Sierra, *Quantum Groups in Two-Dimensional Physics*. Cambridge Monographs on Mathematical Physics. Cambridge University Press, 1996.

[62] M. R. Douglas and G. W. Moore, "D-branes, quivers, and ALE instantons," arXiv:hep-th/9603167.

[63] S. Kachru and E. Silverstein, "4-D conformal theories and strings on orbifolds," *Phys. Rev. Lett.* **80** (1998) 4855–4858, arXiv:hep-th/9802183.

[64] A. E. Lawrence, N. Nekrasov, and C. Vafa, "On conformal field theories in four-dimensions," *Nucl. Phys. B* **533** (1998) 199–209, arXiv:hep-th/9803015.

[65] M. Bershadsky and A. Johansen, "Large N limit of orbifold field theories," *Nucl. Phys. B* **536** (1998) 141–148, arXiv:hep-th/9803249.

[66] S. Gukov, "Comments on N=2 AdS orbifolds," *Phys. Lett. B* **439** (1998) 23–28, arXiv:hep-th/9806180.

[67] I. R. Klebanov and N. A. Nekrasov, "Gravity duals of fractional branes and logarithmic RG flow," *Nucl. Phys. B* **574** (2000) 263–274, arXiv:hep-th/9911096.

[68] T. Skrzypek and A. A. Tseytlin, "On AdS/CFT duality in the twisted sector of string theory on $AdS_5 \times S^5/\mathbb{Z}_2$ orbifold background," *JHEP* **03** (2024) 045, arXiv:2312.13850 [hep-th].

[69] D. le Plat and T. Skrzypek, "Three-point functions from integrability in $\mathcal{N} = 2$ orbifold theories," arXiv:2506.21323 [hep-th].

[70] C. B. Martínez and T. Skrzypek, "Exploring the twisted sector of $\mathbb{Z}_L$ orbifolds: Matching α'-corrections to localisation," arXiv:2512.16984 [hep-th].

[71] N. Beisert and R. Roiban, "The Bethe ansatz for Z_S orbifolds of $\mathcal{N} = 4$ super Yang-Mills theory," *JHEP* **11** (2005) 037, arXiv:hep-th/0510209.

[72] N. Beisert and R. Roiban, "Beauty and the twist: The Bethe ansatz for twisted $\mathcal{N} = 4$ SYM," *JHEP* **08** (2005) 039, arXiv:hep-th/0505187.

[73] X.-J. Wang and Y.-S. Wu, "Integrable spin chain and operator mixing in n=1,2 supersymmetric theories," *Nuclear Physics B* **683** (2004) 363–386, arXiv:hep-th/0311073 [hep-th].

[74] K. Ideguchi, "Semiclassical strings on ads(5) x s(5)/z(m) and operators in orbifold

field theories," *Journal of High Energy Physics* **09** (2004) 008, arXiv:hep-th/0408014 [hep-th].

[75] A. Solovyov, "Bethe ansatz equations for general orbifolds of n=4 sym," *Journal of High Energy Physics* **04** (2008) 013, arXiv:0711.1697 [hep-th].

[76] M. Beccaria and G. Macorini, "Y-system for z_s orbifolds of n=4 sym," *Journal of High Energy Physics* **06** (2011) 004, arXiv:1104.0883 [hep-th].

[77] G. Arutyunov, M. de Leeuw, and S. J. van Tongeren, "Twisting the mirror tba," *Journal of High Energy Physics* **02** (2011) 025, arXiv:1009.4118 [hep-th].

[78] M. de Leeuw and S. J. van Tongeren, "The spectral problem for strings on twisted ads$_5\times$ s^5," *Nuclear Physics B* **860** (2012) 339–376, arXiv:1201.1451 [hep-th].

[79] G. Ferrando, S. Komatsu, G. Lefundes, and D. Serban, "Exact Three-Point Functions in $\mathcal{N}=2$ Superconformal Field Theories: Integrability vs. Localization," arXiv:2503.07295 [hep-th].

[80] A. Gadde, E. Pomoni, and L. Rastelli, "The Veneziano Limit of $\mathcal{N}=2$ Superconformal QCD: Towards the String Dual of $\mathcal{N}=2$ $SU(N_c)$ SYM with $N_f=2N_c$," arXiv:0912.4918 [hep-th].

[81] A. Gadde, E. Pomoni, and L. Rastelli, "Spin Chains in $\mathcal{N}$=2 Superconformal Theories: From the $\mathbb{Z}_2$ Quiver to Superconformal QCD," *JHEP* **06** (2012) 107, arXiv:1006.0015 [hep-th].

[82] E. Pomoni, R. Rabe, and K. Zoubos, "Dynamical spin chains in 4D $\mathcal{N}=2$ SCFTs," *JHEP* **08** (2021) 127, arXiv:2106.08449 [hep-th].

[83] V. Riva and J. L. Cardy, "Scale and conformal invariance in field theory: A Physical counterexample," *Phys. Lett. B* **622** (2005) 339–342, arXiv:hep-th/0504197.

[84] J. Polchinski, "Scale and conformal invariance in quantum field theory," *Nuclear Physics B* **303** no. 2, (1988) 226–236. https://www.sciencedirect.com/science/article/pii/0550321388901794.

[85] A. Dymarsky, Z. Komargodski, A. Schwimmer, and S. Theisen, "On Scale and Conformal Invariance in Four Dimensions," *JHEP* **10** (2015) 171, arXiv:1309.2921 [hep-th].

[86] A. Gimenez-Grau, Y. Nakayama, and S. Rychkov, "Scale without conformal invariance in dipolar ferromagnets," *Phys. Rev. B* **110** no. 2, (2024) 024421, arXiv:2309.02514 [hep-th].

[87] M. S. Costa, T. Hansen, J. Penedones, and E. Trevisani, "Projectors and seed conformal blocks for traceless mixed-symmetry tensors," *JHEP* **07** (2016) 018, arXiv:1603.05551 [hep-th].

[88] D. Simmons-Duffin, "Projectors, Shadows, and Conformal Blocks," *JHEP* **04** (2014) 146, arXiv:1204.3894 [hep-th].

[89] M. S. Costa, J. Penedones, D. Poland, and S. Rychkov, "Spinning Conformal Correlators," *JHEP* **11** (2011) 071, arXiv:1107.3554 [hep-th].

[90] M. Reehorst, E. Trevisani, and A. Vichi, "Mixed Scalar-Current bootstrap in three dimensions," *JHEP* **12** (2020) 156, arXiv:1911.05747 [hep-th].

[91] A. Dymarsky, J. Penedones, E. Trevisani, and A. Vichi, "Charting the space of 3D CFTs with a continuous global symmetry," *JHEP* **05** (2019) 098, arXiv:1705.04278 [hep-th].

[92] A. Dymarsky, F. Kos, P. Kravchuk, D. Poland, and D. Simmons-Duffin, "The 3d Stress-Tensor Bootstrap," *JHEP* **02** (2018) 164, arXiv:1708.05718 [hep-th].

[93] S. Ferrara, A. Grillo, and R. Gatto, "Tensor representations of conformal algebra and conformally covariant operator product expansion," *Annals of Physics* **76** no. 1, (1973) 161–188. https://www.sciencedirect.com/science/article/pii/0003491673904466.

[94] A. M. Polyakov, "Non-Hamiltonian approach to conformal quantum field theory," *Zh. Eksp. Teor. Fiz.* **66** no. 1, (1974) 23–42.

[95] A. Belavin, A. Polyakov, and A. Zamolodchikov, "Infinite conformal symmetry in two-dimensional quantum field theory," *Nuclear Physics B* **241** no. 2, (1984) 333–380. https://www.sciencedirect.com/science/article/pii/055032138490052X.

[96] F. A. Dolan and H. Osborn, "Conformal partial waves and the operator product expansion," *Nucl. Phys. B* **678** (2004) 491–507, arXiv:hep-th/0309180.

[97] R. Rattazzi, V. S. Rychkov, E. Tonni, and A. Vichi, "Bounding scalar operator dimensions in 4D CFT," *JHEP* **12** (2008) 031, arXiv:0807.0004 [hep-th].

[98] S. El-Showk, M. F. Paulos, D. Poland, S. Rychkov, D. Simmons-Duffin, and A. Vichi, "Solving the 3D Ising Model with the Conformal Bootstrap," *Phys. Rev. D* **86** (2012) 025022, arXiv:1203.6064 [hep-th].

[99] S. El-Showk, M. F. Paulos, D. Poland, S. Rychkov, D. Simmons-Duffin, and A. Vichi, "Solving the 3d Ising Model with the Conformal Bootstrap II. c-Minimization and Precise Critical Exponents," *J. Stat. Phys.* **157** (2014) 869, arXiv:1403.4545 [hep-th].

[100] F. Kos, D. Poland, D. Simmons-Duffin, and A. Vichi, "Precision Islands in the Ising and $O(N)$ Models," *JHEP* **08** (2016) 036, arXiv:1603.04436 [hep-th].

[101] D. Poland, S. Rychkov, and A. Vichi, "The Conformal Bootstrap: Theory, Numerical Techniques, and Applications," *Rev. Mod. Phys.* **91** (2019) 015002, arXiv:1805.04405 [hep-th].

[102] C.-H. Chang, V. Dommes, P. Kravchuk, D. Poland, and D. Simmons-Duffin, "Accurate bootstrap bounds from optimal interpolation," arXiv:2509.14307 [hep-th].

[103] C.-H. Chang, V. Dommes, R. S. Erramilli, A. Homrich, P. Kravchuk, A. Liu, M. S. Mitchell, D. Poland, and D. Simmons-Duffin, "Bootstrapping the 3d Ising stress tensor," *JHEP* **03** (2025) 136, arXiv:2411.15300 [hep-th].

[104] D. Pappadopulo, S. Rychkov, J. Espin, and R. Rattazzi, "OPE Convergence in Conformal Field Theory," *Phys. Rev. D* **86** (2012) 105043, arXiv:1208.6449 [hep-th].

[105] V. N. Gribov, "Possible Asymptotic Behavior of Elastic Scattering," *JETP Lett.* **41** (1961) 667–669.

[106] P. D. B. Collins, *An Introduction to Regge Theory and High-Energy Physics*. Cambridge Monographs on Mathematical Physics. Cambridge University Press, Cambridge, UK, 2009.

[107] S. Caron-Huot, "Analyticity in Spin in Conformal Theories," *JHEP* **09** (2017) 078, arXiv:1703.00278 [hep-th].

[108] R. Gopakumar, A. Kaviraj, K. Sen, and A. Sinha, "Conformal Bootstrap in Mellin Space," *Phys. Rev. Lett.* **118** no. 8, (2017) 081601, arXiv:1609.00572 [hep-th].

[109] R. Gopakumar, A. Kaviraj, K. Sen, and A. Sinha, "A Mellin space approach to the conformal bootstrap," *JHEP* **05** (2017) 027, arXiv:1611.08407 [hep-th].

[110] P. Dey, K. Ghosh, and A. Sinha, "Simplifying large spin bootstrap in Mellin space," *JHEP* **01** (2018) 152, arXiv:1709.06110 [hep-th].

[111] A. Bissi, A. Sinha, and X. Zhou, "Selected topics in analytic conformal bootstrap: A guided journey," *Phys. Rept.* **991** (2022) 1–89, arXiv:2202.08475 [hep-th].

[112] M. S. Costa, V. Goncalves, and J. Penedones, "Conformal Regge theory," *JHEP* **12** (2012) 091, arXiv:1209.4355 [hep-th].

[113] M. Hogervorst and S. Rychkov, "Radial Coordinates for Conformal Blocks," *Phys. Rev. D* **87** (2013) 106004, arXiv:1303.1111 [hep-th].

[114] K. Sen and A. Sinha, "On critical exponents without Feynman diagrams," *J. Phys. A* **49** no. 44, (2016) 445401, arXiv:1510.07770 [hep-th].

[115] D. Carmi, J. Penedones, J. A. Silva, and A. Zhiboedov, "Applications of dispersive sum rules: ϵ-expansion and holography," *SciPost Phys.* **10** no. 6, (2021) 145, arXiv:2009.13506 [hep-th].

[116] G. Mussardo, *Statistical Field Theory*. Oxford Graduate Texts. Oxford University Press, 3, 2020.

[117] S. Sachdev, *Quantum Phase Transitions*. Cambridge University Press, 4, 2011.

[118] S. El-Showk and K. Papadodimas, "Emergent Spacetime and Holographic CFTs," *JHEP* **10** (2012) 106, arXiv:1101.4163 [hep-th].

[119] G. P. Korchemsky, "Review of AdS/CFT Integrability, Chapter IV.4: Integrability in QCD and $N < 4$ SYM," *Lett. Math. Phys.* **99** (2012) 425–453, arXiv:1012.4000 [hep-th].

[120] K. Zoubos, "Review of AdS/CFT Integrability, Chapter IV.2: Deformations, Orbifolds and Open Boundaries," *Lett. Math. Phys.* **99** (2012) 375–400, arXiv:1012.3998 [hep-th].

[121] P. Liendo, E. Pomoni, and L. Rastelli, "The Complete One-Loop Dilation Operator of $\mathcal{N} = 2$ SuperConformal QCD," *JHEP* **07** (2012) 003, arXiv:1105.3972 [hep-th].

[122] A. Gadde and L. Rastelli, "Twisted Magnons," *JHEP* **04** (2012) 053, arXiv:1012.2097 [hep-th].

[123] E. Pomoni and C. Sieg, "From N=4 gauge theory to N=2 conformal QCD: three-loop mixing of scalar composite operators," arXiv:1105.3487 [hep-th].

[124] A. Gadde, P. Liendo, L. Rastelli, and W. Yan, "On the Integrability of Planar $N = 2$ Superconformal Gauge Theories," *JHEP* **08** (2013) 015, arXiv:1211.0271 [hep-th].

[125] E. Pomoni, "Integrability in $\mathcal{N} = 2$ superconformal gauge theories," *Nucl. Phys. B* **893** (2015) 21–53, arXiv:1310.5709 [hep-th].

[126] V. Mitev and E. Pomoni, "Exact effective couplings of four dimensional gauge theories with $\mathcal{N} = 2$ supersymmetry," *Phys. Rev. D* **92** no. 12, (2015) 125034, arXiv:1406.3629 [hep-th].

[127] B. Fraser, "Higher rank Wilson loops in the $\mathcal{N} = 2SU(N) \times SU(N)$ conformal quiver," *J. Phys. A* **49** no. 2, (2016) 02LT03, arXiv:1503.05634 [hep-th].

[128] V. Mitev and E. Pomoni, "Exact Bremsstrahlung and Effective Couplings," *JHEP* **06** (2016) 078, arXiv:1511.02217 [hep-th].

[129] V. Niarchos, C. Papageorgakis, and E. Pomoni, "Type-B Anomaly Matching and the 6D (2,0) Theory," *JHEP* **04** (2020) 048, arXiv:1911.05827 [hep-th].

[130] V. Niarchos, C. Papageorgakis, A. Pini, and E. Pomoni, "(Mis-)Matching Type-B Anomalies on the Higgs Branch," *JHEP* **01** (2021) 106, arXiv:2009.08375 [hep-th].

[131] K. Zarembo, "Quiver CFT at strong coupling," *JHEP* **06** (2020) 055, arXiv:2003.00993 [hep-th].

[132] F. Galvagno and M. Preti, "Chiral correlators in $\mathcal{N} = 2$ superconformal quivers," *JHEP* **05** (2021) 201, arXiv:2012.15792 [hep-th].

[133] F. Galvagno and M. Preti, "Wilson loop correlators in $\mathcal{N} = 2$ superconformal quivers," *JHEP* **11** (2021) 023, arXiv:2105.00257 [hep-th].

[134] M. R. Gaberdiel and F. Galvagno, "Worldsheet dual of free $\mathcal{N} = 2$ quiver gauge theories," *JHEP* **10** (2022) 077, arXiv:2206.08795 [hep-th].

[135] A. Dei, P. Ferrero, and L. Rastelli, "On supergravity and noncritical strings," *JHEP* **01** (2025) 117, arXiv:2409.13806 [hep-th].

[136] H. Bertle, E. Pomoni, X. Zhang, and K. Zoubos, "Hidden symmetries of 4D $\mathcal{N} = 2$ gauge theories," *JHEP* **02** (2025) 205, arXiv:2411.11612 [hep-th].

[137] G. Felder, "Elliptic quantum groups," arXiv:hep-th/9412207.

[138] G. Felder and A. Varchenko, "Algebraic Bethe ansatz for the elliptic quantum group $E_{\tau,\eta}(sl(2))$," *Nucl. Phys. B* **480** (1996) 485–503, arXiv:q-alg/9605024.

[139] G. Felder and M. Ren, "Quantum Groups for Restricted SOS Models," *SIGMA* **17** (2021) 005, arXiv:2010.01060 [math.RT].

[140] M. Ren, "Baxterization for the dynamical Yang-Baxter equation," arXiv:2310.04728 [math.RT].

[141] J. Anić and G. Felder, "Restricted quantum groups as graded hopf algebras," 2026. https://arxiv.org/abs/2605.15909.

[142] N. Mann and S. E. Vázquez, "Classical open string integrability," *Journal of High Energy Physics* **2007** no. 04, (Apr., 2007) 065–065. http://dx.doi.org/10.1088/1126-6708/2007/04/065.

[143] O. DeWolfe and N. Mann, "Integrable open spin chains in defect conformal field theory," *Journal of High Energy Physics* **2004** no. 04, (Apr., 2004) 035–035. http://dx.doi.org/10.1088/1126-6708/2004/04/035.

[144] P. N. Bibikov, "Three magnons in an isotropic $s = 1$ ferromagnetic chain as an exactly solvable non-integrable system," *Journal of Statistical Mechanics: Theory and Experiment* **2016** no. 3, (Mar, 2016) 033109. https://dx.doi.org/10.1088/1742-5468/2016/03/033109.

[145] C. N. Yang, "s matrix for the one-dimensional n-body problem with repulsive or attractive δ-function interaction," *Phys. Rev.* **168** (Apr, 1968) 1920–1923. https://link.aps.org/doi/10.1103/PhysRev.168.1920.

[146] L. Iliesiu, M. Koloğlu, R. Mahajan, E. Perlmutter, and D. Simmons-Duffin, "The Conformal Bootstrap at Finite Temperature," *JHEP* **10** (2018) 070, arXiv:1802.10266 [hep-th].

[147] E. Marchetto, A. Miscioscia, and E. Pomoni, "Sum rules & Tauberian theorems at finite temperature," *JHEP* **09** (2024) 044, arXiv:2312.13030 [hep-th].

[148] J. Barrat, E. Marchetto, A. Miscioscia, and E. Pomoni, "Thermal Bootstrap for the Critical O(N) Model," *Phys. Rev. Lett.* **134** no. 21, (2025) 211604, arXiv:2411.00978 [hep-th].

[149] I. Burić, I. Gusev, and A. Parnachev, "Thermal holographic correlators and KMS condition," arXiv:2505.10277 [hep-th].

[150] E. Marchetto, A. Miscioscia, and E. Pomoni, "Broken (super) conformal Ward identities at finite temperature," *JHEP* **12** (2023) 186, arXiv:2306.12417 [hep-th].

[151] N. Benjamin, J. Lee, H. Ooguri, and D. Simmons-Duffin, "Universal asymptotics for high energy CFT data," *JHEP* **03** (2024) 115, arXiv:2306.08031 [hep-th].

[152] L. F. Alday, M. Kologlu, and A. Zhiboedov, "Holographic correlators at finite temperature," *JHEP* **06** (2021) 082, arXiv:2009.10062 [hep-th].

[153] J. M. Deutsch, "Quantum statistical mechanics in a closed system," *Phys. Rev. A* **43** (Feb, 1991) 2046–2049. https://link.aps.org/doi/10.1103/PhysRevA.43.2046.

[154] L. Fidkowski, V. Hubeny, M. Kleban, and S. Shenker, "The Black hole singularity in AdS / CFT," *JHEP* **02** (2004) 014, arXiv:hep-th/0306170.

[155] E. Parisini, K. Skenderis, and B. Withers, "The ambient space formalism," *JHEP* **05** (2024) 296, arXiv:2312.03820 [hep-th].

[156] D. Mazáč, "A Crossing-Symmetric OPE Inversion Formula," *JHEP* **06** (2019) 082, arXiv:1812.02254 [hep-th].

[157] K. Ghosh, M. F. Paulos, and N. Suchel, "Solving 1D crossing and $\mathrm{QFT}_2/\mathrm{CFT}_1$," arXiv:2503.22798 [hep-th].

[158] L. F. Alday and A. Zhiboedov, "Conformal bootstrap with slightly broken higher spin symmetry," *JHEP* **06** (2016) 091, arXiv:1506.04659 [hep-th].

[159] A. L. Fitzpatrick, J. Kaplan, D. Poland, and D. Simmons-Duffin, "The Analytic Bootstrap and AdS Superhorizon Locality," *JHEP* **12** (2013) 004, arXiv:1212.3616 [hep-th].

[160] Z. Komargodski and A. Zhiboedov, "Convexity and Liberation at Large Spin," *JHEP* **11** (2013) 140, arXiv:1212.4103 [hep-th].

[161] J. Barrat, A. Gimenez-Grau, and P. Liendo, "A dispersion relation for defect CFT," *JHEP* **02** (2023) 255, arXiv:2205.09765 [hep-th].

[162] L. Bianchi and D. Bonomi, "Conformal dispersion relations for defects and boundaries," *SciPost Phys.* **15** no. 2, (2023) 055, arXiv:2205.09775 [hep-th].

[163] A. C. Petkou, "Thermal one-point functions and single-valued polylogarithms," *Phys. Lett. B* **820** (2021) 136467, arXiv:2105.03530 [hep-th].

[164] M. Karydas, S. Li, A. C. Petkou, and M. Vilatte, "Conformal Graphs as Twisted Partition Functions," *Phys. Rev. Lett.* **132** no. 23, (2024) 231601, arXiv:2312.00135 [hep-th].

[165] A. Manenti, "Thermal CFTs in momentum space," *JHEP* **01** (2020) 009, arXiv:1905.01355 [hep-th].

[166] A. Bzowski, P. McFadden, and K. Skenderis, "Implications of conformal invariance in momentum space," *JHEP* **03** (2014) 111, arXiv:1304.7760 [hep-th].

[167] A. Bzowski, P. McFadden, and K. Skenderis, "Conformal correlators as simplex integrals in momentum space," *JHEP* **01** (2021) 192, arXiv:2008.07543 [hep-th].

[168] R. Marotta, K. Skenderis, and M. Verma, "Momentum space CFT correlators of non-conserved spinning operators," *JHEP* **03** (2023) 196, arXiv:2212.13135 [hep-th].

[169] S. Caron-Huot, "Asymptotics of thermal spectral functions," *Phys. Rev. D* **79** (2009) 125009, arXiv:0903.3958 [hep-ph].

[170] D. T. Son and A. O. Starinets, "Minkowski-space correlators in ads/cft correspondence: recipe and applications," *Journal of High Energy Physics* **2002** no. 09, (Sept., 2002) 042–042. http://dx.doi.org/10.1088/1126-6708/2002/09/042.

[171] M. Dodelson, C. Iossa, R. Karlsson, A. Lupsasca, and A. Zhiboedov, "Black hole bulk-cone singularities," *JHEP* **07** (2024) 046, arXiv:2310.15236 [hep-th].

[172] H. Kleinert and V. Schulte-Frohlinde, *Critical Properties of ϕ^4-theories*. World Scientific, 2001.

[173] J. Henriksson, "The critical O(N) CFT: Methods and conformal data," *Phys. Rept.* **1002** (2023) 1–72, arXiv:2201.09520 [hep-th].

[174] S. Giombi and X. Yin, "The Higher Spin/Vector Model Duality," *J. Phys. A* **46** (2013) 214003, arXiv:1208.4036 [hep-th].

[175] K. G. Wilson and M. E. Fisher, "Critical exponents in 3.99 dimensions," *Phys. Rev. Lett.* **28** (Jan, 1972) 240–243. https://link.aps.org/doi/10.1103/PhysRevLett.28.240.

[176] K. G. Wilson, "Renormalization group and critical phenomena. i. renormalization group and the kadanoff scaling picture," *Phys. Rev. B* **4** (Nov, 1971) 3174–3183. https://link.aps.org/doi/10.1103/PhysRevB.4.3174.

[177] K. G. Wilson, "Renormalization group and critical phenomena. ii. phase-space cell analysis of critical behavior," *Phys. Rev. B* **4** (Nov, 1971) 3184–3205. https://link.aps.org/doi/10.1103/PhysRevB.4.3184.

[178] K. G. Wilson and J. Kogut, "The renormalization group and the ϵ expansion," *Physics Reports* **12** no. 2, (1974) 75–199. https://www.sciencedirect.com/science/article/pii/0370157374900234.

[179] A. Pelissetto and E. Vicari, "Critical phenomena and renormalization group theory," *Phys. Rept.* **368** (2002) 549–727, arXiv:cond-mat/0012164.

[180] S. K. Kehrein, F. J. Wegner, and Y. M. Pismak, "Conformal symmetry and the spectrum of anomalous dimensions in the n-vector model in $4-\epsilon$ dimensions," *Nuclear Physics B* **402** no. 3, (1993) 669–692. https://www.sciencedirect.com/science/article/pii/0550321393901248.

[181] S. K. Kehrein and F. Wegner, "The Structure of the spectrum of anomalous dimensions in the N vector model in $(4-\epsilon)$-dimensions," *Nucl. Phys. B* **424** (1994) 521–546, arXiv:hep-th/9405123.

[182] S. K. Kehrein, "The Spectrum of critical exponents in ϕ^2 in two-dimensions theory in D = (4-ϵ)-dimensions: Resolution of degeneracies and hierarchical structures," *Nucl. Phys. B* **453** (1995) 777–806, arXiv:hep-th/9507044.

[183] S. Rychkov, "Conformal Bootstrap in Three Dimensions?," arXiv:1111.2115 [hep-th].

[184] A. N. Vasil'ev, Y. M. Pis'mak, and Y. R. Khonkonen, "1/n expansion: Calculation of the exponent ν in the order $1/n^3$ by the conformal bootstrap method," *Theoretical and Mathematical Physics* **50** no. 2, (1982) 127–134. https://doi.org/10.1007/BF01015292.

[185] S. Sachdev, "Polylogarithm identities in a conformal field theory in three-dimensions," *Phys. Lett. B* **309** (1993) 285–288, arXiv:hep-th/9305131.

[186] M. A. Vasiliev, "Higher spin gauge theories in four-dimensions, three-dimensions, and two-dimensions," *Int. J. Mod. Phys. D* **5** (1996) 763–797, arXiv:hep-th/9611024.

[187] M. A. Vasiliev, "Higher spin gauge theories: Star product and AdS space," arXiv:hep-th/9910096.

[188] K. G. Wilson and M. E. Fisher, "Critical exponents in 3.99 dimensions," *Phys. Rev. Lett.* **28** (1972) 240–243.

[189] L. Iliesiu, M. Koloğlu, and D. Simmons-Duffin, "Bootstrapping the 3d Ising model at finite temperature," *JHEP* **12** (2019) 072, arXiv:1811.05451 [hep-th].

[190] S. Giombi, R. Huang, I. R. Klebanov, S. S. Pufu, and G. Tarnopolsky, "The $O(N)$ Model in $4 < d < 6$: Instantons and complex CFTs," *Phys. Rev. D* **101** no. 4, (2020) 045013, arXiv:1910.02462 [hep-th].

[191] O. Diatlyk, F. K. Popov, and Y. Wang, "Beyond $N = \infty$ in Large N conformal vector models at finite temperature," *JHEP* **08** (2024) 219, arXiv:2309.02347 [hep-th].

[192] A. Gimenez-Grau, "Probing magnetic line defects with two-point functions," arXiv:2212.02520 [hep-th].

[193] S. Sachdev and J. Ye, "Universal quantum critical dynamics of two-dimensional antiferromagnets," *Phys. Rev. Lett.* **69** (1992) 2411, arXiv:cond-mat/9204001.

[194] A. C. Petkou and A. Stergiou, "Dynamics of Finite-Temperature Conformal Field Theories from Operator Product Expansion Inversion Formulas," *Phys. Rev. Lett.* **121** no. 7, (2018) 071602, arXiv:1806.02340 [hep-th].

[195] I. Heemskerk, J. Penedones, J. Polchinski, and J. Sully, "Holography from Conformal Field Theory," *JHEP* **10** (2009) 079, arXiv:0907.0151 [hep-th].

[196] M. Ammon and J. Erdmenger, *Gauge/gravity duality: Foundations and applications*. Cambridge University Press, Cambridge, 4, 2015.

[197] A. L. Fitzpatrick, E. Katz, D. Poland, and D. Simmons-Duffin, "Effective Conformal Theory and the Flat-Space Limit of AdS," *JHEP* **07** (2011) 023, arXiv:1007.2412 [hep-th].

[198] A. L. Fitzpatrick and J. Kaplan, "Analyticity and the Holographic S-Matrix," *JHEP* **10** (2012) 127, arXiv:1111.6972 [hep-th].

[199] A. L. Fitzpatrick and J. Kaplan, "Unitarity and the Holographic S-Matrix," *JHEP* **10** (2012) 032, arXiv:1112.4845 [hep-th].

[200] A. L. Fitzpatrick and J. Kaplan, "AdS Field Theory from Conformal Field Theory," *JHEP* **02** (2013) 054, arXiv:1208.0337 [hep-th].

[201] R. Karlsson, A. Parnachev, and P. Tadić, "Thermalization in large-N CFTs," *JHEP* **09** (2021) 205, arXiv:2102.04953 [hep-th].

[202] M. Kulaxizi, G. S. Ng, and A. Parnachev, "Black Holes, Heavy States, Phase Shift and Anomalous Dimensions," *SciPost Phys.* **6** no. 6, (2019) 065, arXiv:1812.03120 [hep-th].

[203] R. Karlsson, M. Kulaxizi, A. Parnachev, and P. Tadić, "Leading Multi-Stress Tensors and Conformal Bootstrap," *JHEP* **01** (2020) 076, arXiv:1909.05775 [hep-th].

[204] Y.-Z. Li, "Heavy-light Bootstrap from Lorentzian Inversion Formula," *JHEP* **07** (2020) 046, arXiv:1910.06357 [hep-th].

[205] R. Karlsson, M. Kulaxizi, A. Parnachev, and P. Tadić, "Black Holes and Conformal Regge Bootstrap," *JHEP* **10** (2019) 046, arXiv:1904.00060 [hep-th].

[206] A. Parnachev, "Near Lightcone Thermal Conformal Correlators and Holography," *J. Phys. A* **54** no. 15, (2021) 155401, arXiv:2005.06877 [hep-th].

[207] Y.-Z. Li and H.-Y. Zhang, "More on heavy-light bootstrap up to double-stress-tensor," *JHEP* **10** (2020) 055, arXiv:2004.04758 [hep-th].

[208] R. Karlsson, M. Kulaxizi, A. Parnachev, and P. Tadić, "Stress tensor sector of conformal correlators operators in the Regge limit," *JHEP* **07** (2020) 019, arXiv:2002.12254 [hep-th].

[209] M. Dodelson, A. Grassi, C. Iossa, D. Panea Lichtig, and A. Zhiboedov, "Holographic

thermal correlators from supersymmetric instantons," *SciPost Phys.* **14** no. 5, (2023) 116, arXiv:2206.07720 [hep-th].

[210] A. L. Fitzpatrick and K.-W. Huang, "Universal Lowest-Twist in CFTs from Holography," *JHEP* **08** (2019) 138, arXiv:1903.05306 [hep-th].

[211] G. Aminov, A. Grassi, and Y. Hatsuda, "Black Hole Quasinormal Modes and Seiberg–Witten Theory," *Annales Henri Poincare* **23** no. 6, (2022) 1951–1977, arXiv:2006.06111 [hep-th].

[212] M. Dodelson, C. Iossa, R. Karlsson, and A. Zhiboedov, "A thermal product formula," *JHEP* **01** (2024) 036, arXiv:2304.12339 [hep-th].

[213] A. L. Fitzpatrick, J. Kaplan, and M. T. Walters, "Virasoro Conformal Blocks and Thermality from Classical Background Fields," *JHEP* **11** (2015) 200, arXiv:1501.05315 [hep-th].

[214] L. F. Alday and A. Bissi, "Unitarity and positivity constraints for CFT at large central charge," *JHEP* **07** (2017) 044, arXiv:1606.09593 [hep-th].

[215] L. F. Alday and A. Bissi, "Loop Corrections to Supergravity on $AdS_5 \times S^5$," *Phys. Rev. Lett.* **119** no. 17, (2017) 171601, arXiv:1706.02388 [hep-th].

[216] I. Burić, I. Gusev, and A. Parnachev, "Holographic Correlators from Thermal Bootstrap," arXiv:2508.08373 [hep-th].

[217] A. Castro and P. J. Martinez, "Revisiting extremal couplings in AdS/CFT," *JHEP* **12** (2024) 157, arXiv:2409.15410 [hep-th].

[218] N. Bobev and H. Paul, "Holographic correlators beyond maximal supersymmetry," *JHEP* **09** (2025) 087, arXiv:2505.20400 [hep-th].

[219] D. Rodriguez-Gomez and J. G. Russo, "Correlation functions in finite temperature CFT and black hole singularities," *JHEP* **06** (2021) 048, arXiv:2102.11891 [hep-th].

[220] G. Festuccia and H. Liu, "Excursions beyond the horizon: Black hole singularities in Yang-Mills theories. I.," *JHEP* **04** (2006) 044, arXiv:hep-th/0506202.

[221] N. Čeplak, H. Liu, A. Parnachev, and S. Valach, "Black hole singularity from OPE," *JHEP* **10** (2024) 105, arXiv:2404.17286 [hep-th].

[222] I. Burić, F. Mangialardi, F. Russo, V. Schomerus, and A. Vichi, "Heavy-Heavy-Light Asymptotics from Thermal Correlators," arXiv:2506.21671 [hep-th].

[223] N. Afkhami-Jeddi, S. Caron-Huot, J. Chakravarty, and A. Maloney, "Imprint of the black hole singularity on thermal two-point functions," arXiv:2510.21673 [hep-th].

[224] E. Parisini, K. Skenderis, and B. Withers, "Embedding formalism for CFTs in general

states on curved backgrounds," *Phys. Rev. D* **107** no. 6, (2023) 066022, arXiv:2209.09250 [hep-th].

[225] G. Policastro, D. T. Son, and A. O. Starinets, "From AdS / CFT correspondence to hydrodynamics," *JHEP* **09** (2002) 043, arXiv:hep-th/0205052.

[226] I. Amado, C. Hoyos-Badajoz, K. Landsteiner, and S. Montero, "Hydrodynamics and beyond in the strongly coupled N=4 plasma," *JHEP* **07** (2008) 133, arXiv:0805.2570 [hep-th].

[227] D. Lovelock, "The Einstein tensor and its generalizations," *J. Math. Phys.* **12** (1971) 498–501.

[228] R. C. Myers, M. F. Paulos, and A. Sinha, "Holographic Hydrodynamics with a Chemical Potential," *JHEP* **06** (2009) 006, arXiv:0903.2834 [hep-th].

[229] X. O. Camanho and J. D. Edelstein, "Causality constraints in AdS/CFT from conformal collider physics and Gauss-Bonnet gravity," *JHEP* **04** (2010) 007, arXiv:0911.3160 [hep-th].

[230] J. de Boer, M. Kulaxizi, and A. Parnachev, "Holographic Lovelock Gravities and Black Holes," *JHEP* **06** (2010) 008, arXiv:0912.1877 [hep-th].

[231] E. Shaghoulian, "Modular Invariance of Conformal Field Theory on $S^1 \times S^3$ and Circle Fibrations," *Phys. Rev. Lett.* **119** no. 13, (2017) 131601, arXiv:1612.05257 [hep-th].

[232] Y. Gobeil, A. Maloney, G. S. Ng, and J.-q. Wu, "Thermal Conformal Blocks," *SciPost Phys.* **7** no. 2, (2019) 015, arXiv:1802.10537 [hep-th].

[233] K. Alkalaev and S. Mandrygin, "One-point thermal conformal blocks from four-point conformal integrals," *JHEP* **10** (2024) 241, arXiv:2407.01741 [hep-th].

[234] K. Allameh and E. Shaghoulian, "Modular invariance and thermal effective field theory in CFT," *JHEP* **01** (2025) 200, arXiv:2402.13337 [hep-th].

[235] I. Buric, F. Russo, V. Schomerus, and A. Vichi, "Thermal one-point functions and their partial wave decomposition," *JHEP* **12** (2024) 021, arXiv:2408.02747 [hep-th].

[236] J. R. David and S. Kumar, "The large N vector model on $\mathrm{S}^1 \times \mathrm{S}^2$," *JHEP* **03** (2025) 169, arXiv:2411.18509 [hep-th].

[237] A. Belin, S. Bintanja, A. Castro, and W. Knop, "Symmetric Product Orbifold Universality and the Mirage of an Emergent Spacetime," arXiv:2502.01734 [hep-th].

[238] R. Kubo, "Statistical mechanical theory of irreversible processes. 1. General theory and simple applications in magnetic and conduction problems," *J. Phys. Soc. Jap.* **12** (1957) 570–586.

[239] P. C. Martin and J. S. Schwinger, "Theory of many particle systems. 1.," *Phys. Rev.* **115** (1959) 1342–1373.

[240] S. W. Hawking and D. N. Page, "Thermodynamics of Black Holes in anti-De Sitter Space," *Commun. Math. Phys.* **87** (1983) 577.

[241] N. Jokela, A. Pönni, and A. Vuorinen, "Small black holes in global AdS spacetime," *Phys. Rev. D* **93** no. 8, (2016) 086004, arXiv:1508.00859 [hep-th].

[242] F. Gliozzi, P. Liendo, M. Meineri, and A. Rago, "Boundary and Interface CFTs from the Conformal Bootstrap," *JHEP* **05** (2015) 036, arXiv:1502.07217 [hep-th].

[243] D. Simmons-Duffin and Y. Xu, "A genus-2 crossing equation in $d \geq 2$," arXiv:2511.07569 [hep-th].

[244] F. Gliozzi, "More constraining conformal bootstrap," *Phys. Rev. Lett.* **111** (2013) 161602, arXiv:1307.3111 [hep-th].

[245] J. Barrat, B. Fiol, E. Marchetto, A. Miscioscia, and E. Pomoni, "Conformal line defects at finite temperature," *SciPost Phys.* **18** no. 1, (2025) 018, arXiv:2407.14600 [hep-th].

[246] M. Reehorst, "Rigorous bounds on irrelevant operators in the 3d Ising model CFT," *JHEP* **09** (2022) 177, arXiv:2111.12093 [hep-th].

[247] A. Bulgarelli, M. Caselle, A. Nada, and M. Panero, "Casimir effect in critical O(N) models from non-equilibrium Monte Carlo simulations," arXiv:2505.20403 [cond-mat.stat-mech].

[248] D. Bernard, M. Gaudin, F. D. M. Haldane, and V. Pasquier, "Yang-Baxter equation in long range interacting system," *J. Phys. A* **26** (1993) 5219–5236, arXiv:hep-th/9301084.

[249] M. de Leeuw, A. Pribytok, and P. Ryan, "Classifying two-dimensional integrable spin chains," *J. Phys. A* **52** no. 50, (2019) 505201, arXiv:1904.12005 [math-ph].

[250] M. de Leeuw, C. Paletta, A. Pribytok, A. L. Retore, and P. Ryan, "Classifying Nearest-Neighbor Interactions and Deformations of AdS," *Phys. Rev. Lett.* **125** no. 3, (2020) 031604, arXiv:2003.04332 [hep-th].

[251] M. de Leeuw, C. Paletta, A. Pribytok, A. L. Retore, and P. Ryan, "Yang-Baxter and the Boost: splitting the difference," *SciPost Phys.* **11** (2021) 069, arXiv:2010.11231 [math-ph].

[252] L. Corcoran, M. de Leeuw, and B. Pozsgay, "Integrable models on Rydberg atom chains," *SciPost Phys.* **18** no. 4, (2025) 139, arXiv:2405.15848 [cond-mat.str-el].

[253] T. McLoughlin and A. Spiering, "Chaotic spin chains in AdS/CFT," *JHEP* **09** (2022) 240, arXiv:2202.12075 [hep-th].

[254] P. Liendo and L. Rastelli, "The Complete One-loop Spin Chain of N =1 SQCD," *JHEP* **10** (2012) 117, arXiv:1111.5290 [hep-th].

[255] B. Basso, S. Komatsu, and P. Vieira, "Structure Constants and Integrable Bootstrap in Planar N=4 SYM Theory," arXiv:1505.06745 [hep-th].

[256] N. Chai, S. Chaudhuri, C. Choi, Z. Komargodski, E. Rabinovici, and M. Smolkin, "Symmetry Breaking at All Temperatures," *Phys. Rev. Lett.* **125** no. 13, (2020) 131603.

[257] Z. Komargodski and F. K. Popov, "Temperature-Resistant Order in 2+1 Dimensions," arXiv:2412.09459 [hep-th].

[258] B. Hawashin, J. Rong, and M. M. Scherer, "Ultraviolet-Complete Local Field Theory of Persistent Symmetry Breaking in 2+1 Dimensions," *Phys. Rev. Lett.* **134** no. 4, (2025) 041602, arXiv:2409.10606 [hep-th].

[259] Y. Han, X. Huang, Z. Komargodski, A. Lucas, and F. K. Popov, "Entropic Order," arXiv:2503.22789 [cond-mat.stat-mech].

[260] A. M. Polyakov, "Thermal Properties of Gauge Fields and Quark Liberation," *Phys. Lett. B* **72** (1978) 477–480.

[261] I. Affleck, "Conformal field theory approach to the Kondo effect," *Acta Phys. Polon. B* **26** (1995) 1869–1932, arXiv:cond-mat/9512099.

[262] G. Cuomo, Z. Komargodski, and M. Mezei, "Localized magnetic field in the O(N) model," *JHEP* **02** (2022) 134, arXiv:2112.10634 [hep-th].

[263] A. Gimenez-Grau, E. Lauria, P. Liendo, and P. van Vliet, "Bootstrapping line defects with O(2) global symmetry," *JHEP* **11** (2022) 018, arXiv:2208.11715 [hep-th].

[264] L. Bianchi, D. Bonomi, and E. de Sabbata, "Analytic bootstrap for the localized magnetic field," *JHEP* **04** (2023) 069, arXiv:2212.02524 [hep-th].

[265] L. Hu, Y.-C. He, and W. Zhu, "Solving conformal defects in 3D conformal field theory using fuzzy sphere regularization," *Nature Commun.* **15** no. 1, (2024) 9013, arXiv:2308.01903 [cond-mat.stat-mech].

[266] S. Giombi, R. Roiban, and A. A. Tseytlin, "Half-BPS Wilson loop and AdS_2/CFT_1," *Nucl. Phys. B* **922** (2017) 499–527, arXiv:1706.00756 [hep-th].

[267] P. Liendo, C. Meneghelli, and V. Mitev, "Bootstrapping the half-BPS line defect," *JHEP* **10** (2018) 077, arXiv:1806.01862 [hep-th].

[268] S. Giombi and S. Komatsu, "Exact Correlators on the Wilson Loop in $\mathcal{N} = 4$ SYM: Localization, Defect CFT, and Integrability," *JHEP* **05** (2018) 109, arXiv:1802.05201 [hep-th]. [Erratum: JHEP 11, 123 (2018)].

[269] P. Ferrero and C. Meneghelli, "Bootstrapping the half-BPS line defect CFT in N=4

supersymmetric Yang–Mills theory at strong coupling," *Phys. Rev. D* **104** no. 8, (2021) L081703, arXiv:2103.10440 [hep-th].

[270] A. Cavaglià, N. Gromov, J. Julius, and M. Preti, "Integrability and conformal bootstrap: One dimensional defect conformal field theory," *Phys. Rev. D* **105** no. 2, (2022) L021902, arXiv:2107.08510 [hep-th].

[271] J. Barrat, P. Liendo, G. Peveri, and J. Plefka, "Multipoint correlators on the supersymmetric Wilson line defect CFT," *JHEP* **08** (2022) 067, arXiv:2112.10780 [hep-th].

[272] D. Artico, J. Barrat, and G. Peveri, "Perturbative bootstrap of the Wilson-line defect CFT: multipoint correlators," *JHEP* **02** (2025) 190, arXiv:2410.08271 [hep-th].

[273] J. R. David and S. Kumar, "Thermal one-point functions: CFT's with fermions, large d and large spin," *JHEP* **10** (2023) 143, arXiv:2307.14847 [hep-th].